

NASA Technical Memorandum 4124

Wind-Tunnel Investigation of Aerodynamic Characteristics and Wing Pressure Distributions of an Airplane With Variable-Sweep Wings Modified for Laminar Flow

James B. Hallissy and Pamela S. Phillips
Langley Research Center
Hampton, Virginia



National Aeronautics and
Space Administration
Office of Management
Scientific and Technical
Information Division

1989

Summary

A wind-tunnel investigation has been conducted to evaluate the aerodynamic characteristics and wing pressure distributions of a variable-wing-sweep aircraft having wing panels that were modified to promote laminar flow. The modified wing section shapes were incorporated over most of the exposed outer wing panel span and were obtained by extending the leading edge and adding thickness to the existing wing upper surface forward of 60 percent chord. Two different wing configurations, one designed for a Mach number of 0.7 and one for 0.8, were tested on the model simultaneously, with one wing configuration on the left side and the other on the right. The investigations were conducted at Mach numbers from 0.20 to 0.90 for wing sweep angles of 20°, 25°, 30°, and 35°. Longitudinal, lateral, and directional aerodynamic characteristics of the modified and baseline configurations, and selected pressure distributions for the modified configuration, are presented in graphical form without analysis. A complete tabulation of the pressure data for the modified configuration is available as a microfiche supplement. Test results indicate that the stability and control characteristics were not significantly altered as a result of the modifications and that the rolling moments resulting from the asymmetric wing configuration were within the prescribed limits of angles of attack below wing stall. Also, comparison of the measured wing pressure distributions with predicted values (not presented) generally showed good agreement.

Introduction

During the mid-1970's, NASA began the Aircraft Energy Efficiency (ACEE) Program to look at ways of making commercial transport aircraft more efficient. One area of research that has received considerable attention is laminar flow. In order to design wings that effectively utilize laminar flow, it is necessary to understand the influence of cross-flow (CF) and Tollmien-Schlichting (TS) instabilities on boundary-layer transition for representative transport wing configurations.

A flight experiment designed to provide a data base on the effect of wing sweep on boundary-layer transition was conducted using the F-111 transonic aircraft technology (TACT) aircraft with a modified airfoil contour designed to promote laminar flow over part of the wing panel (ref. 1), but the results were compromised by a very limited span for the modified wing section. In order to augment the data base obtained in that experiment, NASA has defined and conducted a Variable Sweep Transition Flight Experiment (VSTFE) using a modified F-14A

aircraft (refs. 2, 3, and 4). The objective of this experiment was to obtain accurate in-flight measurements of boundary-layer transition location for wing pressure distributions, sweep angles, and flight conditions representative of future laminar flow transport aircraft. By using the results obtained from analysis of these wing pressure distributions with a boundary-layer stability code and from flight-measured transition data, the interaction of CF and TS instabilities on boundary-layer transition can be studied. These results could then be used to develop a reliable method of predicting boundary-layer transition for this type of aircraft configuration.

To obtain flight data for a representative wing configuration, the F-14A wing outer panel was modified by using the technique of reference 5 in which a foam and fiberglass "glove" is built up on the existing wing panel to produce a wing of the desired shape. The desired wing shapes were designed to produce pressure gradients favorable for laminar flow over most of the wing upper surface forward of 60 percent chord. Two different design conditions were selected, and a separate wing configuration was developed for each condition by using computational techniques described in references 6 and 7. The two different wing configurations were to be flown simultaneously on the test aircraft, with one configuration applied to the left wing and the other to the right wing.

In order to evaluate the stability and control characteristics of this asymmetric wing configuration, a wind-tunnel investigation was conducted in the National Transonic Facility (NTF) using a 1/16-scale model of the F-14A aircraft. Another objective of this investigation was to verify the predicted pressure distributions for each of the wing designs for a range of Mach numbers, angles of attack, and wing sweep angles. The model was tested with the baseline F-14A wing and with the modified wings. Based on these test results and other constraints, the decision was made to make minor modifications to the inboard region of one glove and to conduct the flight experiment with that glove on the left side and an unmodified (baseline F-14A) wing on the right. These modifications to the glove were developed using the same computational techniques as the original design described in reference 6, and the flight test was conducted without additional wind-tunnel testing. At the time of this publication, the flight test program has been completed but published results are not yet available.

The present paper describes the wind-tunnel investigation conducted in NTF in support of the flight experiment and presents the wind-tunnel test results without analysis. These tests were conducted in the air mode at NTF, at Mach numbers from 0.2 to

0.9, wing sweep angles of 20°, 25°, 30°, and 35°, and angles of sideslip up to 10°. Both the baseline F-14A and the modified wing configurations were tested. Aerodynamic force and moment data for both the baseline and modified configurations and selected wing pressure data for the modified configuration are presented in graphical form. A tabulation of the wing pressure coefficients pertinent to the investigation is available as a microfiche supplement.

Symbols

The aerodynamic force and moment data presented herein are referenced to the body axis system with the exception of the lift and drag coefficients, which are referenced to the stability axis system. The moment reference center is located at fuselage station 33.254 and waterline 9.375. Coefficients for all configurations are based on the wing geometry of the baseline wing at a leading-edge sweep angle of 20°. Symbols in parentheses are used in the supplement.

A	axial force
b	reference wing span, for $\Lambda = 20^\circ$ (48.100 in.)
C_A	axial-force coefficient, $A/q_\infty S$
C_D	drag coefficient, $D/q_\infty S$
C_L	lift coefficient, $L/q_\infty S$
C_l	rolling-moment coefficient, $l/q_\infty S b$
C_m	pitching-moment coefficient, $m/q_\infty S \bar{c}$
C_N	normal force coefficient, $N/q_\infty S$
C_n	yawing-moment coefficient, $n/q_\infty S b$
C_p (CP)	pressure coefficient, $\frac{p-p_\infty}{q_\infty}$
C_Y	side force coefficient, $Y/q_\infty S$
c (C)	local wing chord
\bar{c}	mean geometric chord, for $\Lambda = 20^\circ$ (7.350 in.)
c_r	local chord of wing reference planform
D	drag force

L	lift force
l	rolling moment
M (MACH)	free-stream Mach number
m	pitching moment
N	normal force
n	yawing moment
p	local pressure
p_∞	free-stream static pressure
q_∞	free-stream dynamic pressure
S	reference wing area (2.207 ft ²)
x (X)	distance aft of wing leading edge (streamwise for $\Lambda = 20^\circ$)
x_r	distance aft of wing reference planform leading edge
Y	side force
y	distance left or right of model centerline
z_r	distance upward from a reference waterline
α (ALPHA)	model angle of attack, deg
β (BETA)	model angle of sideslip, deg
η (ETA)	fractional span position of orifice rows, $\frac{y}{b/2}$, for $\Lambda = 20^\circ$
Λ	nominal wing sweep angle

Abbreviations:

BL	buttock line
FS	fuselage station
LE	leading edge of reference planform
WL	waterline

Model Description

The general arrangement of the airplane model used for this investigation is shown in figure 1, and photographs of the model installed in the National Transonic Facility (NTF) are presented in figure 2. The baseline configuration was a 1/16-scale model of the F-14A aircraft with the wing pivot located longitudinally at fuselage station 32.763, laterally 6.687 in. outboard of the plane of symmetry, and canted 1.5° outboard. The wing leading-edge sweep angle was manually adjusted to sweep angles of 20° , 25° , 30° , and 35° . The model was equipped with flow-through nacelles that were configured with boat-tailed nozzles that simulated engine mass flow at cruise flight conditions. The model was mounted in the tunnel with a centerline sting arrangement shown in figure 2. Use of this sting arrangement required significant variation of the model geometry from that of the actual airplane in the aft centerbody region. These variations, however, were not expected to be of any significance for this investigation. Horizontal tail and rudder deflection angles were zero for all data presented herein.

The basic F-14A wing configuration, designated the baseline wing in this report, and two modified wing designs were tested in this investigation. The modified wing configurations, designated wing B and wing C, were developed for different design conditions but were designed to be tested simultaneously on the left and right sides, respectively, of the same aircraft. Consequently, only a left-hand panel for the wing B configuration and only a right-hand panel for the wing C configuration were fabricated for the model, and the wings were designed to generate approximately the same amount of lift as the basic wing at comparable angles of attack. The modified wing shapes were designed to promote laminar flow over the forward half of the outer (variable sweep) wing panel for cruise lift coefficients at a Mach number of 0.7 and an altitude of 35 000 ft for wing B, and at a Mach number of 0.8 and an altitude of 20 000 ft for wing C. For the wind-tunnel model, the modified shapes were obtained by fabricating new outer wing panels of steel.

Several constraints were placed on the glove design as a result of practical considerations. A requirement to maintain spoiler effectiveness for low-speed flight control restricted the aft limit of the glove to the spoiler hingeline ($0.60c$) and the maximum glove thickness on the aircraft at that location to 1.00 in. (0.062 in. model scale). In order to install pressure tubes on the aircraft, the aircraft glove thickness could not be less than 0.25 in. (0.016 in. model scale) anywhere on the wing. Over the aircraft

leading-edge slat-wing joint, a minimum glove thickness of 0.65 in. (0.041 in. model scale) was required to prevent a surface discontinuity that would otherwise occur because of slat deflection under aerodynamic load. To minimize load on the glove fairing around the leading edge, the maximum forward extension of the aircraft wing resulting from glove thickness at the leading edge was restricted to not more than 2 in. (0.125 in. model scale). In order to permit roll control without the use of spoilers during the cruise portion of flight, the modified wings were designed so that the rolling-moment coefficient induced by the wing asymmetry would not exceed ± 0.01 .

The modified wing configurations developed to meet these constraints were designed by using numerical computation techniques and methods described in references 6 and 7. The resulting model wing configurations are shown in plan view in figure 3, and typical variation of the glove section shape is shown in figure 4. The glove extended spanwise from BL 8.125 ($\eta = 0.338$) to BL 21.746 ($\eta = 0.904$) and chordwise from the spoiler hingeline ($0.60c$) forward around the leading edge, and faired into the basic wing lower surface contour ahead of the 5-percent chord line. The side edges of both gloves (streamwise for $\Lambda = 20^\circ$) were not blended into the basic wing contours but ended abruptly with a vertical step down to the basic wing contour. For the wing B configuration, the aft edge of the glove terminated abruptly with an aft-facing vertical step, and the leading edge was parallel to and 0.125 in. (model scale) forward of the baseline wing leading edge. For the wing C configuration, the aft edge of the glove terminated with an aft-facing ramp of approximately 45° slope, and the leading edge of the glove extended forward of the baseline wing a distance of 1 percent of the local chord, resulting in a leading edge that was swept 0.16° more than the baseline wing. This wing sweep differential was maintained for all model configurations with the modified wing panels, and all references to wing sweep angle in this report refer to the nominal sweep angle. Numerical values of the leading-edge offsets and sweep angles for wings B and C are noted in figure 3, and geometric details of the modified and baseline sections are presented in tables I, II, and III.

The new model wing panels incorporating the glove geometry were fabricated from VascoMax C-200 steel and each was instrumented with 60 flush pressure orifices of 0.013-in diameter arranged in 3 streamwise rows for $\Lambda = 20^\circ$, as shown in figure 3 and tabulated in table IV. Each row consisted of 19 orifices on the upper surface and 1 orifice near

the leading edge on the lower surface. The baseline (unmodified) wing tested for comparison had no pressure instrumentation.

Apparatus and Procedures

Facility

These investigations were conducted in the National Transonic Facility (NTF) at the Langley Research Center. This facility is a closed circuit, continuous flow, pressurized wind tunnel that can use either gaseous nitrogen at ambient or cryogenic temperatures or air at ambient temperatures as a test medium. The tunnel has a test section that is 2.5 m square with slotted top and bottom walls of 6-percent openness ratio and can operate continuously at Mach numbers from 0.2 to 1.2. Additional details about this facility can be obtained from reference 8.

The present investigations were conducted in air at Mach numbers from 0.2 to 0.9. For the 0.2 Mach number conditions, data were obtained at a stagnation pressure of 2 atm and a chord Reynolds number of 2.6 million. Data at the higher Mach numbers were obtained near the tunnel minimum operating pressure of 1 atm, resulting in chord Reynolds numbers ranging from approximately 3.3 million to 4.3 million, depending on Mach number.

Boundary-Layer Transition

Boundary-layer transition was fixed on the model by using transition strips composed of Carborundum grains set in a plastic adhesive. The roughness particle sizes were selected according to the method of reference 9. Transition strips were located 1.5 in. aft of the nose; 0.5 in. aft of the leading edges of the inlets (external surfaces), vertical and horizontal tails, ventral fins, and inboard (fixed) wing; and 0.5 in. aft (for $\Lambda = 20^\circ$) of the leading edge on the lower surface of the outer wing panels. In order to prevent an unrealistic laminar separation at the wing shock or at the glove trailing-edge step for the low Reynolds numbers of this test, transition was also fixed on the outer wing panel upper surface, even though the program objectives were to obtain laminar flow in that region at full-scale flight conditions. Two transition configurations for the wing upper surface were investigated for the modified wing panels in the 20° sweep position: (1) transition strip located 0.5 in. rearward of the wing leading edge, and (2) transition strip located at 47 percent of the local chord (measured streamwise). Wing pressure data for the forward transition location indicated the presence of wing trailing-edge flow separation at the 0.8 Mach number cruise condition which was not evident for the aft transition location. This flow separation resulted

from the relatively thicker boundary layer associated with the forward transition location and was not considered to be a realistic simulation of the cruise condition airflow at flight Reynolds numbers. Consequently, all data presented herein were obtained with the aft transition location. For wing sweeps greater than 20° , the transition strip remained in the same physical location on the wing as for the 20° sweep configuration. Transition strips for the baseline wing were also located 0.5 in. aft of the leading edge on the lower surface and at 47 percent of the local chord on the upper surface.

Measurements and Corrections

Aerodynamic forces and moments for the model were measured using an internally mounted six-component strain-gauge balance. Model attitude was set by using a combination of sting support system pitch and roll to achieve the desired angles of attack and sideslip. For runs in which sideslip angles were zero, model angles of attack were measured using a single-axis accelerometer system mounted within the model. For other runs, the model attitude was measured by using model support system pitch and roll indicators, and the resulting angles were corrected for aeroelastic deflection of the support system resulting from aerodynamic loads on the model. The tunnel flow angularity, determined by testing the model in both upright and inverted positions, was negligible for the conditions of this investigation, and no corrections were applied. Balance forces were adjusted to a condition of free-stream static pressure acting over the sting cavity area, but no adjustments were made for internal drag of the flow-through nacelles.

Wing surface pressures for the modified wing panels were measured by using electronically scanned pressure transducer modules located in the nose of the model. The modules were not maintained at a fixed temperature but were calibrated frequently during the testing sequence to compensate for the effects of temperature variation on the sensitivity and bias of the transducers.

The data for this investigation were obtained in a "pitch-pause" mode, with several seconds on test condition to allow the data to stabilize before recording.

The accuracy of the data presented herein, based on the instrumentation accuracy, is estimated to be as follows:

C_N	± 0.011
C_A	± 0.0008
C_m	± 0.005

C_l	± 0.0001
C_n	± 0.001
C_Y	± 0.027
C_p	± 0.009
α	$\pm 0.1^\circ$
β	$\pm 0.1^\circ$
M	+0.001 to -0.005

(Coefficient values are based on a nominal dynamic pressure of 500 lb-ft⁻².)

Presentation of Results

The results of this investigation are presented without analysis. The basic aerodynamic force and moment data are presented in figures 5 through 20. Figures 5 through 8 compare the longitudinal characteristics of the basic (F-14A) and the modified wing configurations. Figures 9 through 12 compare the lateral-directional characteristics of the basic and modified configurations at zero sideslip. Figures 13 through 16 present the lateral-directional characteristics of the basic wing configuration, and figures 17 through 20 present the lateral-directional characteristics of the modified configuration through the full range of sideslip angles tested.

Selected pressure data for angles of attack encompassing the cruise lift coefficients are presented in graphical form in figures 21 through 24 for wing B. Figure 21 presents data for wing B at the 20° sweep configuration for the range of Mach numbers tested between 0.6 and 0.825. Figures 22 through 24 present data for wing B at the remaining sweep angles, but only for the two design Mach numbers of 0.7 and 0.8. The corresponding pressure coefficient data for wing C are presented in figures 25 through 28 in a similar sequence.

Wing pressure coefficient data for the modified wing at all test points relevant to this report are tabulated in a microfiche supplement that is available on request.¹ A run schedule is included here as table V to assist the reader in locating pressure data for specific test conditions within this supplement.

For assistance in locating specific plotted data the reader is referred to table VI, which presents a summary of the data figures organization.

Concluding Remarks

A wind-tunnel investigation has been conducted to evaluate the aerodynamic characteristics and wing

pressure distributions of a variable-wing-sweep aircraft having wing panels that were modified to promote laminar flow. Two modified wing configurations designed to have pressure distributions favorable for laminar flow over the forward half of the upper surface at Mach numbers of 0.7 and 0.8, respectively, were investigated. Modified wing section shapes were incorporated over most of the exposed outer wing panel span and were obtained by extending the leading edge and adding thickness to the existing wing upper surface forward of 60-percent chord. The two different wing configurations were tested on the model simultaneously, with the 0.7 Mach number design on the left side and the 0.8 Mach number design on the right. The investigations were conducted at Mach numbers from 0.20 to 0.90 for wing sweep angles of 20°, 25°, 30°, and 35°. Longitudinal, lateral, and directional aerodynamic characteristics of the modified and baseline configurations, and selected pressure distributions for the modified configurations, are presented in graphical form without analysis. A complete tabulation of the pressure data for the modified configuration is included as a microfiche supplement. Test results indicate that the stability and control characteristics are not significantly altered as a result of the modifications and that the rolling moments resulting from the asymmetric wing configuration were within the prescribed limits at angles of attack below wing stall. Also, comparison of the measured wing pressure distributions with predicted values (not presented) generally showed good agreement.

NASA Langley Research Center
Hampton, VA 23665-5225
June 6, 1989

References

1. Runyan, L. James; Navran, Brent H.; and Rozendaal, Rodger A.: *F-111 Natural Laminar Flow Glove Flight Test Data Analysis and Boundary Layer Stability Analysis*. NASA CR-166051, 1984.
2. Meyer, Robert R.; Trujillo, Bianca M.; and Bartlett, Dennis W.: *F-14 VSTFE and Results of the Cleanup Flight Test Program. Research in Natural Laminar Flow and Laminar-Flow Control*, Jerry N. Hefner and Francis E. Sabo, compilers, NASA CP-2487, Part 3, 1987, pp. 819-844.
3. Rozendaal, R. A.: *Variable-Sweep Transition Flight Experiment (VSTFE)—Stability Code Development and Clean-up Glove Data Analysis. Research in Natural Laminar Flow and Laminar-Flow Control*, Jerry N. Hefner and Frances E. Sabo, compilers, NASA CP-2487, Part 3, 1987, pp. 845-859.

¹ Requests for supplement to NASA TM-4124 should be addressed to NASA Langley Research Center, Transonic Aerodynamics Branch, Mail Stop 294, Hampton, VA 23665-5225.

4. Waggoner, E. G.; Campbell, R. L.; Phillips, P. S.; and Hallissy, J. B.: Design and Test of an NLF Wing Glove for the Variable-Sweep Transition Flight Experiment. *Research in Natural Laminar Flow and Laminar-Flow Control*, Jerry N. Hefner and Frances E. Sabo, compilers, NASA CP-2487, Part 3, 1987, pp. 753-776.
5. Bohn-Meyer, Marta; and Jiran, Fred: Techniques for Modifying Airfoils and Fairings on Aircraft Using Foam and Fiberglass. AIAA-81-2445, Nov. 1981.
6. Waggoner, Edgar G.; Campbell, Richard L.; and Phillips, Pamela S.: Computational Wing Design in Support of an NLF Variable Sweep Transition Flight Experiment. AIAA-85-4074, Oct. 1985.
7. Rozendaal, Rodger A.: *Variable Sweep Transition Flight Experiment (VSTFE)—Parametric Pressure Distribution Boundary Layer Stability Study and Wing Glove Design Task*. NASA CR-3992, 1986.
8. Fuller, Dennis E.: *Guide for Users of the National Transonic Facility*. NASA TM-83124, 1981.
9. Braslow, Albert L.; and Knox, Eugene C.: *Simplified Method for Determination of Critical Height of Distributed Roughness Particles for Boundary-Layer Transition at Mach Numbers From 0 to 5*. NACA TN 4363, 1958.

Table I. Baseline Wing Definition

(a) Span station 7.95; $c_r = 7.904$;

FS at LE = 31.432; ref. WL = 9.996

(b) Span station 10.25; $c_r = 7.176$;

FS at LE = 32.262; ref. WL = 9.946

x_r/c_r	Upper surface z_r/c_r	Lower surface z_r/c_r
0.00000	0.00756	0.00756
.00191	.01357	.00182
.00496	.01710	-.00176
.00995	.02101	-.00548
.02000	.02672	-.01013
.03993	.03485	-.01567
.06000	.04095	-.01922
.08000	.04582	-.02178
.10000	.04983	-.02375
.12000	.05317	-.02532
.14000	.05596	-.02661
.16000	.05827	-.02768
.18000	.06017	-.02857
.20000	.06170	-.02932
.22000	.06291	-.02994
.24000	.06381	-.03046
.26000	.06444	-.03087
.28000	.06482	-.03120
.30000	.06496	-.03144
.32000	.06489	-.03160
.34000	.06462	-.03168
.36000	.06416	-.03169
.38000	.06352	-.03163
.40000	.06271	-.03150
.42000	.06175	-.03130
.44000	.06064	-.03105
.46000	.05938	-.03073
.48000	.05800	-.03036
.50000	.05648	-.02993
.52000	.05485	-.02945
.56000	.05124	-.02834
.60000	.04722	-.02706
.64000	.04284	-.02562
.68000	.03812	-.02405
.70000	.03566	-.02322
.72000	.03313	-.02236
.74000	.03054	-.02148
.76000	.02790	-.02058
.78000	.02521	-.01966
.80000	.02247	-.01872
.82000	.01970	-.01777
.84000	.01689	-.01680
.86000	.01405	-.01582
.88000	.01119	-.01484
.90000	.00830	-.01385
.92000	.00540	-.01285
.94000	.00249	-.01185
.96000	-.00043	-.01085
.98000	-.00335	-.00984
1.00000	-.00628	-.00884

x_r/c_r	Upper surface z_r/c_r	Lower surface z_r/c_r
0.00000	0.00878	0.00878
.00191	.01488	.00324
.00496	.01831	-.00023
.00995	.02205	-.00362
.02000	.02742	-.00778
.03993	.03498	-.01273
.06000	.04063	-.01589
.08000	.04519	-.01819
.10000	.04901	-.01997
.12000	.05226	-.02142
.14000	.05502	-.02263
.16000	.05737	-.02366
.18000	.05934	-.02455
.20000	.06097	-.02534
.22000	.06229	-.02604
.24000	.06331	-.02665
.26000	.06406	-.02720
.28000	.06456	-.02767
.30000	.06481	-.02808
.32000	.06483	-.02843
.34000	.06464	-.02871
.36000	.06424	-.02893
.38000	.06365	-.02909
.40000	.06288	-.02918
.42000	.06193	-.02920
.44000	.06081	-.02917
.46000	.05953	-.02907
.48000	.05811	-.02890
.50000	.05654	-.02868
.52000	.05484	-.02839
.56000	.05107	-.02765
.60000	.04685	-.02668
.64000	.04224	-.02552
.68000	.03730	-.02417
.70000	.03473	-.02343
.72000	.03209	-.02266
.74000	.02939	-.02185
.76000	.02665	-.02100
.78000	.02386	-.02013
.80000	.02103	-.01923
.82000	.01818	-.01831
.84000	.01529	-.01736
.86000	.01239	-.01639
.88000	.00947	-.01541
.90000	.00653	-.01442
.92000	.00359	-.01342
.94000	.00064	-.01241
.96000	-.00231	-.01139
.98000	-.00526	-.01037
1.00000	-.00821	-.00935

Table I. Continued

(c) Span station 12.55; $c_r = 6.441$;
FS at LE = 33.099; ref. WL = 9.880

x_r/c_r	Upper surface z_r/c_r	Lower surface z_r/c_r
0.00000	0.00722	0.00722
.00191	.01327	.00165
.00496	.01657	-.00173
.00995	.02033	-.00503
.02000	.02564	-.00897
.03993	.03300	-.01357
.06000	.03852	-.01650
.08000	.04301	-.01863
.10000	.04682	-.02029
.12000	.05010	-.02164
.14000	.05294	-.02277
.16000	.05540	-.02375
.18000	.05751	-.02461
.20000	.05930	-.02537
.22000	.06078	-.02606
.24000	.06198	-.02668
.26000	.06291	-.02723
.28000	.06359	-.02772
.30000	.06402	-.02816
.32000	.06421	-.02853
.34000	.06419	-.02884
.36000	.06395	-.02909
.38000	.06351	-.02928
.40000	.06287	-.02940
.42000	.06205	-.02945
.44000	.06105	-.02944
.46000	.05989	-.02936
.48000	.05856	-.02921
.50000	.05708	-.02900
.52000	.05546	-.02871
.56000	.05182	-.02795
.60000	.04770	-.02694
.64000	.04317	-.02570
.68000	.03828	-.02424
.70000	.03572	-.02343
.72000	.03310	-.02258
.74000	.03042	-.02168
.76000	.02770	-.02074
.78000	.02492	-.01977
.80000	.02211	-.01876
.82000	.01927	-.01772
.84000	.01640	-.01665
.86000	.01351	-.01556
.88000	.01061	-.01445
.90000	.00770	-.01332
.92000	.00478	-.01217
.94000	.00185	-.01102
.96000	-.00107	-.00986
.98000	-.00400	-.00869
1.00000	-.00692	-.00753

(d) Span station 14.85; $c_r = 5.706$;
FS at LE = 33.936; ref. WL = 9.804

x_r/c_r	Upper surface z_r/c_r	Lower surface z_r/c_r
0.00000	0.00316	0.00316
.00191	.00928	-.00259
.00496	.01260	-.00581
.00995	.01642	-.00904
.02000	.02180	-.01292
.03993	.02928	-.01739
.06000	.03490	-.02019
.08000	.03949	-.02220
.10000	.04341	-.02375
.12000	.04682	-.02501
.14000	.04981	-.02606
.16000	.05243	-.02696
.18000	.05472	-.02775
.20000	.05671	-.02844
.22000	.05840	-.02906
.24000	.05982	-.02962
.26000	.06098	-.03010
.28000	.06189	-.03052
.30000	.06256	-.03088
.32000	.06301	-.03117
.34000	.06323	-.03139
.36000	.06324	-.03155
.38000	.06304	-.03163
.40000	.06265	-.03164
.42000	.06207	-.03158
.44000	.06131	-.03144
.46000	.06038	-.03123
.48000	.05928	-.03094
.50000	.05802	-.03057
.52000	.05662	-.03014
.56000	.05338	-.02905
.60000	.04964	-.02768
.64000	.04545	-.02605
.68000	.04087	-.02418
.70000	.03846	-.02316
.72000	.03598	-.02209
.74000	.03342	-.02097
.76000	.03081	-.01980
.78000	.02815	-.01859
.80000	.02544	-.01734
.82000	.02270	-.01606
.84000	.01992	-.01474
.86000	.01712	-.01340
.88000	.01430	-.01203
.90000	.01146	-.01064
.92000	.00861	-.00923
.94000	.00575	-.00781
.96000	.00290	-.00638
.98000	.00004	-.00494
1.00000	-.00282	-.00350

Table I. Continued

(e) Span station 17.15; $c_r = 4.971$;
FS at LE = 34.774; ref. WL = 9.729

(f) Span station 19.45; $c_r = 4.236$;
FS at LE = 35.611; ref. WL = 9.653

x_r/c_r	Upper surface z_r/c_r	Lower surface z_r/c_r
0.00000	-0.00210	-0.00210
.00191	.00412	-.00787
.00496	.00754	-.01123
.00995	.01134	-.01427
.02000	.01680	-.01799
.03993	.02441	-.02226
.06000	.03016	-.02490
.08000	.03488	-.02674
.10000	.03893	-.02814
.12000	.04249	-.02926
.14000	.04565	-.03019
.16000	.04845	-.03098
.18000	.05094	-.03167
.20000	.05314	-.03227
.22000	.05507	-.03280
.24000	.05675	-.03325
.26000	.05817	-.03363
.28000	.05936	-.03395
.30000	.06032	-.03419
.32000	.06106	-.03436
.34000	.06158	-.03446
.36000	.06189	-.03447
.38000	.06200	-.03441
.40000	.06191	-.03426
.42000	.06164	-.03404
.44000	.06118	-.03373
.46000	.06054	-.03334
.48000	.05974	-.03286
.50000	.05877	-.03230
.52000	.05765	-.03167
.56000	.05496	-.03015
.60000	.05173	-.02833
.64000	.04802	-.02622
.68000	.04388	-.02384
.70000	.04168	-.02256
.72000	.03939	-.02122
.74000	.03702	-.01982
.76000	.03458	-.01837
.78000	.03209	-.01687
.80000	.02954	-.01532
.82000	.02694	-.01374
.84000	.02431	-.01211
.86000	.02164	-.01046
.88000	.01894	-.00877
.90000	.01623	-.00706
.92000	.01349	-.00533
.94000	.01075	-.00358
.96000	.00800	-.00183
.98000	.00525	-.00006
1.00000	.00249	.00171

x_r/c_r	Upper surface z_r/c_r	Lower surface z_r/c_r
0.00000	-0.00919	-0.00919
.00191	-.00300	-.01499
.00496	.00061	-.01831
.00995	.00452	-.02131
.02000	.01008	-.02487
.03993	.01787	-.02883
.06000	.02378	-.03118
.08000	.02965	-.03278
.10000	.03287	-.03396
.12000	.03659	-.03488
.14000	.03993	-.03563
.16000	.04294	-.03626
.18000	.04566	-.03679
.20000	.04810	-.03722
.22000	.05030	-.03758
.24000	.05226	-.03786
.26000	.05399	-.03806
.28000	.05550	-.03818
.30000	.05679	-.03822
.32000	.05788	-.03818
.34000	.05876	-.03805
.36000	.05944	-.03784
.38000	.05992	-.03753
.40000	.06022	-.03715
.42000	.06033	-.03667
.44000	.06026	-.03610
.46000	.06001	-.03545
.48000	.05960	-.03470
.50000	.05902	-.03387
.52000	.05828	-.03296
.56000	.05634	-.03087
.60000	.05384	-.02846
.64000	.05083	-.02573
.68000	.04735	-.02272
.70000	.04545	-.02111
.72000	.04347	-.01943
.74000	.04139	-.01769
.76000	.03923	-.01590
.78000	.03700	-.01404
.80000	.03471	-.01214
.82000	.03235	-.01019
.84000	.02994	-.00820
.86000	.02749	-.00617
.88000	.02500	-.00410
.90000	.02249	-.00201
.92000	.01994	.00011
.94000	.01738	.00225
.96000	.01481	.00440
.98000	.01223	.00656
1.00000	.00965	.00873

Table I. Concluded

(g) Span station 21.75; $c_r = 3.501$;
FS at LE = 38.448; ref. WL = 9.578

x_r/c_r	Upper surface z_r/c_r	Lower surface z_r/c_r
0.00000	−0.01912	−0.01912
.00191	−.01295	−.02525
.00496	−.00937	−.02851
.00995	−.00540	−.03139
.02000	.00037	−.03470
.03993	.00844	−.03816
.06000	.01456	−.04002
.08000	.01963	−.04117
.10000	.02404	−.04195
.12000	.02796	−.04251
.14000	.03151	−.04293
.16000	.03474	−.04322
.18000	.03771	−.04342
.20000	.04043	−.04353
.22000	.04293	−.04354
.24000	.04521	−.04347
.26000	.04729	−.04332
.28000	.04917	−.04308
.30000	.05085	−.04275
.32000	.05235	−.04234
.34000	.05366	−.04184
.36000	.05479	−.04125
.38000	.05574	−.04058
.40000	.05652	−.03982
.42000	.05712	−.03897
.44000	.05755	−.03803
.46000	.05781	−.03700
.48000	.05791	−.03588
.50000	.05785	−.03468
.52000	.05764	−.03339
.56000	.05676	−.03054
.60000	.05531	−.02735
.64000	.05333	−.02385
.68000	.05087	−.02003
.70000	.04947	−.01801
.72000	.04796	−.01592
.74000	.04635	−.01376
.76000	.04466	−.01154
.78000	.04287	−.00926
.80000	.04101	−.00692
.82000	.03908	−.00452
.84000	.03708	−.00208
.86000	.03503	.00040
.88000	.03292	.00292
.90000	.03078	.00548
.92000	.02860	.00806
.94000	.02639	.01067
.96000	.02416	.01329
.98000	.02192	.01592
1.00000	.01968	.01856

(h) Span station 24.04; $c_r = 2.766$;
FS at LE = 37.285; ref. WL = 9.503

x_r/c_r	Upper surface z_r/c_r	Lower surface z_r/c_r
0.00000	−0.03451	−0.03451
.00191	−.02816	−.04097
.00496	−.02443	−.04400
.00995	−.02028	−.04663
.02000	−.01435	−.04935
.03993	−.00591	−.05135
.06000	.00053	−.05167
.08000	.00587	−.05149
.10000	.01053	−.05115
.12000	.01470	−.05076
.14000	.01850	−.05036
.16000	.02200	−.04995
.18000	.02525	−.04951
.20000	.02827	−.04903
.22000	.03109	−.04851
.24000	.03373	−.04793
.26000	.03618	−.04729
.28000	.03847	−.04658
.30000	.04060	−.04580
.32000	.04256	−.04495
.34000	.04437	−.04401
.36000	.04602	−.04299
.38000	.04752	−.04187
.40000	.04887	−.04067
.42000	.05007	−.03938
.44000	.05112	−.03799
.46000	.05202	−.03650
.48000	.05278	−.03492
.50000	.05340	−.03324
.52000	.05388	−.03147
.56000	.05444	−.02763
.60000	.05449	−.02341
.64000	.05405	−.01884
.68000	.05317	−.01392
.70000	.05257	−.01135
.72000	.05187	−.00869
.74000	.05107	−.00597
.76000	.05019	−.00317
.78000	.04923	−.00031
.80000	.04820	.00261
.82000	.04709	.00558
.84000	.04592	.00859
.86000	.04470	.01166
.88000	.04343	.01475
.90000	.04212	.01788
.92000	.04078	.02104
.94000	.03941	.02421
.96000	.03802	.02740
.98000	.03662	.03060
1.00000	.03521	.03380

Table II. Wing B Glove Definition

(a) Span station 8.13; $c_r = 7.855$;
FS at LE = 31.488; ref. WL = 9.992

(b) Span station 10.25; $c_r = 7.176$;
FS at LE = 32.262; ref. WL = 9.946

Upper surface	
x_r/c_r	z_r/c_r
-0.01591	0.00768
-.01397	.01289
-.01087	.01752
-.00580	.02226
.00441	.02868
.02466	.03700
.04504	.04302
.06536	.04785
.08568	.05190
.10600	.05538
.12632	.05840
.14664	.06104
.16695	.06334
.18727	.06534
.20759	.06708
.22791	.06856
.24823	.06981
.26854	.07082
.28886	.07162
.30918	.07222
.32950	.07259
.34982	.07276
.37014	.07273
.39045	.07246
.41077	.07195
.43109	.07114
.45141	.07008
.47173	.06871
.49205	.06705
.51236	.06511
.55300	.06031
.59364	.05436
Lower surface	
-0.01591	0.00768
-.01397	.00243
-.01087	-.00090
-.00580	-.00405
.00441	-.00826
.02466	-.01355
.04504	-.01724
.06536	-.02008
.08568	-.02236

Upper surface	
x_r/c_r	z_r/c_r
-0.01742	0.00686
-.01548	.01208
-.01237	.01672
-.00730	.02146
.00293	.02789
.02321	.03622
.04363	.04225
.06397	.04709
.08432	.05115
.10467	.05463
.12502	.05766
.14537	.06029
.16572	.06260
.18606	.06461
.20641	.06635
.22676	.06783
.24711	.06908
.26746	.07009
.28781	.07089
.30815	.07149
.32850	.07186
.34885	.07203
.36920	.07200
.38955	.07174
.40990	.07122
.43024	.07042
.45059	.06935
.47094	.06797
.49129	.06632
.51164	.06437
.55234	.05957
.59303	.05361
Lower surface	
-0.01742	0.00686
-.01548	.00170
-.01237	-.00156
-.00730	-.00440
.00293	-.00816
.02321	-.01236
.04363	-.01513
.06397	-.01721
.08432	-.01892

Table II. Continued

(c) Span station 12.55; $c_r = 6.441$;
FS at LE = 33.099; ref. WL = 9.879

Upper surface	
x_r/c_r	z_r/c_r
-0.01941	0.00513
-.01746	.00943
-.01435	.01352
-.00927	.01816
.00098	.02472
.02130	.03346
.04175	.03973
.06214	.04476
.08253	.04902
.10292	.05269
.12331	.05590
.14370	.05875
.16408	.06126
.18447	.06348
.20486	.06544
.22525	.06714
.24564	.06861
.26602	.06985
.28641	.07086
.30680	.07163
.32719	.07218
.34758	.07250
.36797	.07260
.38835	.07246
.40874	.07206
.42913	.07142
.44952	.07051
.46991	.06933
.49030	.06787
.51068	.06613
.55146	.06178
.59224	.05626
Lower surface	
x_r/c_r	z_r/c_r
-0.01941	0.00513
-.01746	.00055
-.01435	-.00248
-.00927	-.00490
.00098	-.00837
.02130	-.01272
.04175	-.01550
.06214	-.01741
.08253	-.01901

(d) Span station 17.15; $c_r = 4.971$;
FS at LE = 34.774; ref. WL = 9.729

Upper surface	
x_r/c_r	z_r/c_r
-0.02515	-0.00295
-.02319	.00109
-.02007	.00440
-.01495	.00860
-.00465	.01501
.01578	.02436
.03636	.03121
.05686	.03670
.07737	.04138
.09787	.04544
.11837	.04904
.13887	.05226
.15938	.05513
.17988	.05771
.20038	.06002
.22089	.06208
.24139	.06390
.26189	.06547
.28240	.06681
.30290	.06791
.32340	.06879
.34390	.06942
.36441	.06983
.38491	.07001
.40541	.06992
.42592	.06957
.44642	.06895
.46692	.06806
.48743	.06690
.50793	.06550
.54893	.06202
.58994	.05777
Lower surface	
x_r/c_r	z_r/c_r
-0.02515	-0.00295
-.02319	-.00785
-.02007	-.01138
-.01495	-.01428
-.00465	-.01796
.01578	-.02246
.03636	-.02505
.05686	-.02664
.07737	-.02782
.09787	-.02882

Table II. Concluded

(e) Span station 21.75; $c_r = 3.501$;
FS at LE = 36.448; ref. WL = 9.578

Upper surface	
x_r/c_r	z_r/c_r
-0.03570	-0.02208
-.03372	-.01551
-.03056	-.01070
-.02539	-.00568
-.01499	.00121
.00566	.01037
.02644	.01739
.04716	.02331
.06787	.02850
.08858	.03314
.10930	.03732
.13001	.04113
.15073	.04463
.17144	.04788
.19215	.05088
.21287	.05367
.23358	.05623
.25430	.05858
.27501	.06071
.29572	.06264
.31644	.06436
.33715	.06585
.35787	.06713
.37858	.06819
.39929	.06901
.42001	.06958
.44072	.06988
.46144	.06991
.48215	.06965
.50286	.06909
.54429	.06712
.58572	.06410
Lower surface	
-0.03570	-0.02208
-.03372	-.02911
-.03056	-.03221
-.02539	-.03464
-.01499	-.03753
.00566	-.04021
.02644	-.04150
.04716	-.04205
.06787	-.04249
.08858	-.04285

Table III. Wing C Glove Definition

(a) Span station 8.13; $c_r = 7.855$;
FS at LE = 31.488; ref. WL = 9.992

Upper surface	
x_r/c_r	z_r/c_r
-0.01000	0.01265
-.00828	.01975
-.00377	.02599
.00281	.03137
.01450	.03761
.03622	.04538
.05735	.05067
.07804	.05463
.09854	.05774
.11891	.06025
.13919	.06226
.15940	.06385
.17956	.06517
.19969	.06619
.21978	.06696
.23985	.06753
.25991	.06791
.27996	.06812
.29999	.06816
.32003	.06805
.34006	.06774
.36008	.06722
.38011	.06649
.40013	.06559
.42014	.06447
.44015	.06320
.46015	.06174
.48015	.06013
.50015	.05837
.52014	.05648
.56010	.05229
.57009	.05113
.58007	.04992
.59000	.04823
Lower surface	
x_r/c_r	z_r/c_r
-0.01000	0.01265
-.00907	.00751
-.00254	-.00071
.00270	-.00392
.00901	-.00684
.01970	-.01071
.03987	-.01570
.05999	-.01903
.08000	-.02151
.10000	-.02347

(b) Span station 10.25; $c_r = 7.176$;
FS at LE = 32.262; ref. WL = 9.946

Upper surface	
x_r/c_r	z_r/c_r
-0.01000	0.01378
-.00824	.02105
-.00363	.02725
.00303	.03248
.01475	.03839
.03644	.04559
.05751	.05044
.07814	.05410
.09858	.05702
.11892	.05944
.13918	.06142
.15939	.06304
.17954	.06442
.19966	.06552
.21976	.06640
.23983	.06708
.25989	.06757
.27994	.06788
.29998	.06802
.32001	.06799
.34005	.06776
.36008	.06729
.38010	.06661
.40012	.06575
.42014	.06464
.44015	.06336
.46016	.06188
.48016	.06024
.50015	.05843
.52014	.05648
.56011	.05216
.57010	.05098
.58008	.04978
.59003	.04820
Lower surface	
x_r/c_r	z_r/c_r
-0.01000	0.01378
-.00907	.00852
-.00258	.00051
.00271	-.00262
.00904	-.00512
.01971	-.00859
.03988	-.01299
.05999	-.01595
.08000	-.01819
.10000	-.01997

Table III. Continued

(c) Span station 12.55; $c_r = 6.441$;
FS at LE = 33.099; ref. WL = 9.879

Upper surface	
x_r/c_r	z_r/c_r
-0.01000	0.01222
-.00815	.01958
-.00354	.02558
.00303	.03076
.01482	.03665
.03651	.04365
.05755	.04835
.07815	.05193
.09858	.05484
.11890	.05729
.13915	.05934
.15935	.06107
.17950	.06259
.19963	.06385
.21972	.06489
.23980	.06575
.25986	.06642
.27991	.06691
.29995	.06723
.31999	.06739
.34002	.06738
.36006	.06720
.38009	.06684
.40013	.06630
.42016	.06556
.44019	.06461
.46023	.06351
.48026	.06223
.50029	.06078
.52031	.05912
.56033	.05517
.57033	.05407
.58031	.05285
.59000	.04877
Lower surface	
-0.01000	0.12222
-.00907	.00700
-.00254	-.00111
.00273	-.00416
.00906	-.00664
.01972	-.00980
.03988	-.01384
.05999	-.01657
.08000	-.01863
.10000	-.02029

(d) Span station 14.85; $c_r = 5.706$;
FS at LE = 33.936; ref. WL = 9.804

Upper surface	
x_r/c_r	z_r/c_r
-0.01000	0.00816
-.00817	.01557
-.00359	.02157
.00296	.02680
.01476	.03278
.03646	.03990
.05750	.04471
.07811	.04839
.09853	.05141
.11885	.05399
.13911	.05619
.15931	.05809
.17946	.05979
.19958	.06125
.21968	.06250
.23976	.06358
.25982	.06448
.27987	.06520
.29991	.06577
.31995	.06619
.33998	.06642
.36002	.06649
.38005	.06638
.40008	.06608
.42012	.06558
.44015	.06488
.46018	.06400
.48022	.06295
.50025	.06173
.52027	.06208
.56029	.05673
.57029	.05573
.58028	.05452
.59000	.05062
Lower surface	
-0.01000	0.00816
-.00907	.00299
-.00242	-.00537
.00279	-.00826
.00907	-.01065
.01973	-.01375
.03988	-.01766
.05999	-.02026
.08000	-.02220
.10000	-.02375

Table III. Continued

(e) Span station 17.15; $c_r = 4.971$;
FS at LE = 34.774; ref. WL = 9.729

Upper surface	
x_r/c_r	z_r/c_r
-0.01000	0.00290
-.00825	.01031
-.00366	.01646
.00295	.02172
.01470	.02774
.03640	.03500
.05745	.03994
.07806	.04376
.09848	.04690
.11880	.04963
.13905	.05201
.15925	.05409
.17941	.05599
.19953	.05766
.21963	.05916
.23971	.06050
.25977	.06166
.27982	.06267
.29986	.06353
.31990	.06424
.33993	.06477
.35997	.06514
.38000	.06534
.40003	.06534
.42006	.06515
.44010	.06475
.46013	.06416
.48016	.06341
.50019	.06248
.52022	.06132
.56025	.05831
.57025	.05744
.58023	.05624
.59000	.05258
Lower surface	
-0.01000	0.00290
-.00907	-.00230
-.00246	-.01058
.00282	-.01365
.00911	-.01590
.01974	-.01882
.03988	-.02253
.05999	-.02497
.08000	-.02674
.10000	-.02814

(f) Span station 19.45; $c_r = 4.236$;
FS at LE = 35.611; ref. WL = 9.653

Upper surface	
x_r/c_r	z_r/c_r
-0.01000	0.00290
-.00825	.01031
-.00366	.01646
.00295	.02172
.01470	.02774
.03640	.03500
.05745	.03994
.07806	.04376
.09848	.04690
.11880	.04963
.13905	.05201
.15925	.05409
.17941	.05599
.19953	.05766
.21963	.05916
.23971	.06050
.25977	.06166
.27982	.06267
.29986	.06353
.31990	.06424
.33993	.06477
.35997	.06514
.38000	.06534
.40003	.06534
.42006	.06515
.44010	.06475
.46013	.06416
.48016	.06341
.50019	.06248
.52022	.06132
.56025	.05831
.57025	.05744
.58023	.05624
.59000	.05258
Lower surface	
-0.01000	0.00290
-.00907	-.00230
-.00246	-.01058
.00282	-.01365
.00911	-.01590
.01974	-.01882
.03988	-.02253
.05999	-.02497
.08000	-.02674
.10000	-.02814

Table III. Concluded

(g) Span station 21.75; $c_r = 3.501$;
 FS at LE = 36.448; ref. WL = 9.578

Upper surface	
x_r/c_r	z_r/c_r
-0.01000	-0.01212
-.00845	-.00686
-.00464	.00016
.00167	.00631
.01312	.01379
.03493	.02258
.05613	.02845
.07683	.03302
.09734	.03680
.11774	.04006
.13806	.04295
.15833	.04553
.17855	.04788
.19875	.05004
.21892	.05200
.23906	.05379
.25919	.05542
.27931	.05690
.29941	.05824
.31950	.05943
.33958	.06047
.35966	.06138
.37972	.06214
.39978	.06276
.41984	.06319
.43990	.06345
.45995	.06351
.47999	.06339
.50004	.06309
.52007	.06260
.56010	.06110
.57014	.06069
.58014	.05959
.59000	.05572
Lower surface	
-0.01000	-0.01212
-.00826	-.01914
-.00124	-.02725
.00365	-.03002
.00955	-.03222
.01992	-.03497
.03993	-.03816
.06000	-.04002
.08000	-.04117
.10000	-.04195

Table IV. Orifice Locations

(a) Wing B

$\eta = 0.522$ $c = 6.57$ in.		$\eta = 0.676$ $c = 5.38$ in.		$\eta = 0.832$ $c = 4.21$ in.	
Orifice	x/c	Orifice	x/c	Orifice	x/c
1	0.010	21	0.011	41	0.010
2	.025	22	.025	42	.025
3	.050	23	.050	43	.050
4	.075	24	.074	44	.075
5	.100	25	.099	45	.100
6	.150	26	.150	46	.151
7	.200	27	.200	47	.200
8	.250	28	.250	48	.251
9	.300	29	.300	49	.301
10	.350	30	.349	50	.350
11	.400	31	.399	51	.402
12	.450	32	.450	52	.451
13	.499	33	.499	53	.501
14	.550	34	.549	54	.552
15	.601	35	.598	55	.602
16	.699	36	.698	56	.702
17	.799	37	.798	57	.803
18	.900	38	.898	58	.902
19	.949	39	.948	59	.953
20	.026	40	.026	60	.026

(b) Wing C

$\eta = 0.522$ $c = 6.51$ in.		$\eta = 0.676$ $c = 5.32$ in.		$\eta = 0.832$ $c = 4.15$ in.	
Orifice	x/c	Orifice	x/c	Orifice	x/c
101	0.011	121	0.013	141	0.010
102	.025	122	.025	142	.025
103	.048	123	.050	143	.051
104	.074	124	.076	144	.076
105	.099	125	.100	145	.101
106	.140	126	.144	146	.150
107	.200	127	.198	147	.202
108	.250	128	.250	148	.252
109	.300	129	.299	149	.303
110	.350	130	.349	150	.352
111	.401	131	.400	151	.402
112	.450	132	.450	152	.452
113	.500	133	.500	153	.503
114	.551	134	.550	154	.553
115	.601	135	.600	155	.604
116	.700	136	.701	156	.704
117	.800	137	.800	157	.804
118	.905	138	.901	158	.905
119	.950	139	.950	159	.956
120	.026	140	.026	160	.025

Table V. Run Schedule for Pressure Data in Microfiche Supplement

(a) $\Lambda = 20.0^\circ$; Transition = $0.47c$

Mach number	Run number for—						
	$\beta = -10.0^\circ$	$\beta = -7.5^\circ$	$\beta = -5.0^\circ$	$\beta = 0.0^\circ$	$\beta = 5.0^\circ$	$\beta = 7.5^\circ$	$\beta = 10.0^\circ$
0.200	25	43, 44	20	2	19	42, 46	24
.600		48	29	10	28	49	
.675			31	9	30		
.700			23	3	22		
.725			33	8	32		
.750		50	35	7	34	51	
.775			37	6, 18	36		
.800			27	4	26		
.825			39	5	38		
.850							
.875							
.900							

(b) $\Lambda = 20.0^\circ$; Transition = 0.5 in.

Mach number	Run number for—		
	$\beta = -5.0^\circ$	$\beta = 0.0^\circ$	$\beta = 5.0^\circ$
0.200	17	12	16
.600		13	
.675			
.700		14	
.725			
.750			
.775			
.800		15	
.825			
.850			
.875			
.900			

(c) $\Lambda = 25.0^\circ$; Transition = $0.47c$

Mach number	Run number for—		
	$\beta = -5.0^\circ$	$\beta = 0.0^\circ$	$\beta = 5.0^\circ$
0.200		99	
.600	101	100	102
.675		103	
.700	106	104	105
.725		107	
.750	110	108	109
.775		111	
.800	113	112	114
.825		115	
.850		116	
.875		117	
.900			

Table V. Concluded

(d) $\Lambda = 30.0^\circ$; Transition = $0.47c$

Mach number	Run number for—		
	$\beta = -5.0^\circ$	$\beta = 0.0^\circ$	$\beta = 5.0^\circ$
0.200	72	54	71
.600		52	
.675		55	
.700	62	56	61
.725		57	
.750		58	
.775		59	
.800	64	60	63
.825		67	
.850	66	68	65
.875		69	
.900		70	73

(e) $\Lambda = 35.0^\circ$; Transition = $0.47c$

Mach number	Run number for—		
	$\beta = -5.0^\circ$	$\beta = 0.0^\circ$	$\beta = 5.0^\circ$
0.200	77	76	78
.600		79	
.675		80	
.700	82	81	83
.725		84	
.750		85	
.775		86	
.800	88	87	89
.825		90	
.850	92	91	93
.875		94	
.900	96	95	97

Table VI. Graphical Data Summary

Figure content	Wing sweep, deg	Figure number
Longitudinal aerodynamic characteristics of the baseline and modified wing configurations.	20	5
	25	6
	30	7
	35	8
Lateral-directional aerodynamic characteristics of the baseline and modified wing configurations with $\beta = 0^\circ$.	20	9
	25	10
	30	11
	35	12
Lateral-directional aerodynamic characteristics of the baseline wing configuration for a range of sideslip angles.	20	13
	25	14
	30	15
	35	16
Lateral-directional aerodynamic characteristics of the modified wing configuration for a range of sideslip angles.	20	17
	25	18
	30	19
	35	20
Selected pressure coefficient data for wing B. $M = 0.6$ through 0.8 .	20	21
Selected pressure coefficient data for wing B. $M = 0.7$ and 0.8 .	25	22
Selected pressure coefficient data for wing B. $M = 0.7$ and 0.8 .	30	23
Selected pressure coefficient data for wing B. $M = 0.7$ and 0.8 .	35	24
Selected pressure coefficient data for wing C. $M = 0.6$ through 0.8 .	20	25
Selected pressure coefficient data for wing C. $M = 0.7$ and 0.8 .	25	26
Selected pressure coefficient data for wing C. $M = 0.7$ and 0.8 .	30	27
Selected pressure coefficient data for wing C. $M = 0.7$ and 0.8 .	35	28

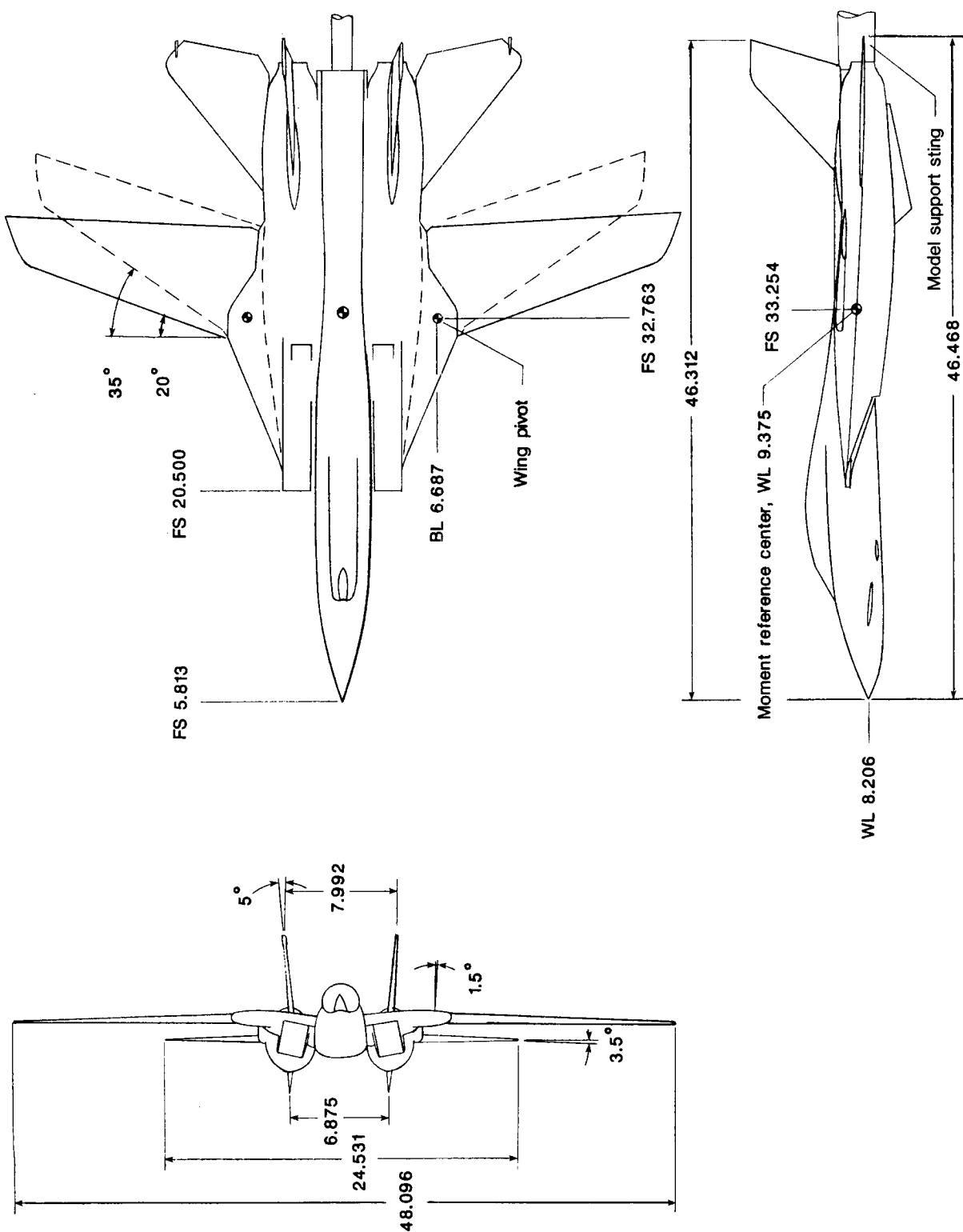
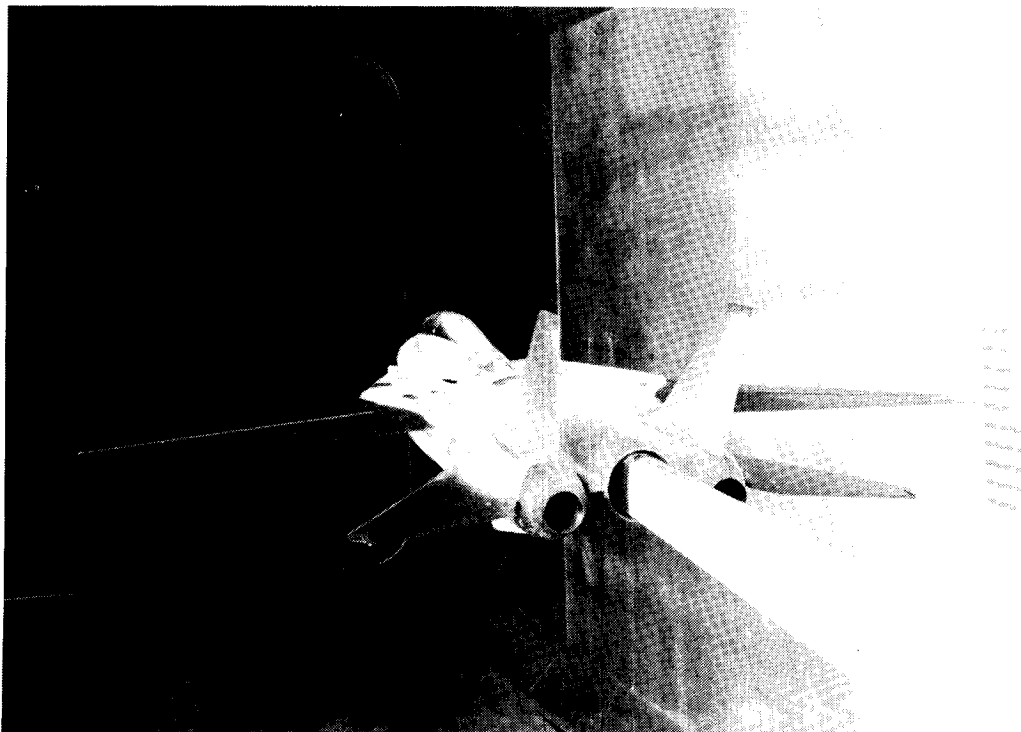
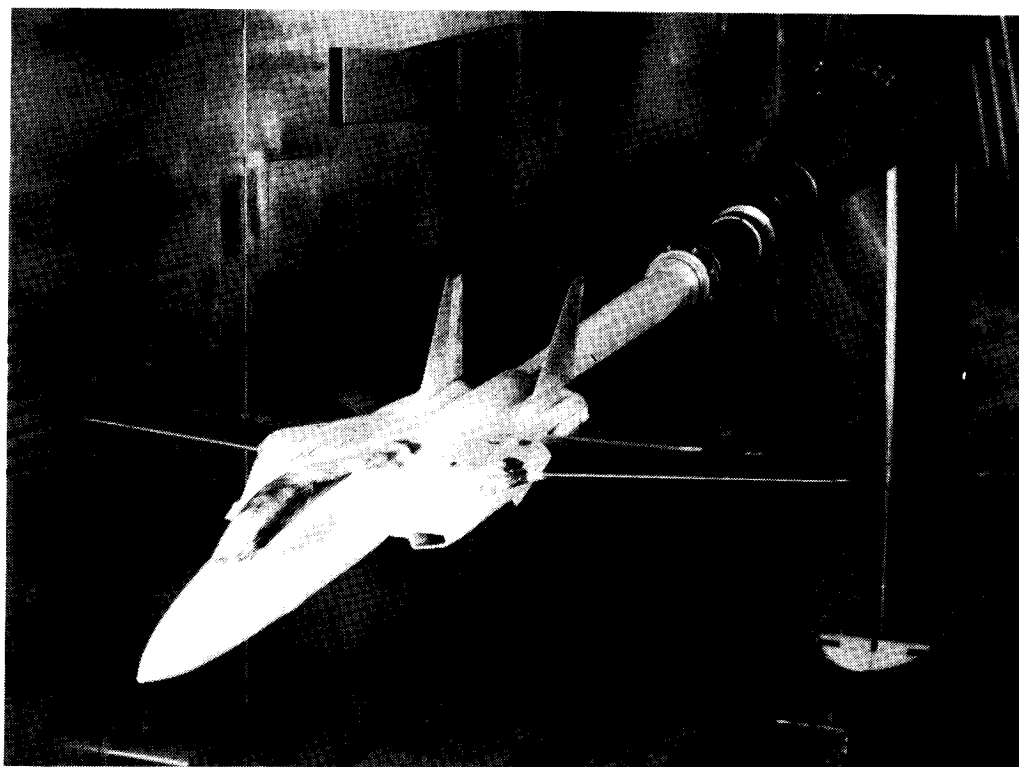


Figure 1. General arrangement of the 1/16-scale model. All dimensions in inches unless otherwise noted.

ORIGINAL PAGE
BLACK AND WHITE PHOTOGRAPH

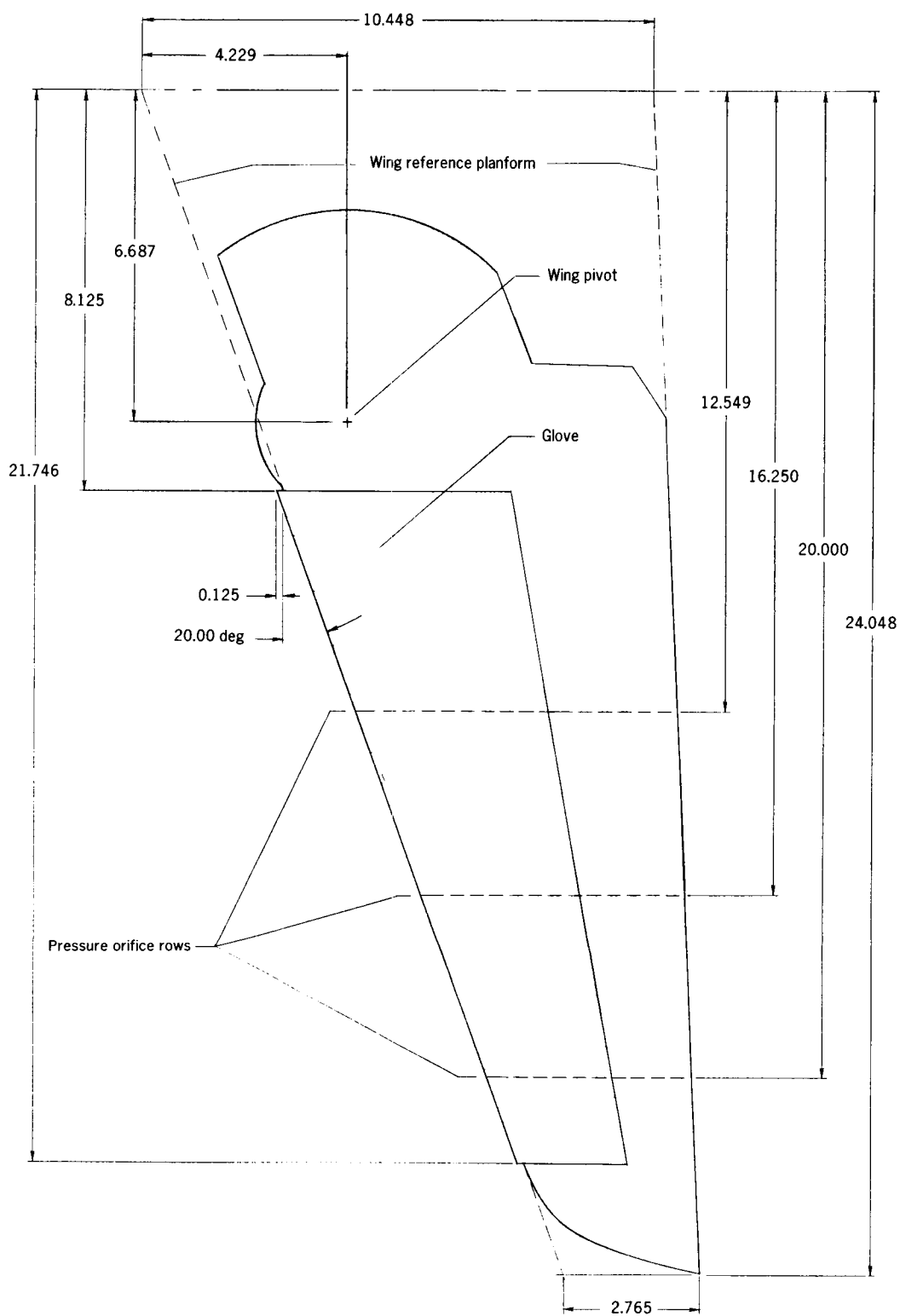


L-85-14,126



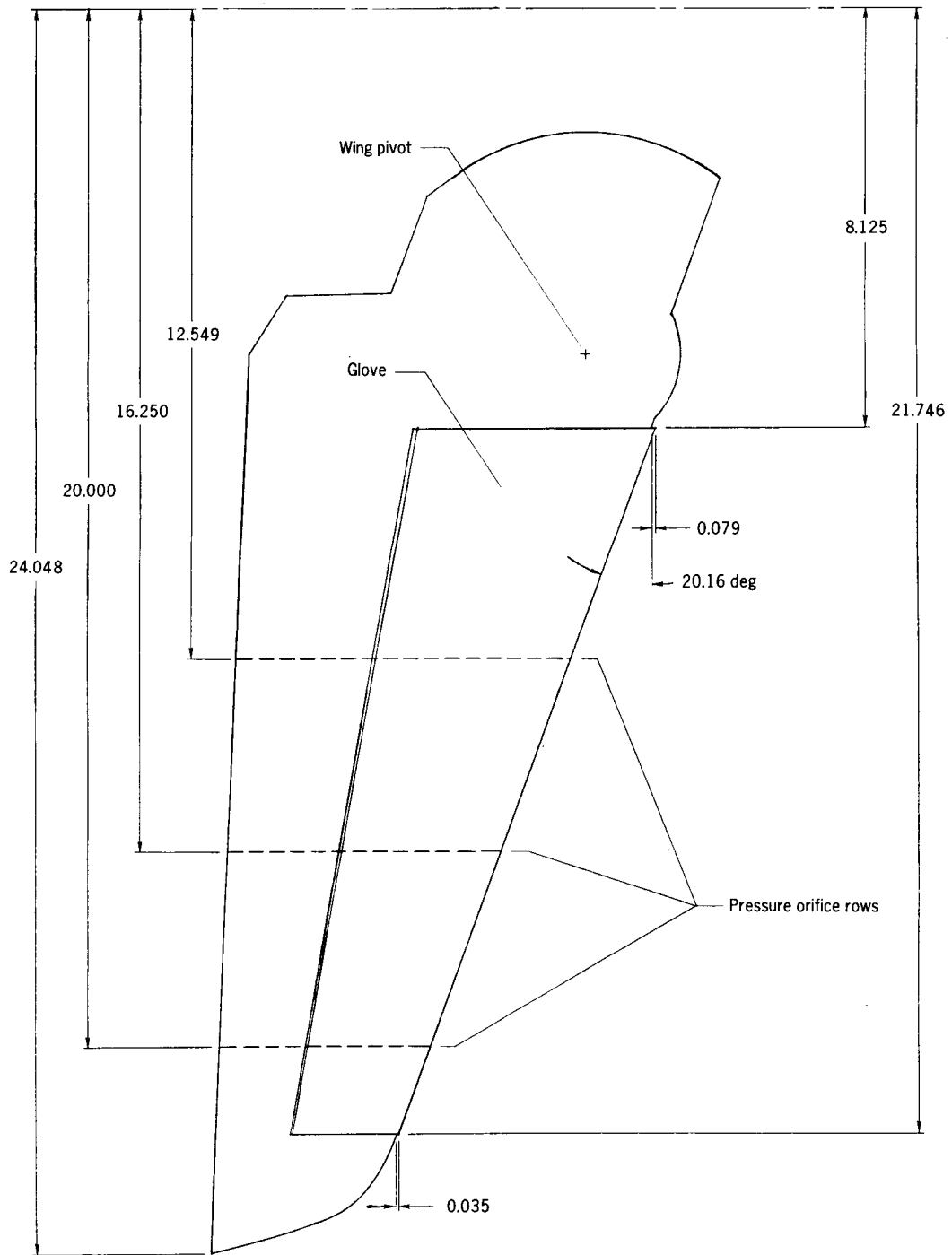
L-85-14,119

Figure 2. Model mounted in NTF.



(a) Wing B.

Figure 3. Model wing planform details. Dimensions in inches unless otherwise noted.



(b) Wing C.

Figure 3. Concluded.

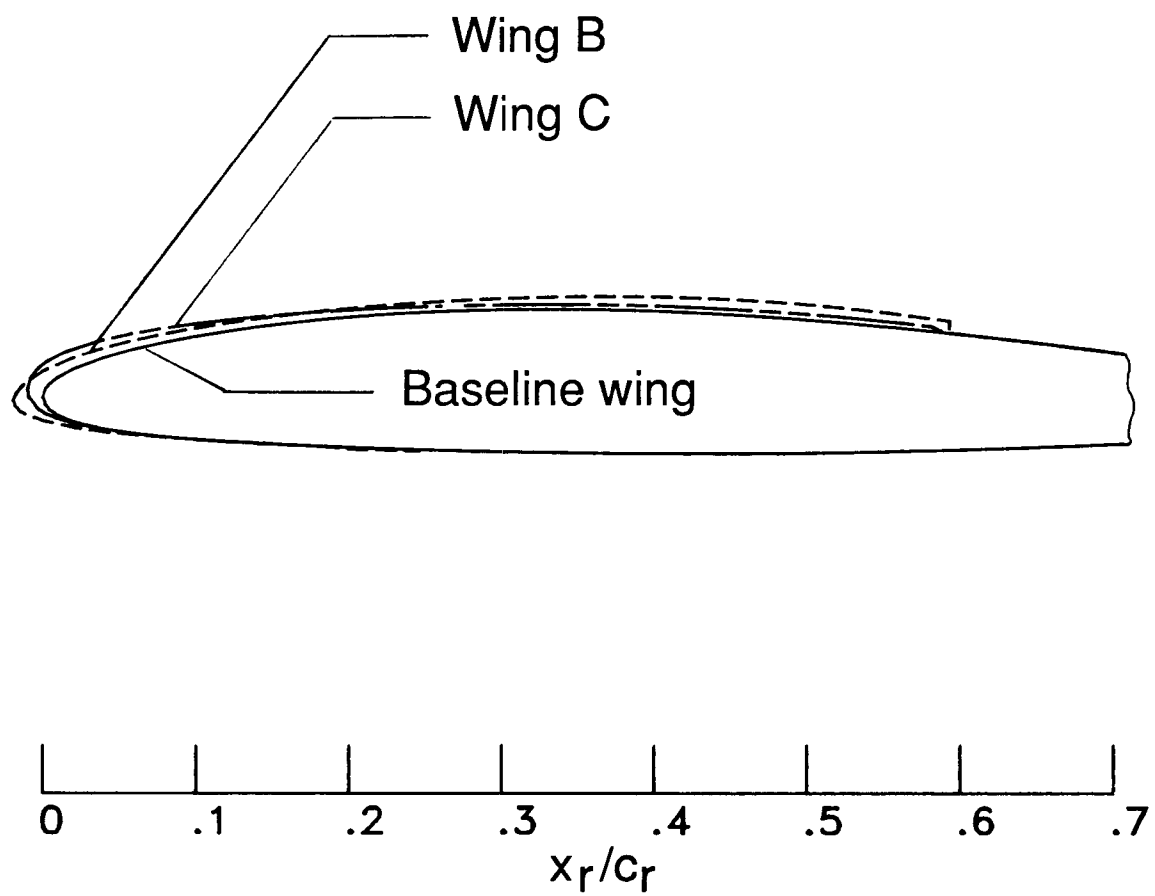
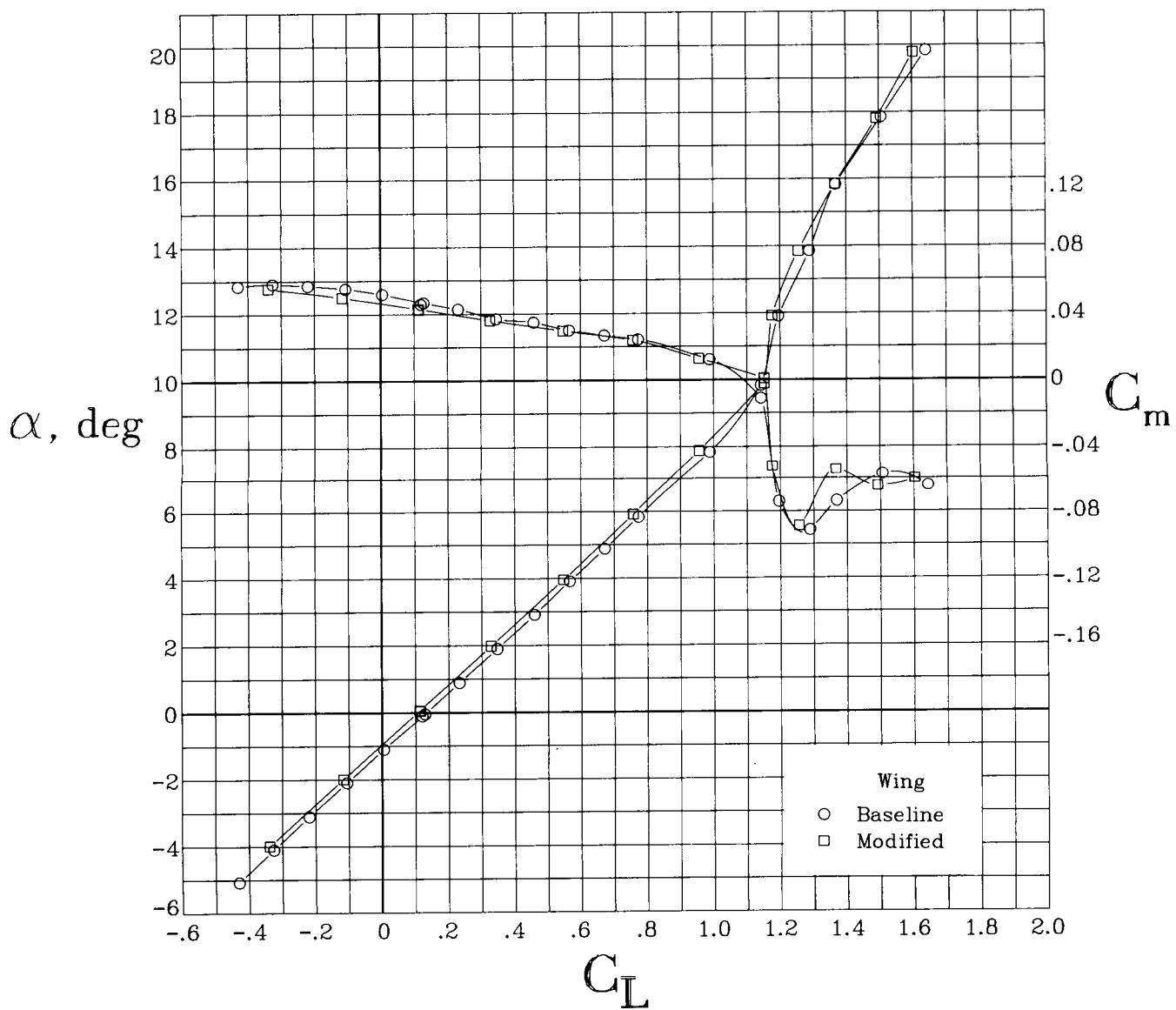
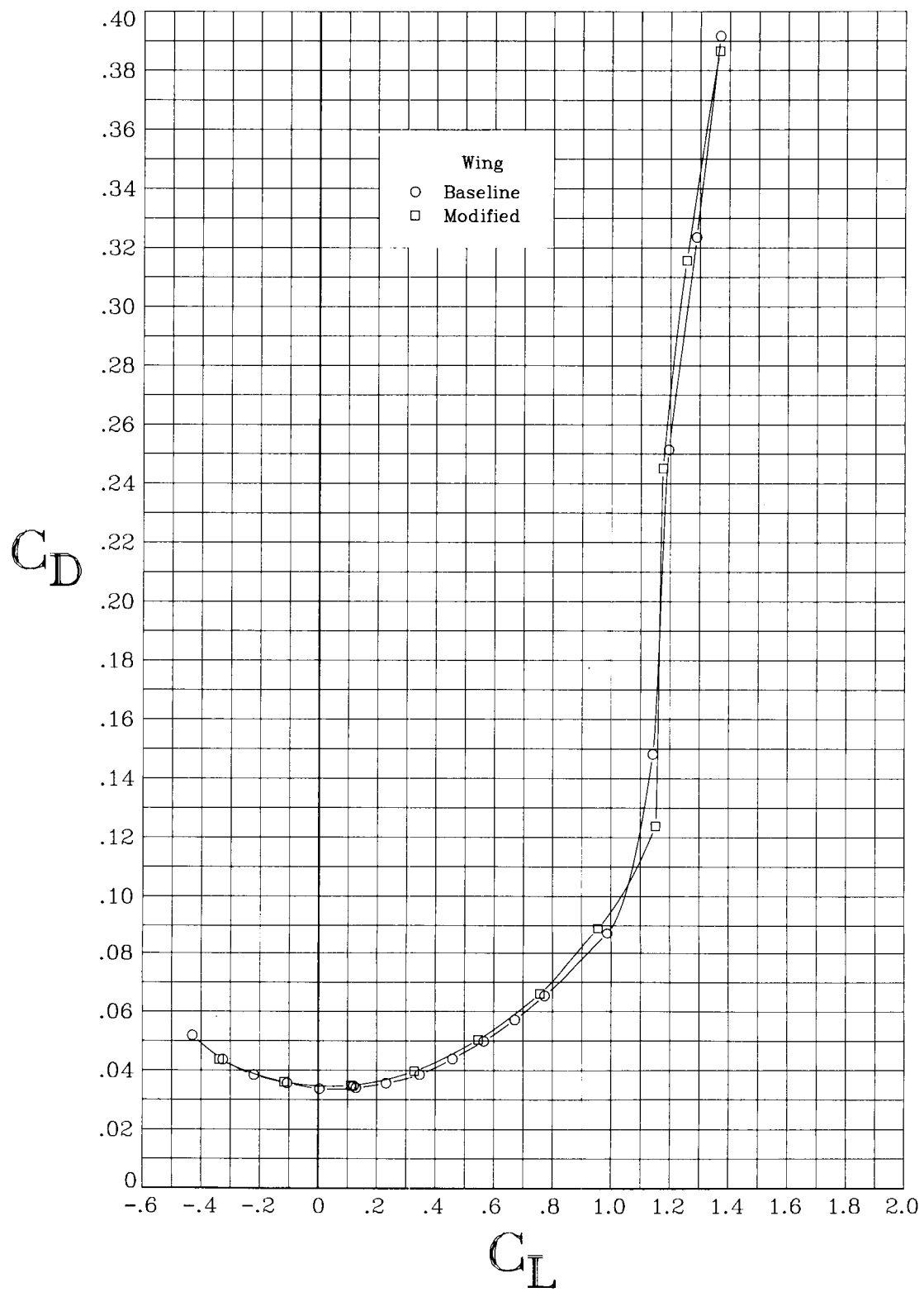


Figure 4. Comparison of glove section shapes for wings B and C.



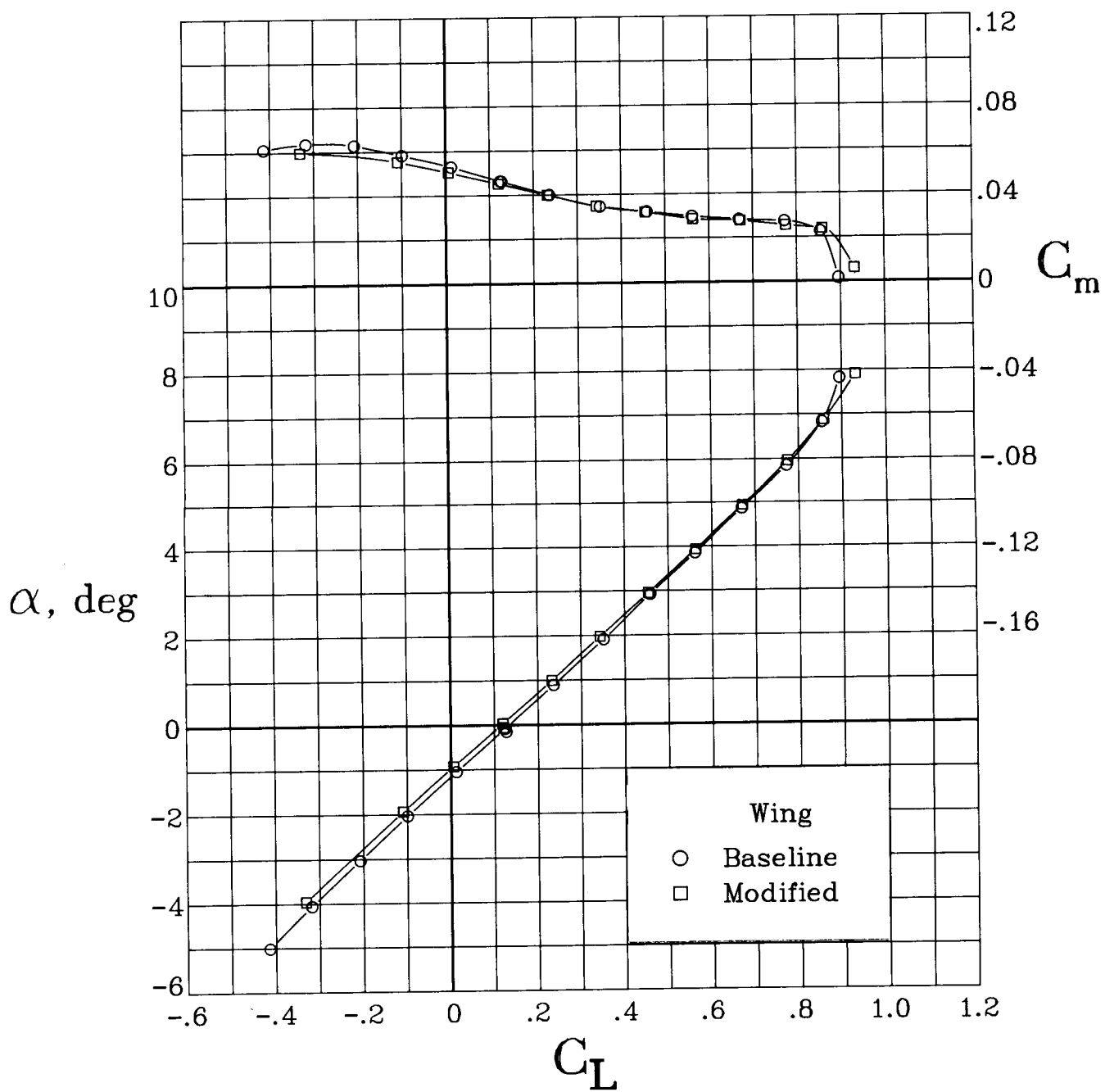
(a) $M = 0.20$.

Figure 5. Longitudinal aerodynamic characteristics of the baseline and modified wing configurations, with wings swept 20° . $\beta = 0^\circ$.



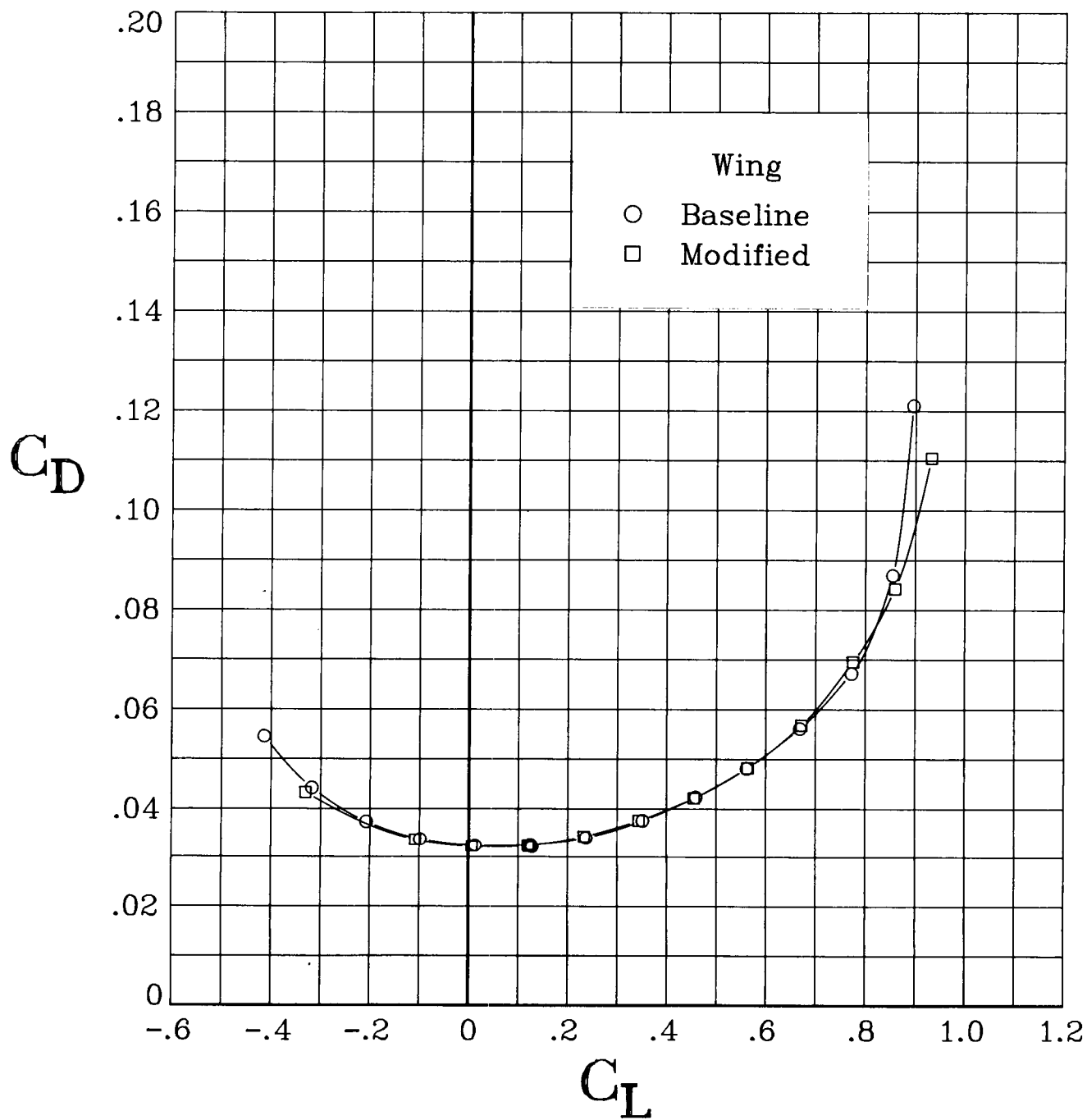
(a) Concluded.

Figure 5. Continued.



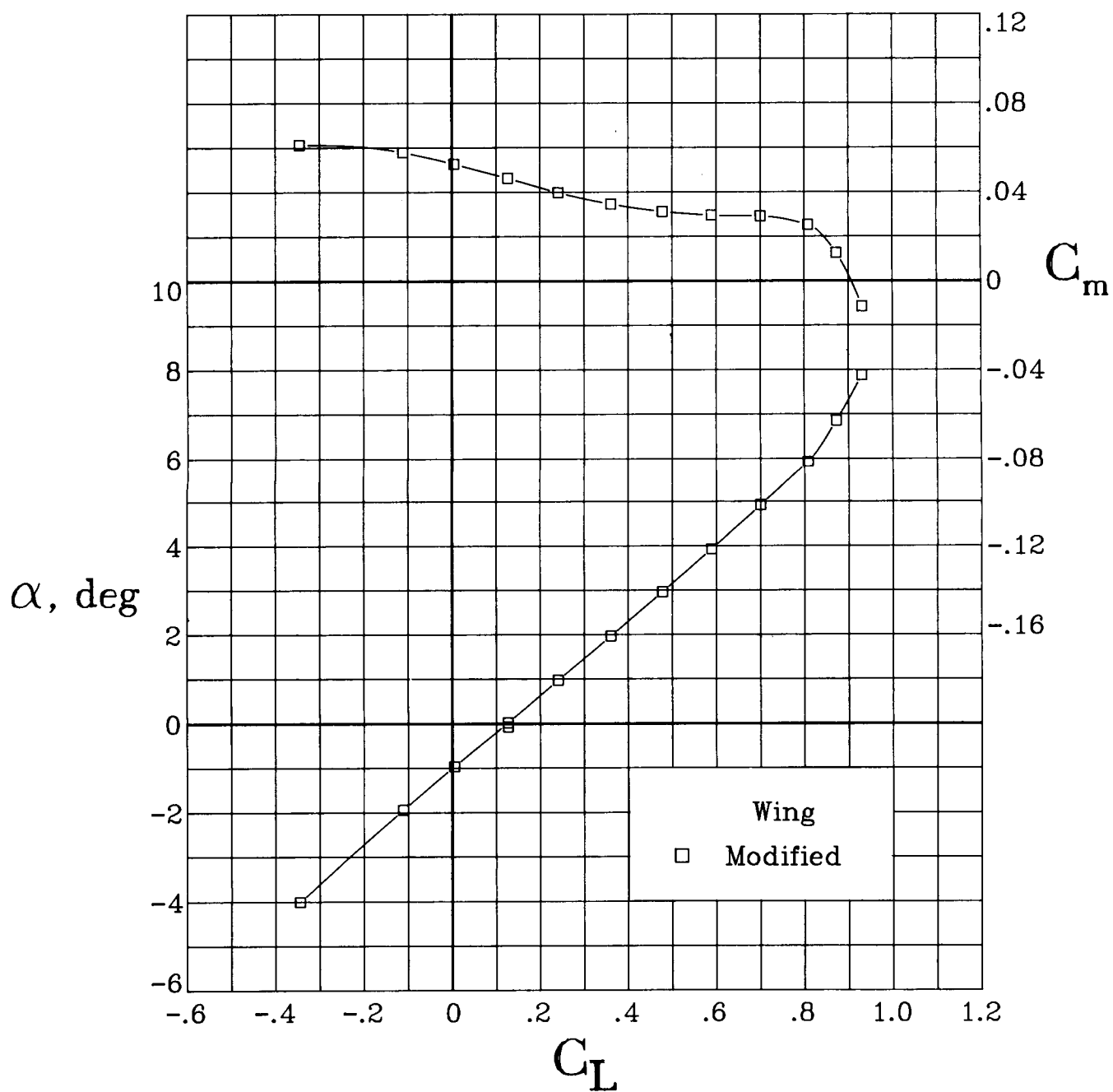
(b) $M = 0.60$.

Figure 5. Continued.



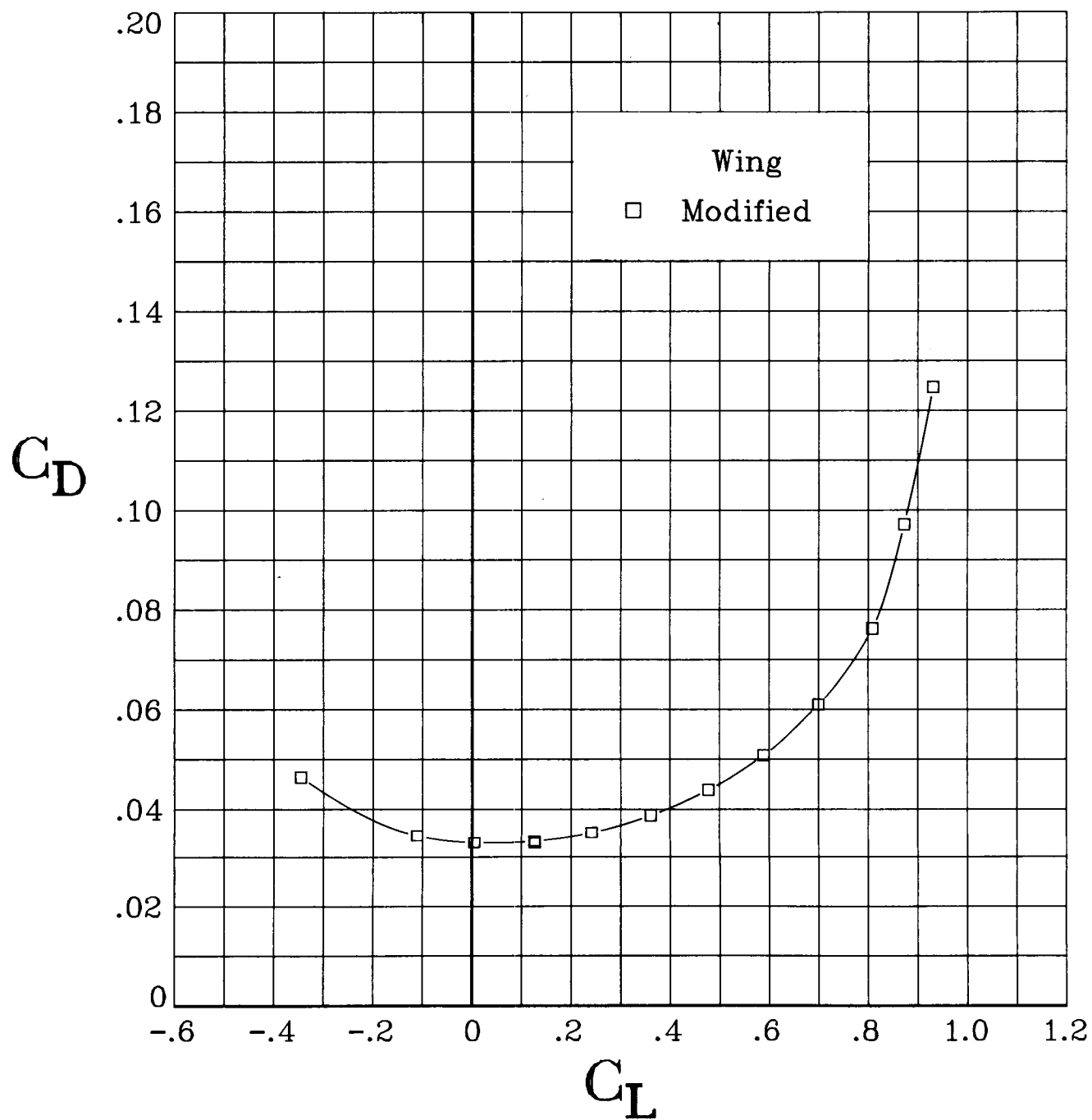
(b) Concluded.

Figure 5. Continued.



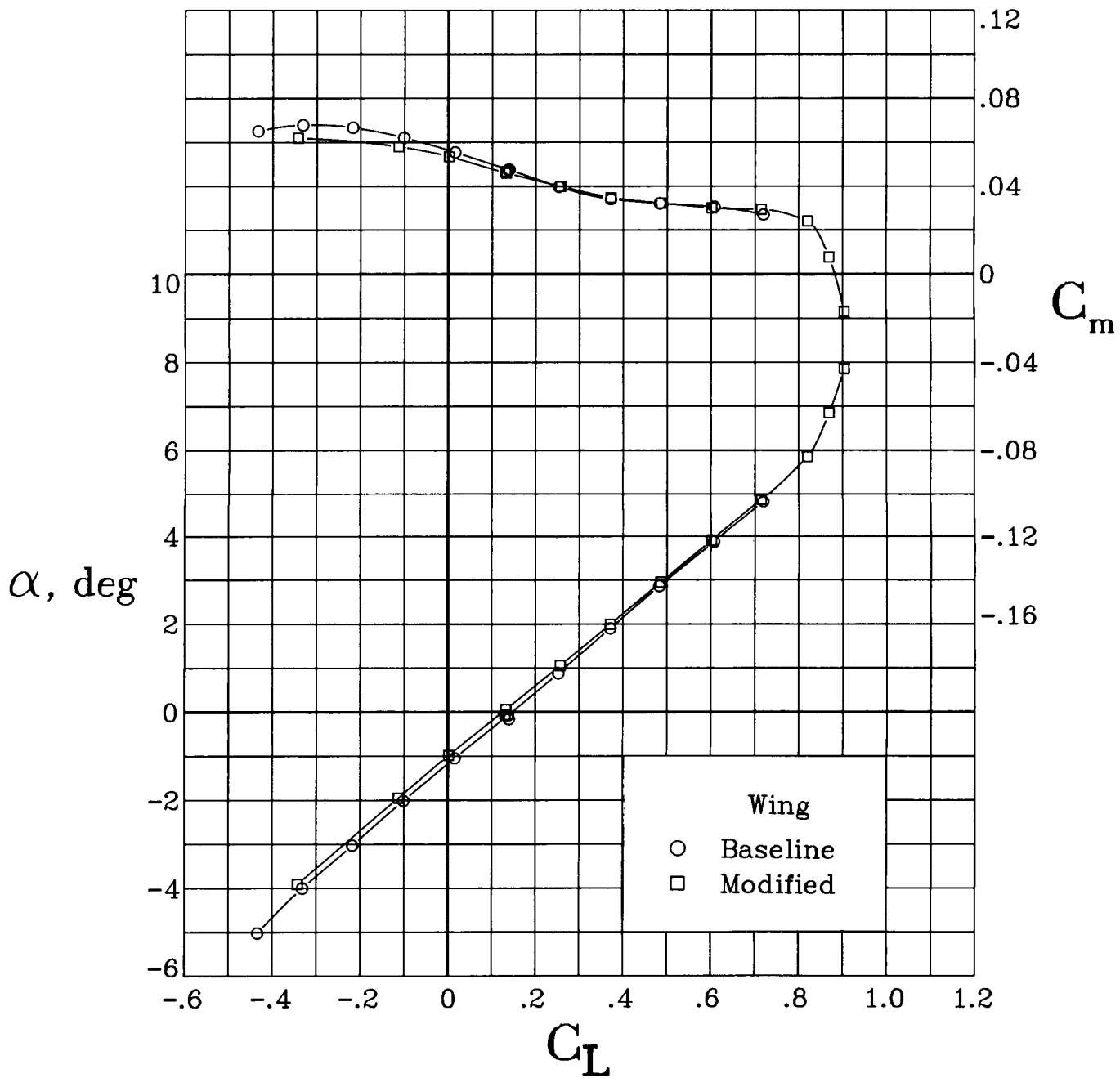
(c) $M = 0.675$.

Figure 5. Continued.



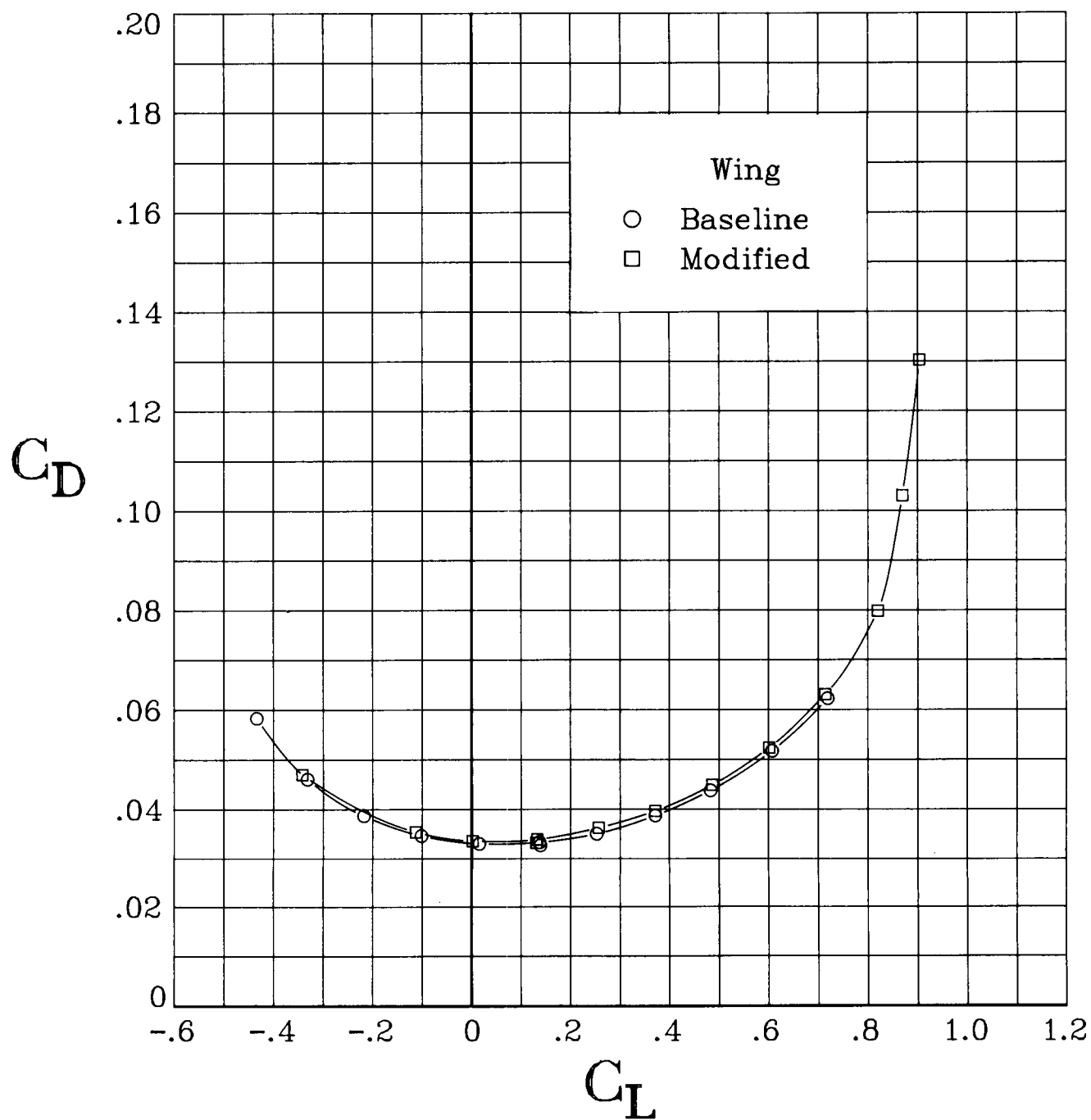
(c) Concluded.

Figure 5. Continued.



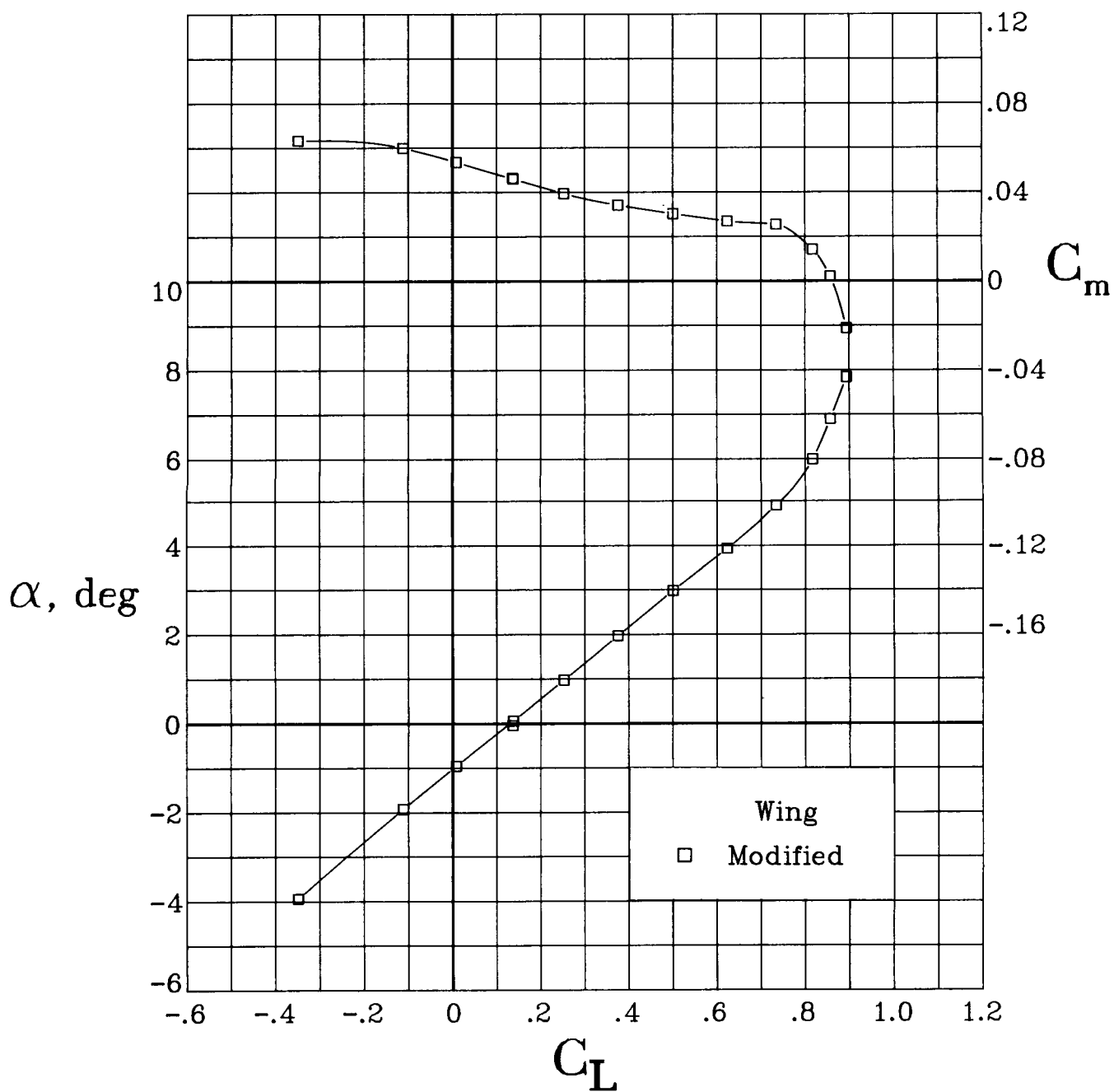
(d) $M = 0.70$.

Figure 5. Continued.



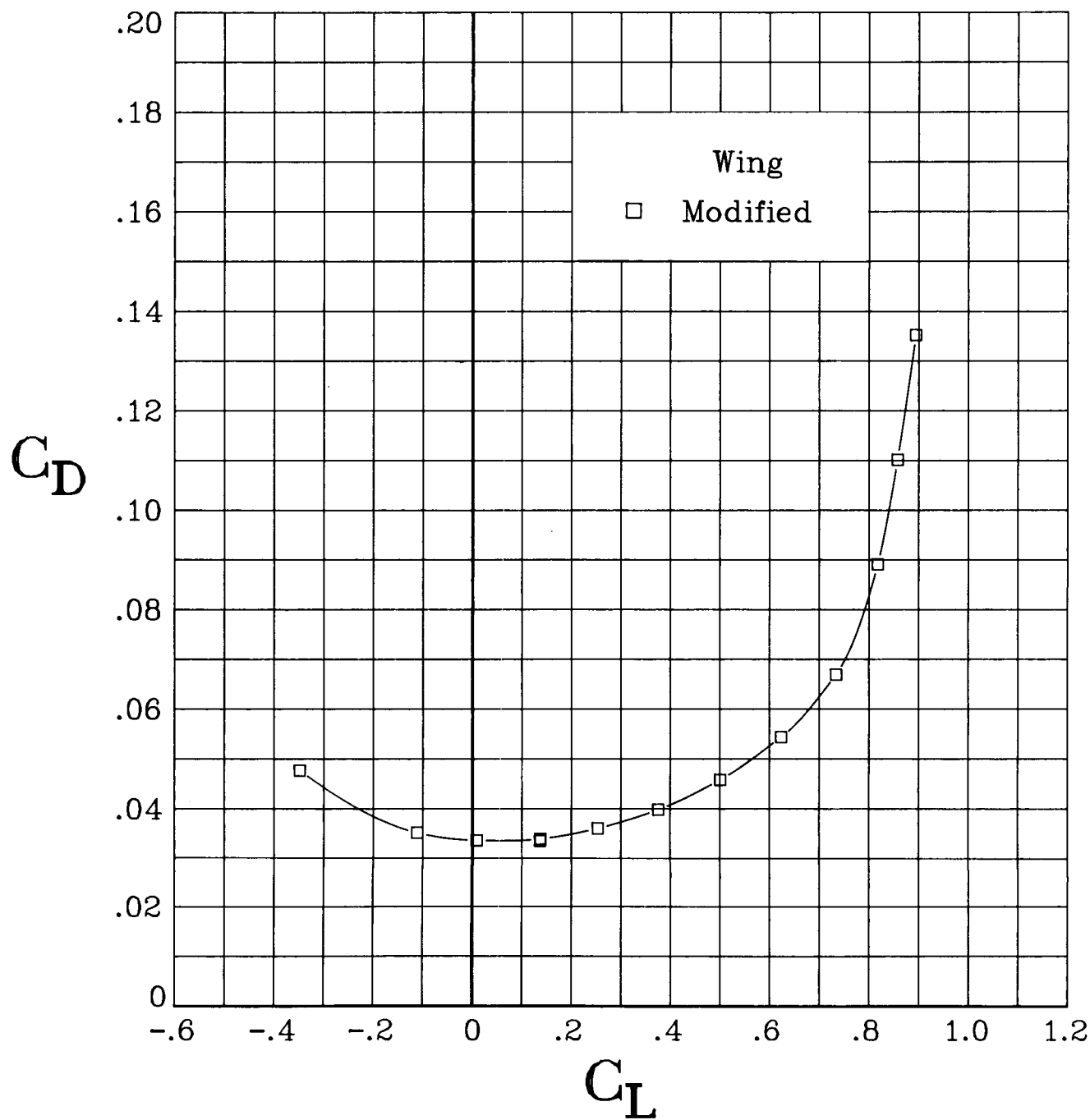
(d) Concluded.

Figure 5. Continued.



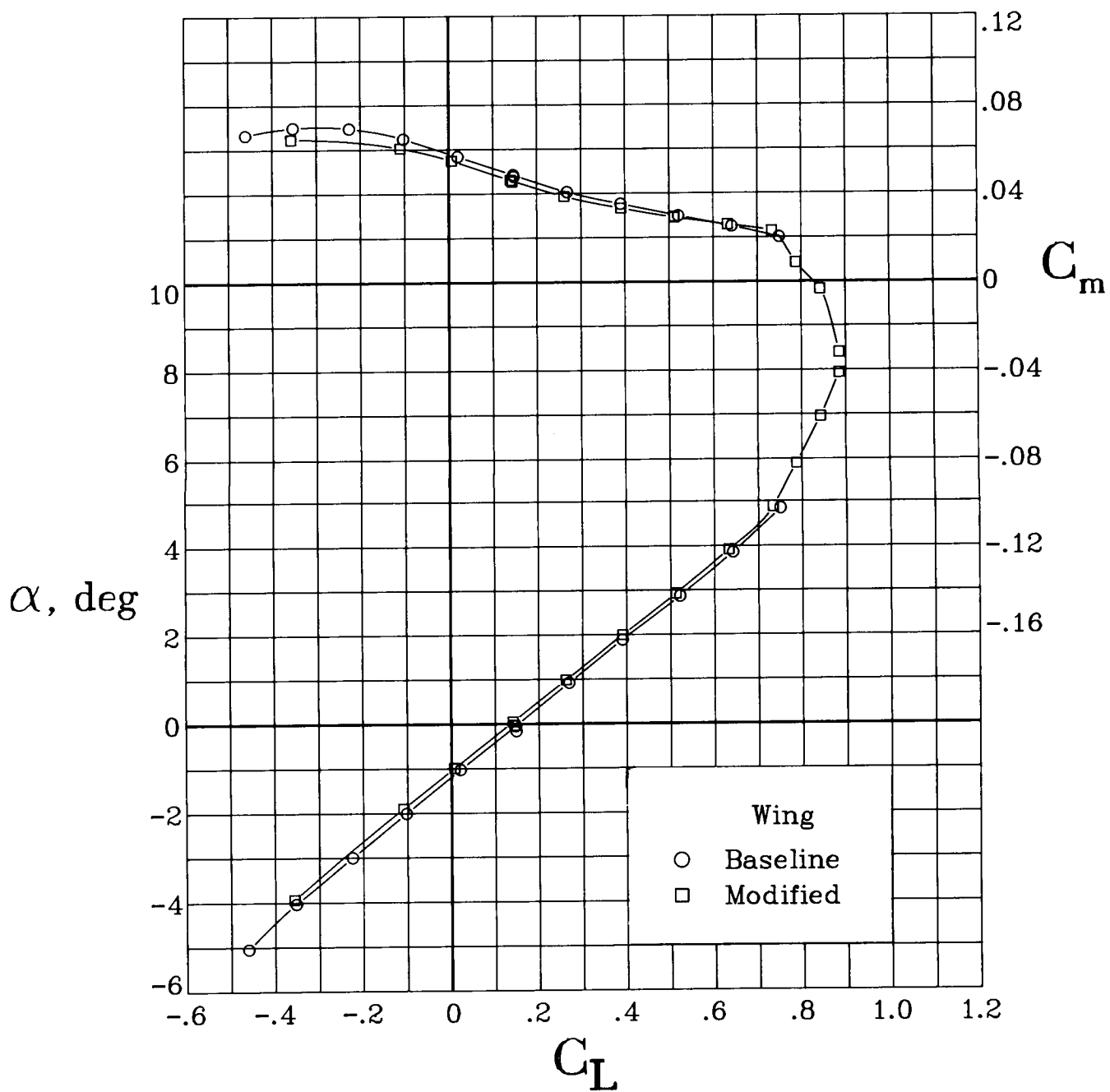
(e) $M = 0.725$.

Figure 5. Continued.



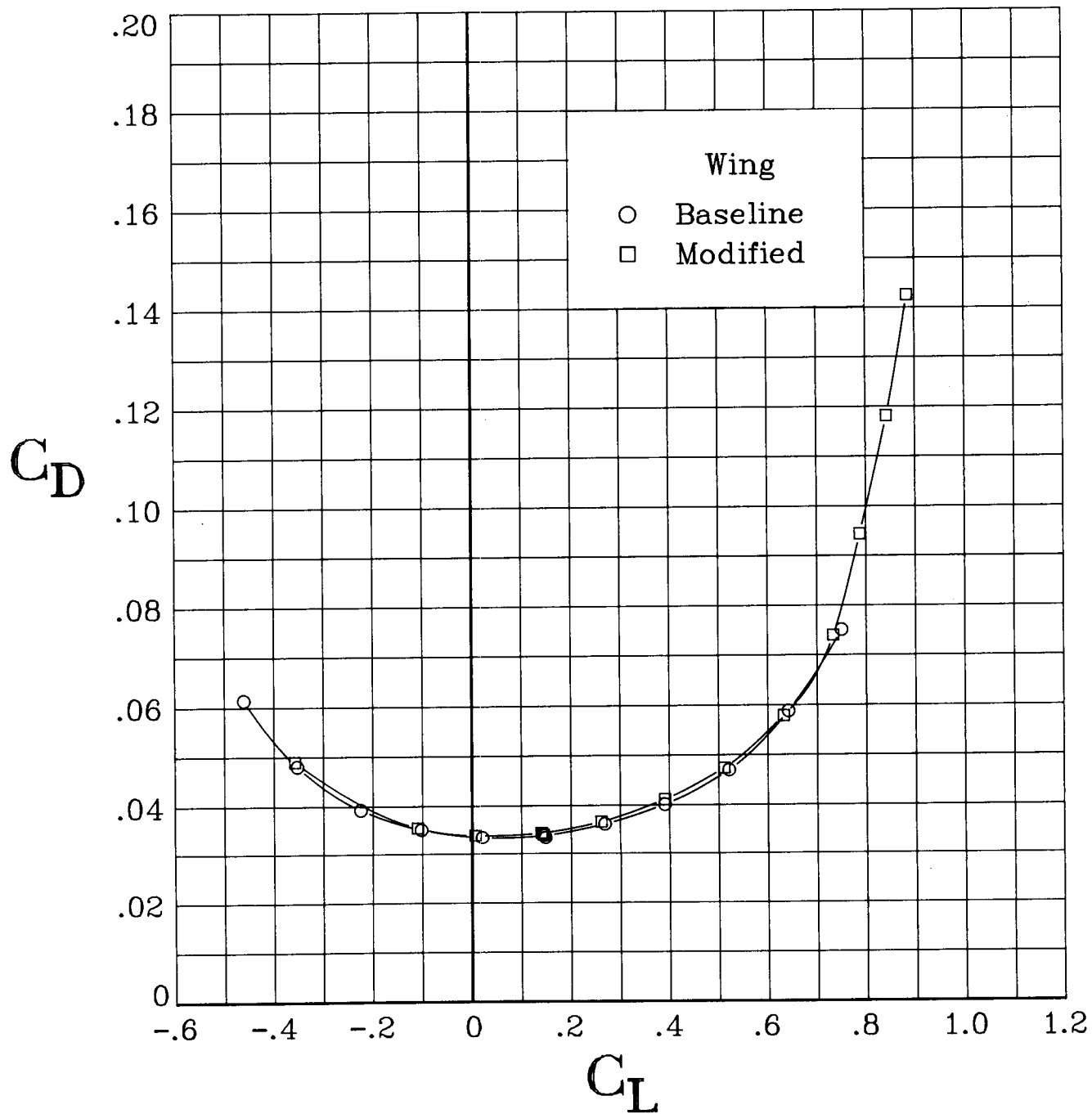
(e) Concluded.

Figure 5. Continued.



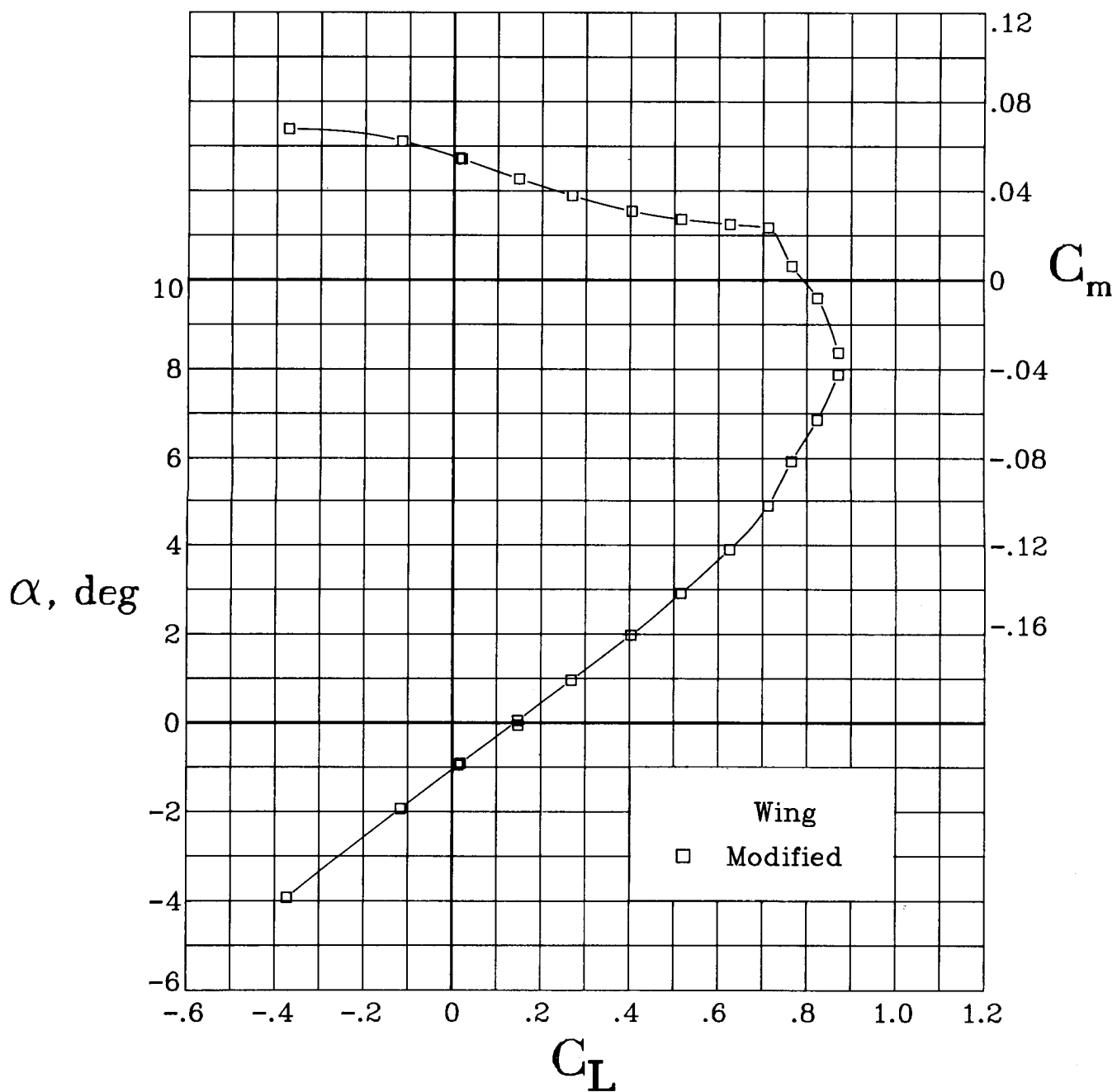
(f) $M = 0.75$.

Figure 5. Continued.



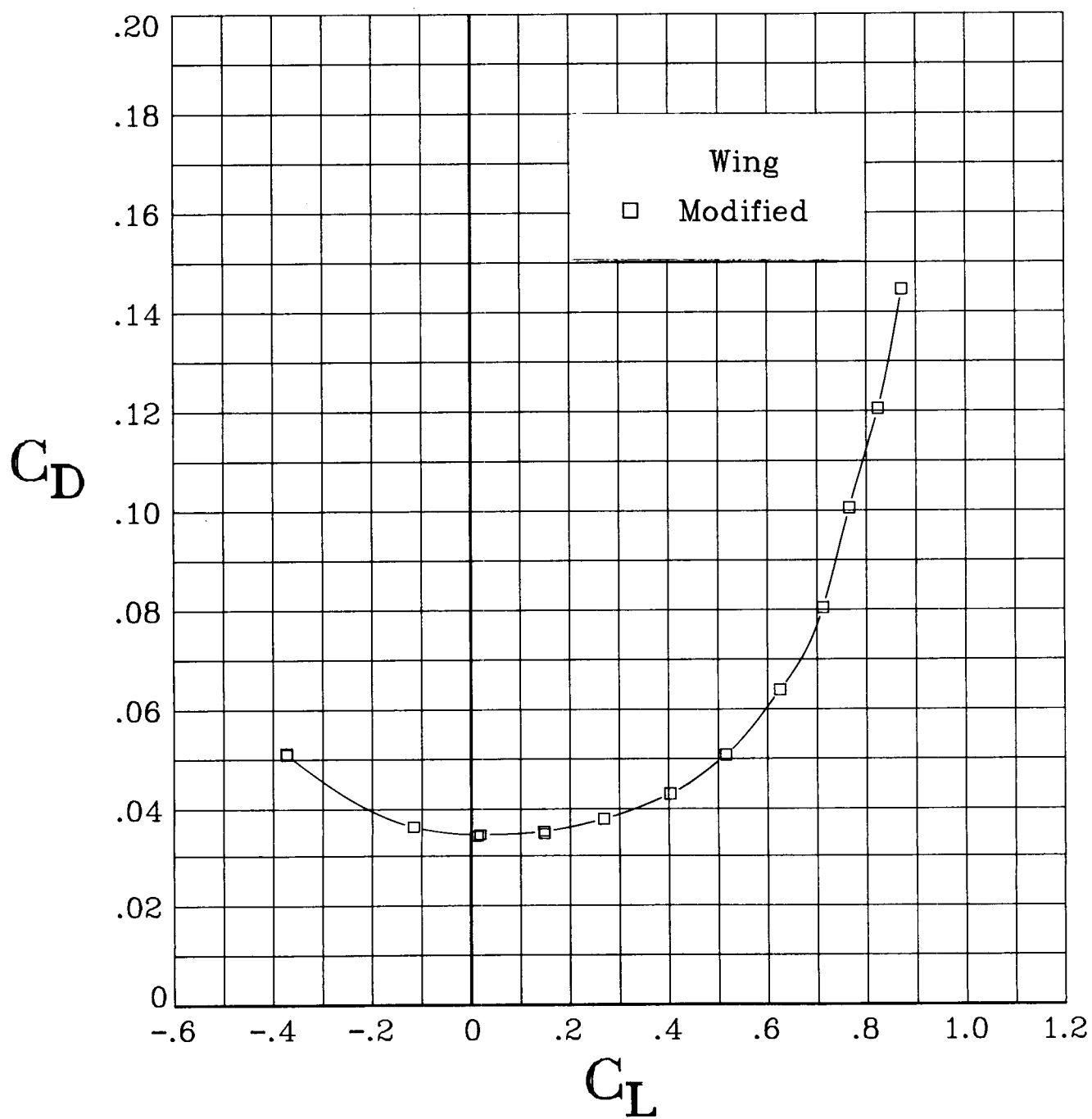
(f) Concluded.

Figure 5. Continued.



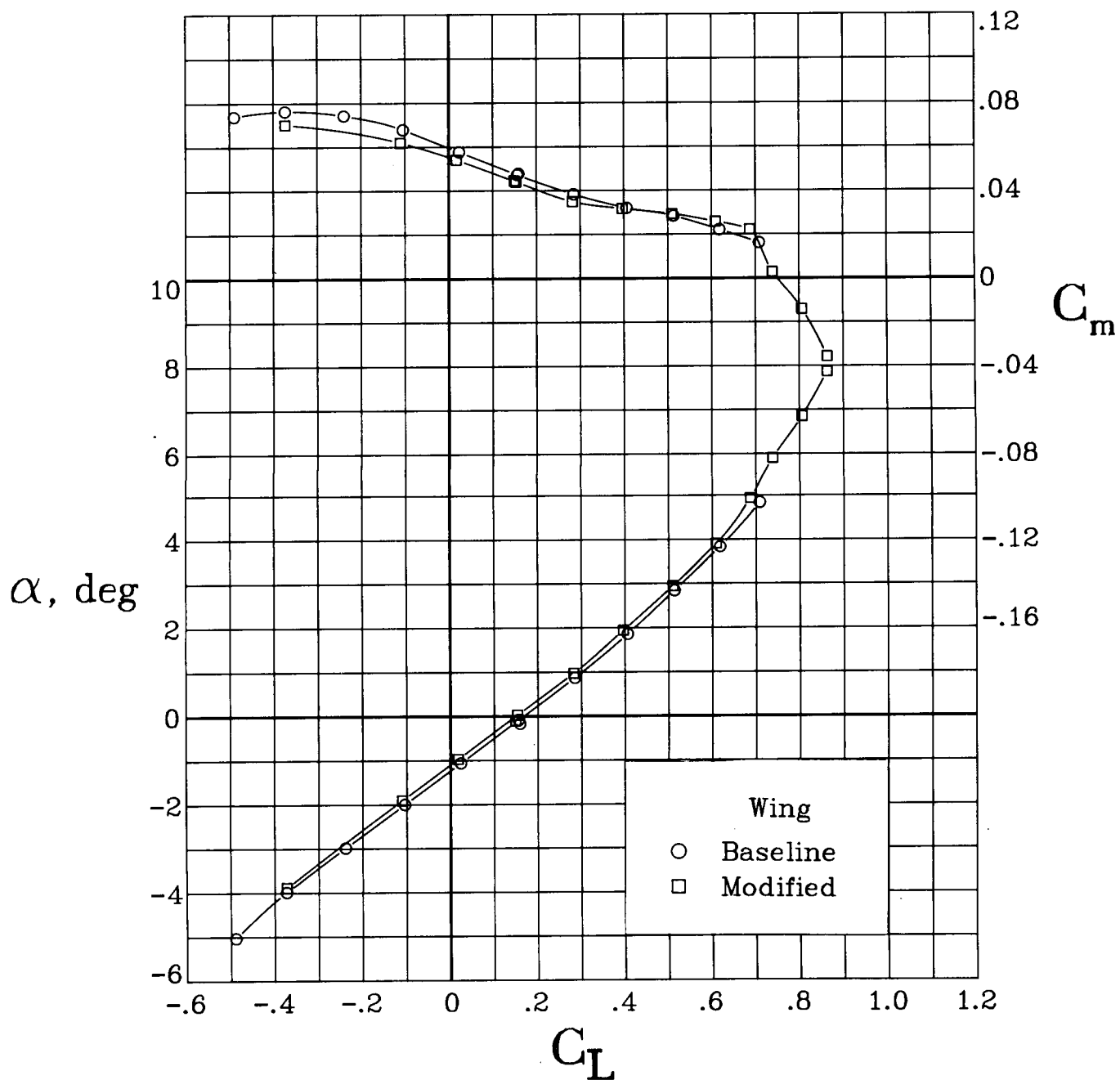
(g) $M = 0.775$.

Figure 5. Continued.



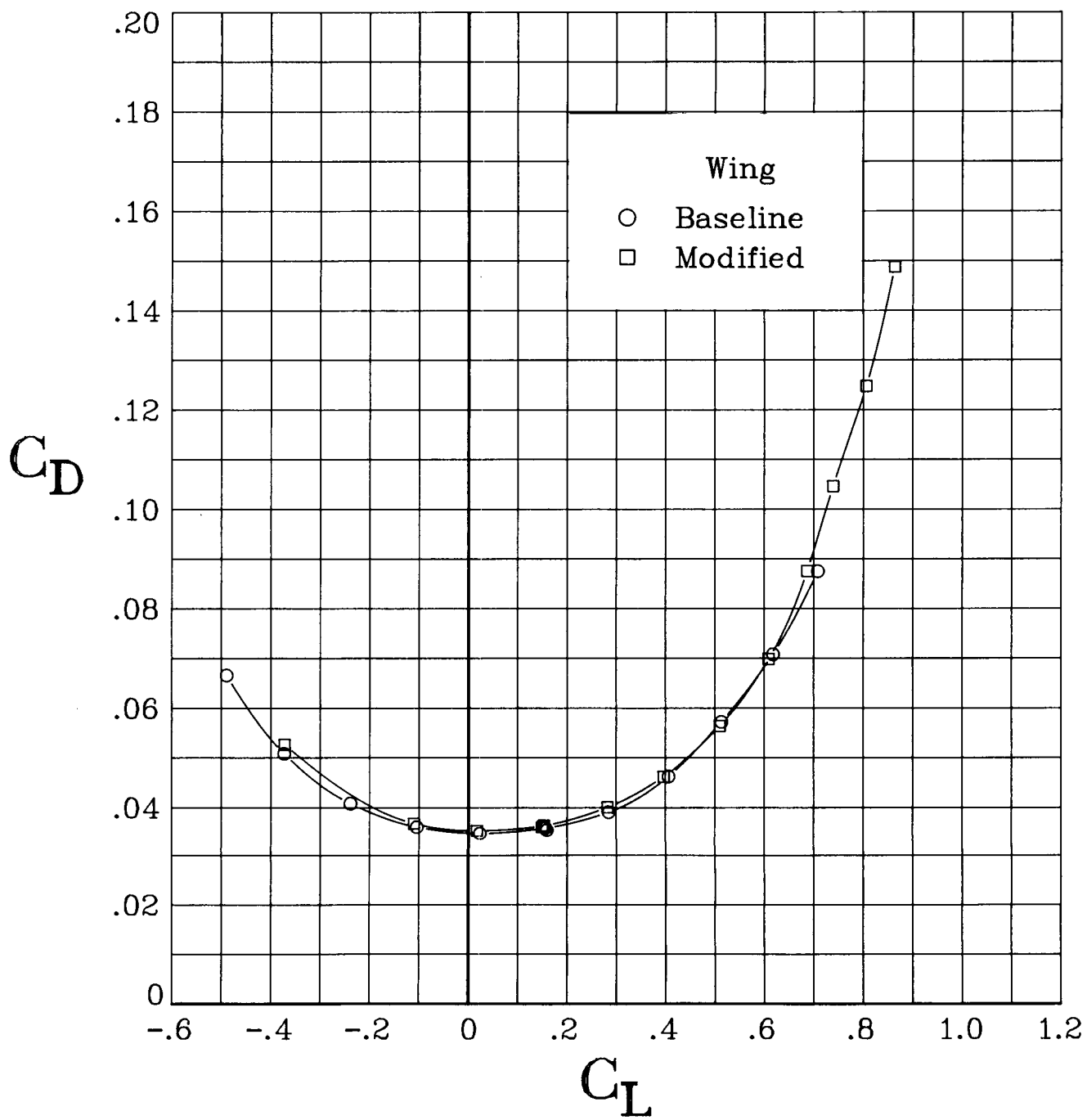
(g) Concluded.

Figure 5. Continued.



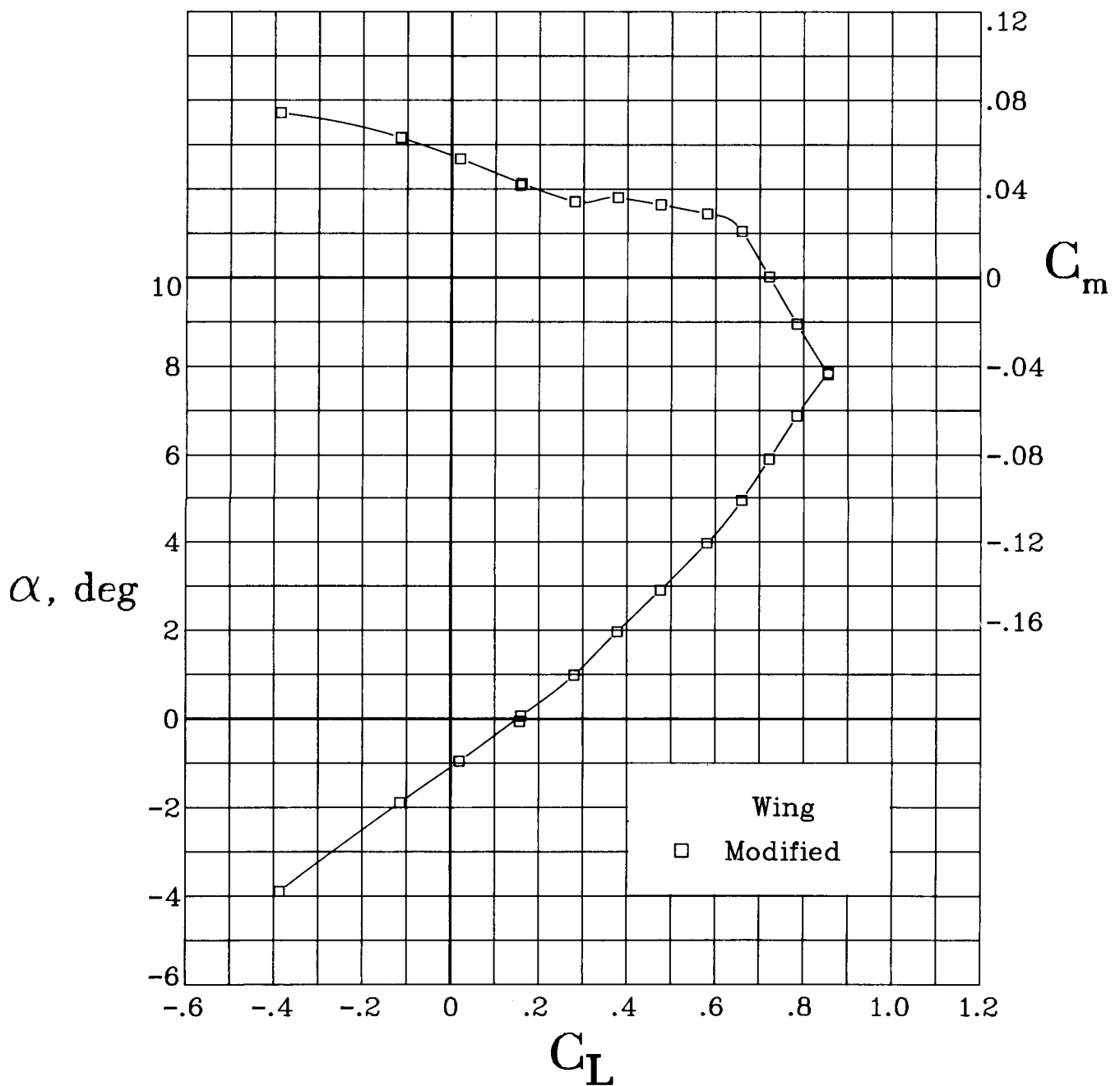
(h) $M = 0.80$.

Figure 5. Continued.



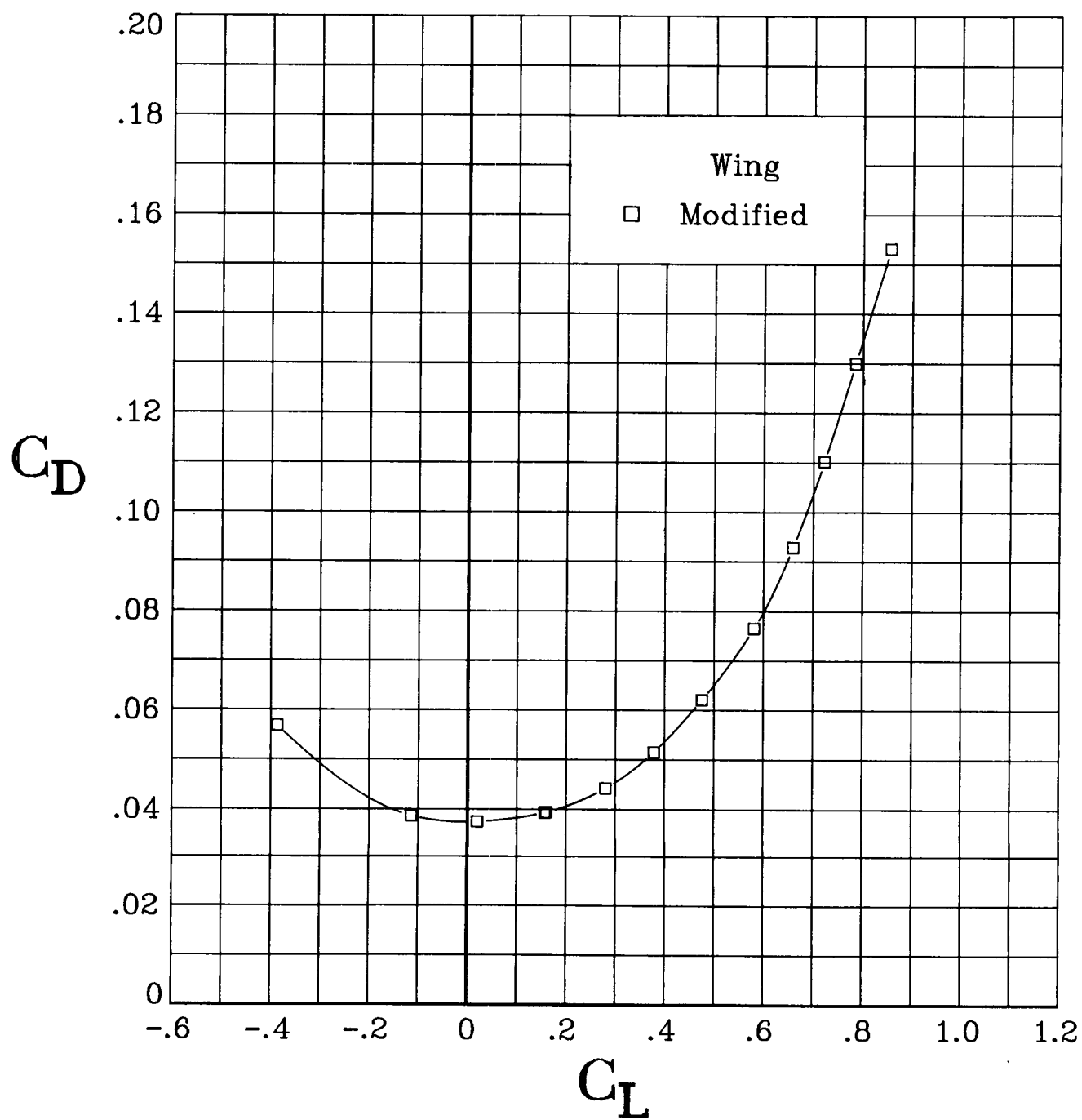
(h) Concluded.

Figure 5. Continued.



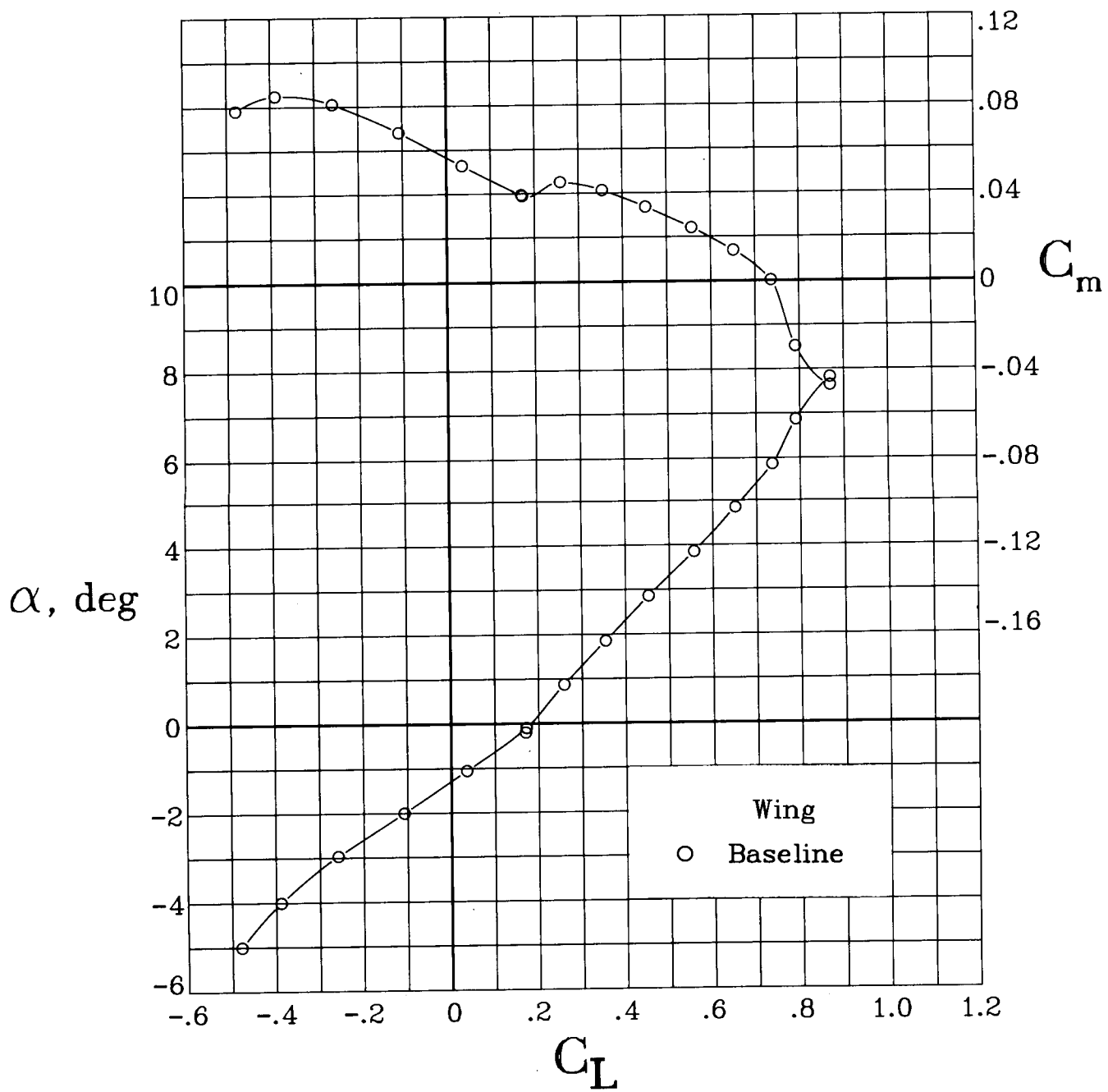
(i) $M = 0.825$.

Figure 5. Continued.



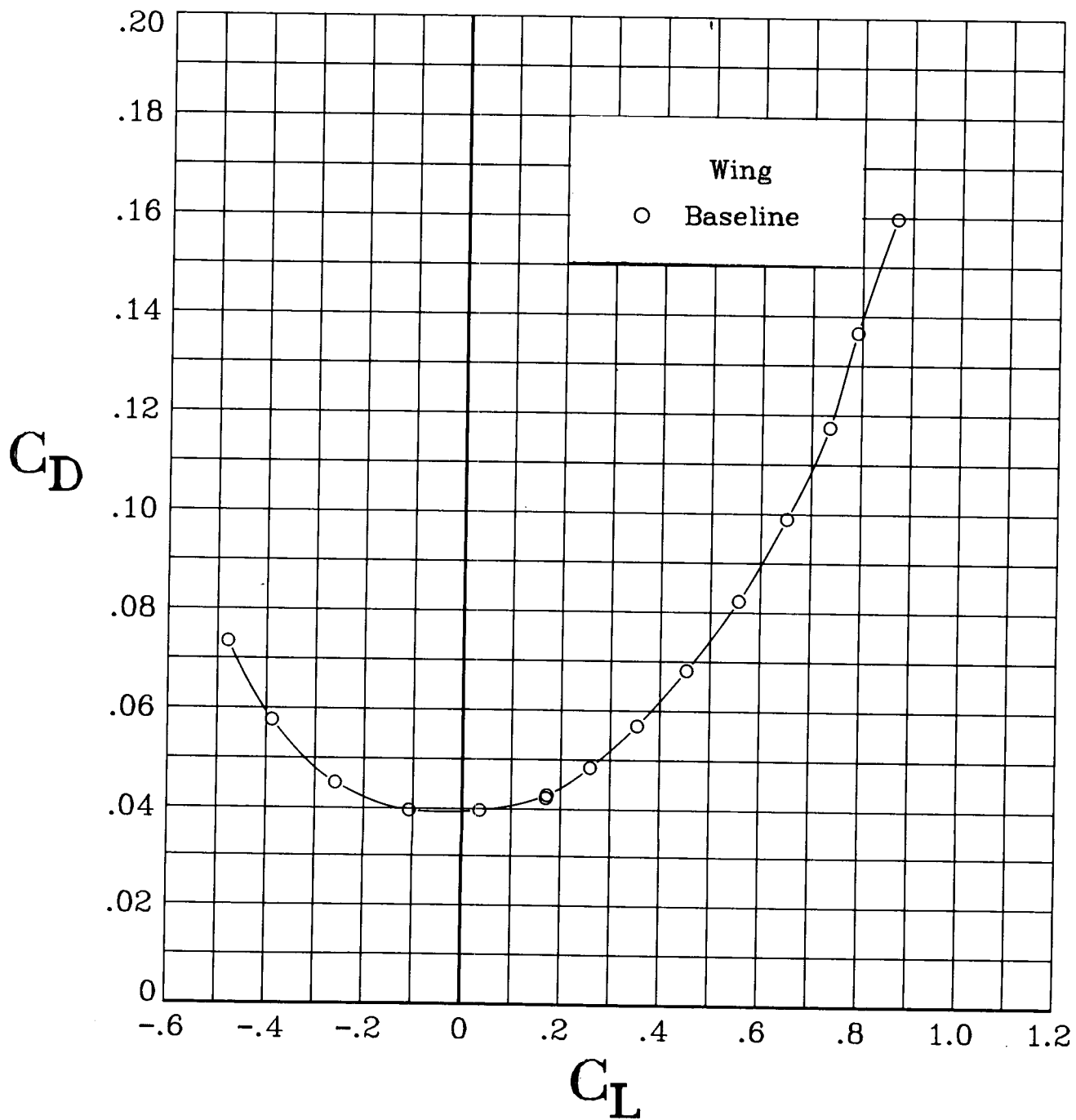
(i) Concluded.

Figure 5. Continued.



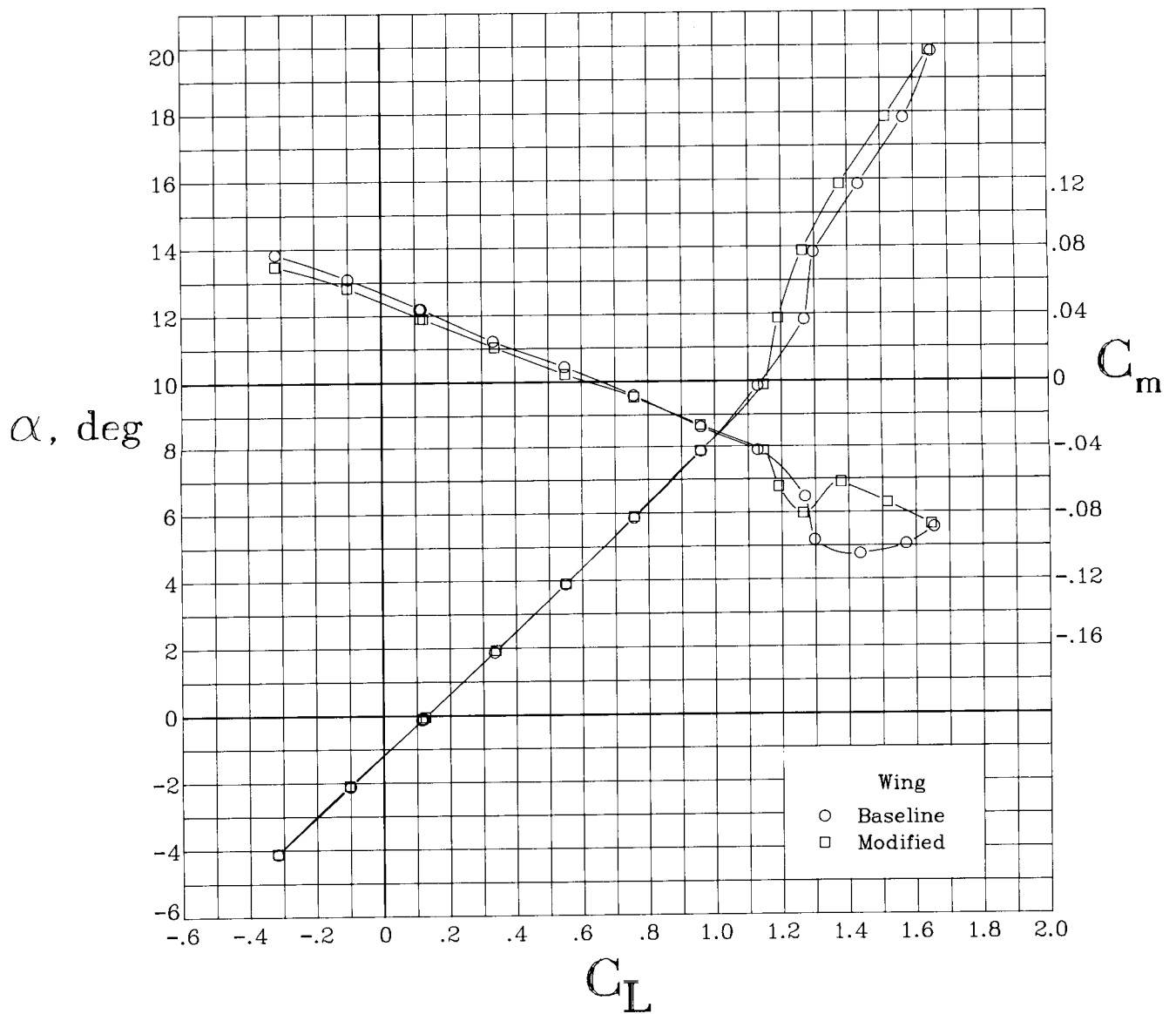
(j) $M = 0.85$.

Figure 5. Continued.



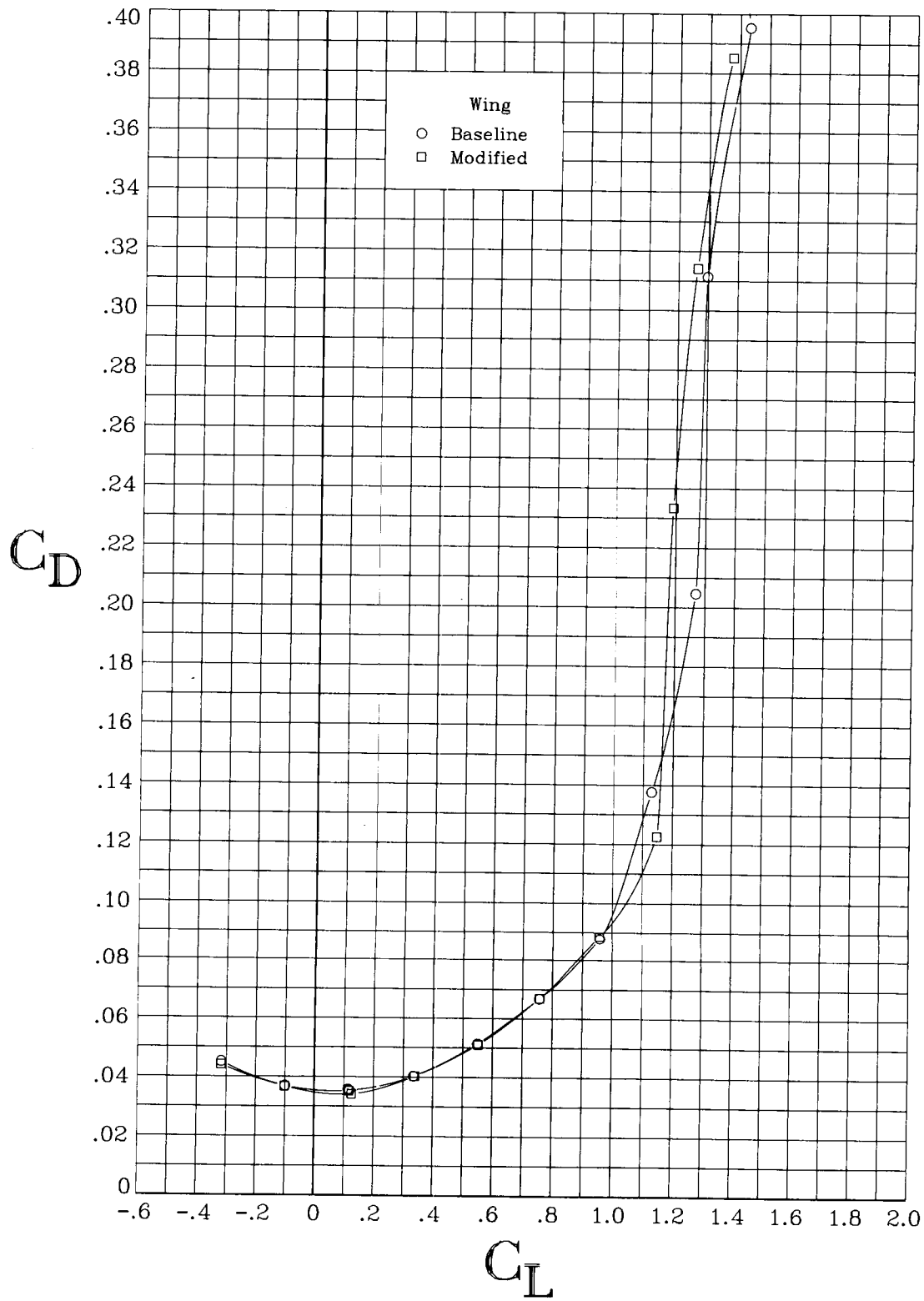
(j) Concluded.

Figure 5. Concluded.



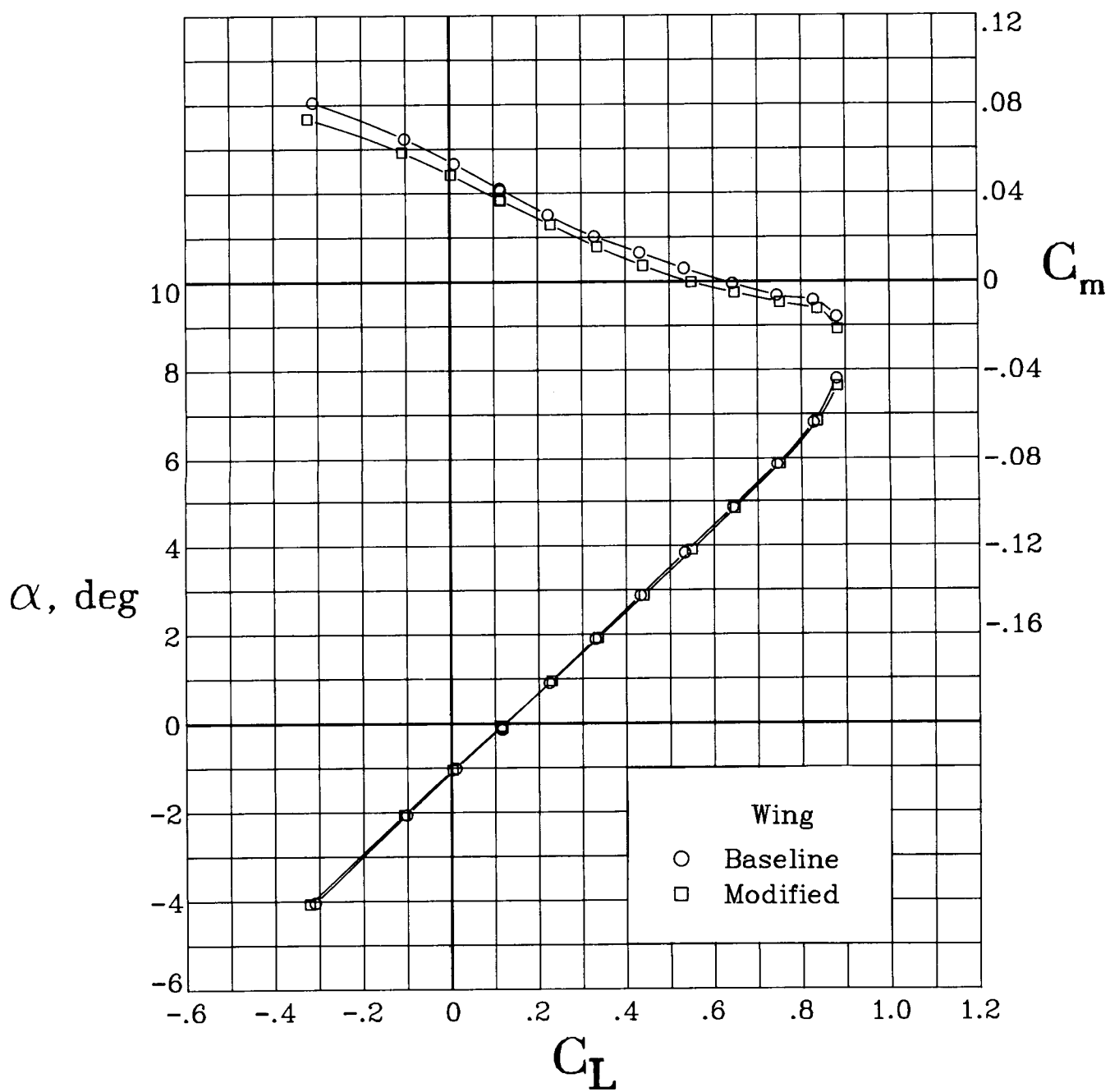
(a) $M = 0.20$.

Figure 6. Longitudinal aerodynamic characteristics of the baseline and modified wing configurations, with wings swept 25° . $\beta = 0^\circ$.



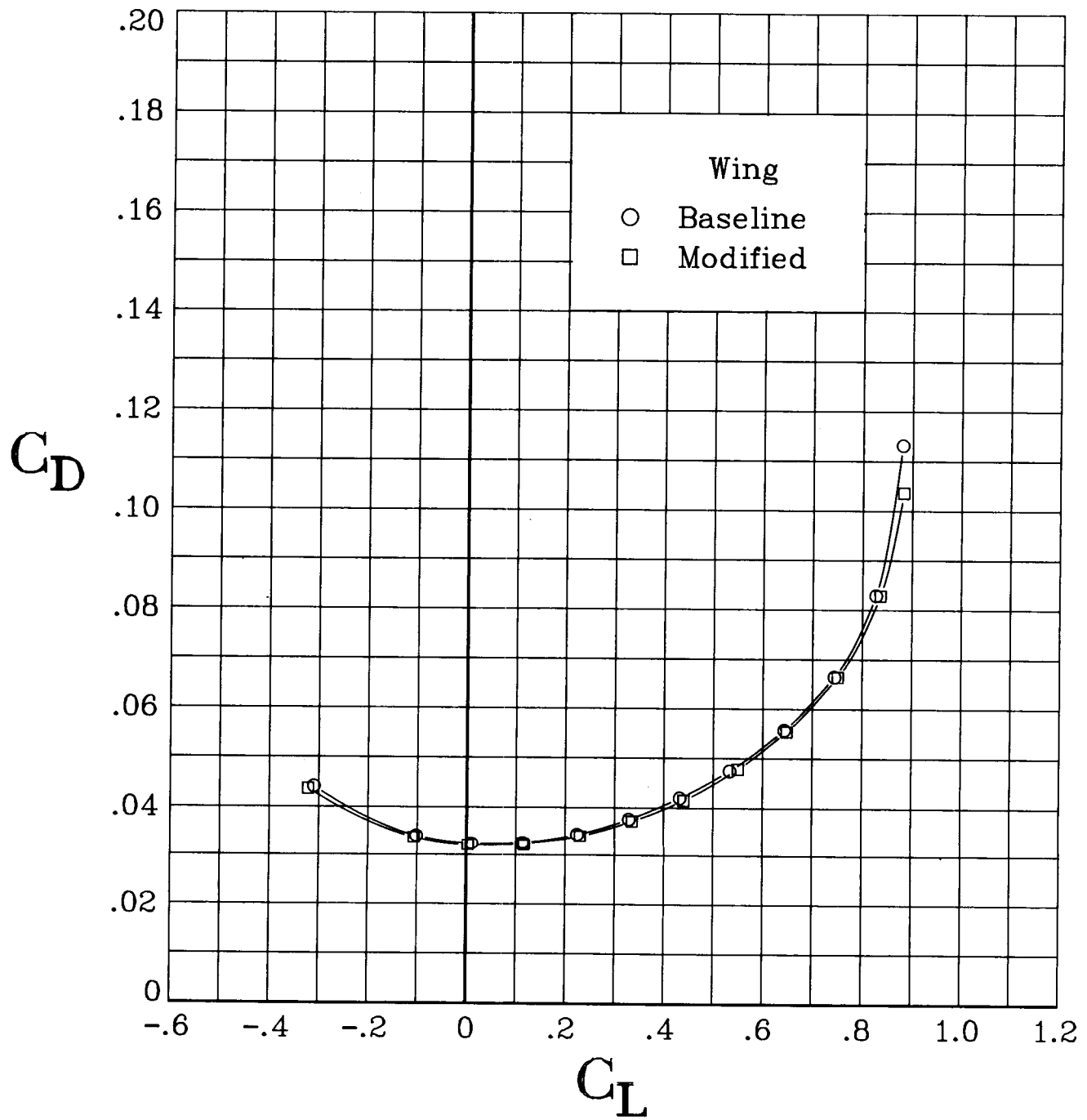
(a) Concluded.

Figure 6. Continued.



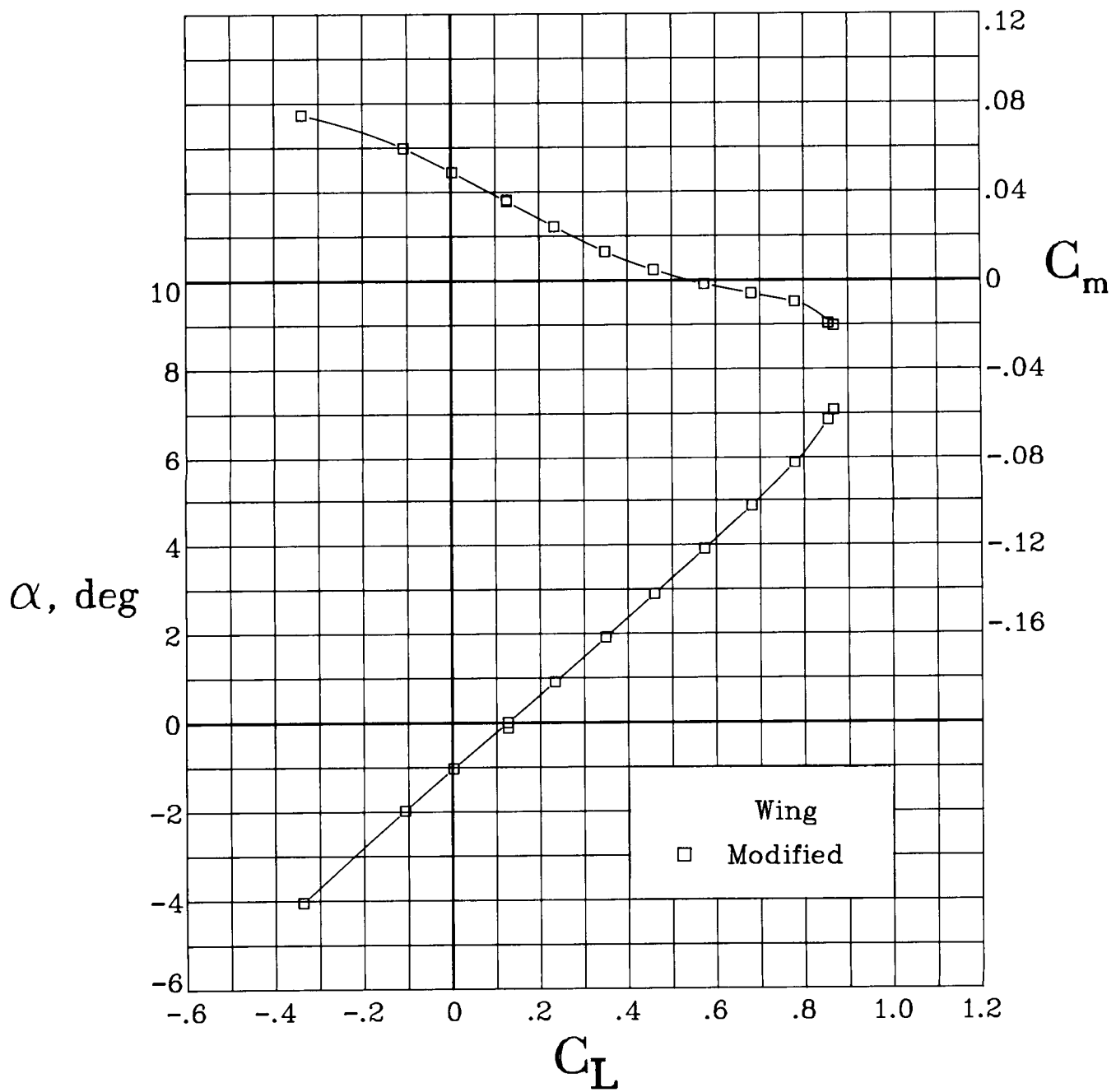
(b) $M = 0.60$.

Figure 6. Continued.



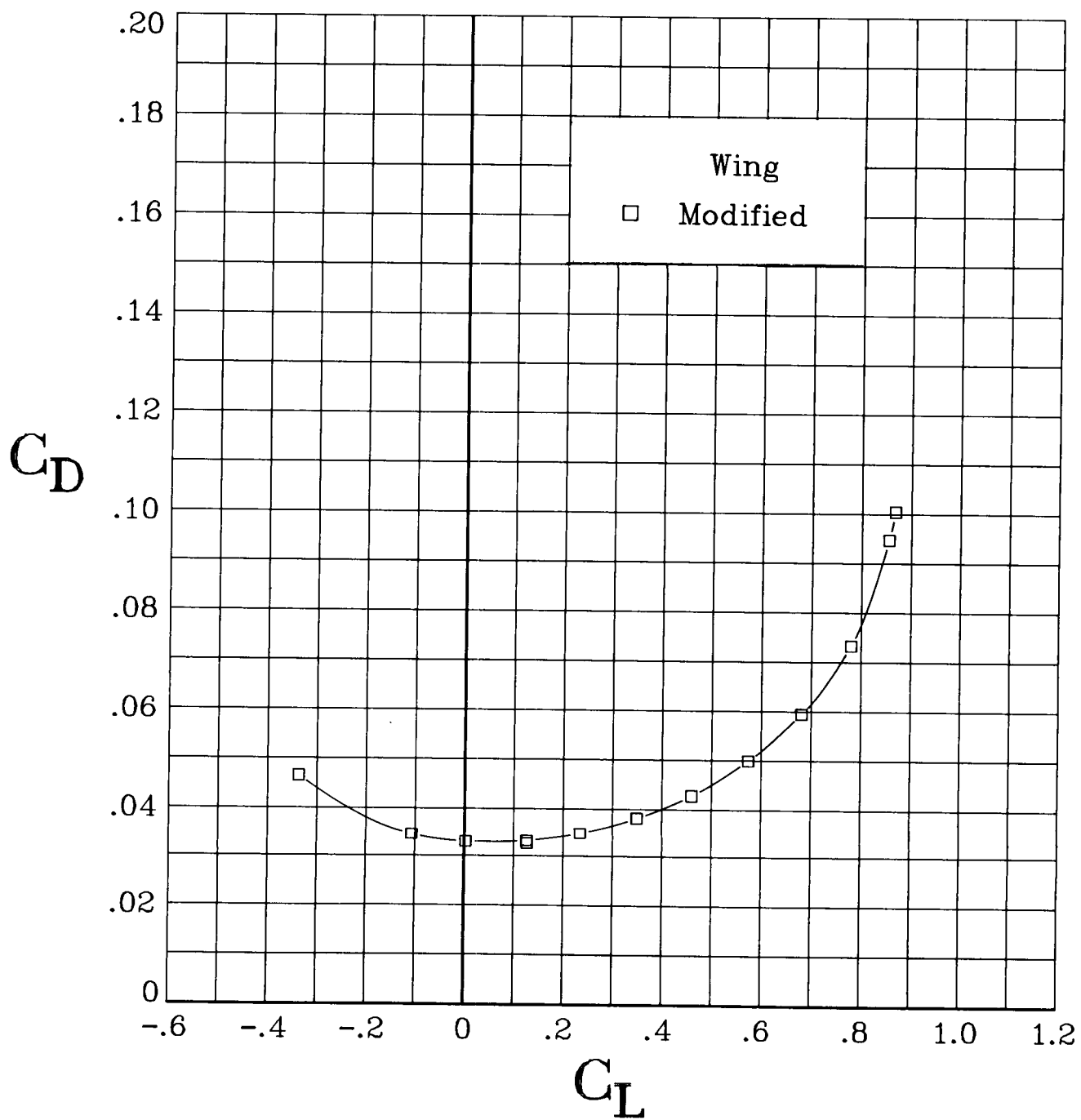
(b) Concluded.

Figure 6. Continued.



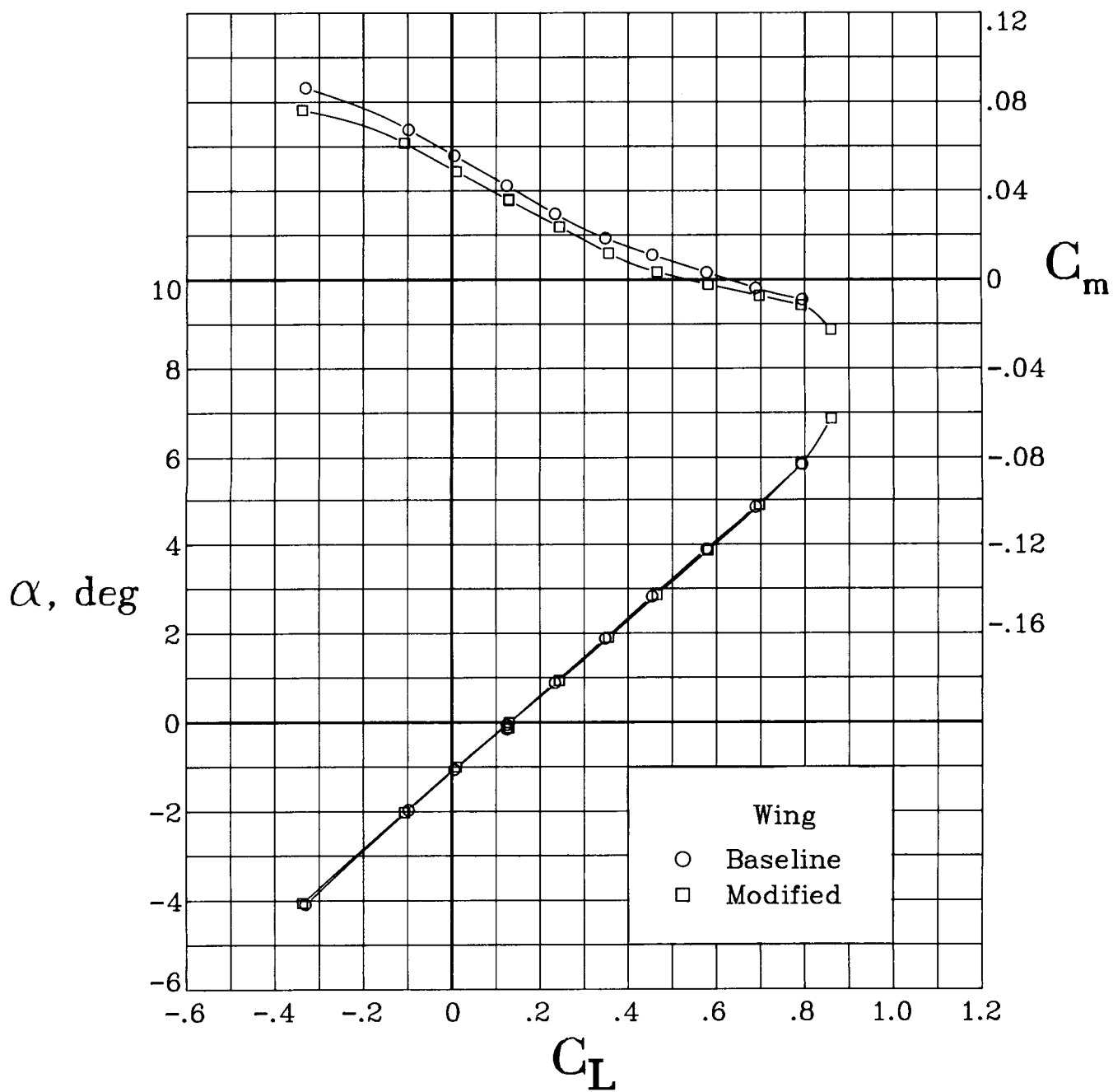
(c) $M = 0.675$.

Figure 6. Continued.



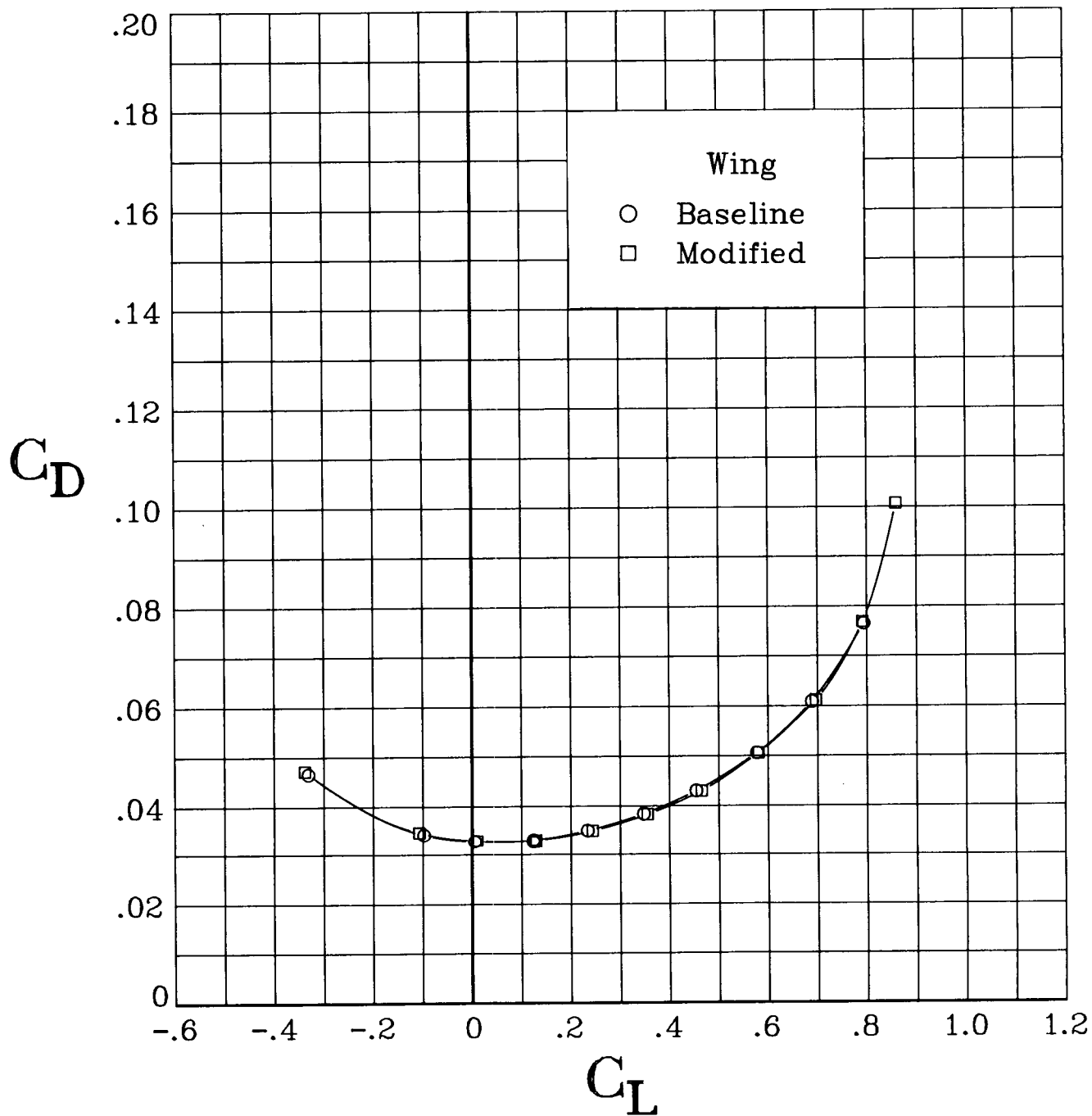
(c) Concluded.

Figure 6. Continued.



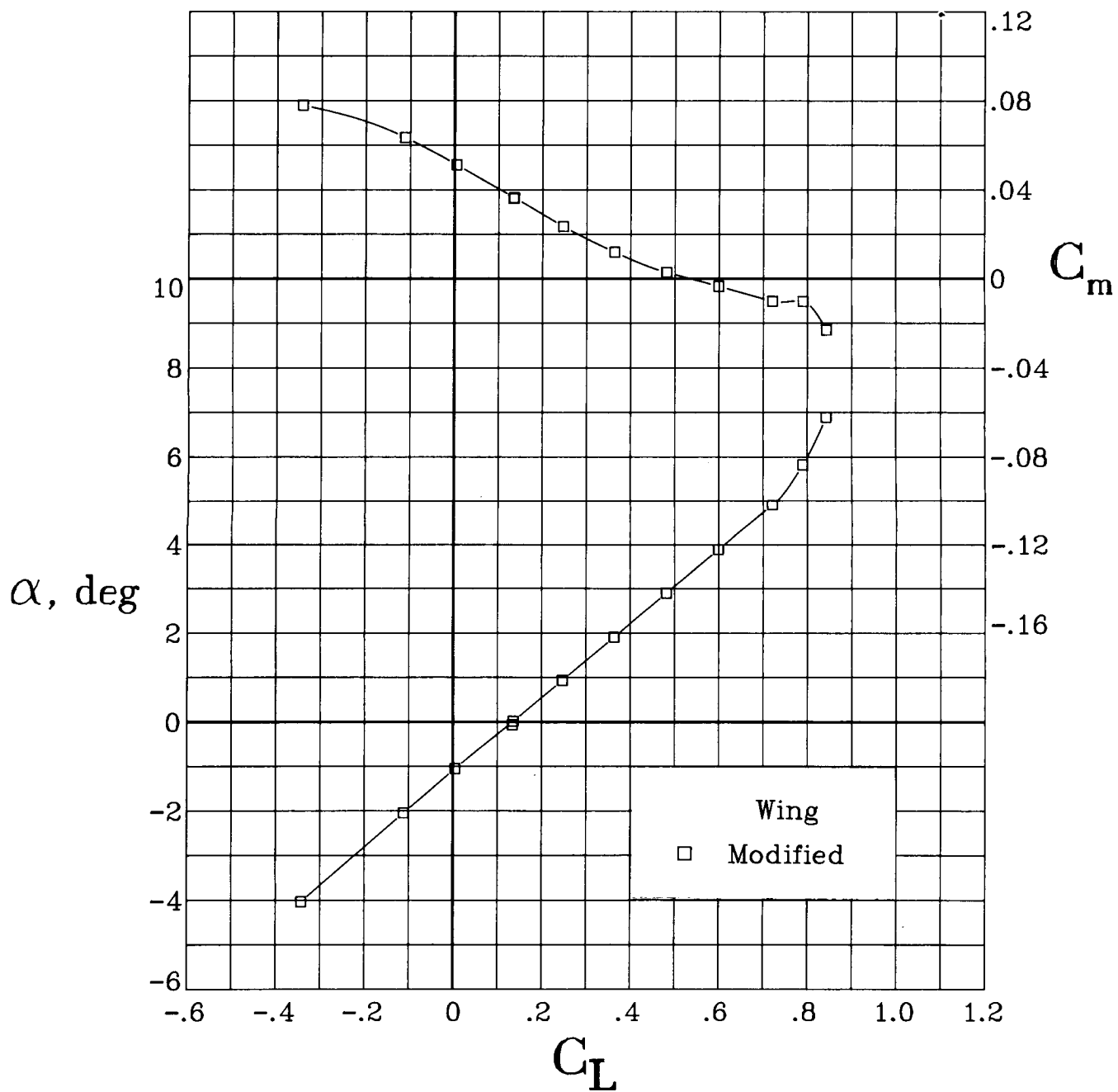
(d) $M = 0.70$.

Figure 6. Continued.



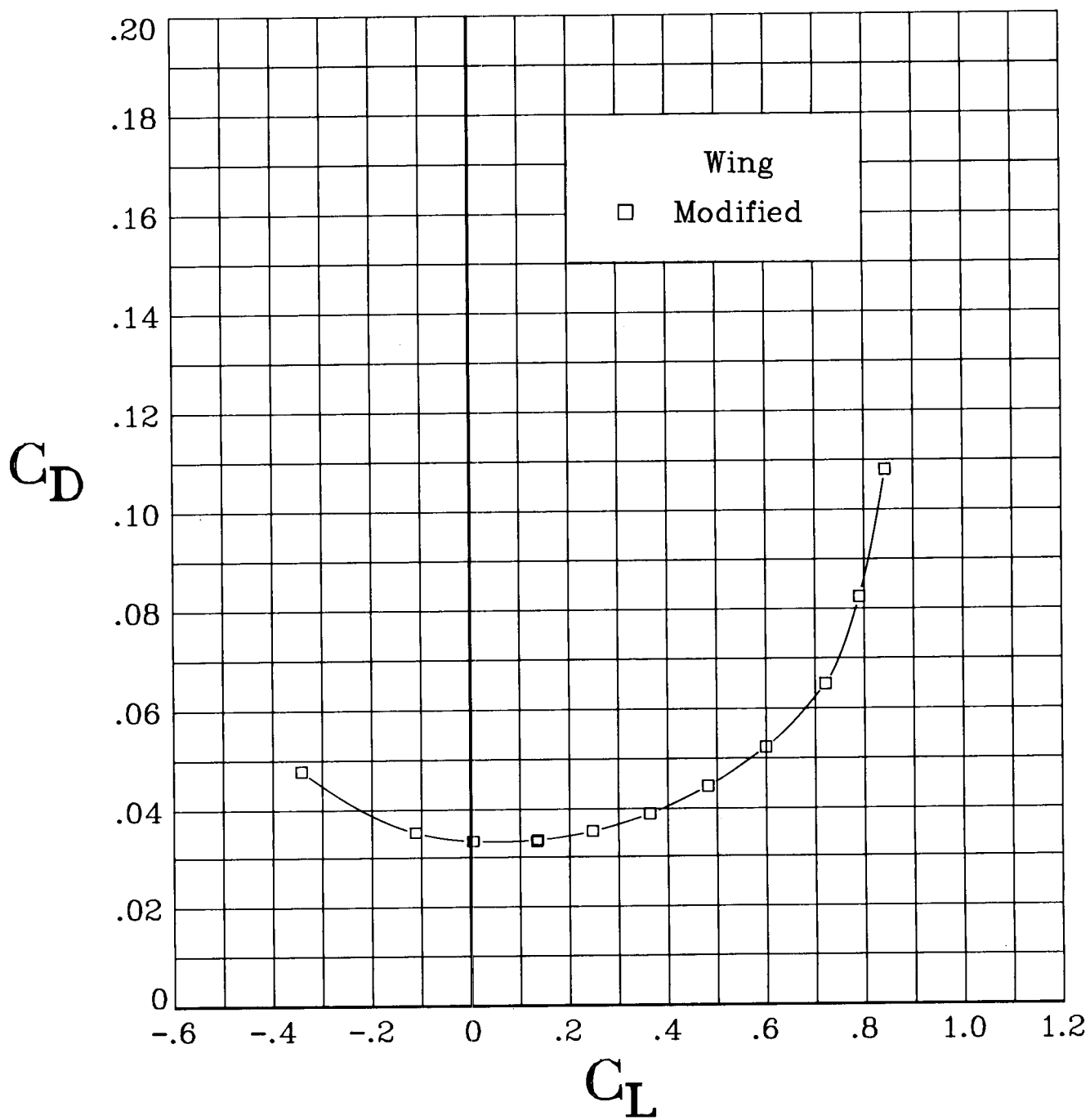
(d) Concluded.

Figure 6. Continued.



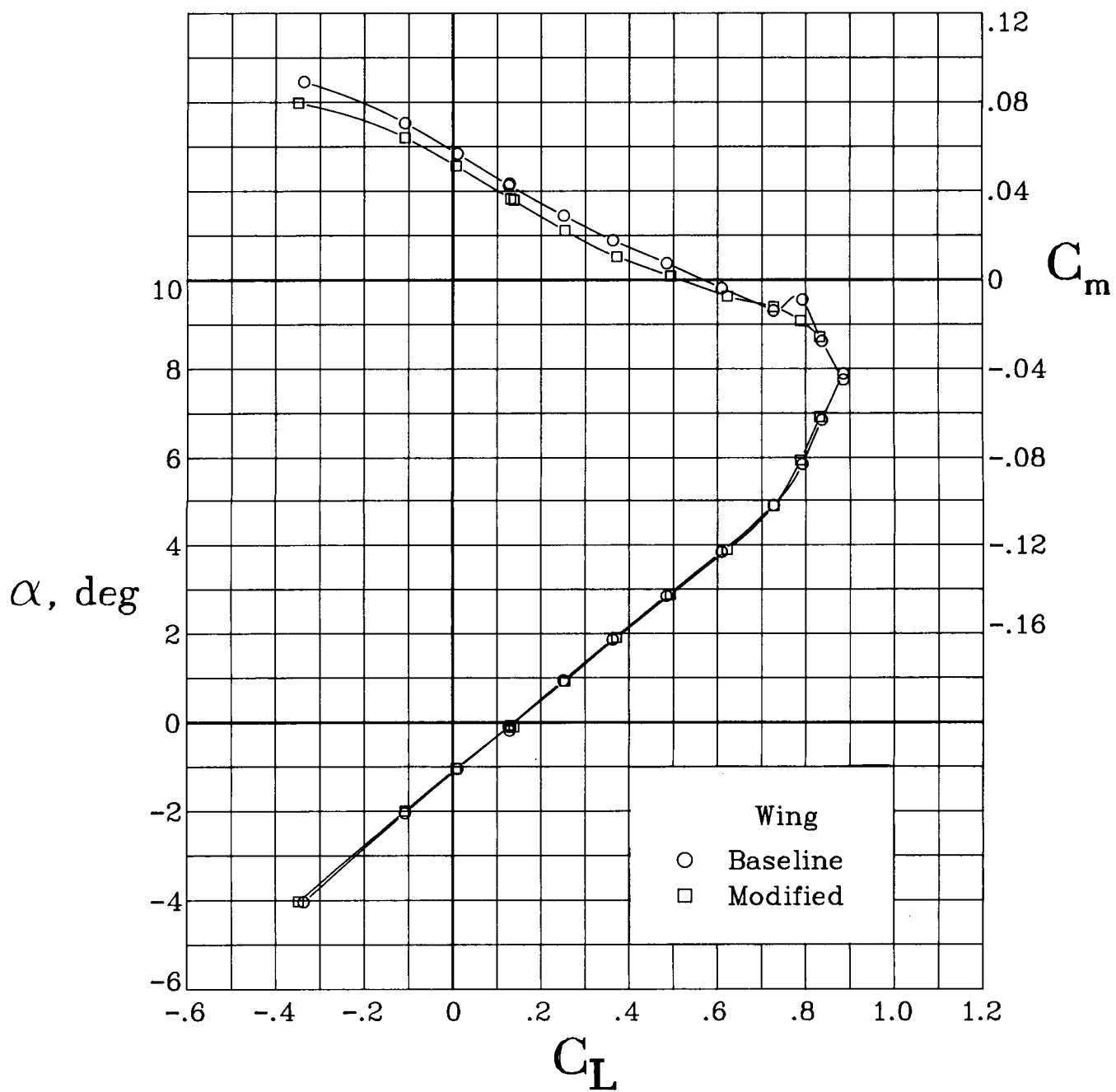
(e) $M = 0.725$.

Figure 6. Continued.



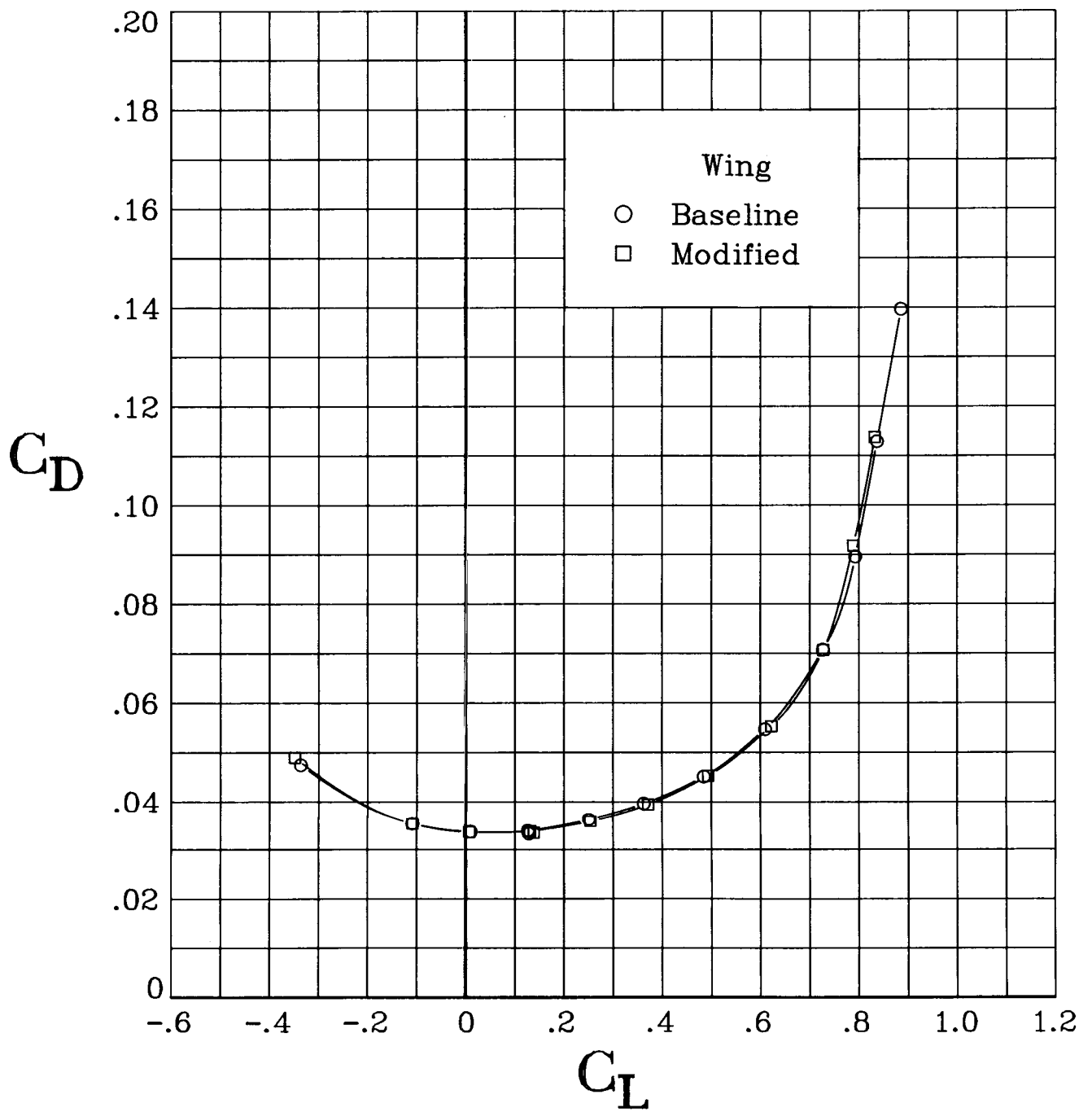
(e) Concluded.

Figure 6. Continued.



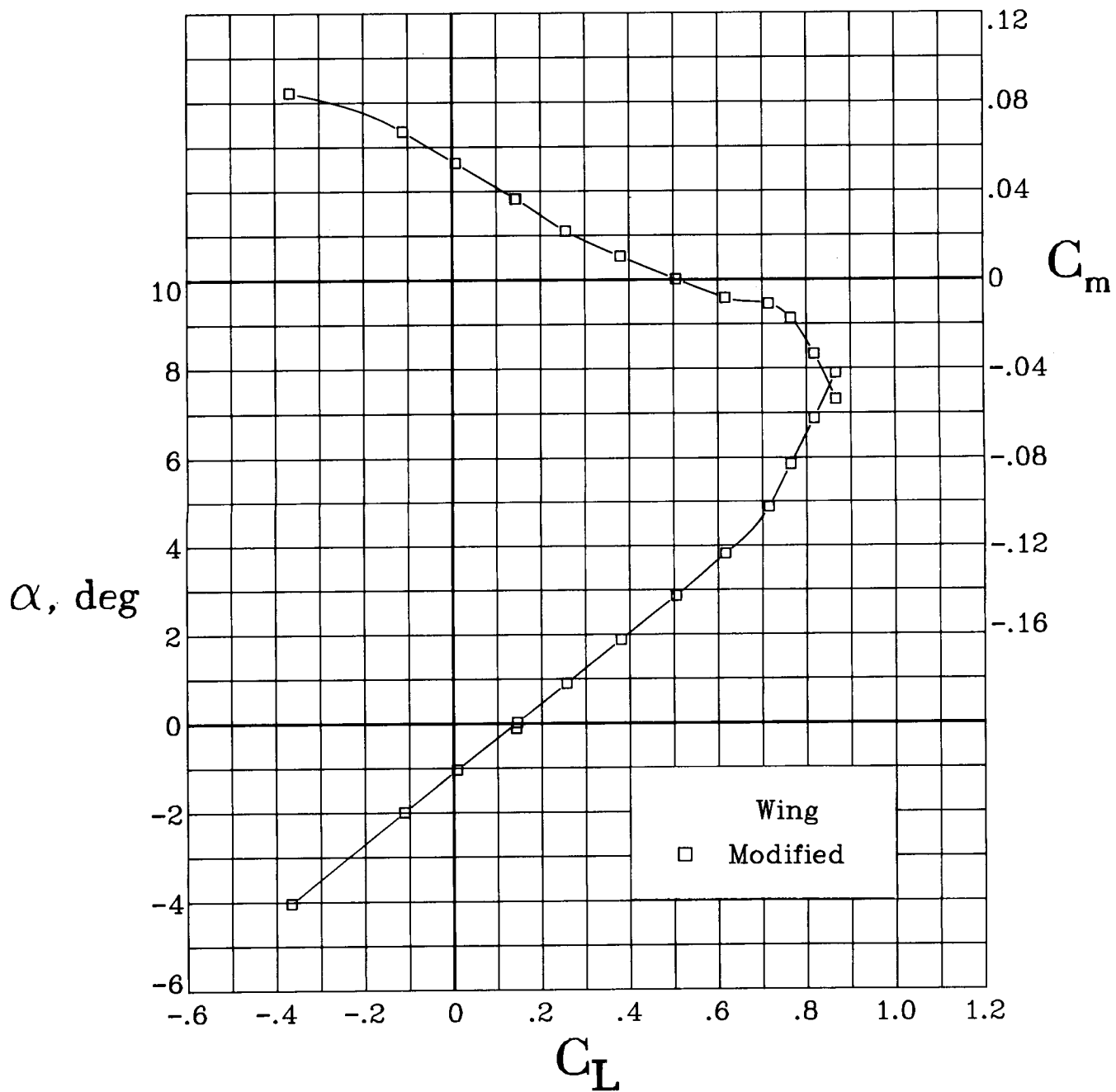
(f) $M = 0.75$.

Figure 6. Continued.



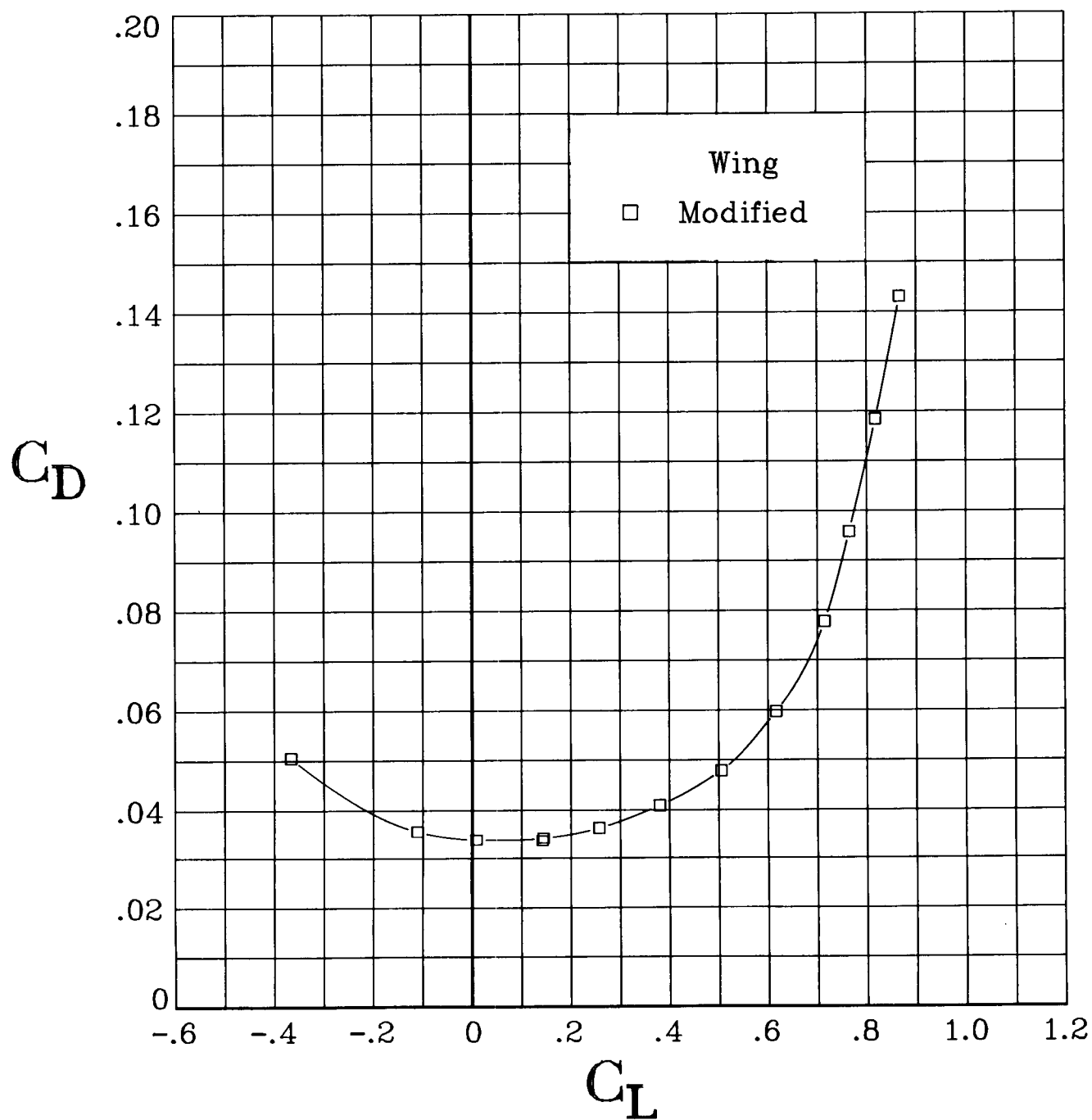
(f) Concluded.

Figure 6. Continued.



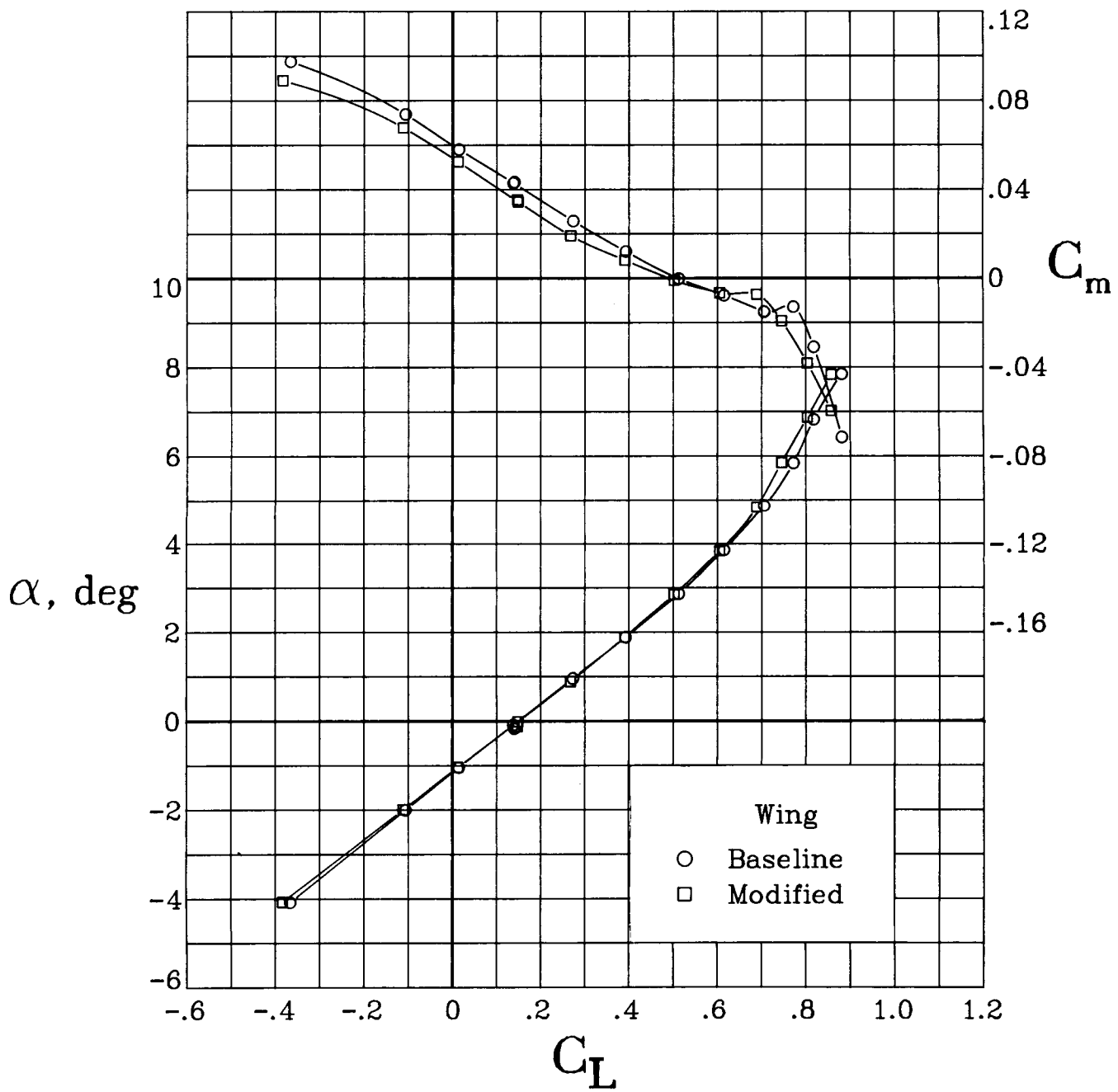
(g) $M = 0.775$.

Figure 6. Continued.



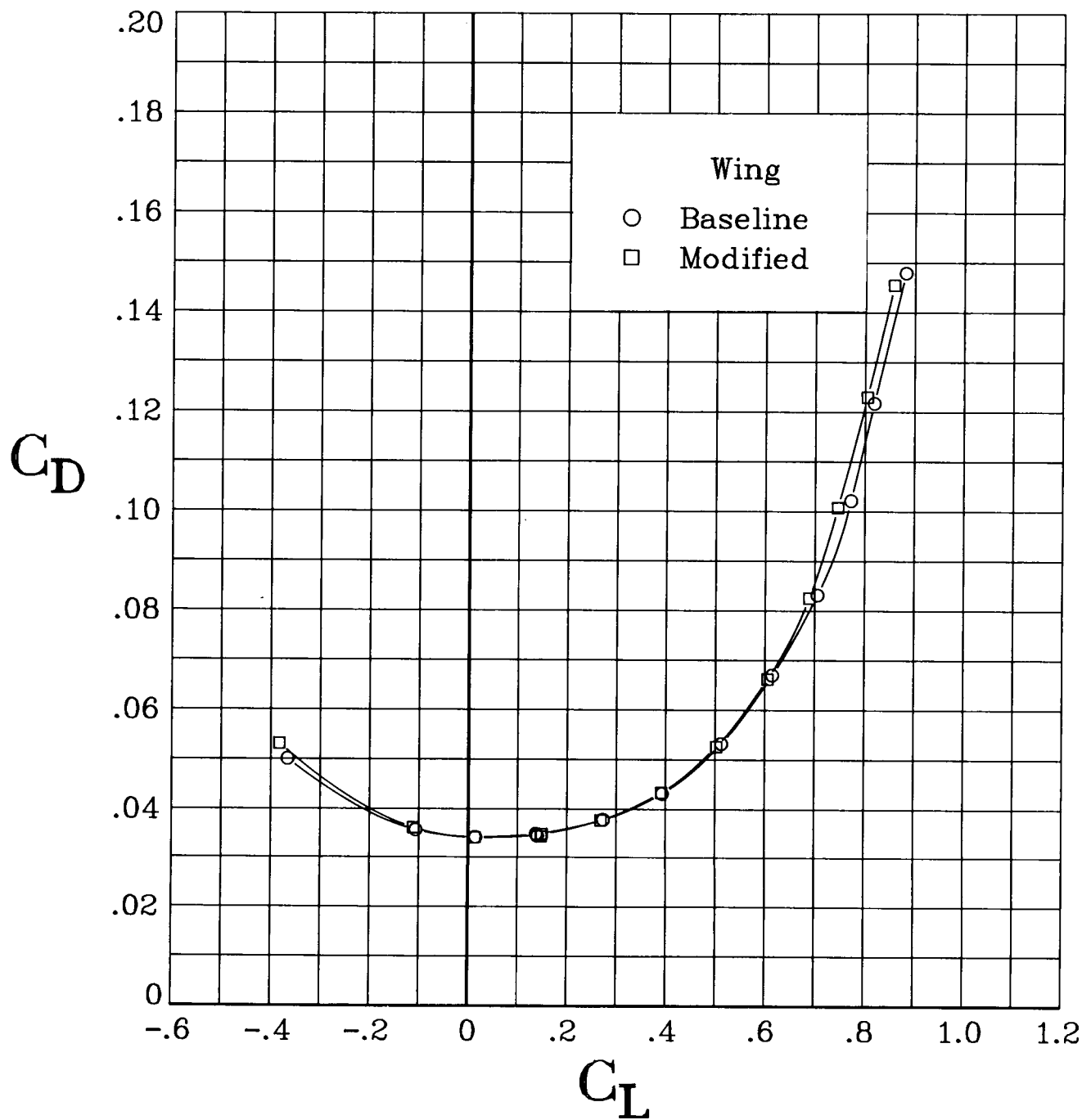
(g) Concluded.

Figure 6. Continued.



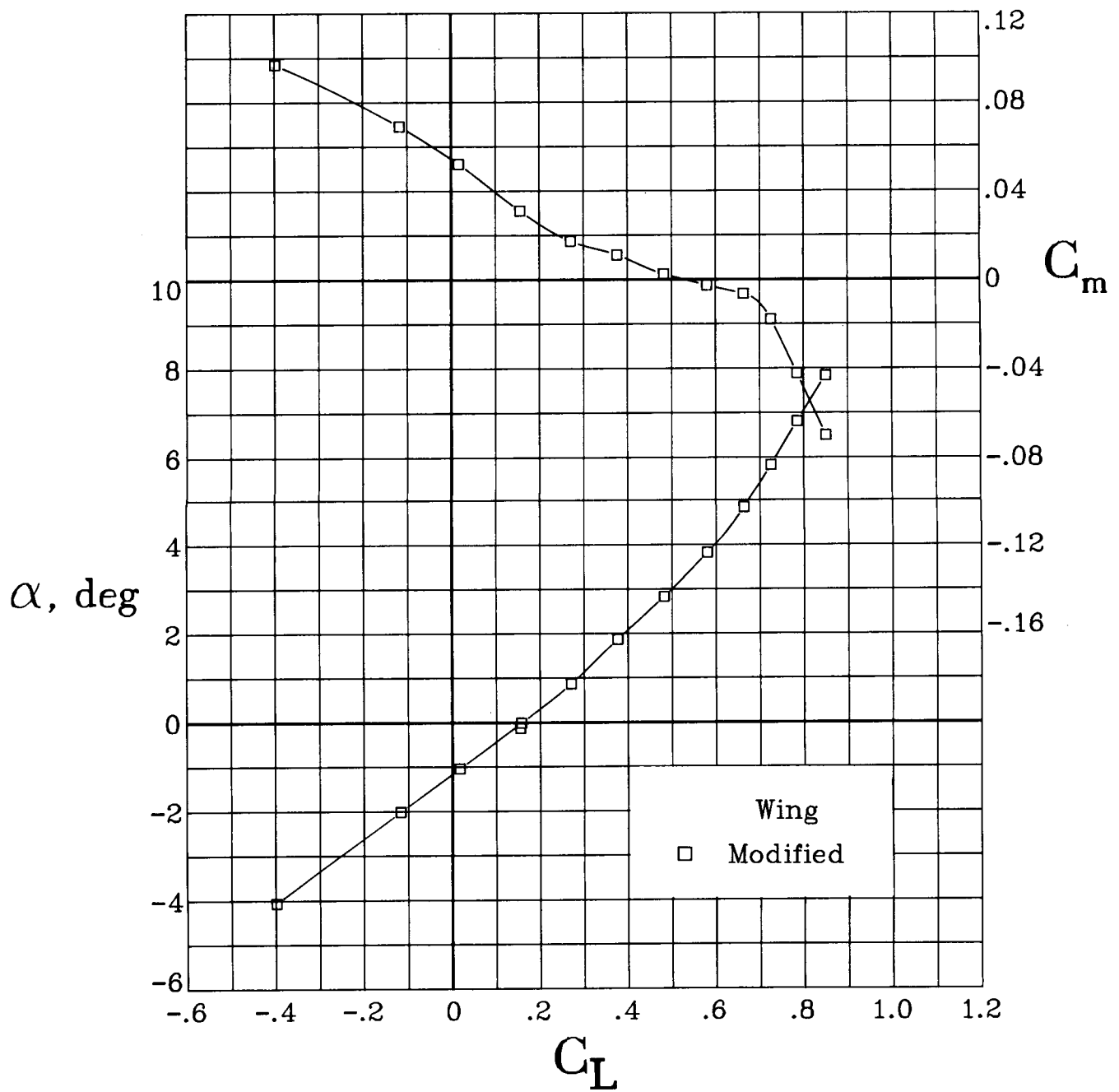
(h) $M = 0.80$.

Figure 6. Continued.



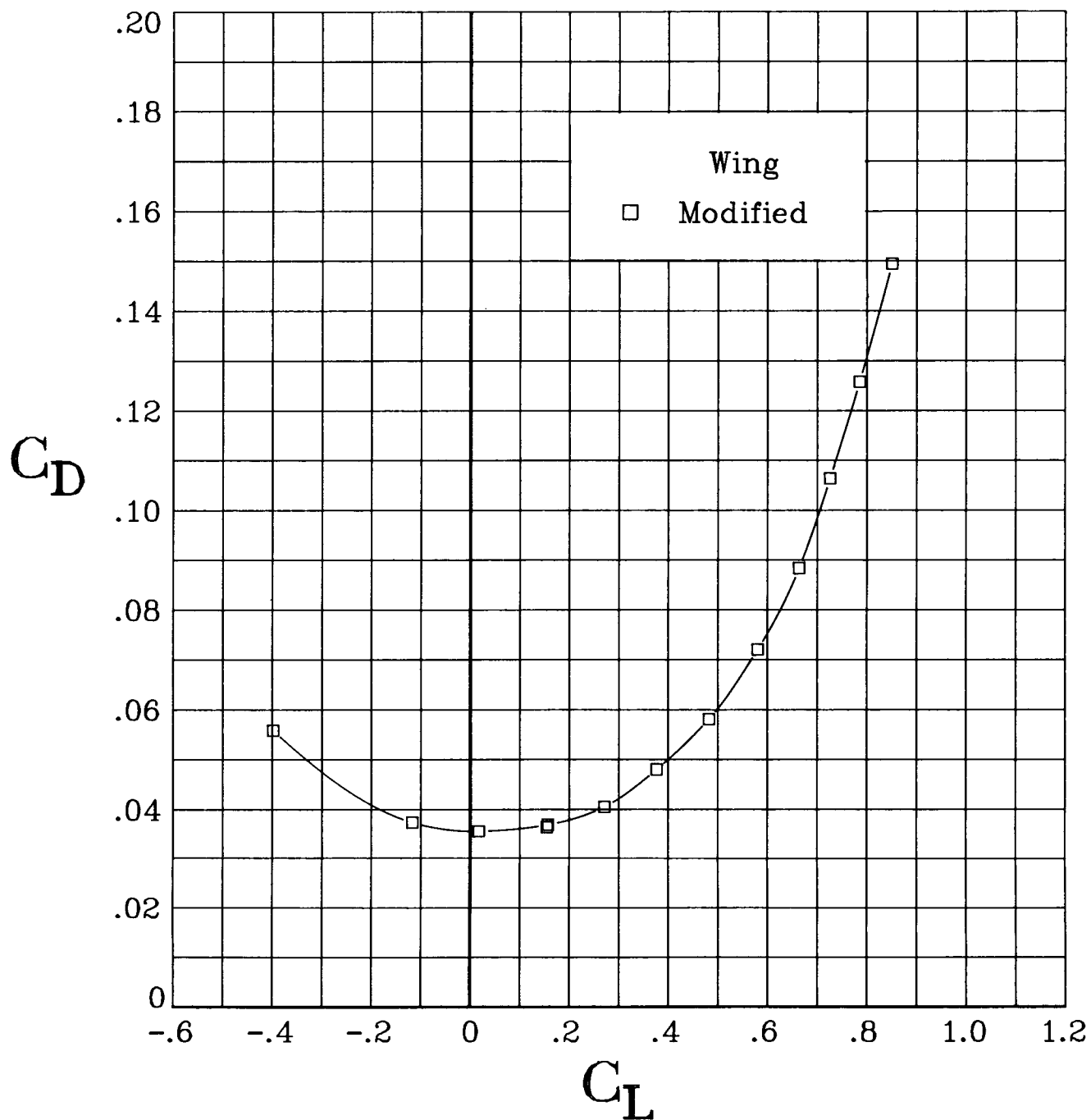
(h) Concluded.

Figure 6. Continued.



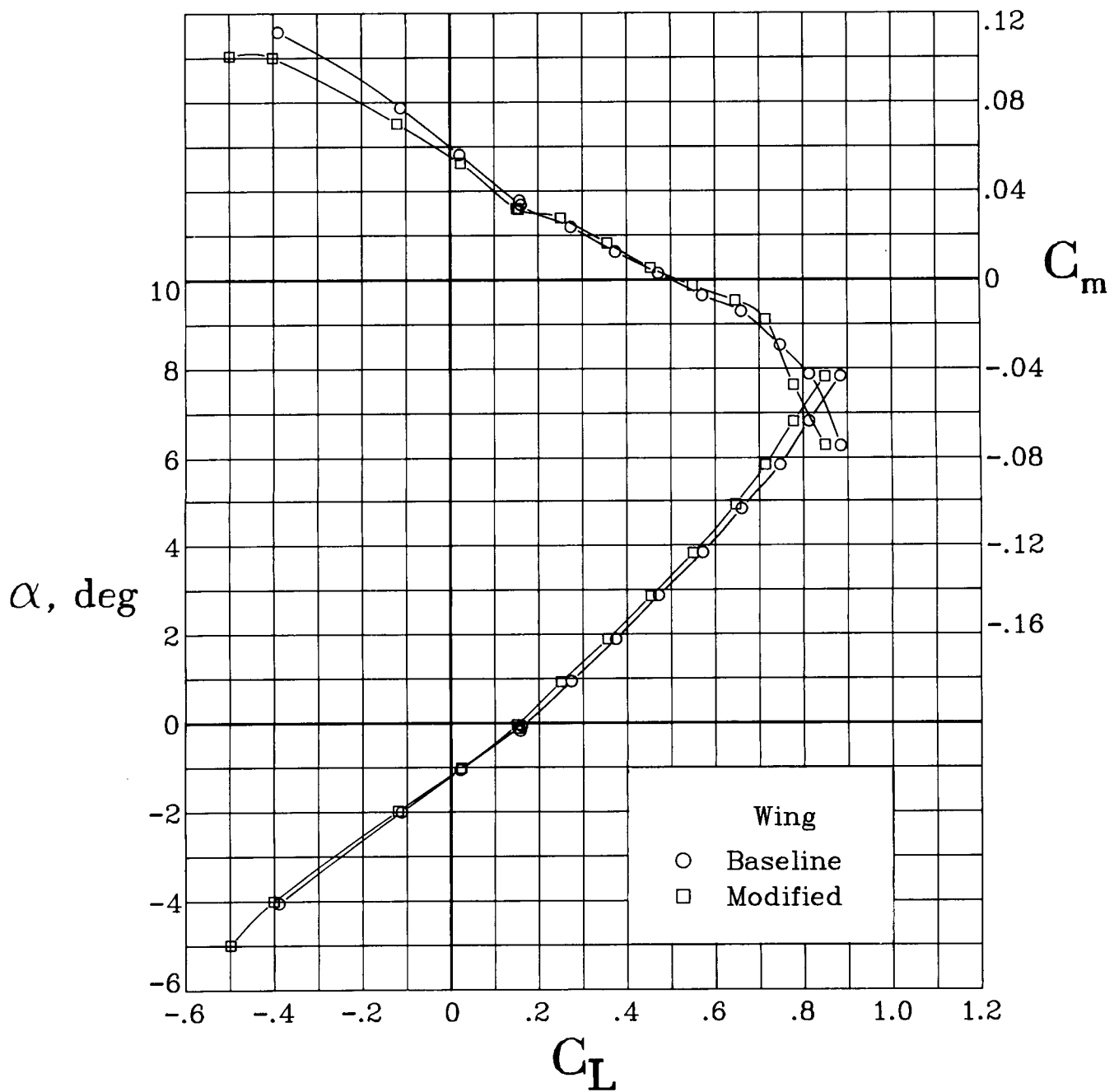
(i) $M = 0.825$.

Figure 6. Continued.



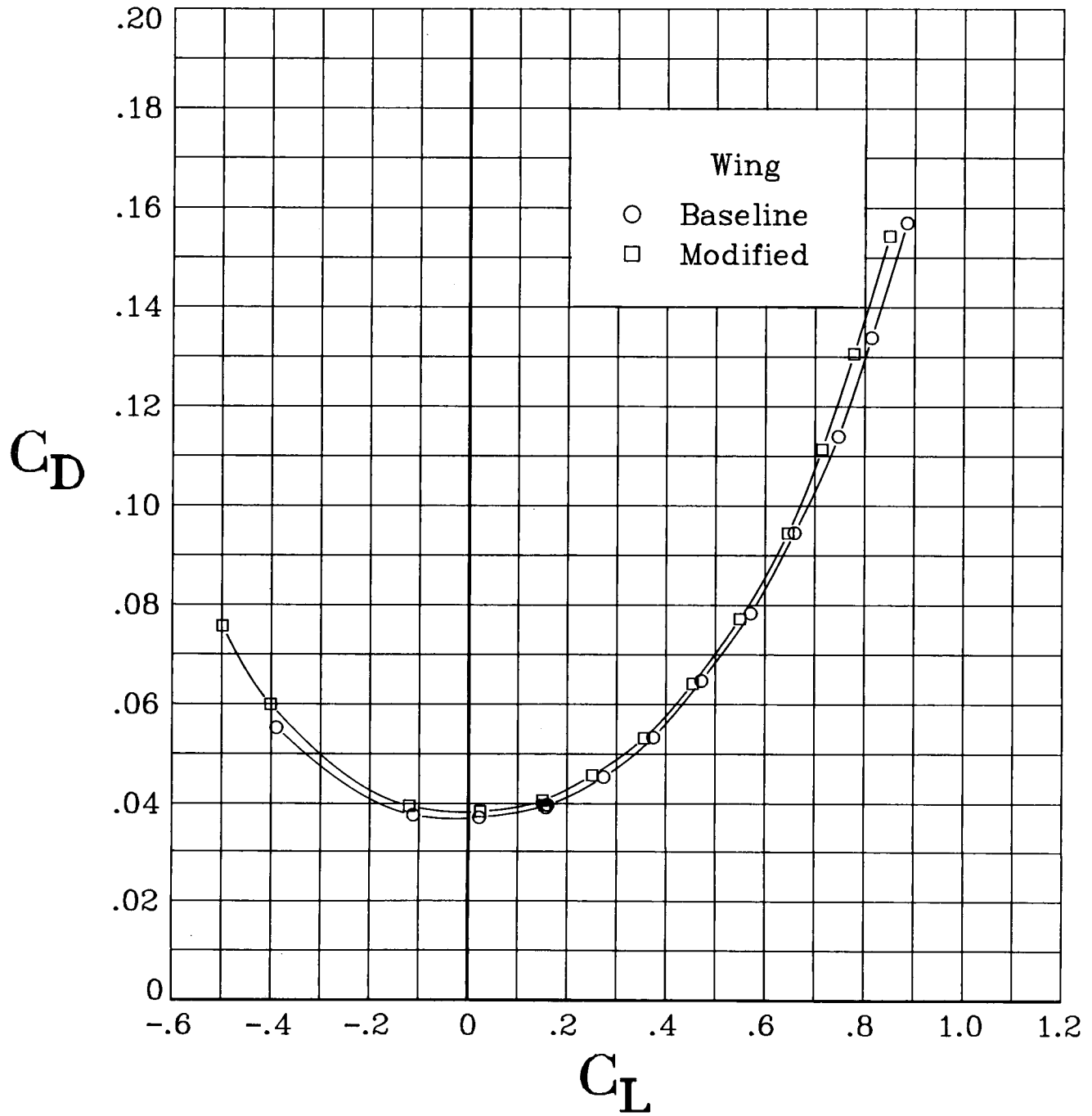
(i) Concluded.

Figure 6. Continued.



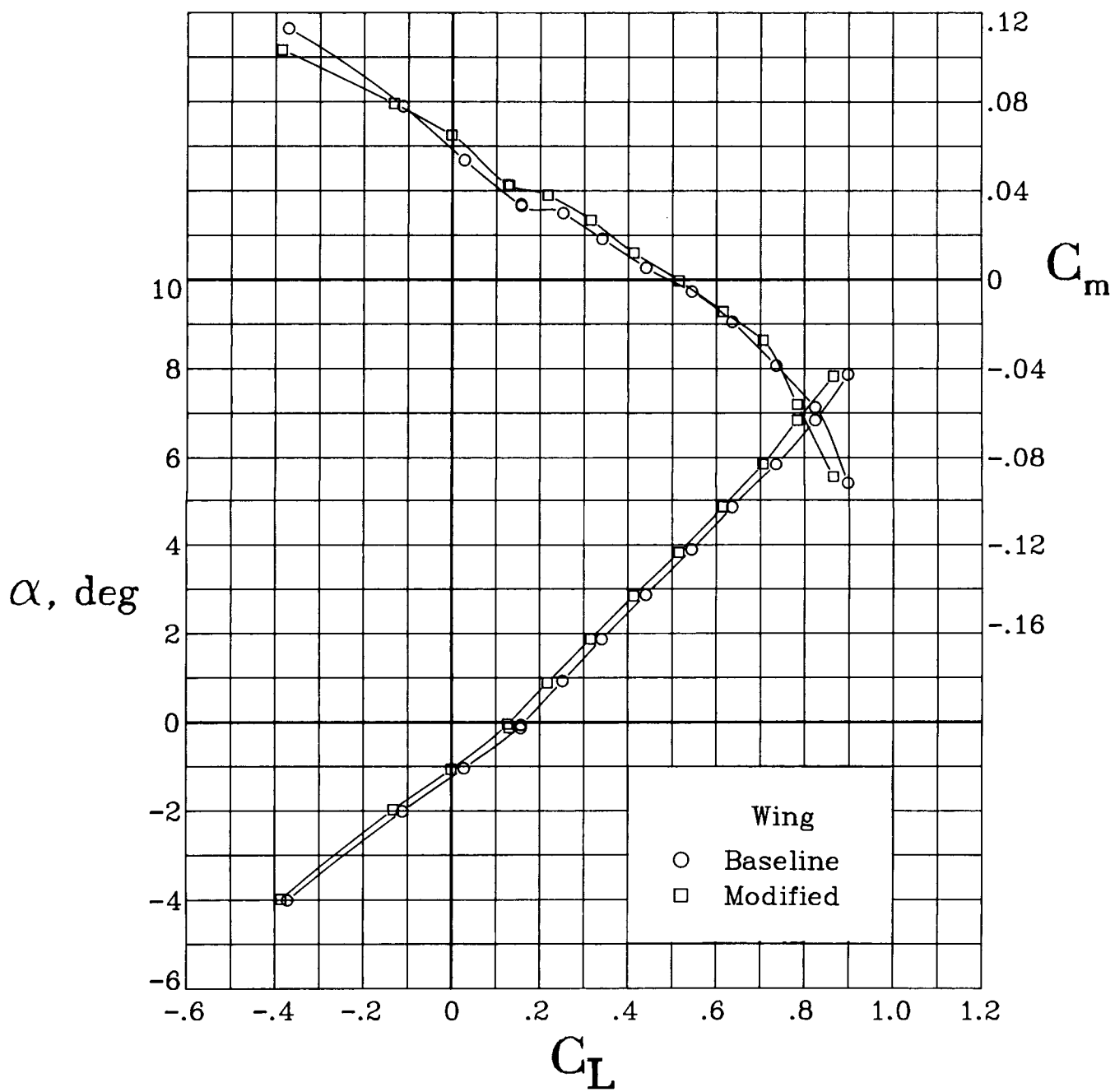
(j) $M = 0.85$.

Figure 6. Continued.



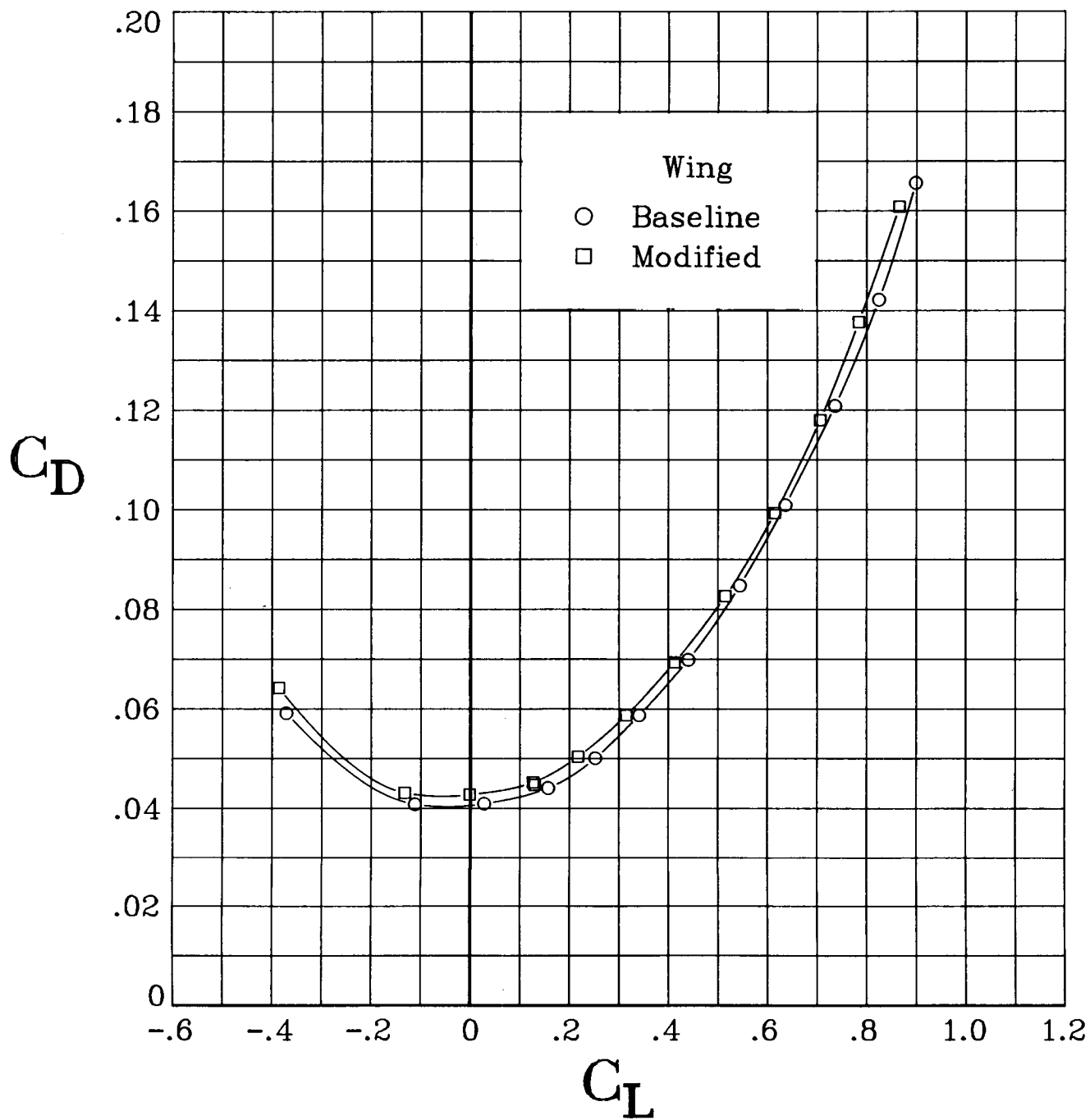
(j) Concluded.

Figure 6. Continued.



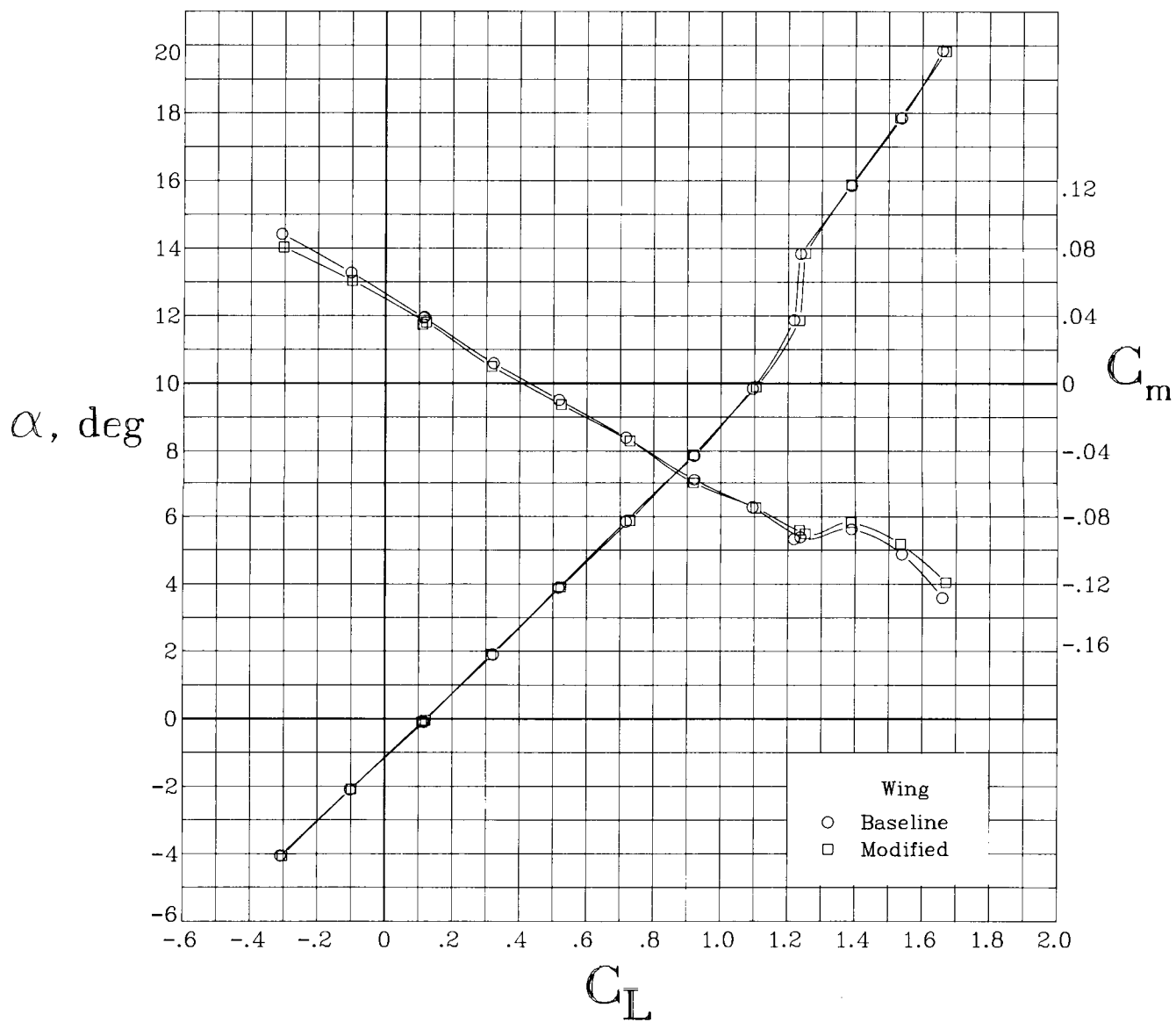
(k) $M = 0.875$.

Figure 6. Continued.



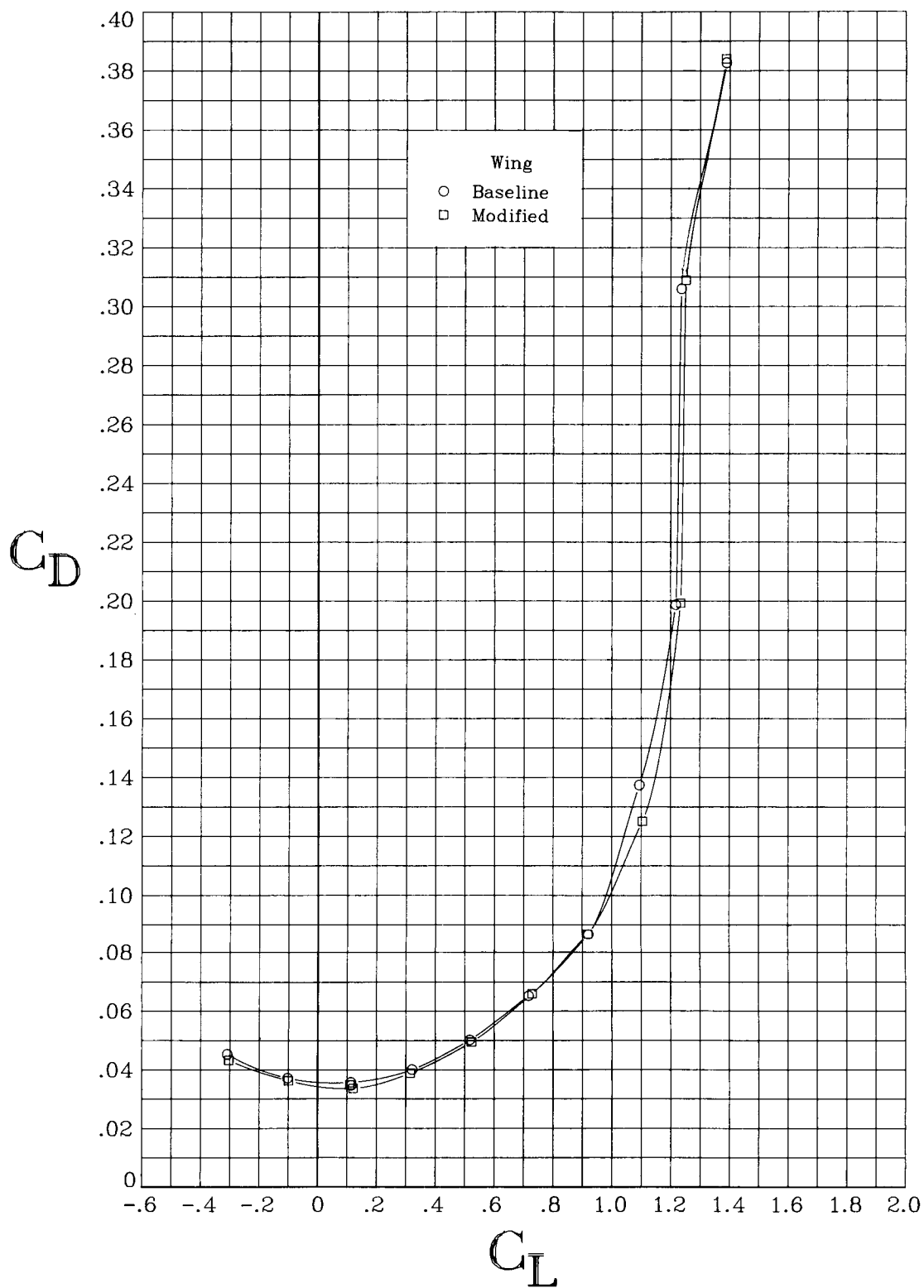
(k) Concluded.

Figure 6. Concluded.



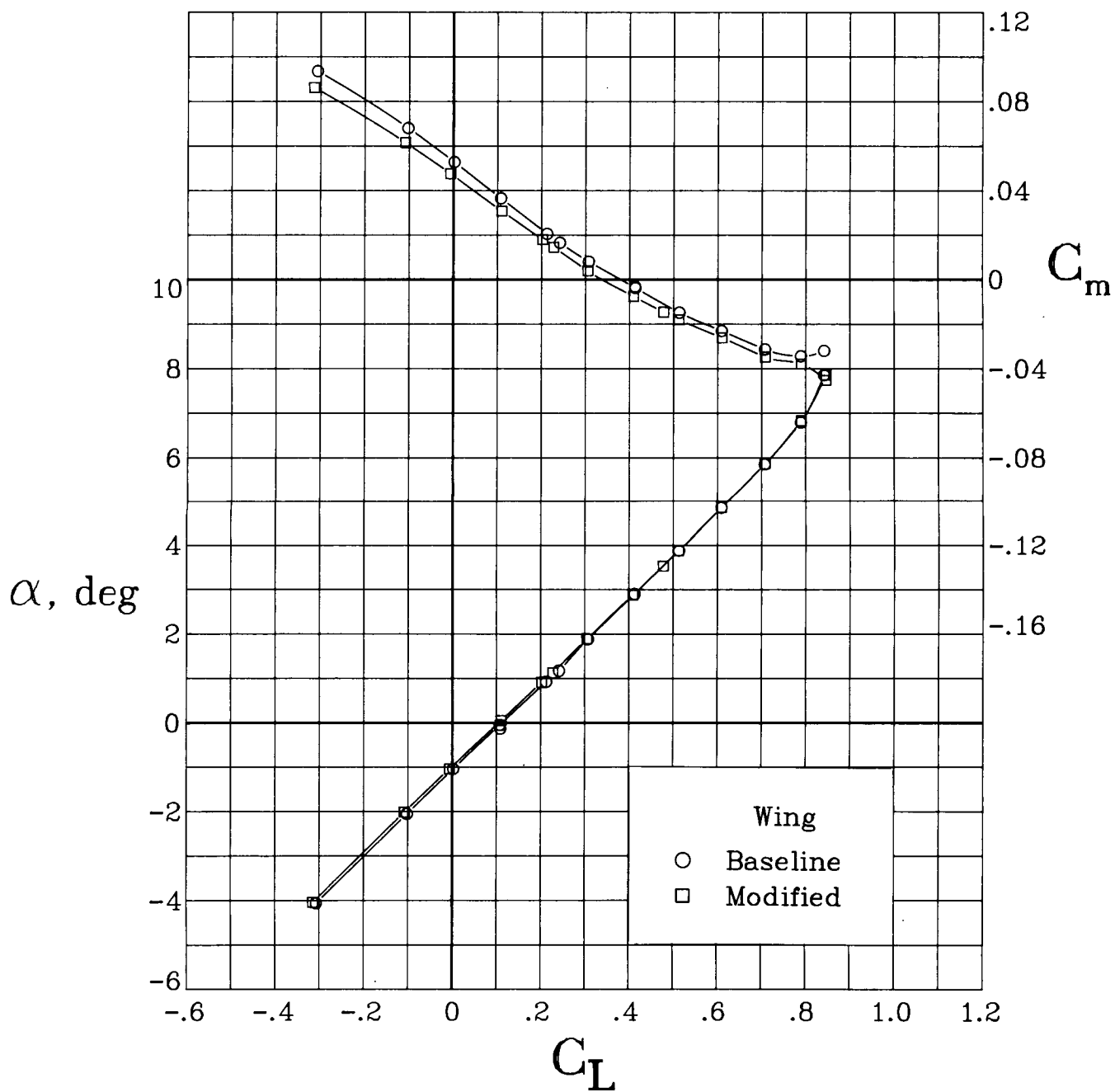
(a) $M = 0.20$.

Figure 7. Longitudinal aerodynamic characteristics of the baseline and modified wing configurations, with wings swept 30° . $\beta = 0^\circ$.



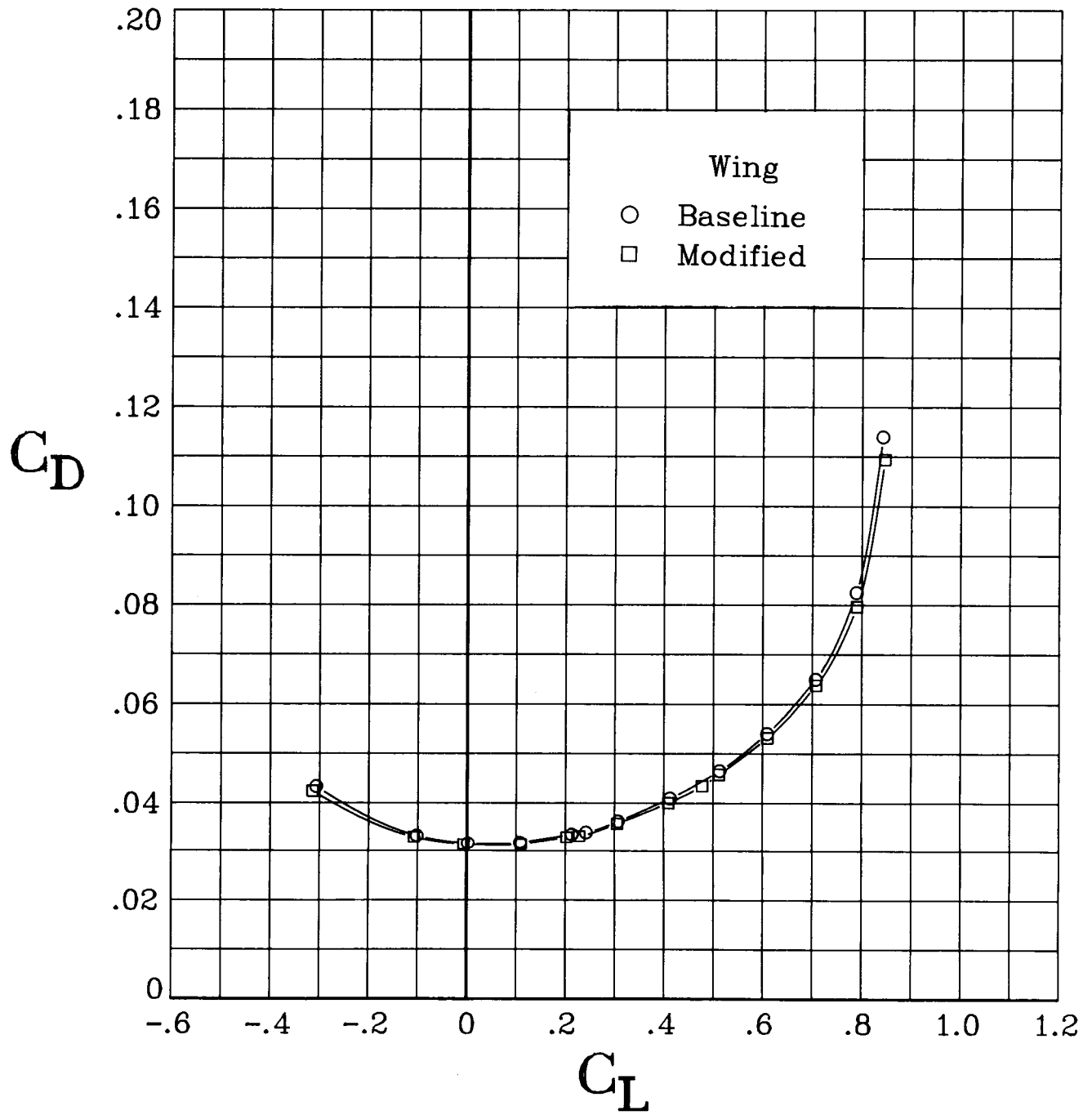
(a) Concluded.

Figure 7. Continued.



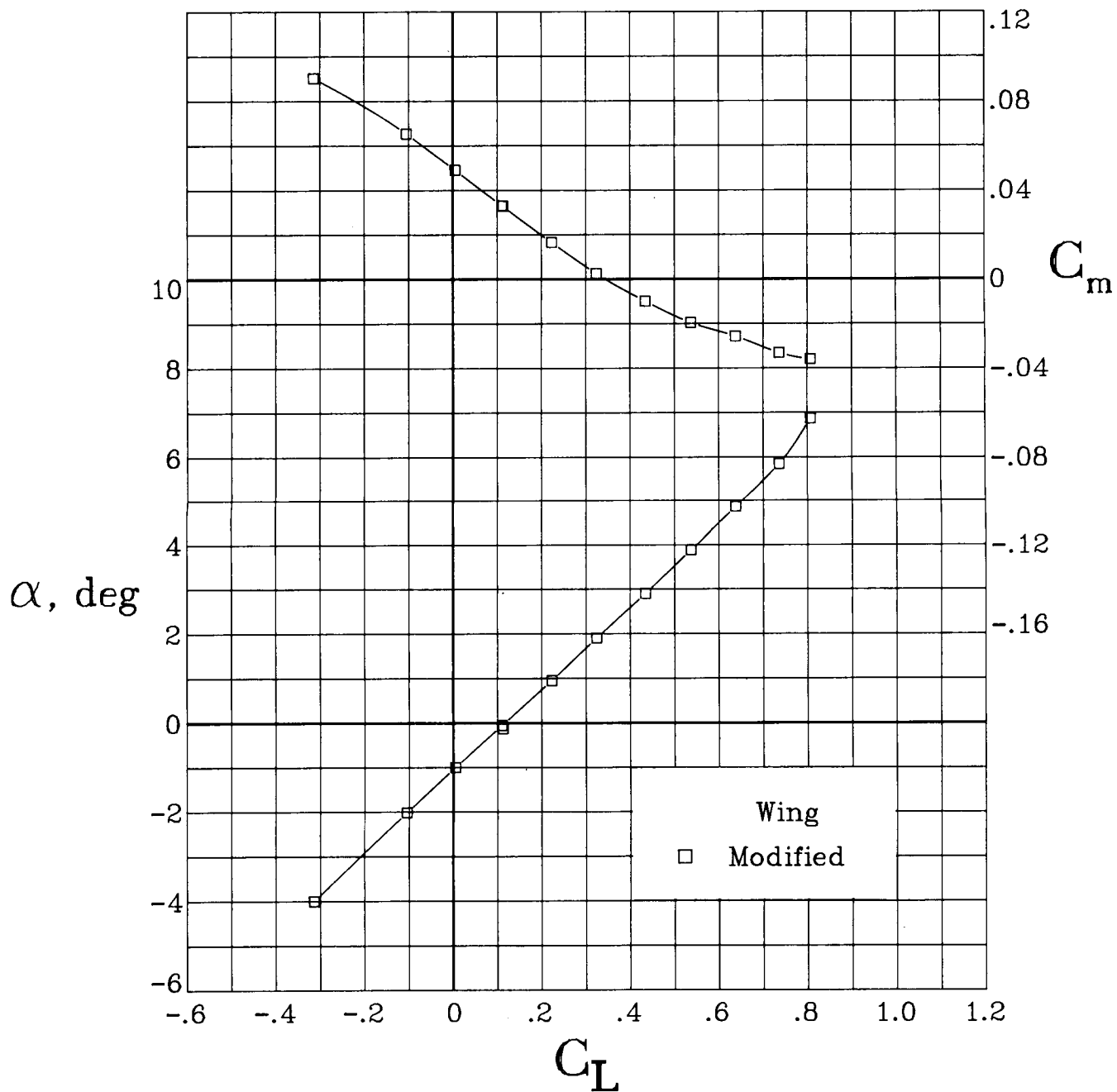
(b) $M = 0.60$.

Figure 7. Continued.



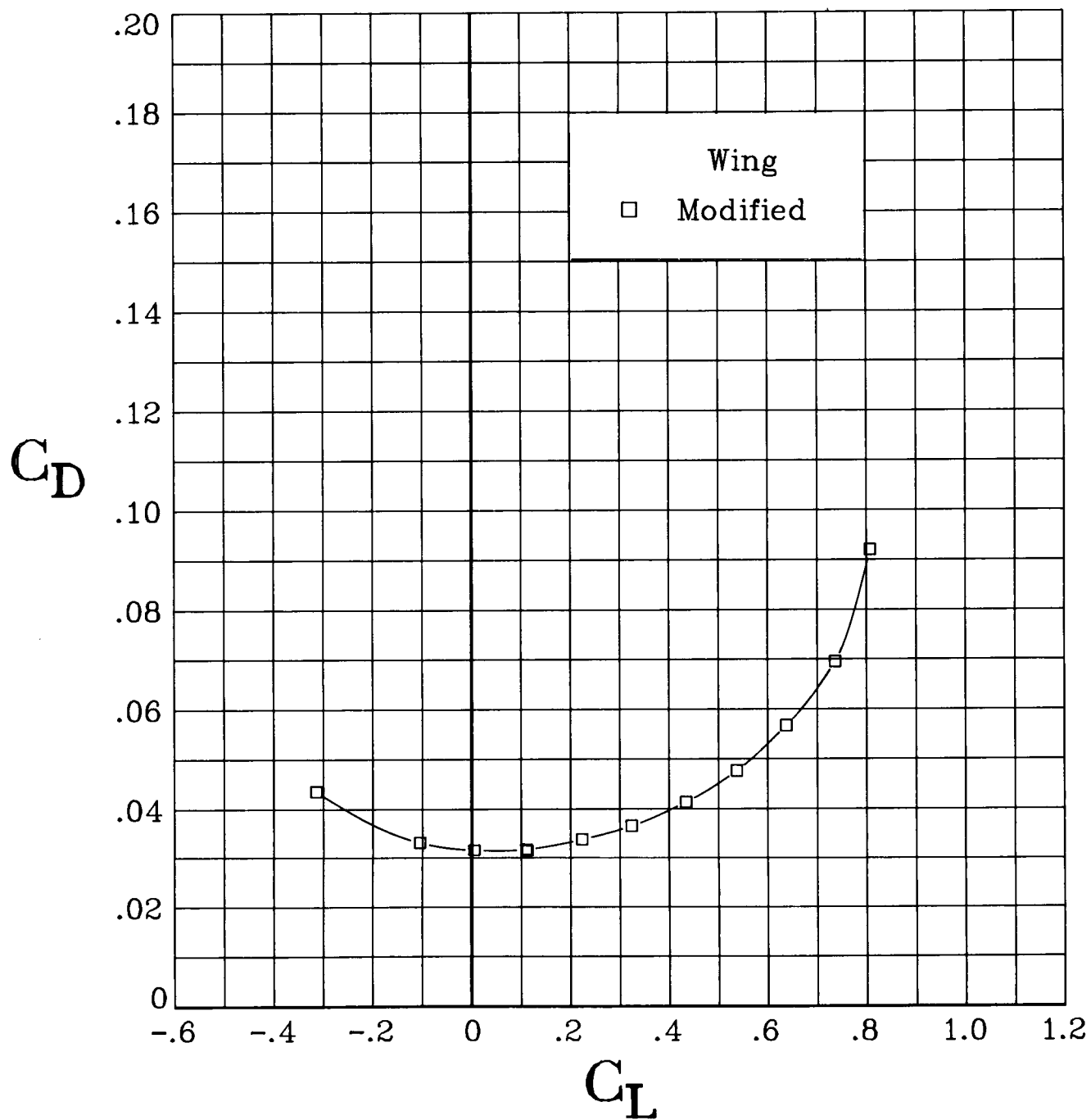
(b) Concluded.

Figure 7. Continued.



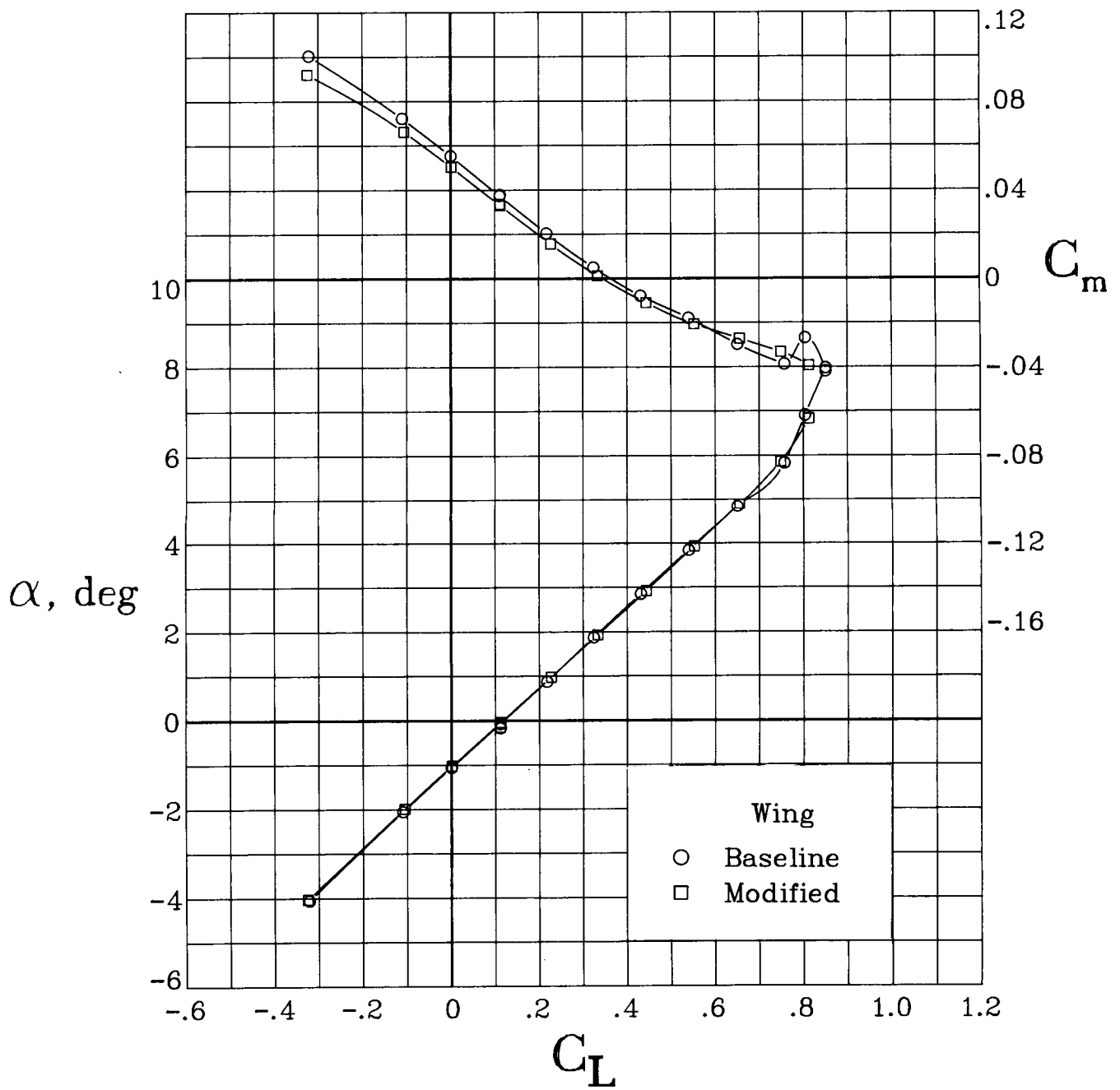
(c) $M = 0.675$.

Figure 7. Continued.



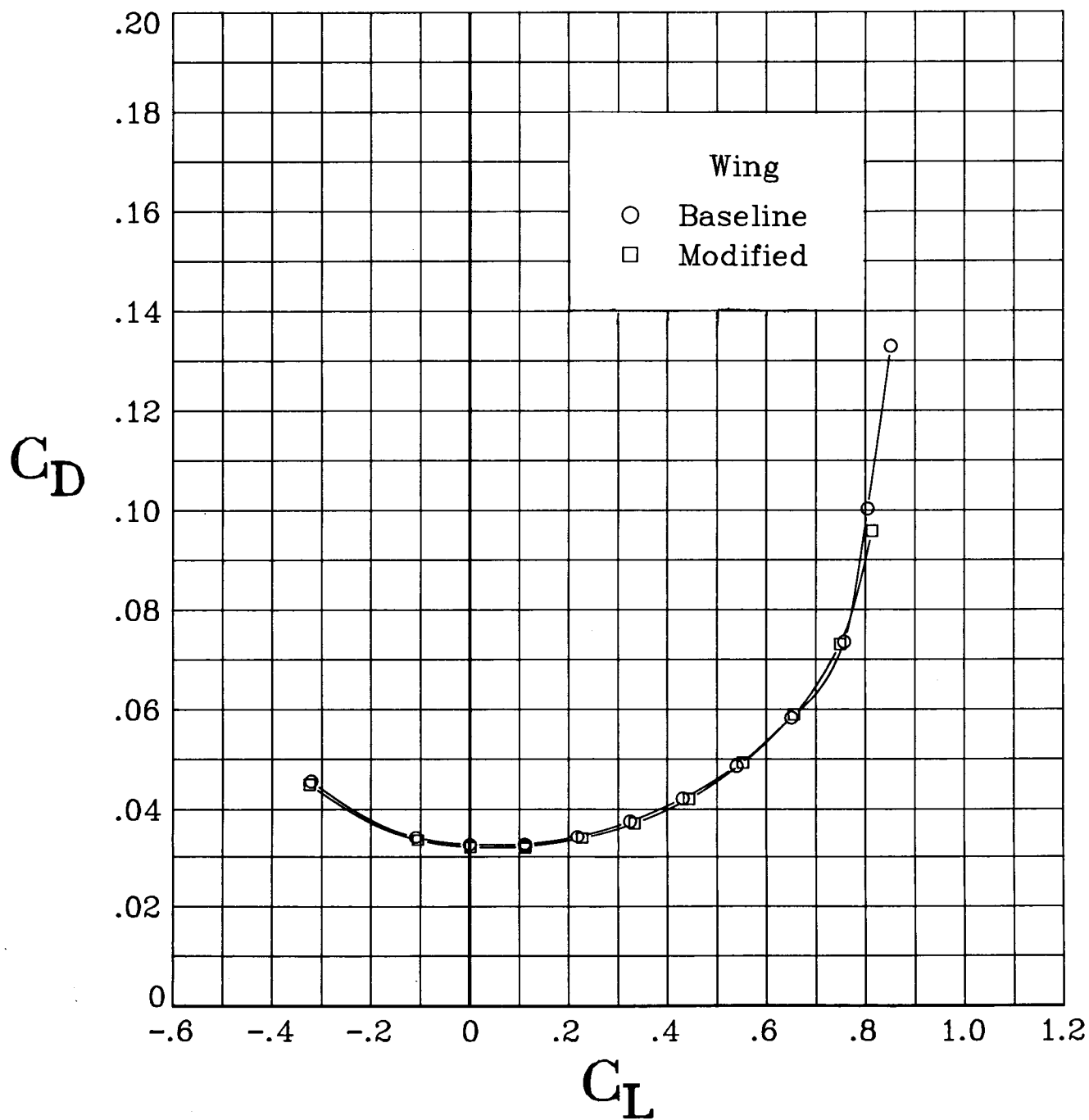
(c) Concluded.

Figure 7. Continued.



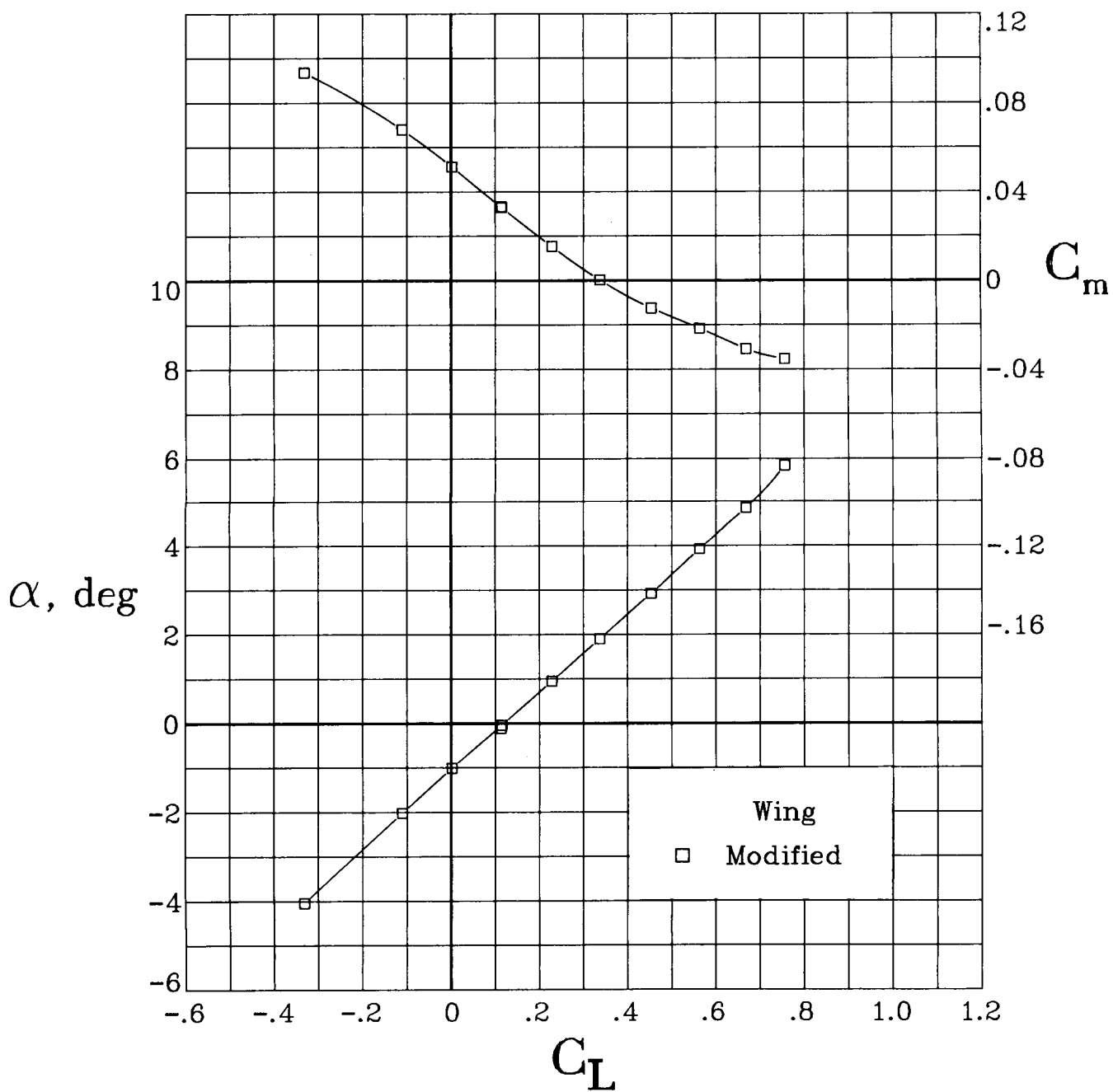
(d) $M = 0.70$.

Figure 7. Continued.



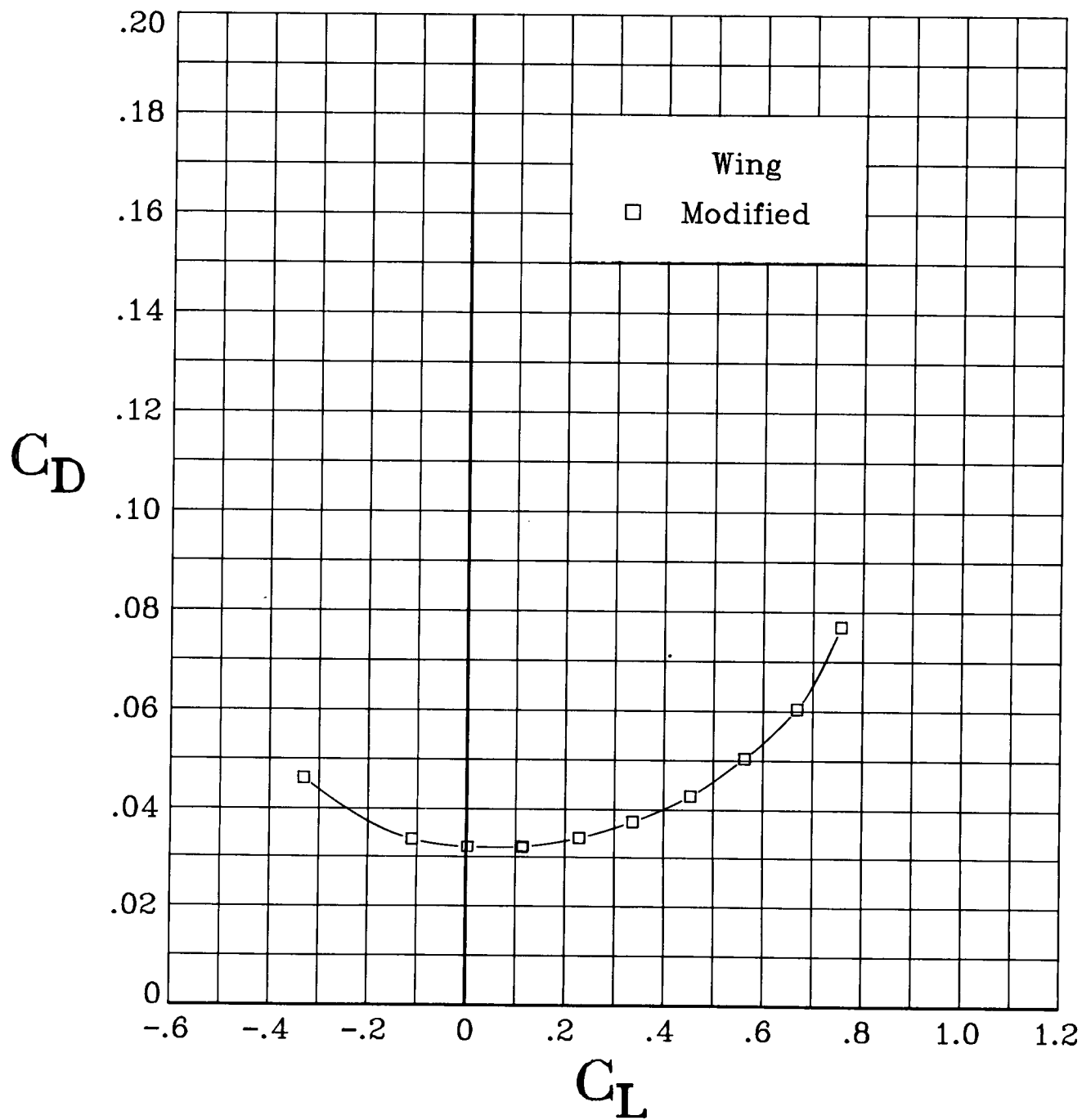
(d) Concluded.

Figure 7. Continued.



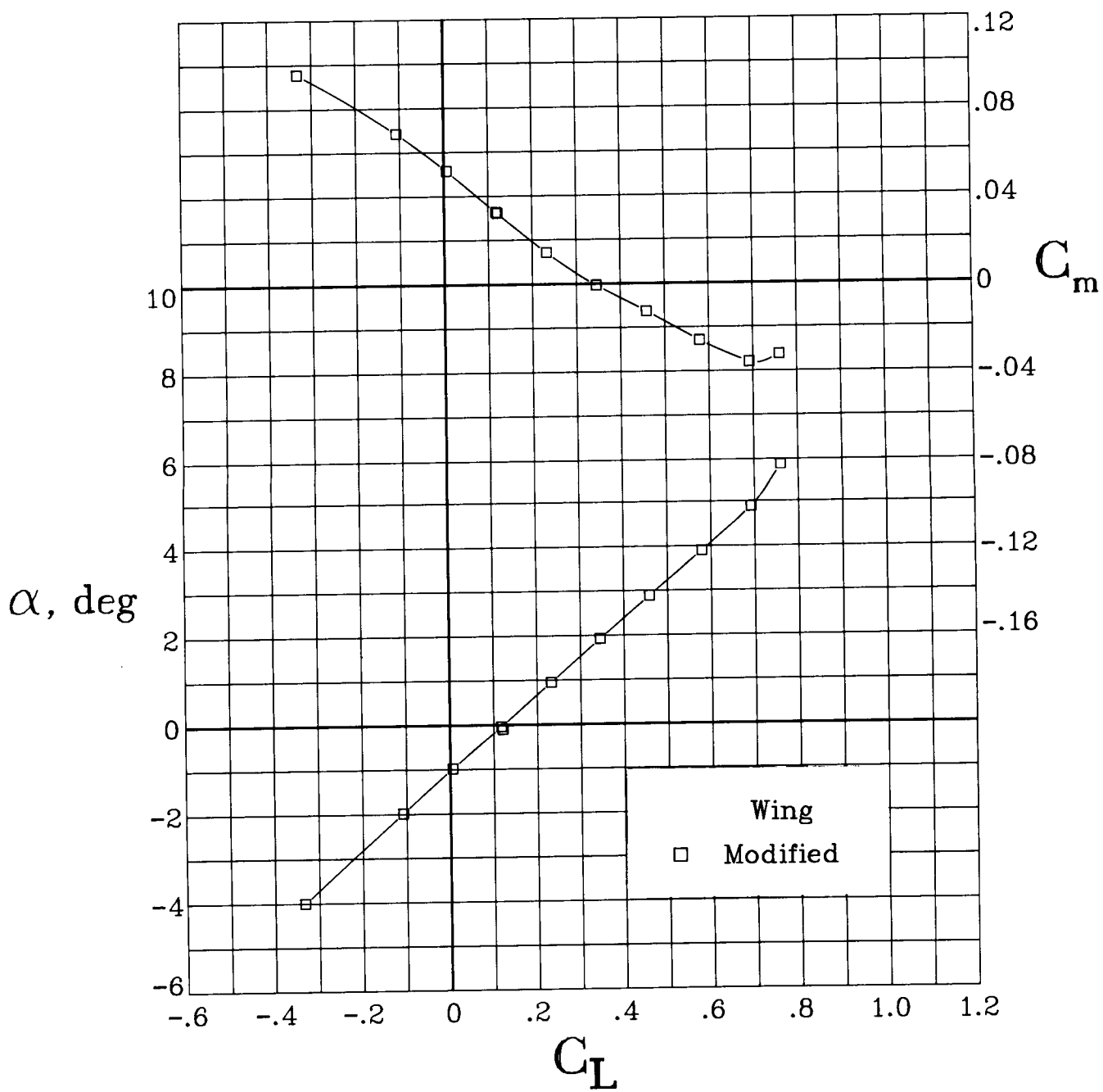
(e) $M = 0.725$.

Figure 7. Continued.



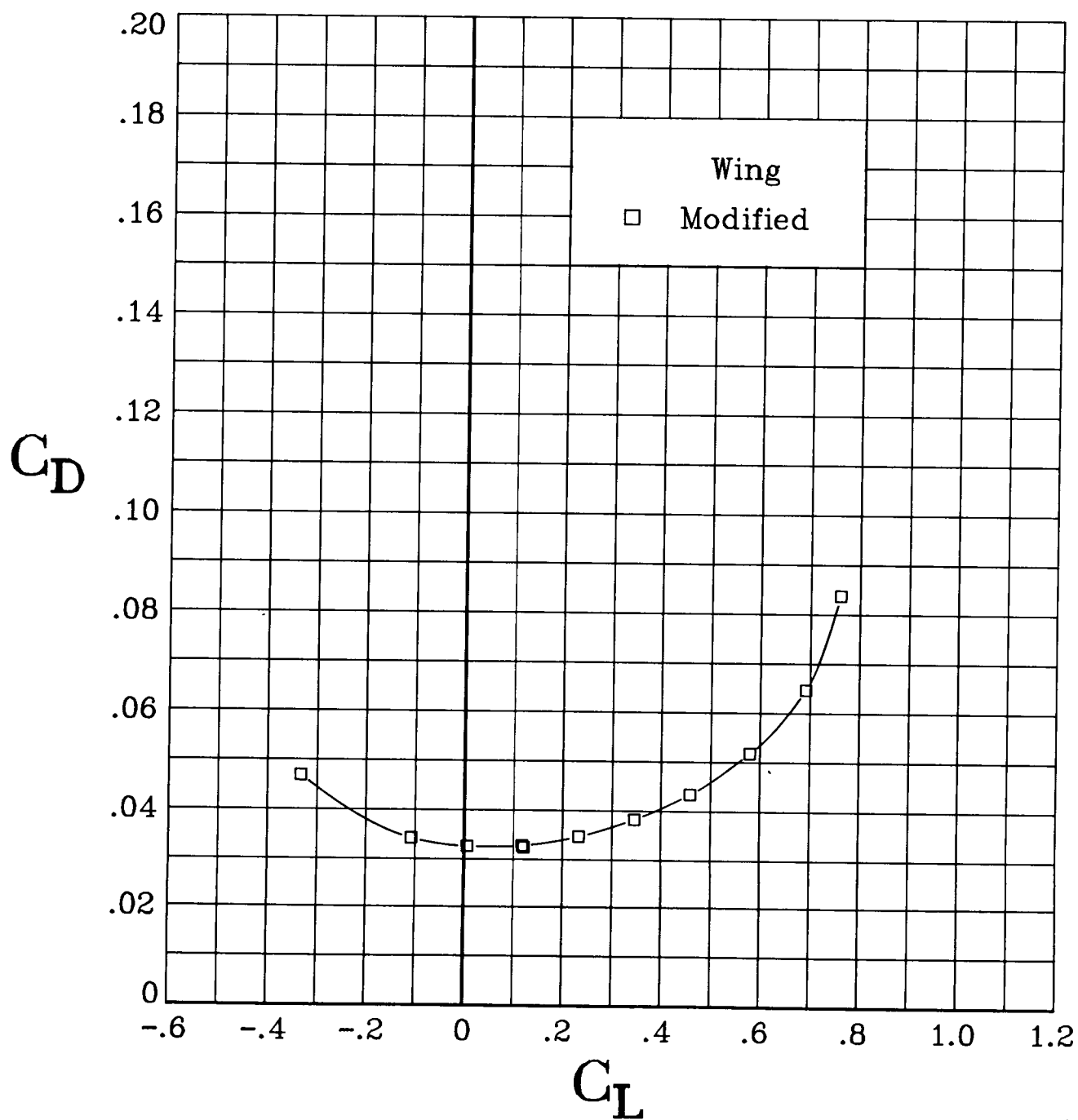
(e) Concluded.

Figure 7. Continued.



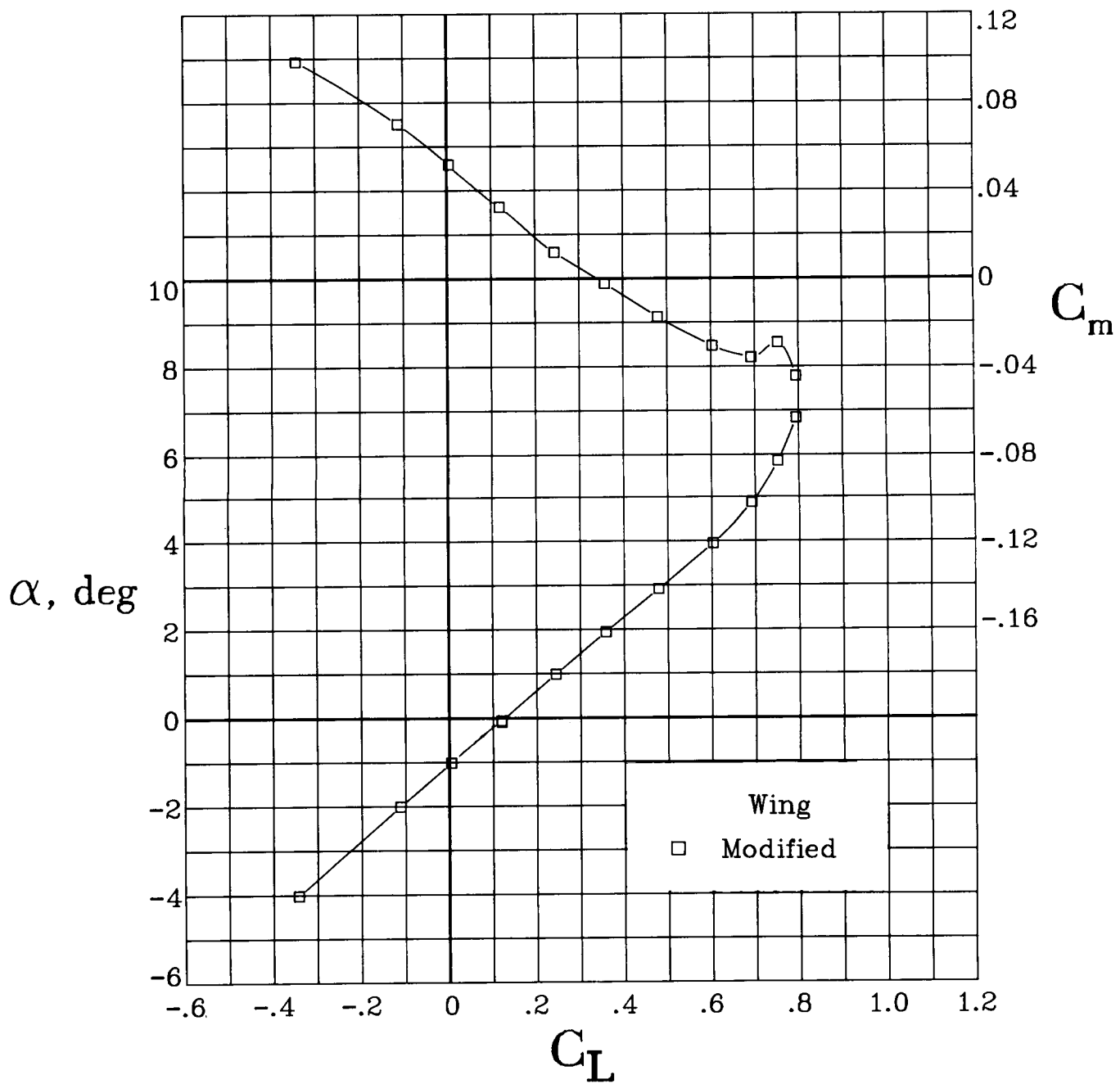
(f) $M = 0.75$.

Figure 7. Continued.



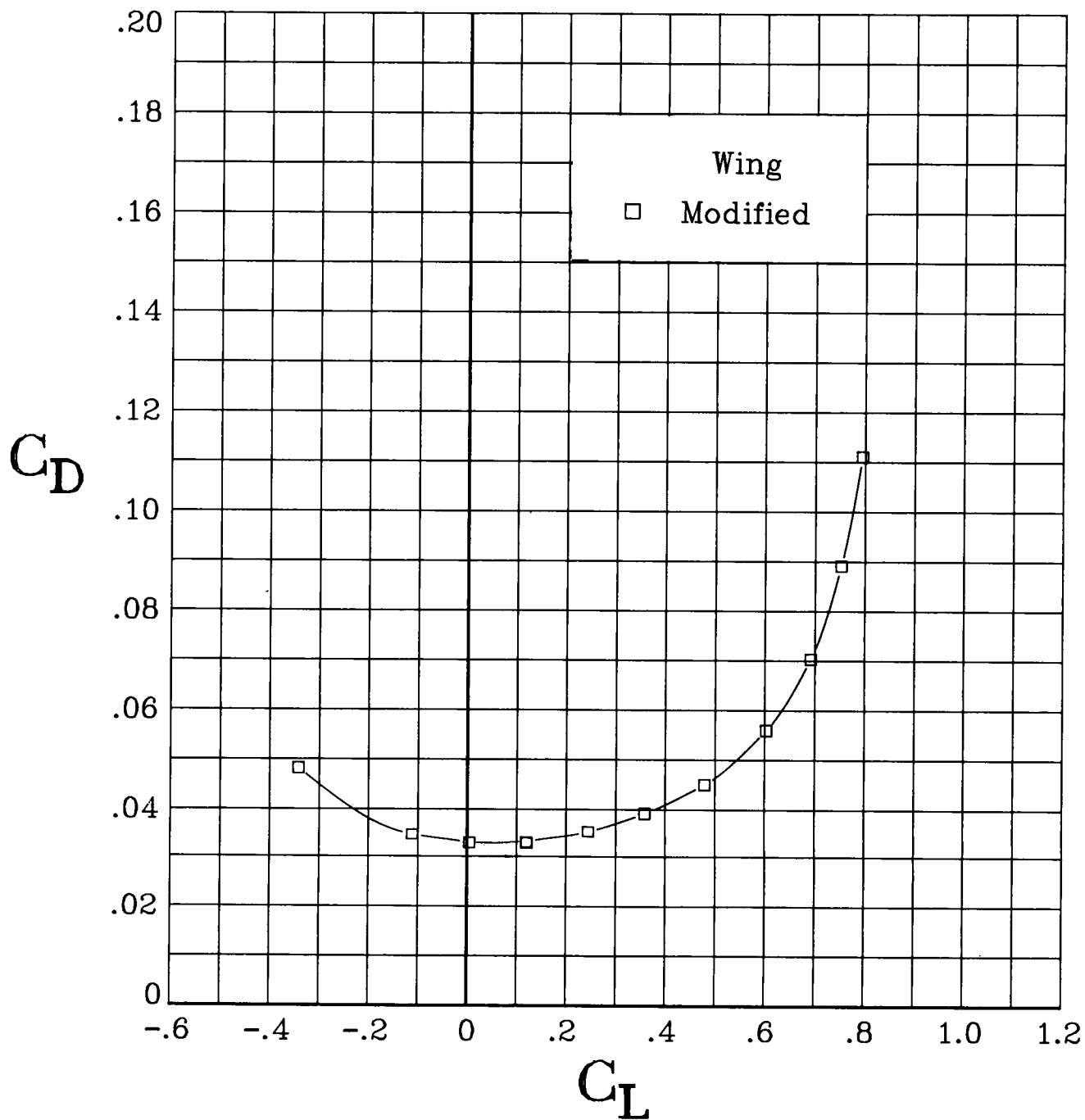
(f) Concluded.

Figure 7. Continued.



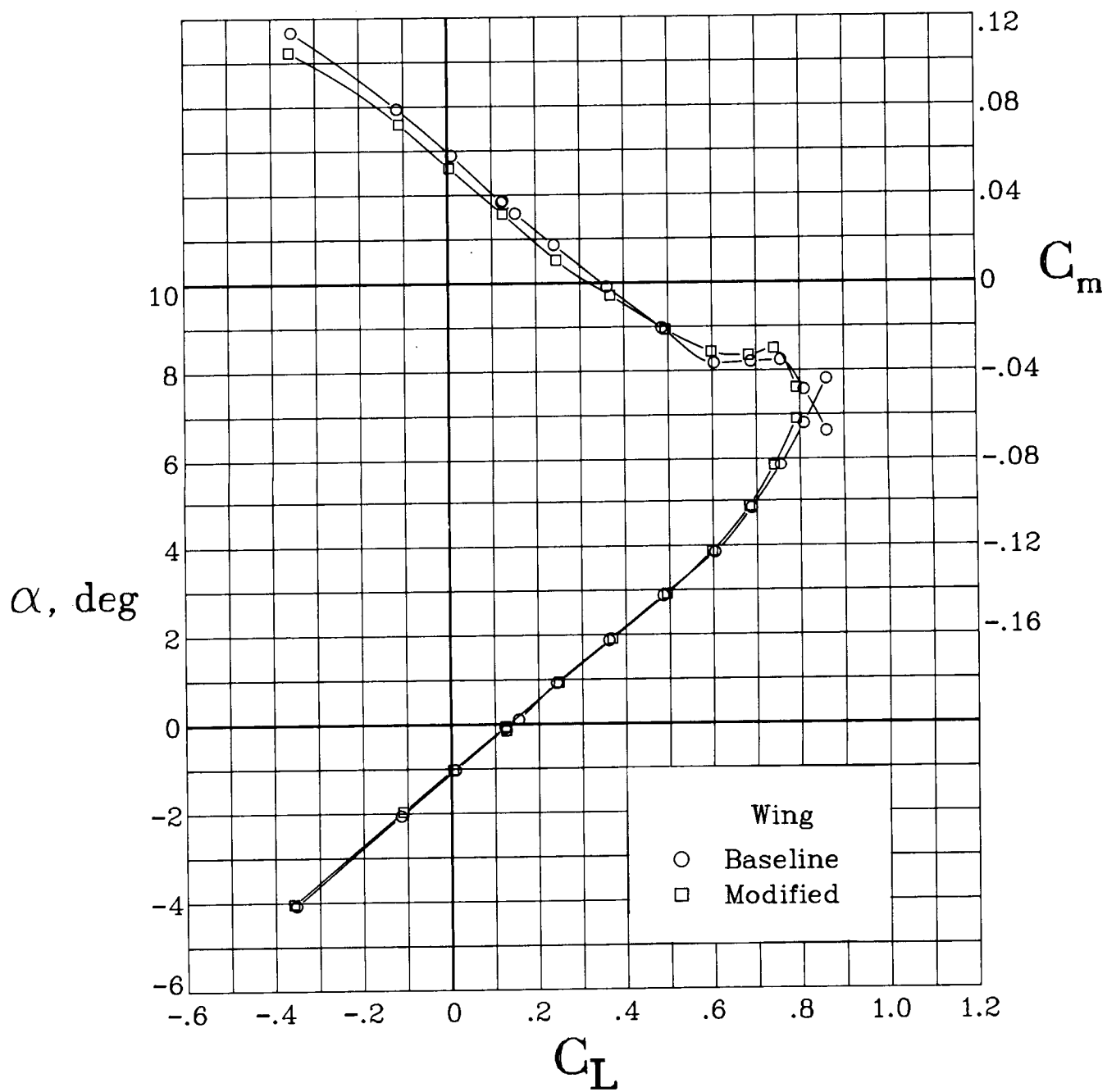
(g) $M = 0.775$.

Figure 7. Continued.



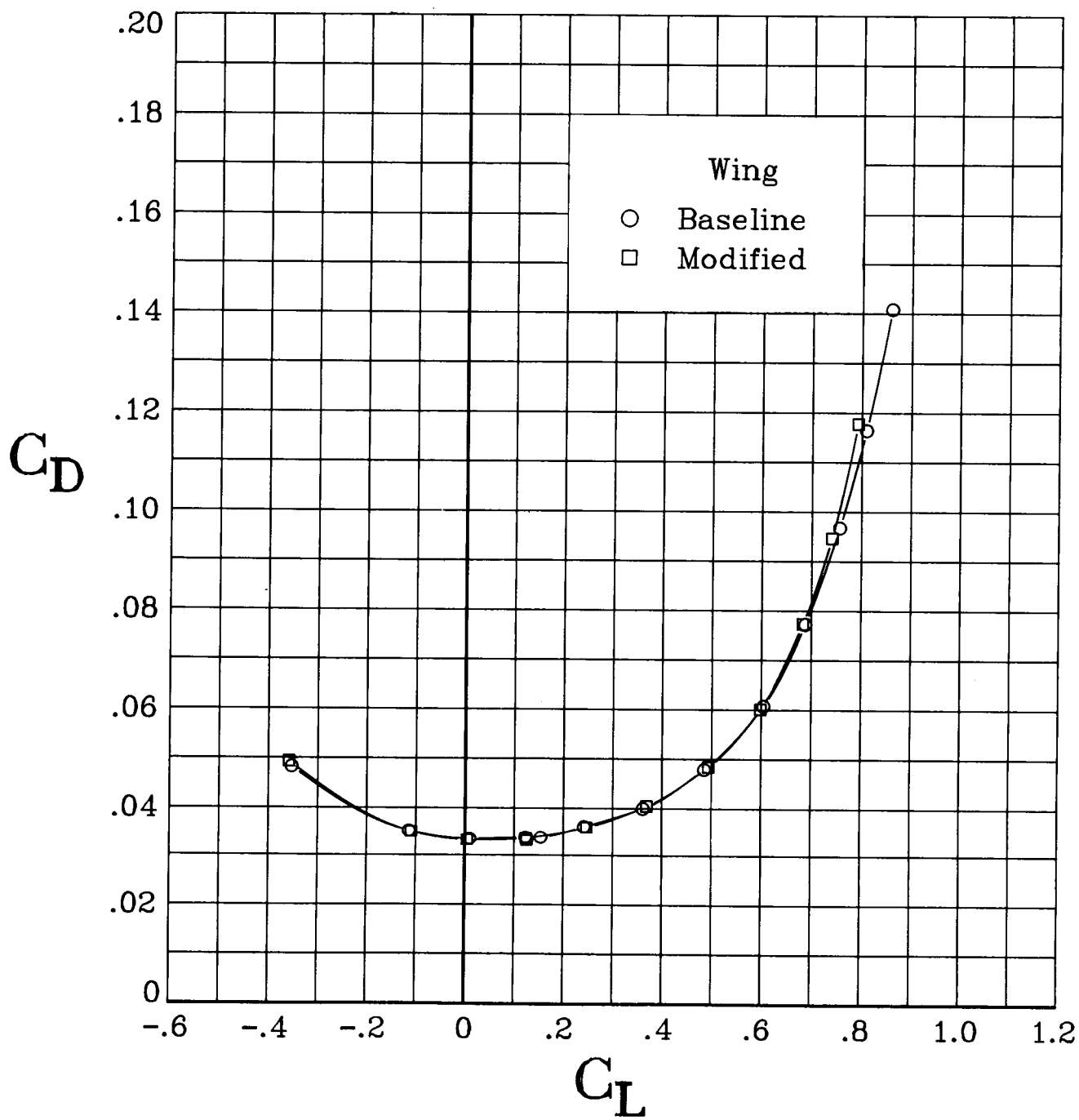
(g) Concluded.

Figure 7. Continued.



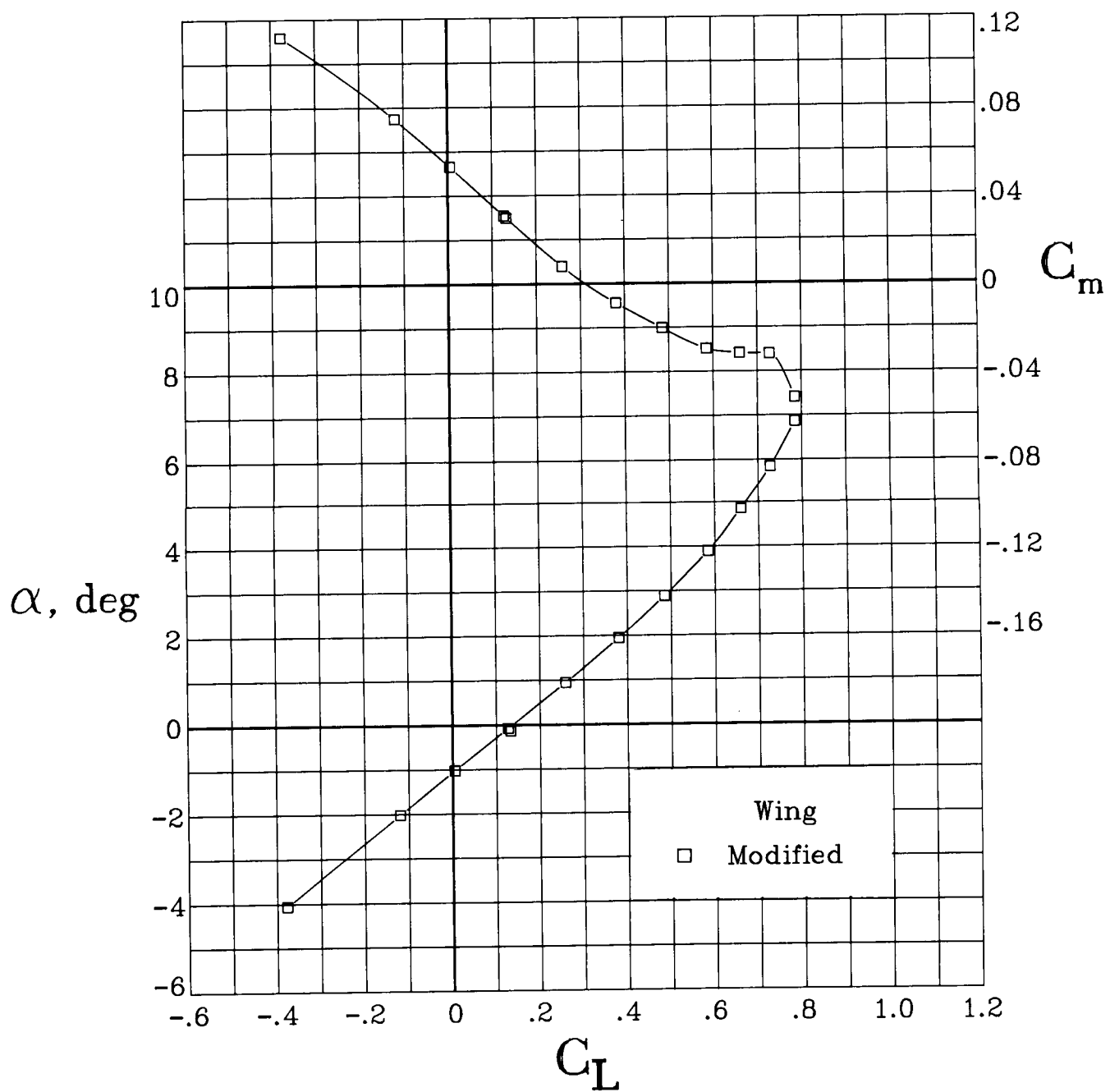
(h) $M = 0.80$.

Figure 7. Continued.



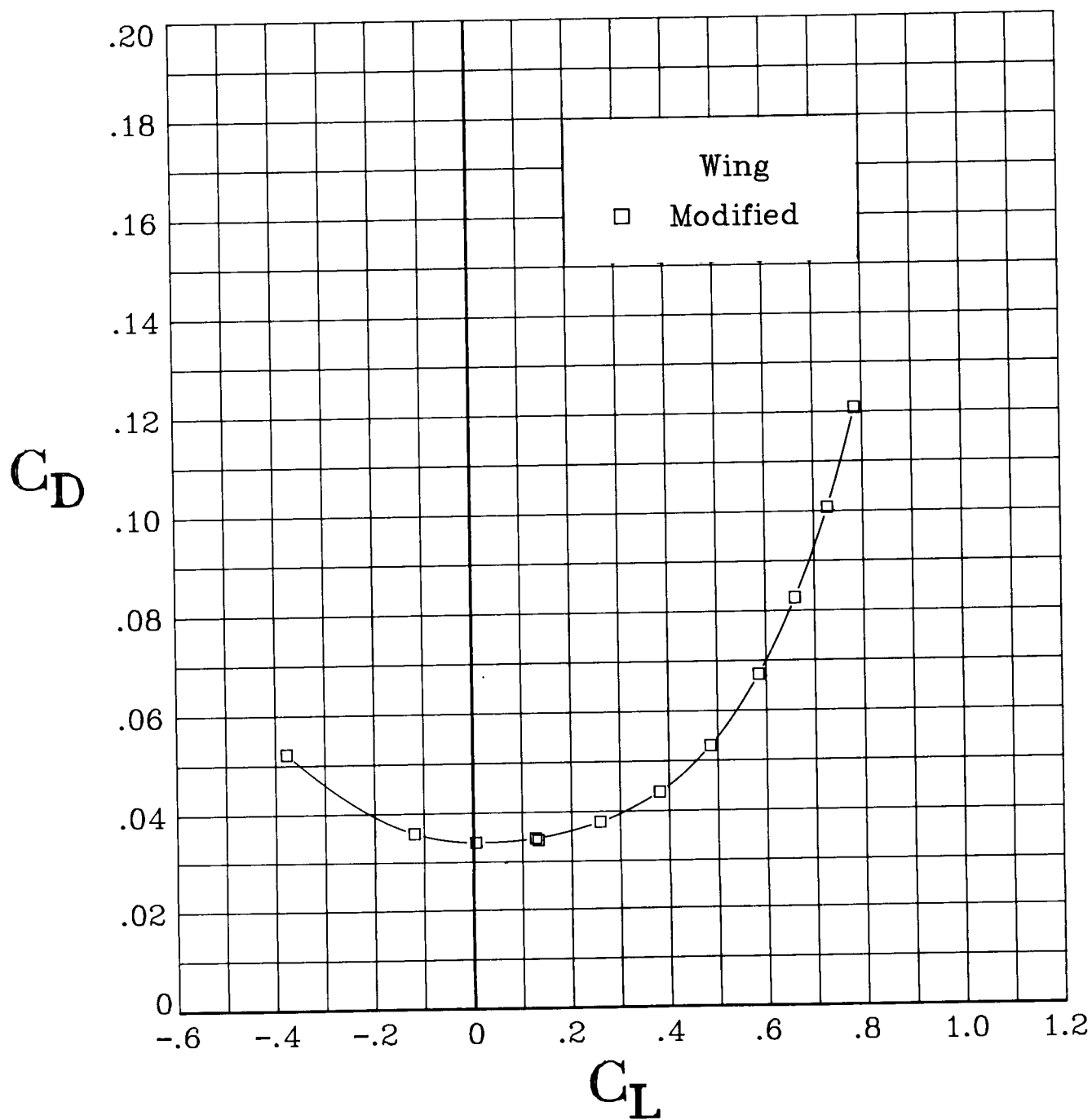
(h) Concluded.

Figure 7. Continued.



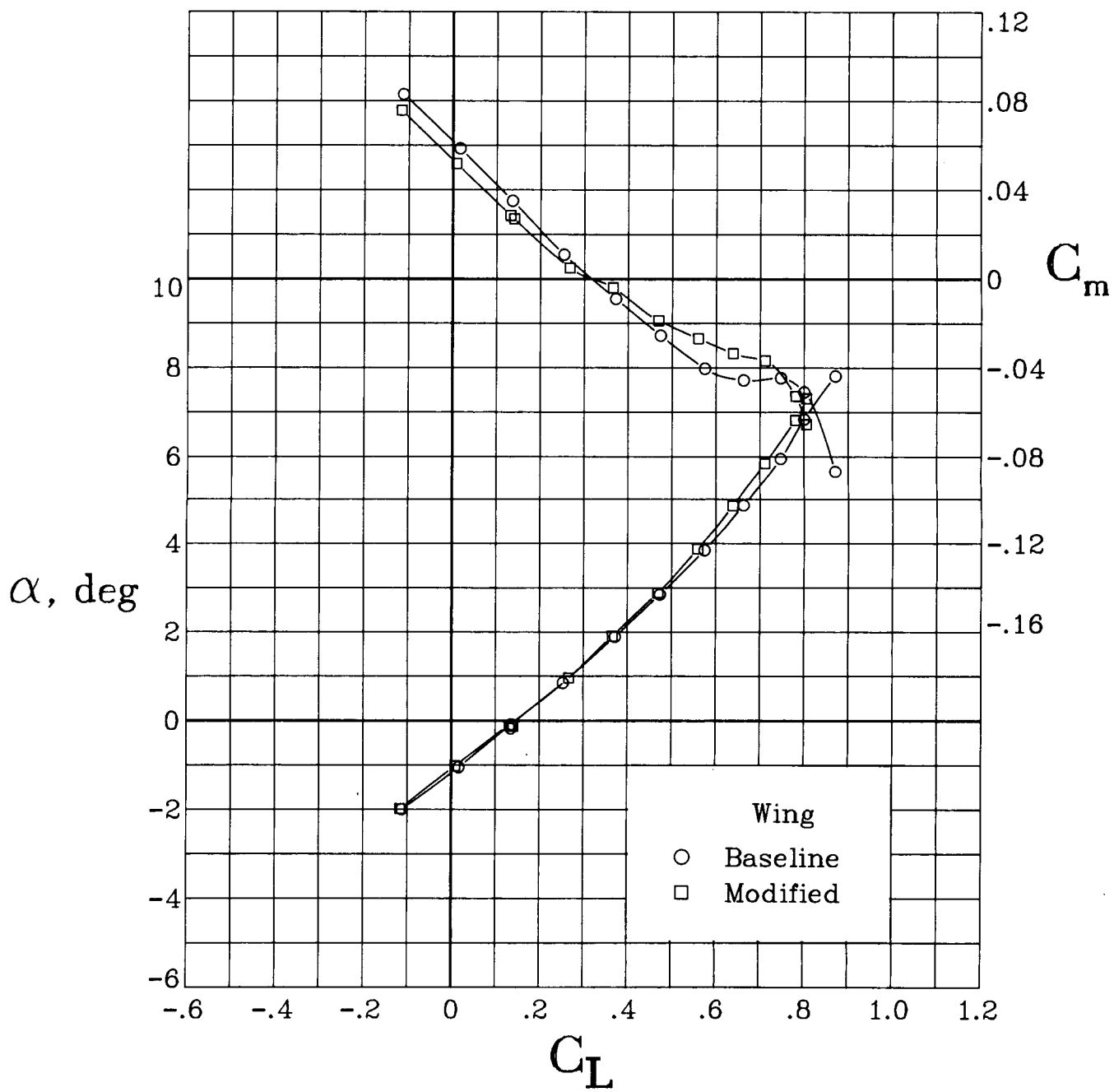
(i) $M = 0.825$.

Figure 7. Continued.



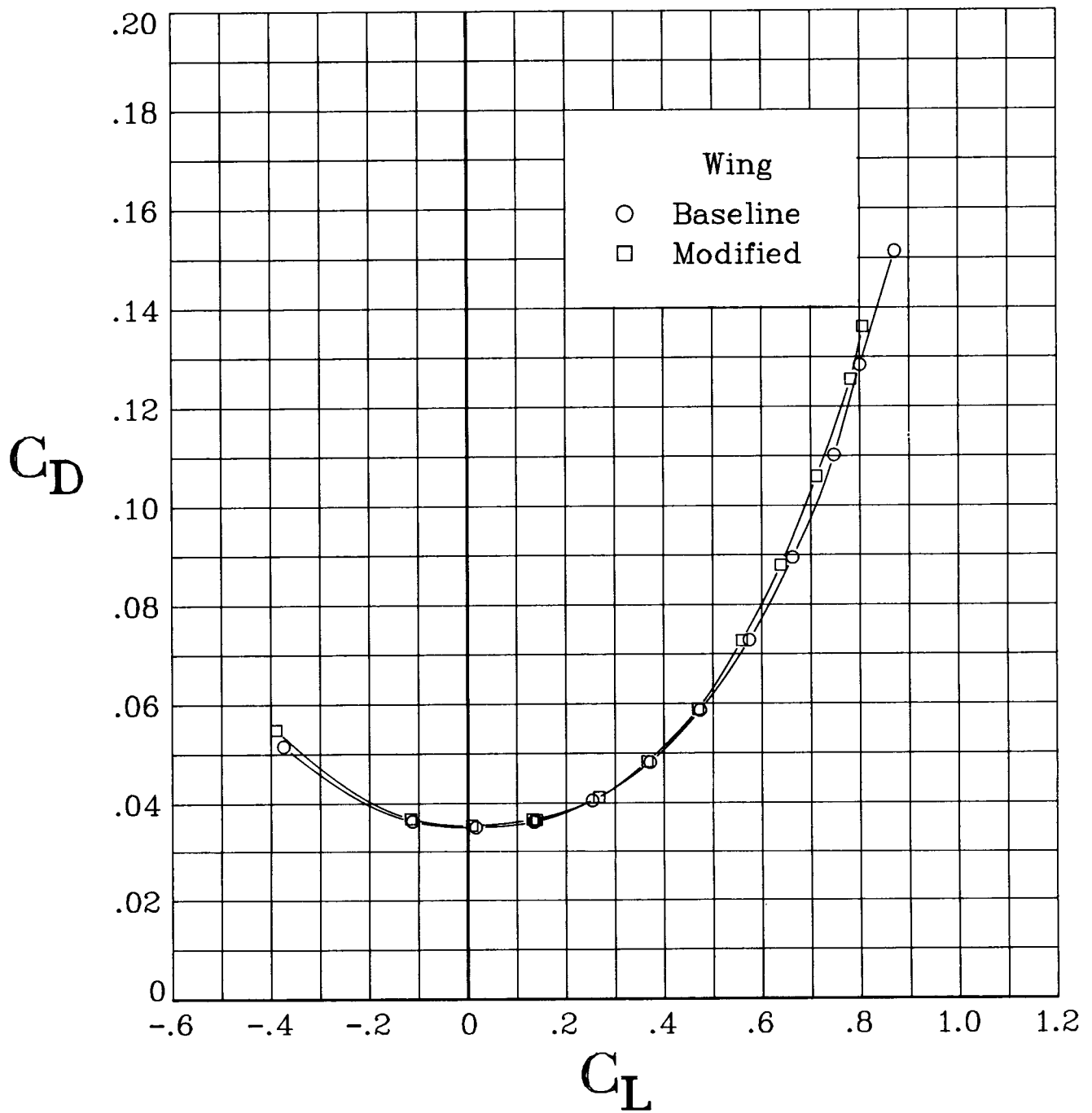
(i) Concluded.

Figure 7. Continued.



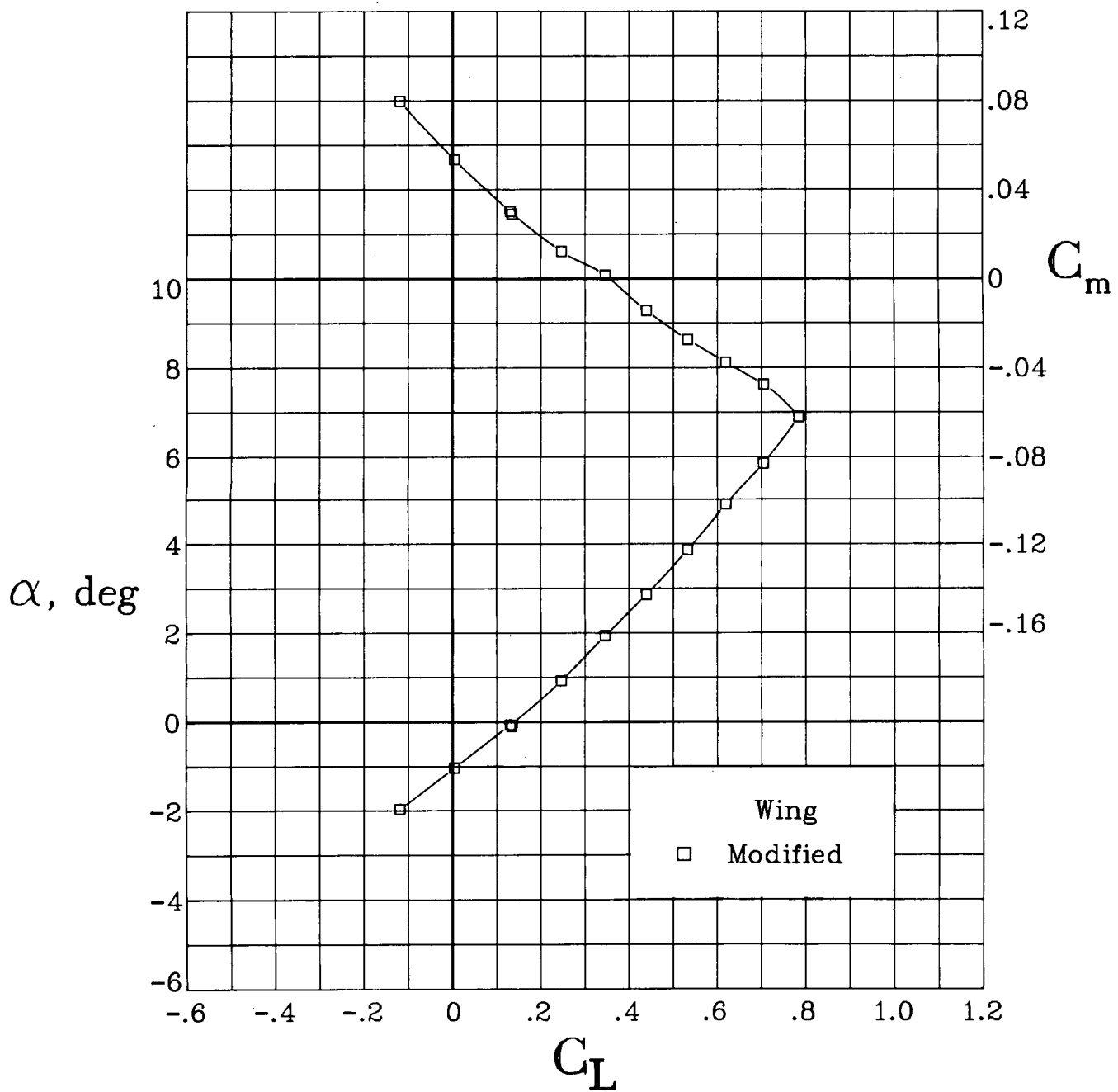
(j) $M = 0.85$.

Figure 7. Continued.



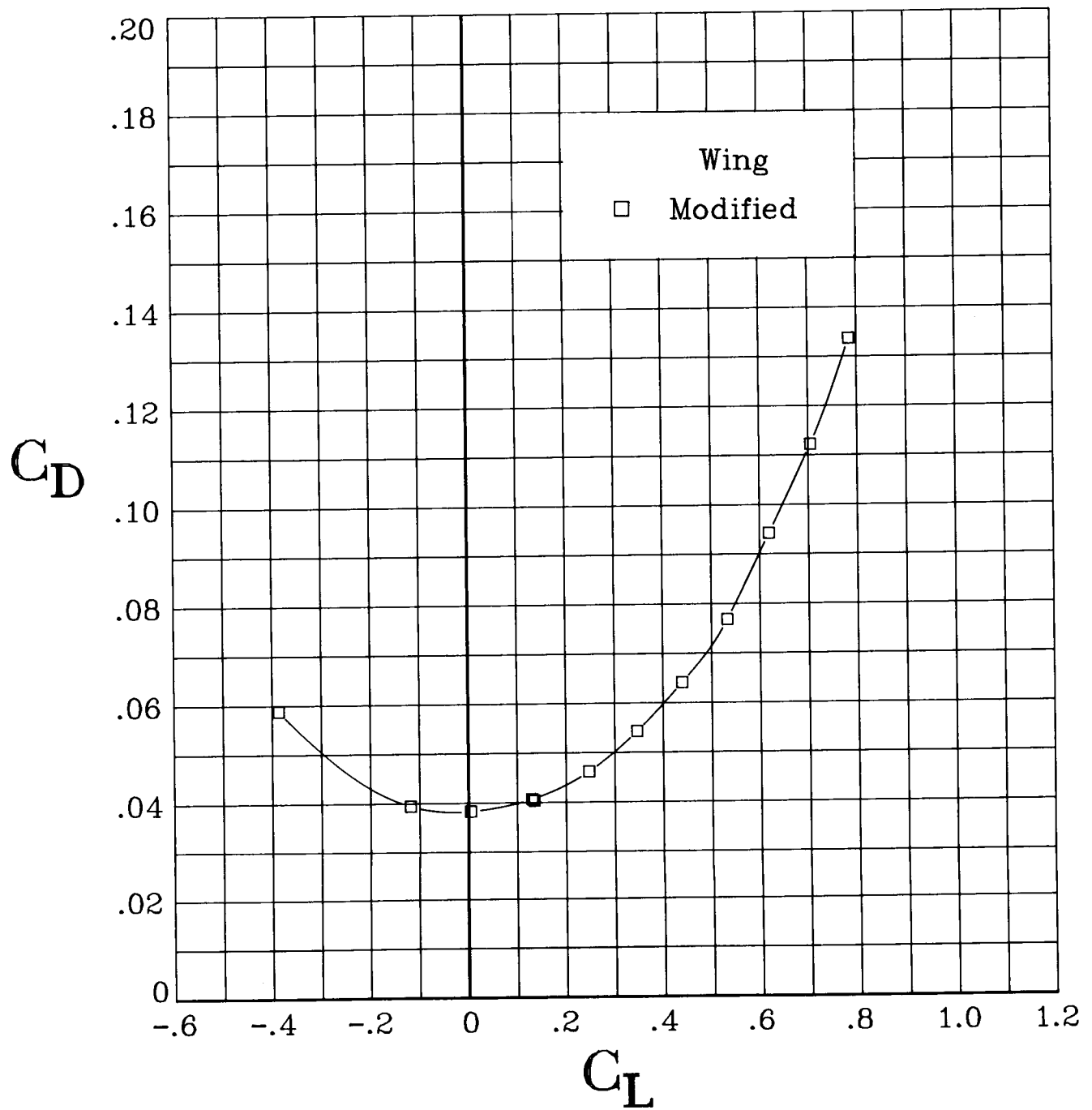
(j) Concluded.

Figure 7. Continued.



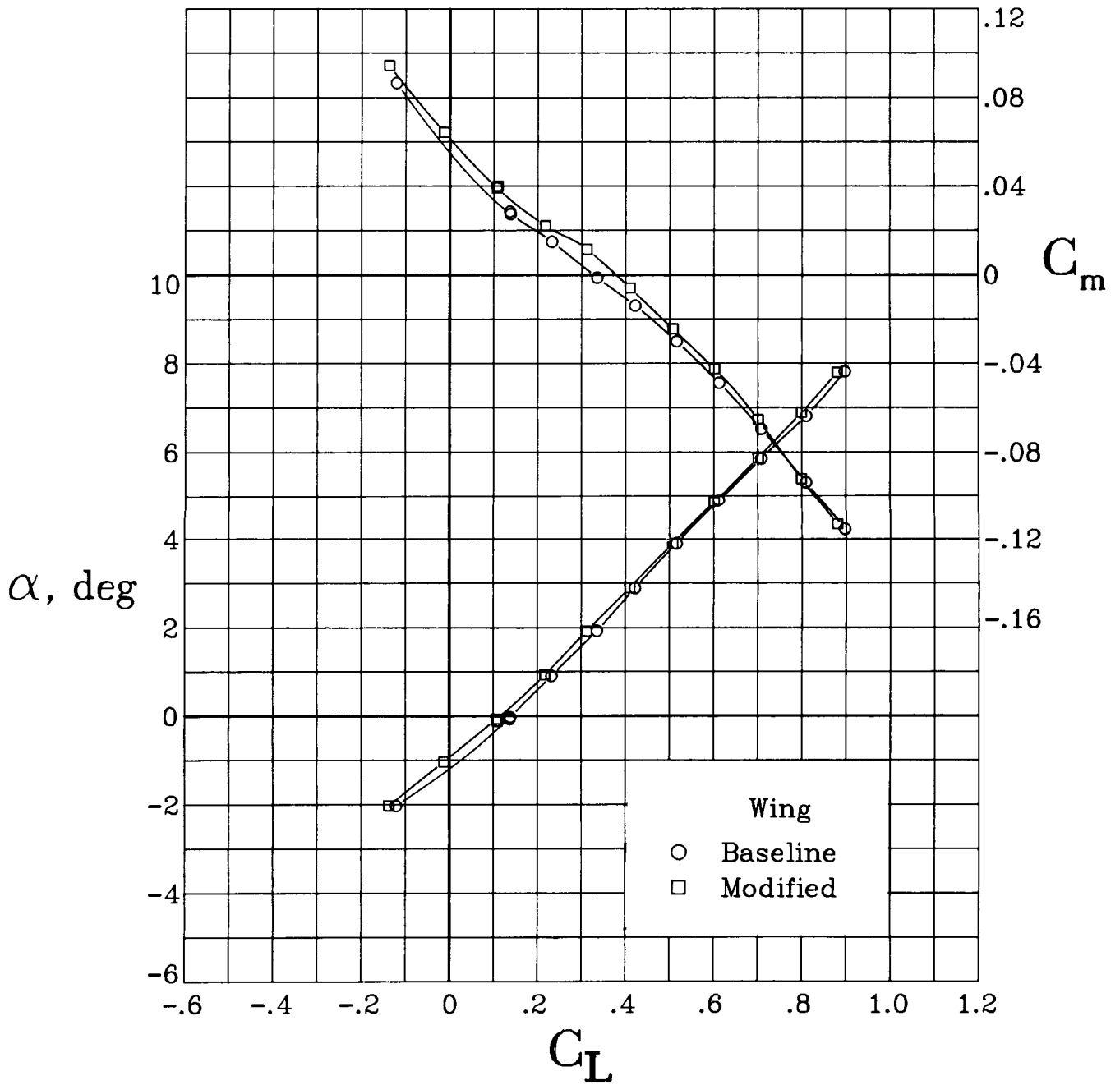
(k) $M = 0.875$.

Figure 7. Continued.



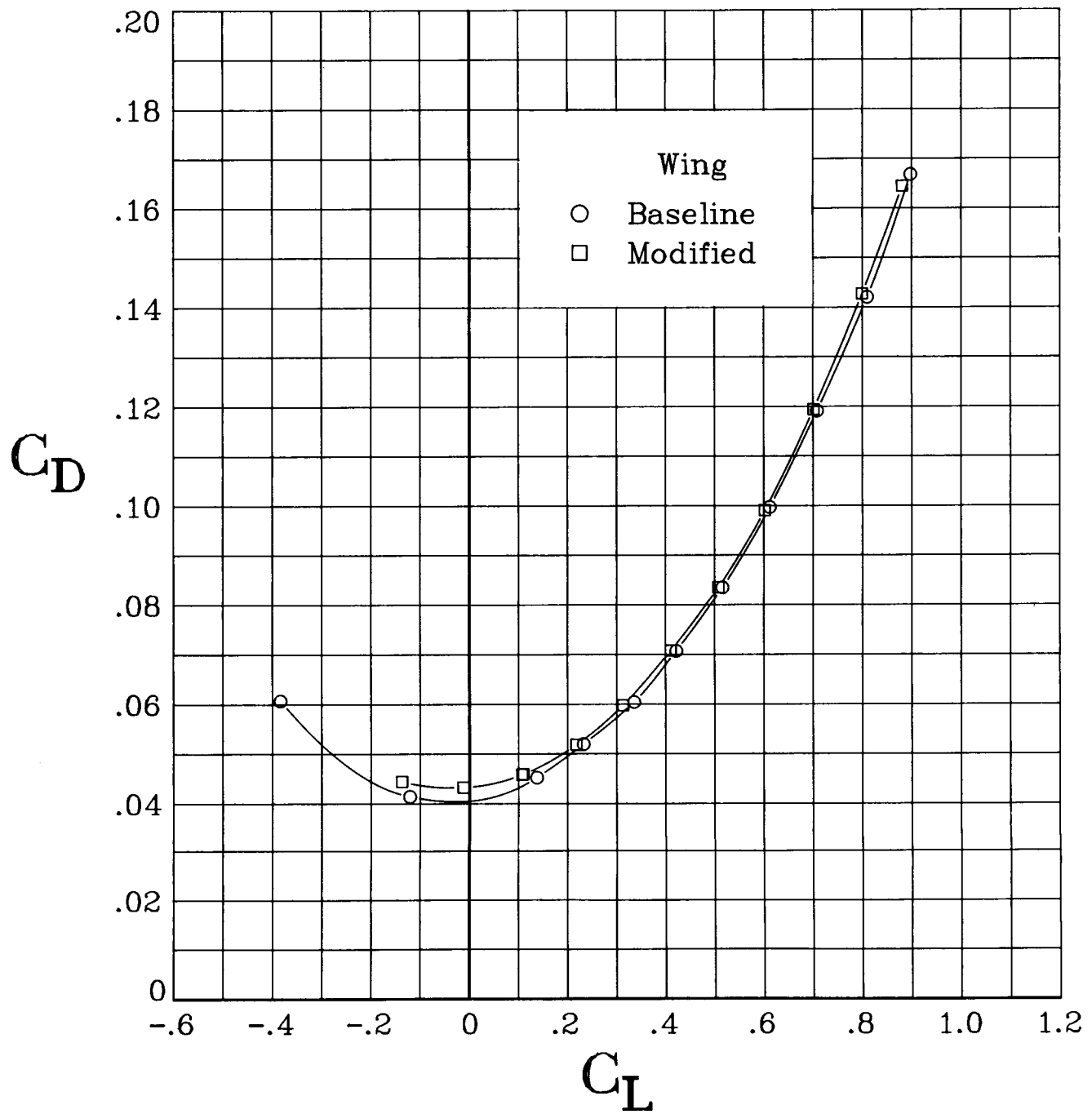
(k) Concluded.

Figure 7. Continued.



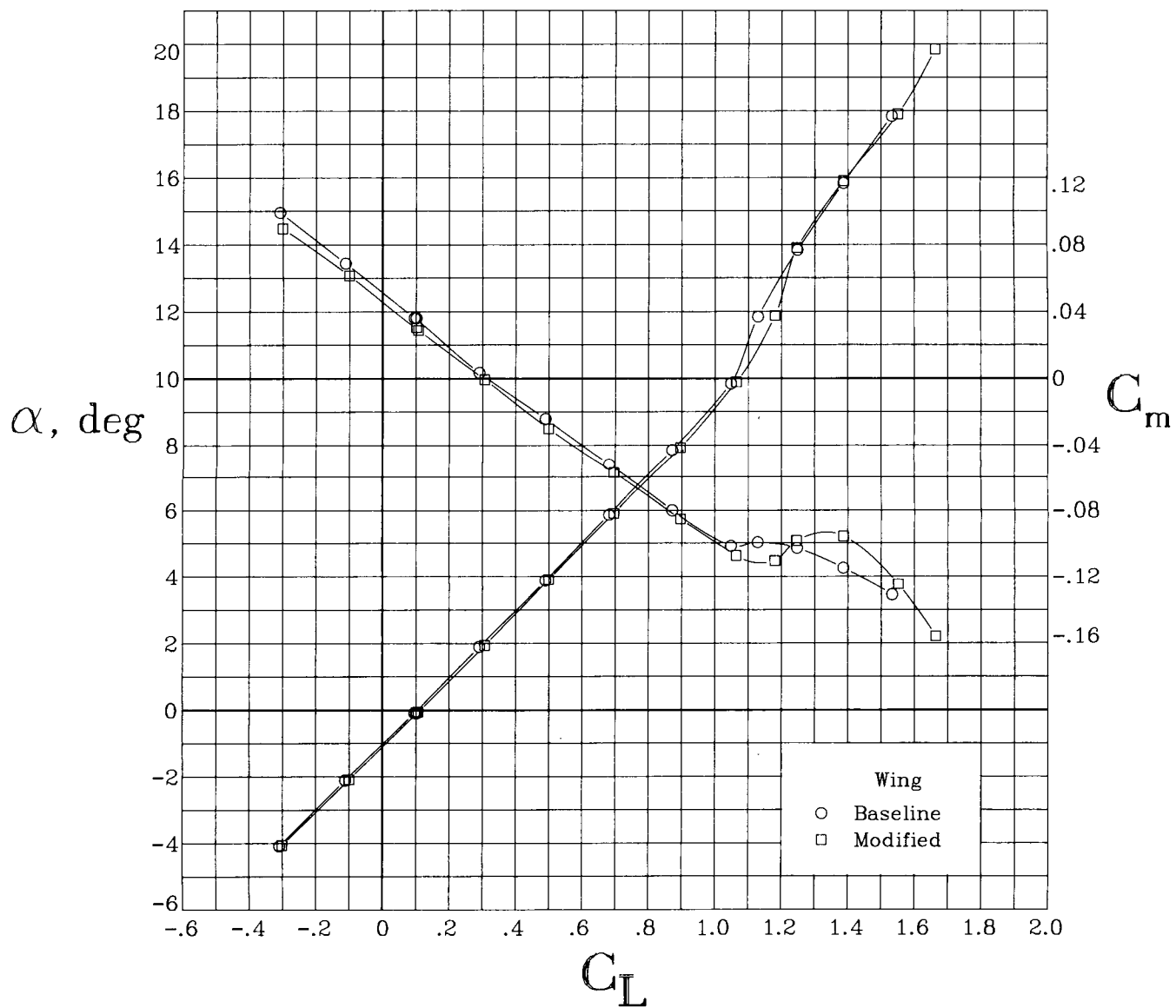
(1) $M = 0.90$.

Figure 7. Continued.



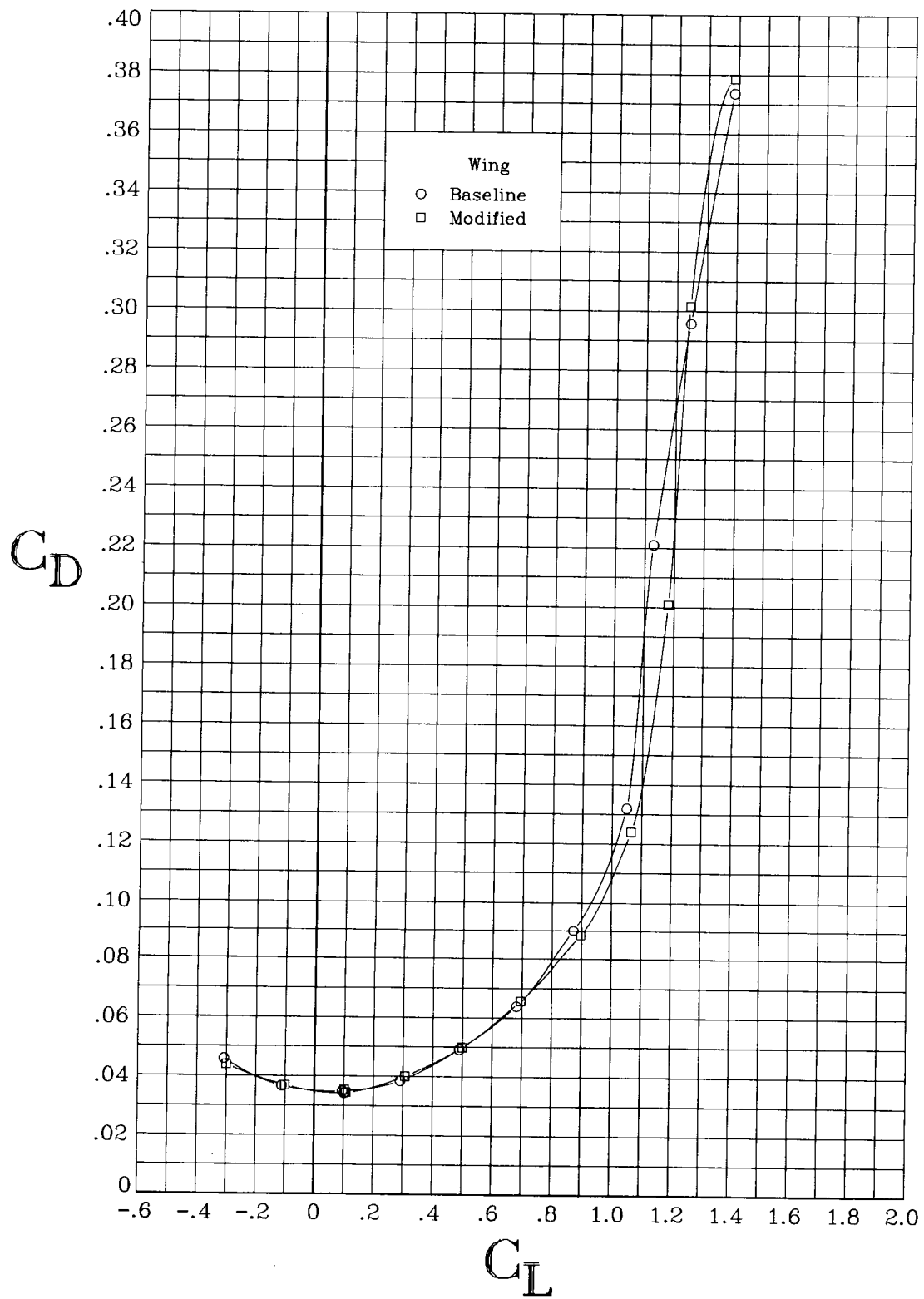
(l) Concluded.

Figure 7. Concluded.



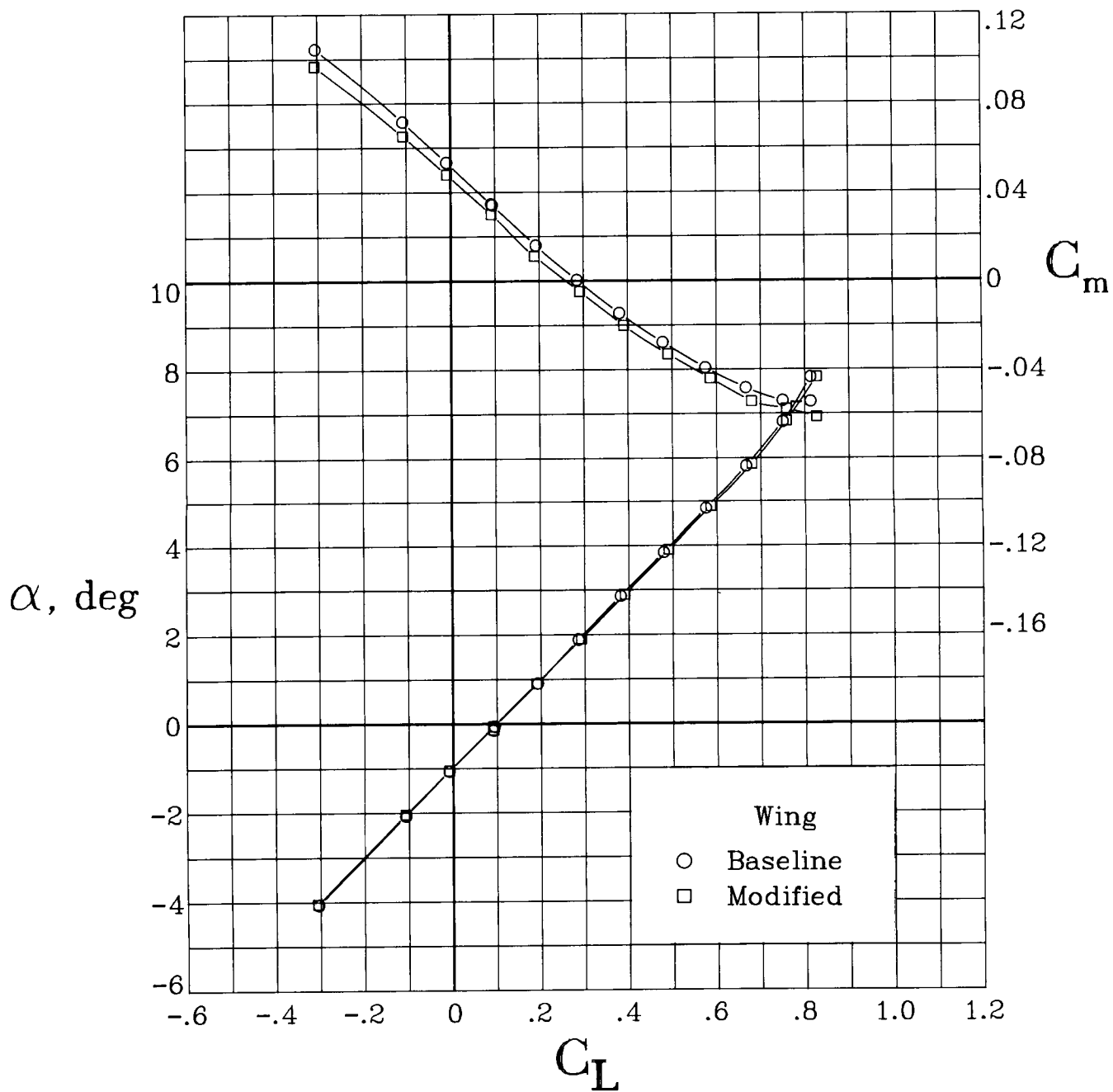
(a) $M = 0.20$.

Figure 8. Longitudinal aerodynamic characteristics of the baseline and modified wing configurations, with wings swept 35° . $\beta = 0^\circ$.



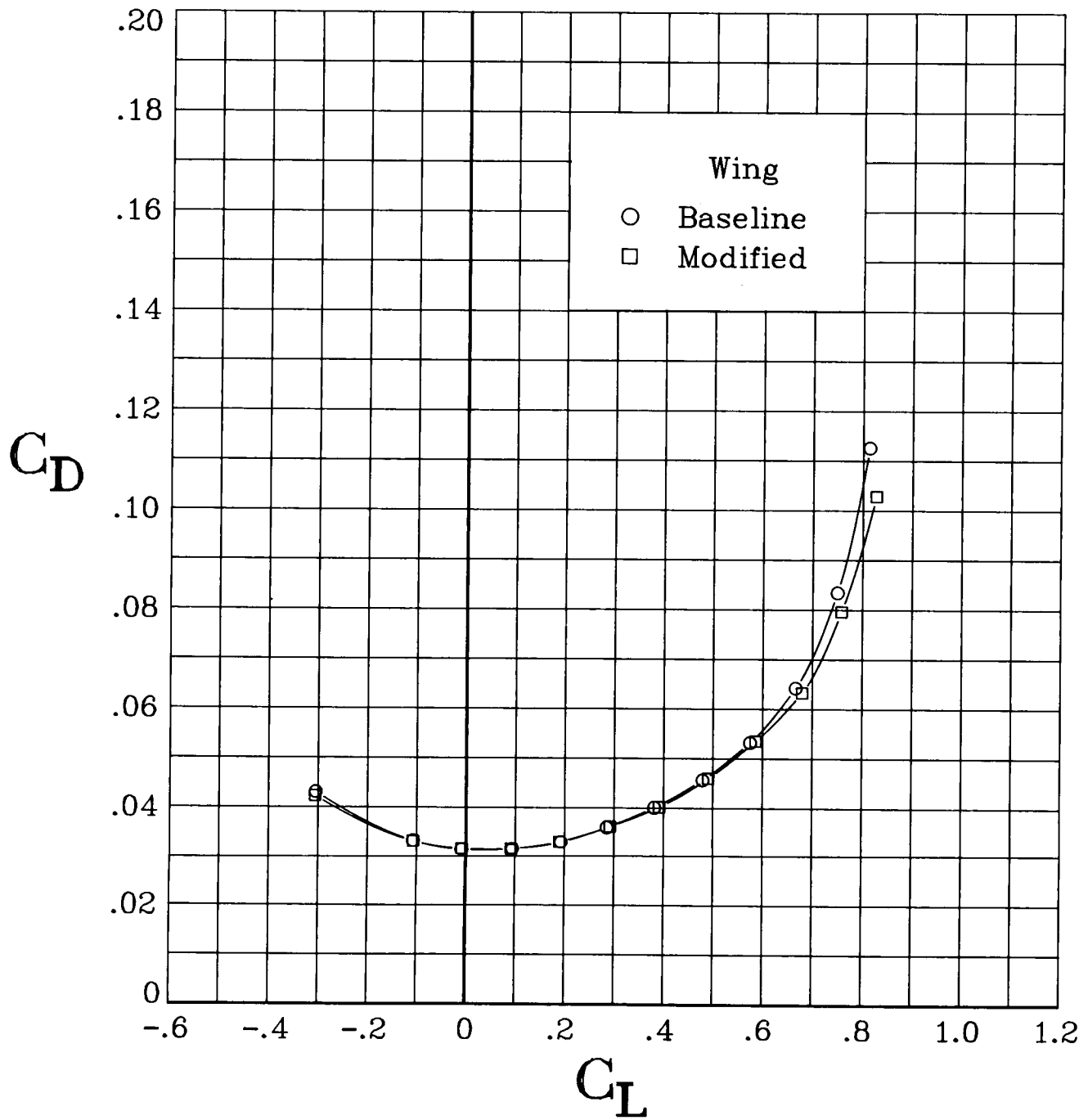
(a) Concluded.

Figure 8. Continued.



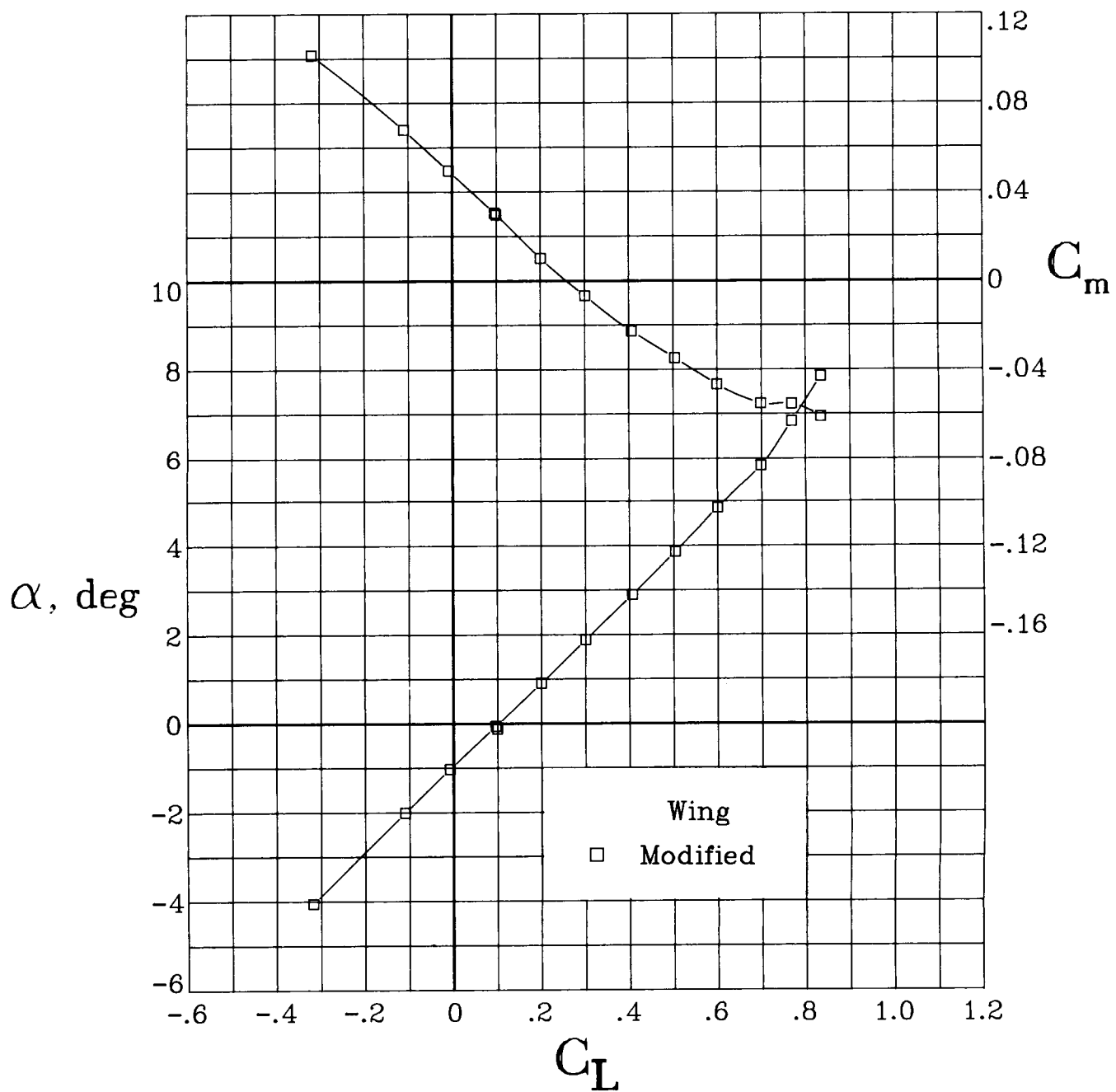
(b) $M = 0.60$.

Figure 8. Continued.



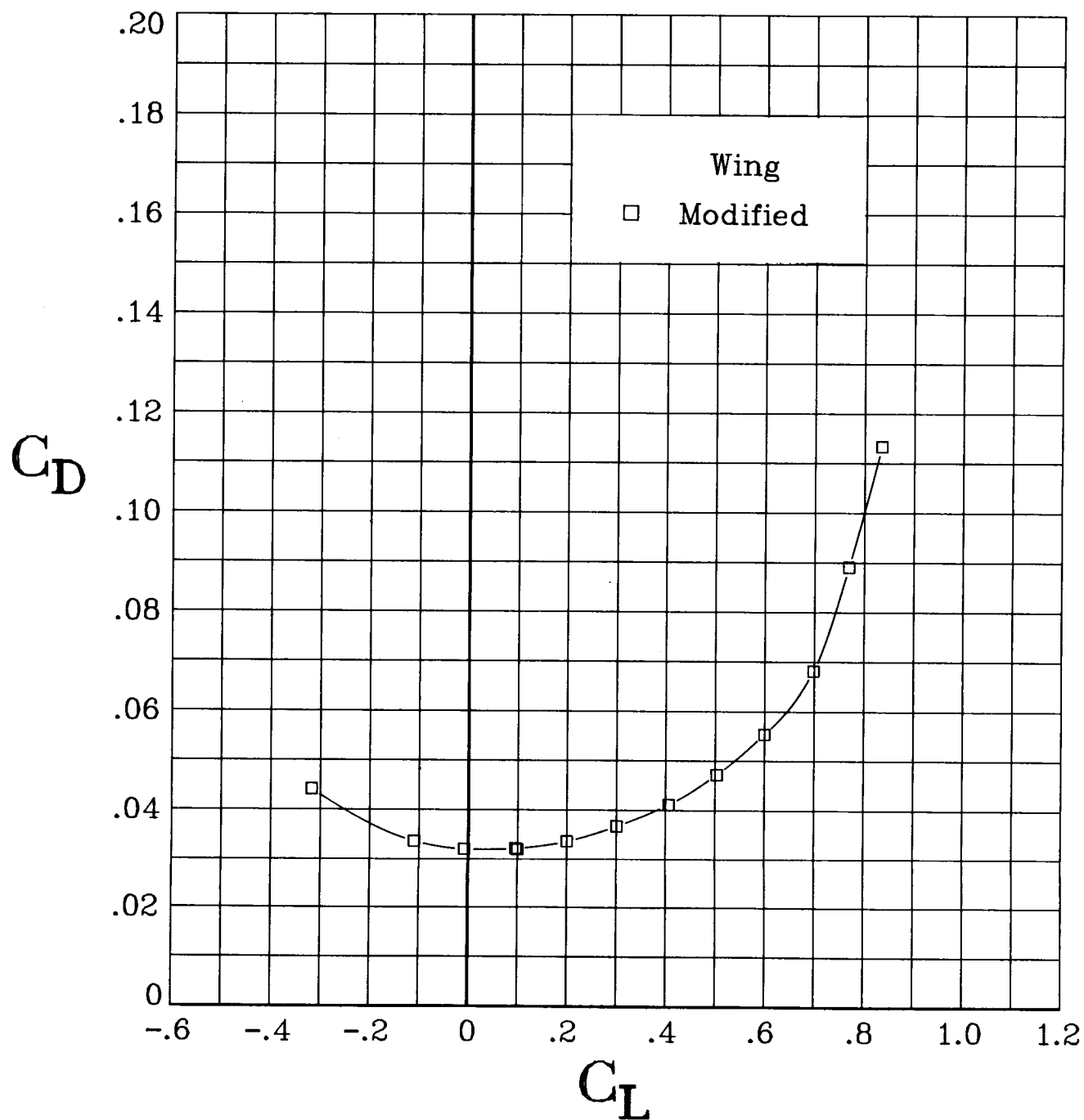
(b) Concluded.

Figure 8. Continued.



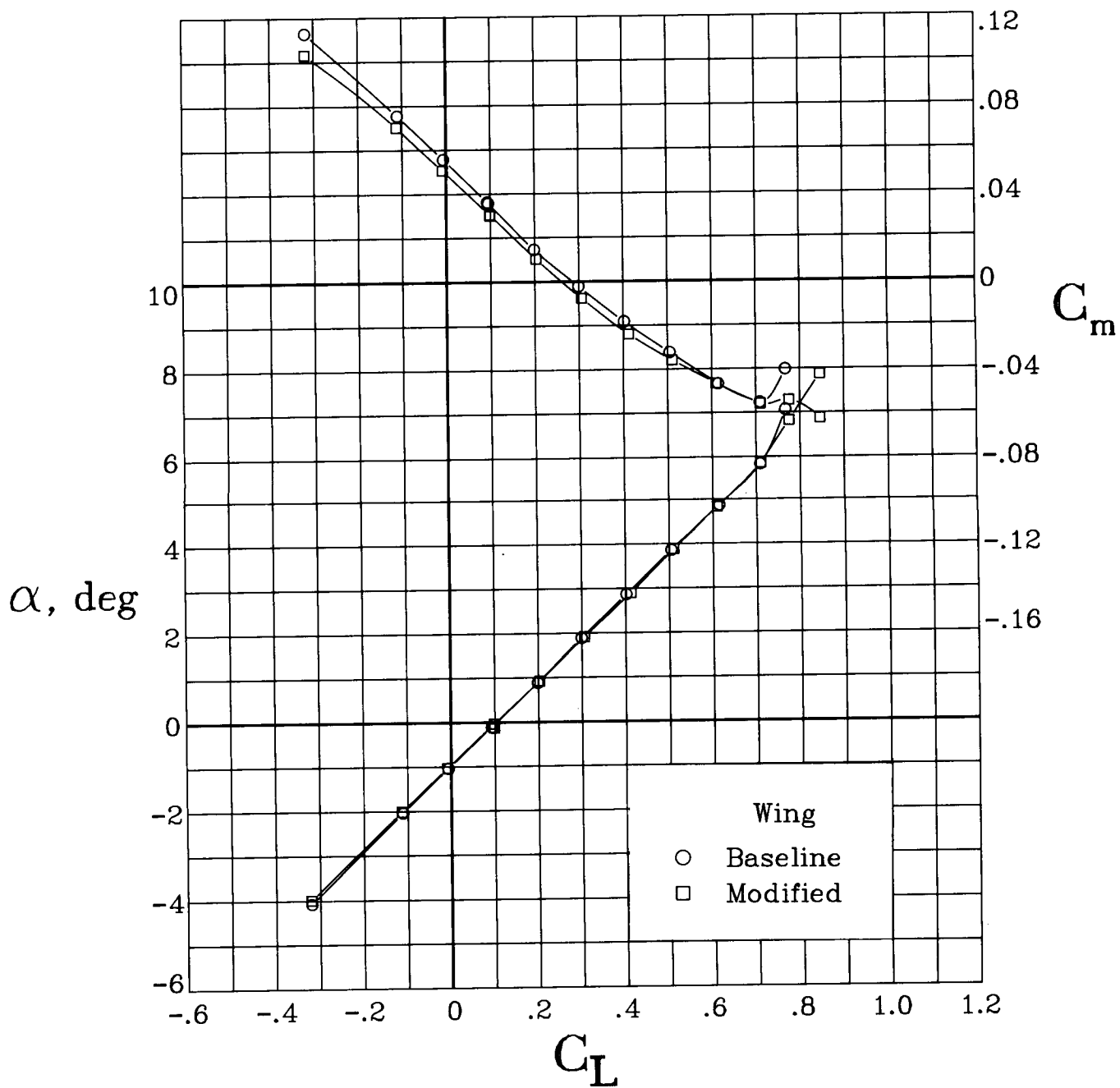
(c) $M = 0.675$

Figure 8. Continued.



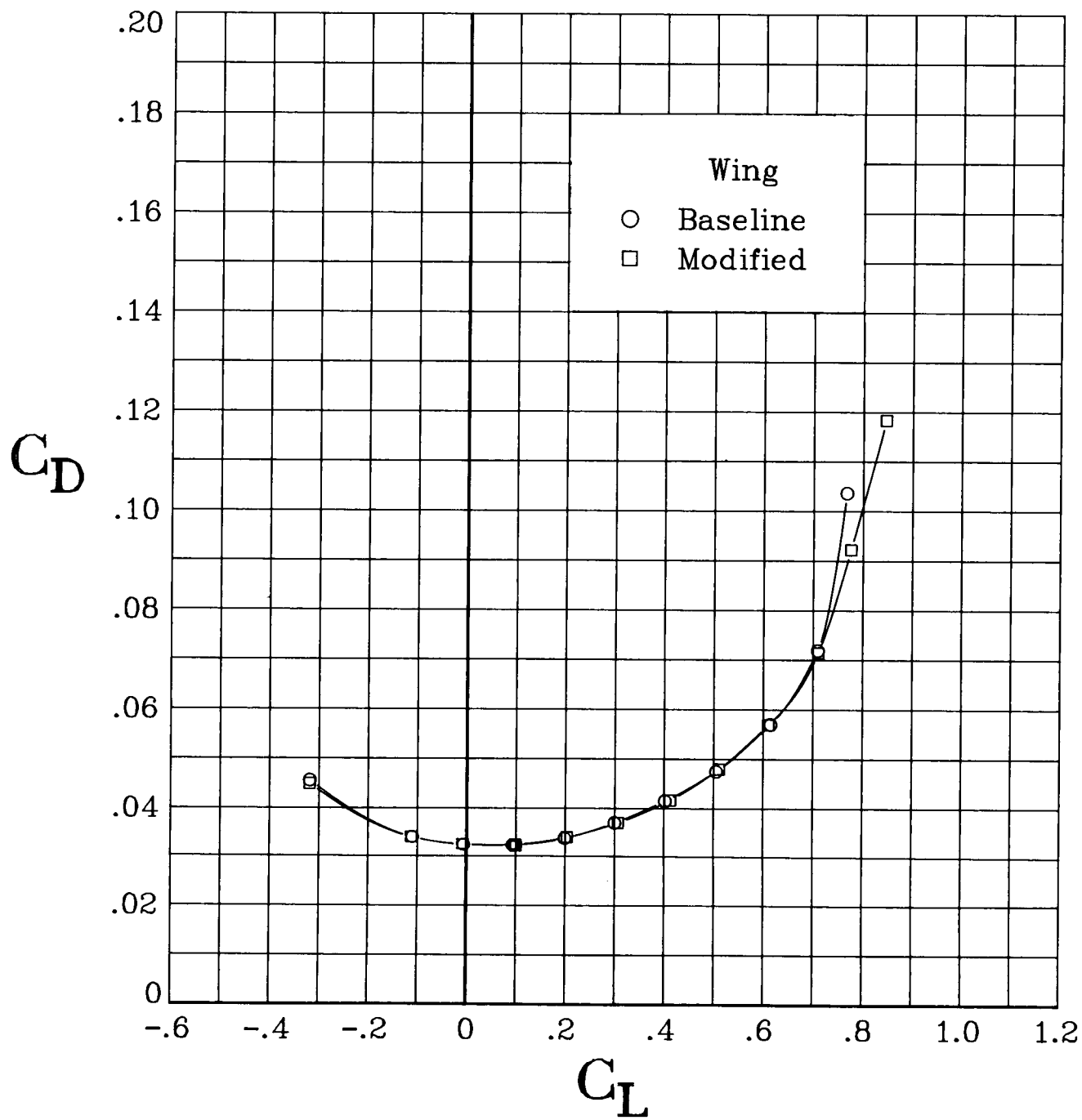
(c) Concluded.

Figure 8. Continued.



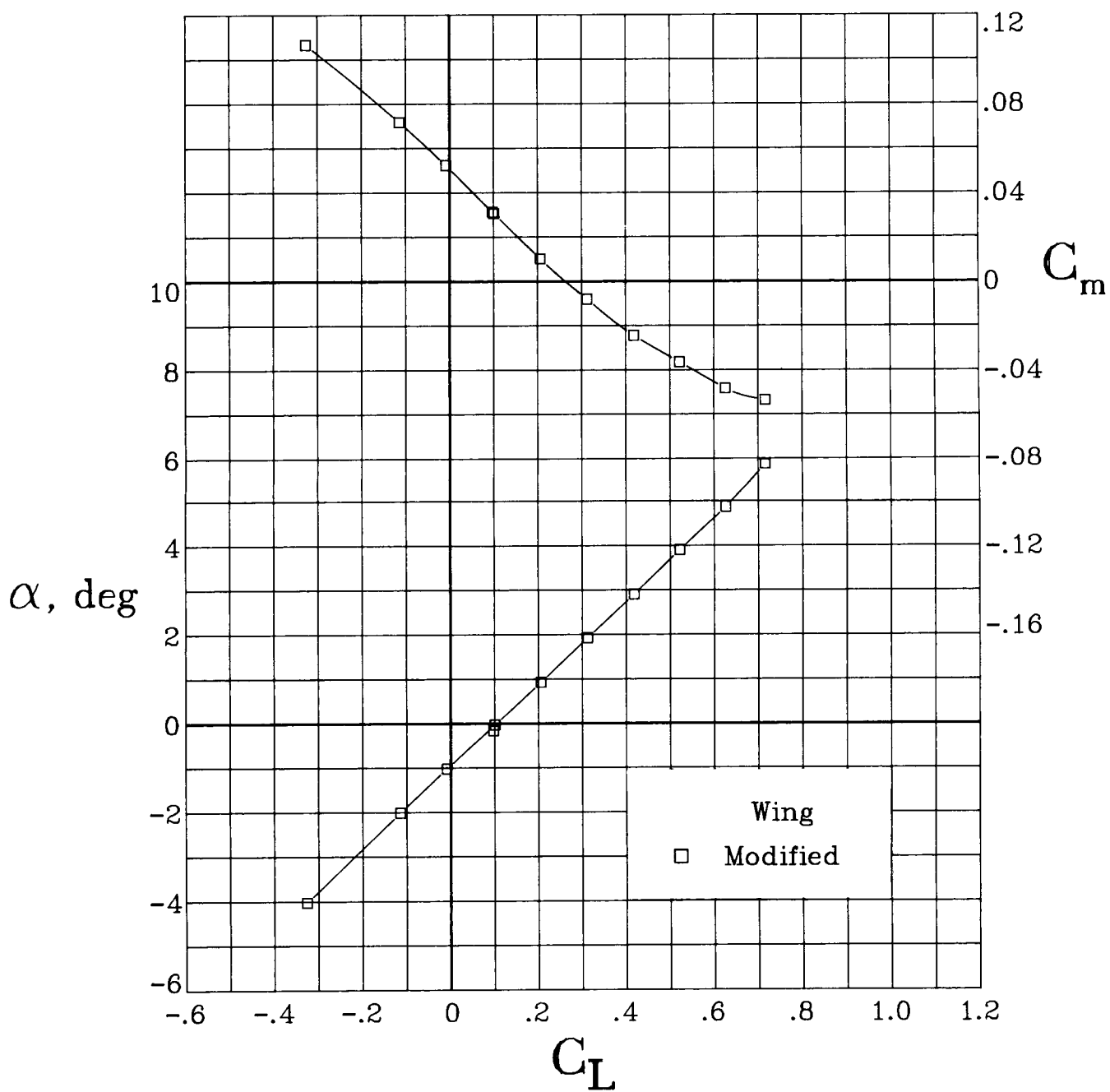
(d) $M = 0.70$.

Figure 8. Continued.



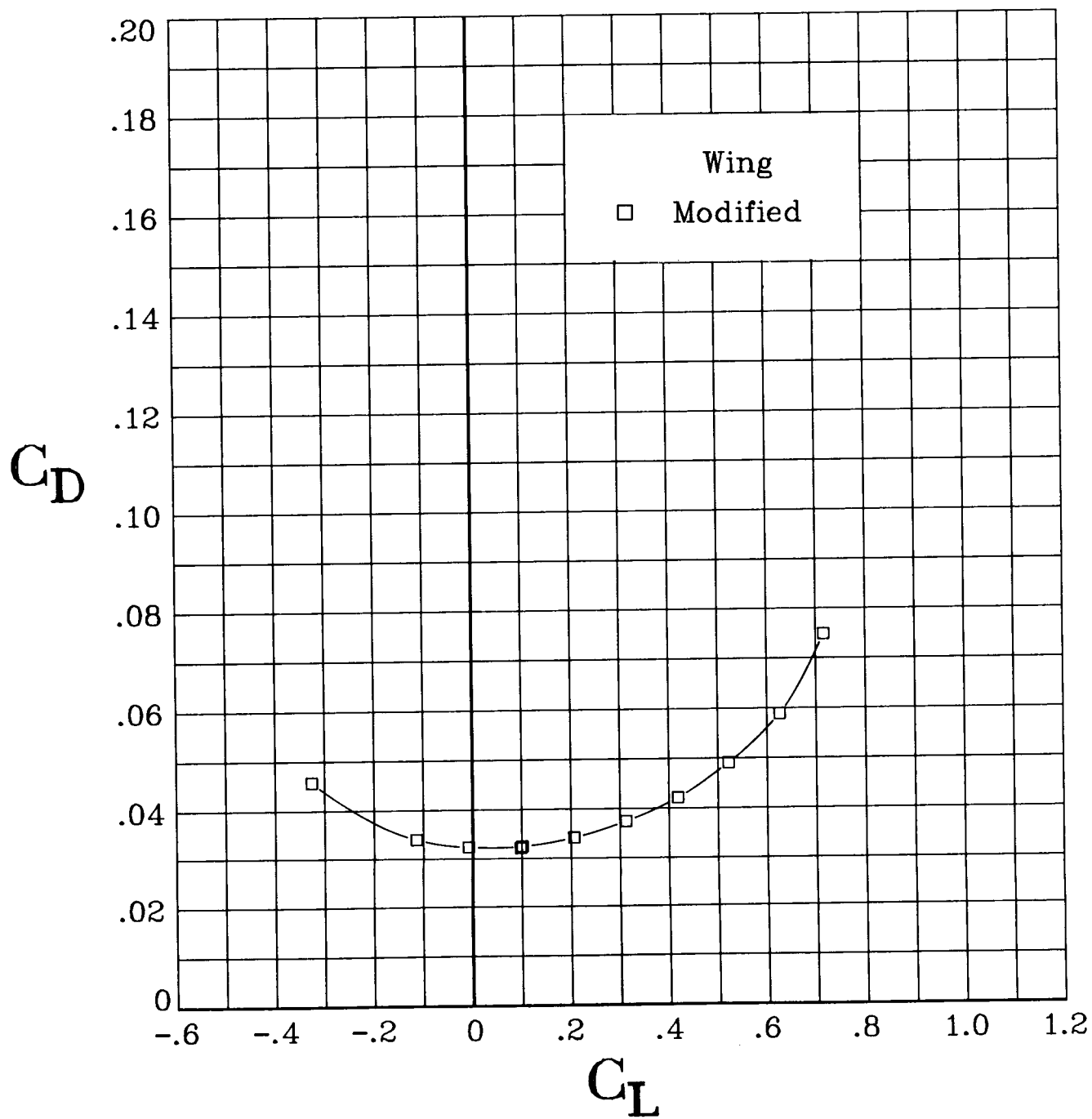
(d) Concluded.

Figure 8. Continued.



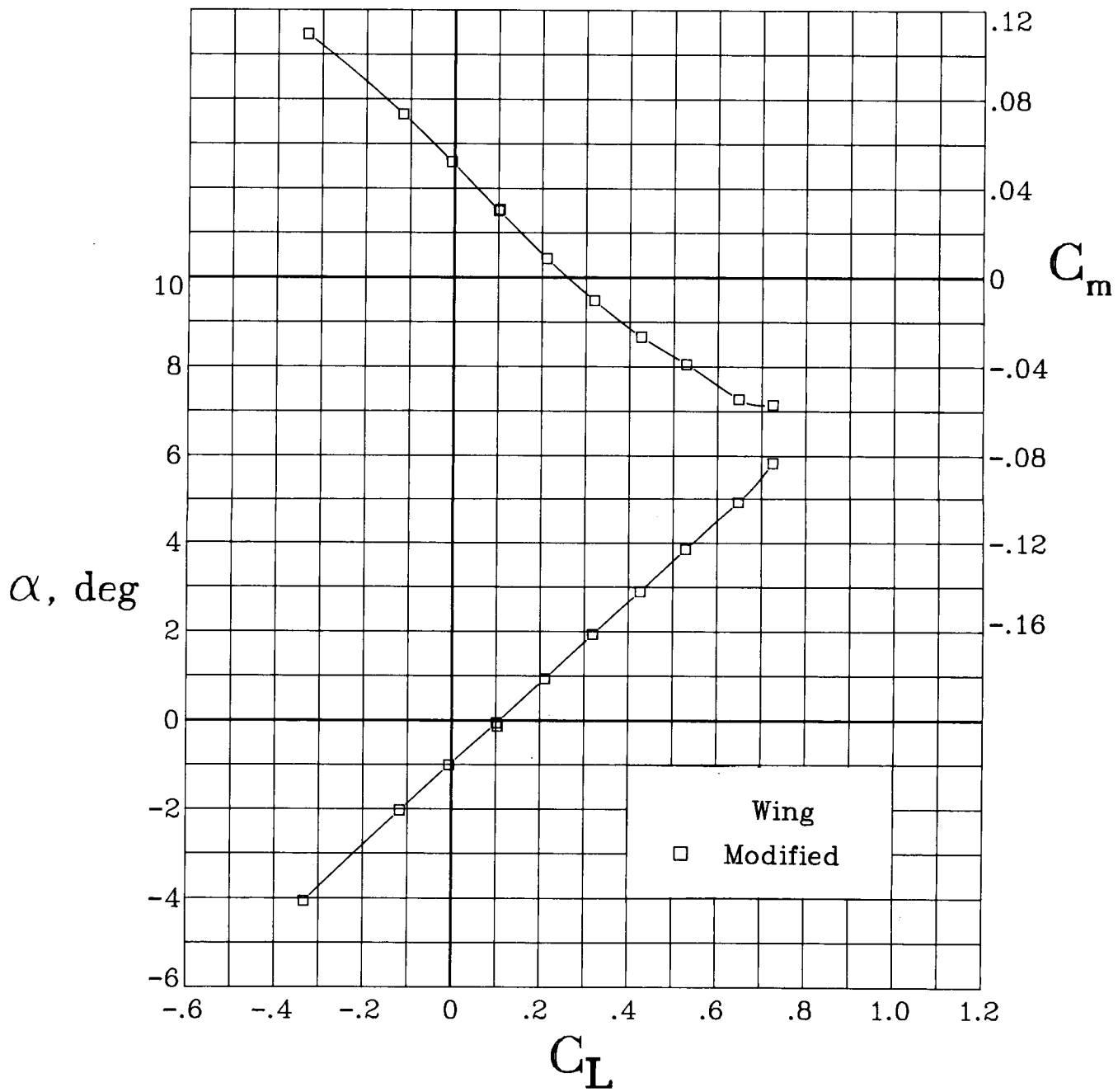
(e) $M = 0.725$.

Figure 8. Continued.



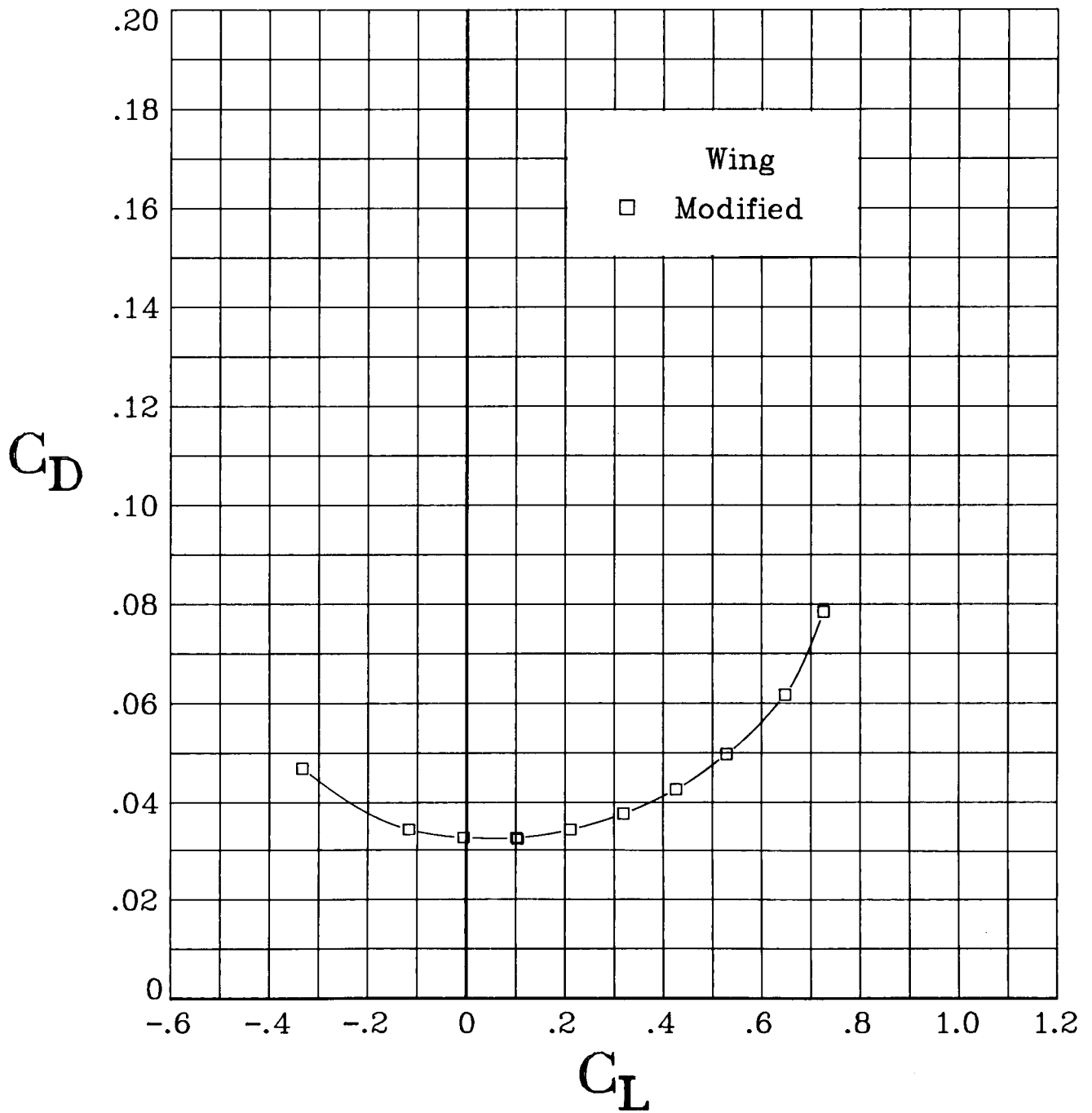
(e) Concluded.

Figure 8. Continued.



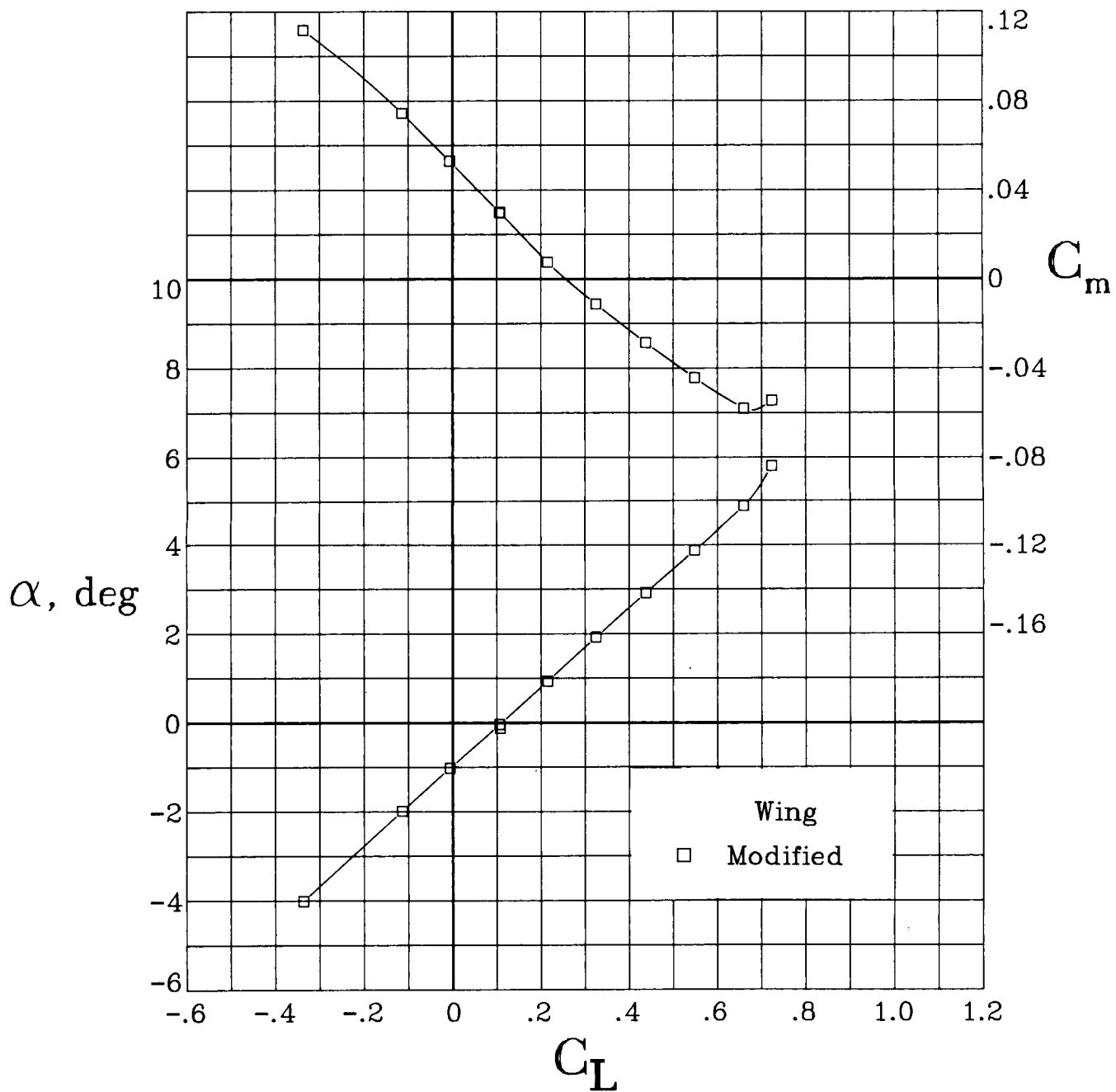
(f) $M = 0.75$.

Figure 8. Continued.



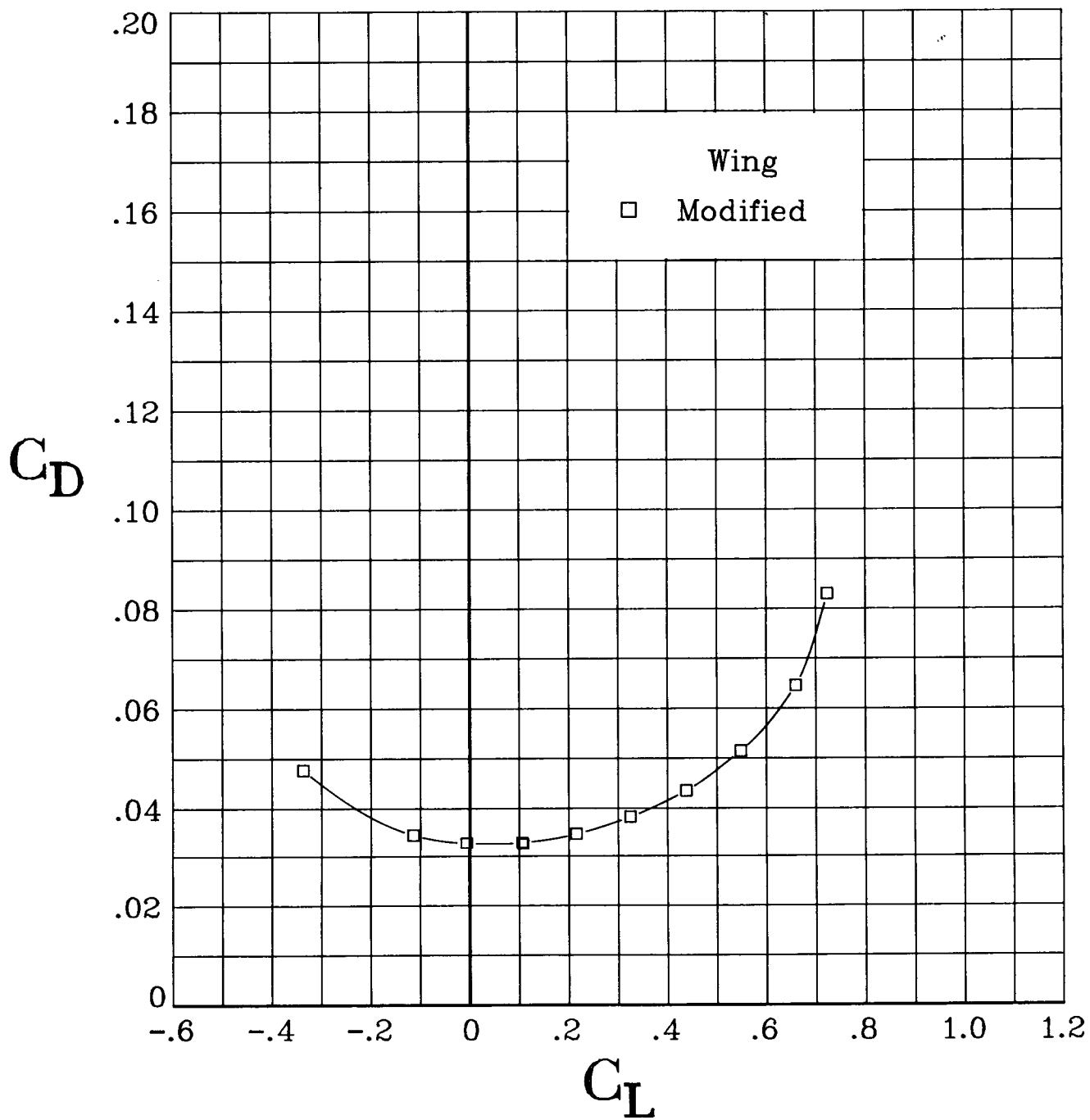
(f) Concluded.

Figure 8. Continued.



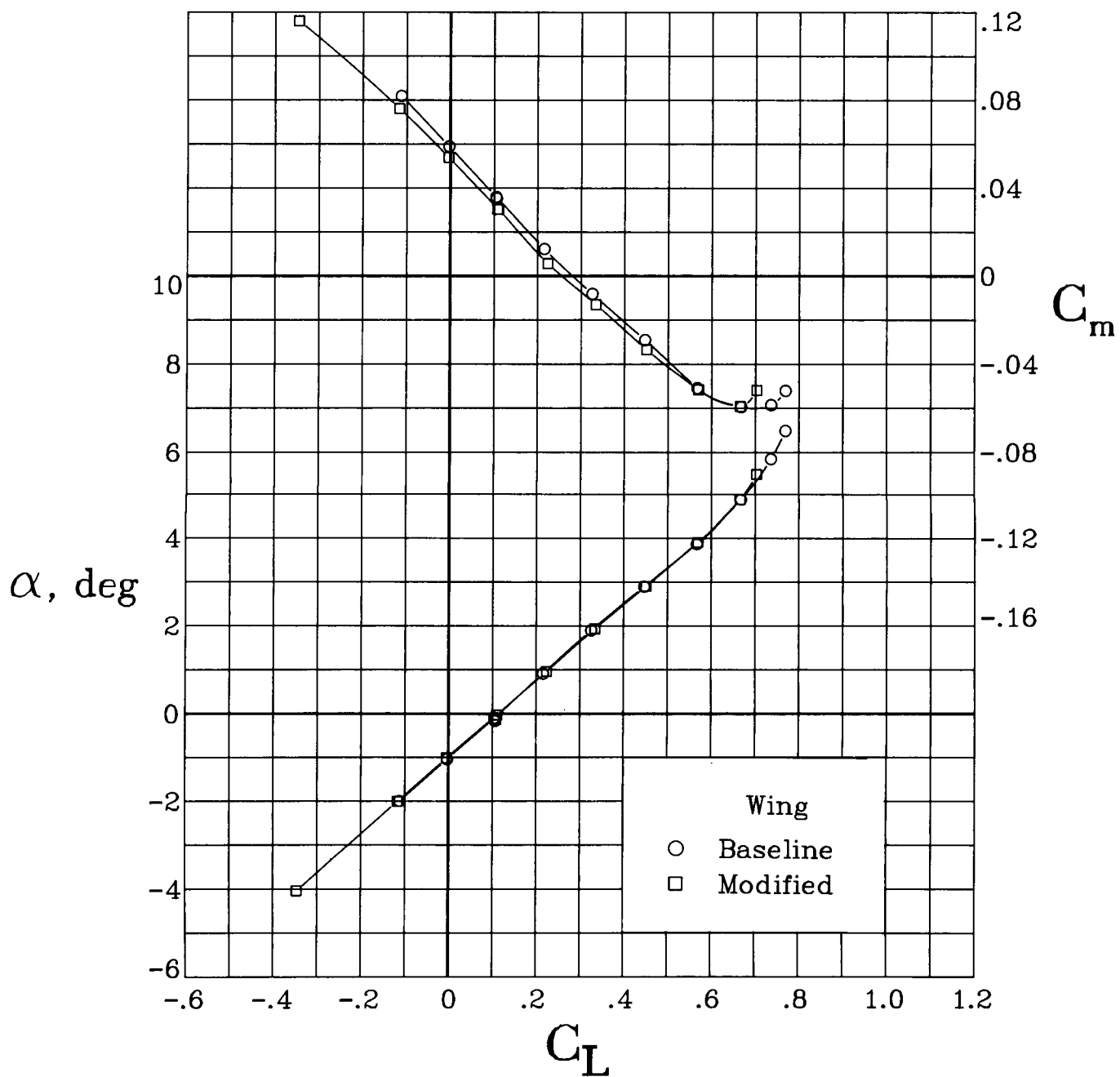
(g) $M = 0.775$.

Figure 8. Continued.



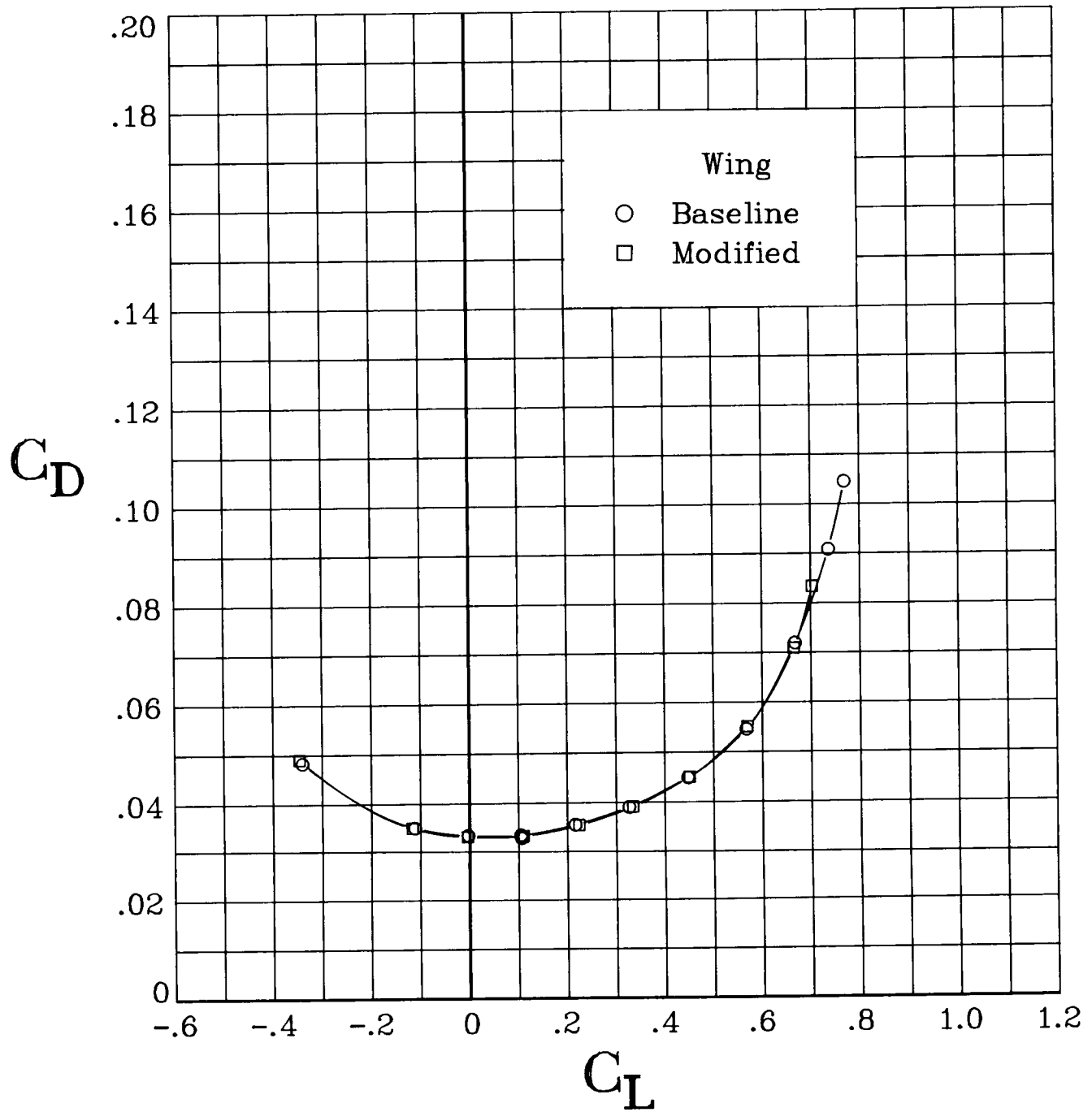
(g) Concluded.

Figure 8. Continued.



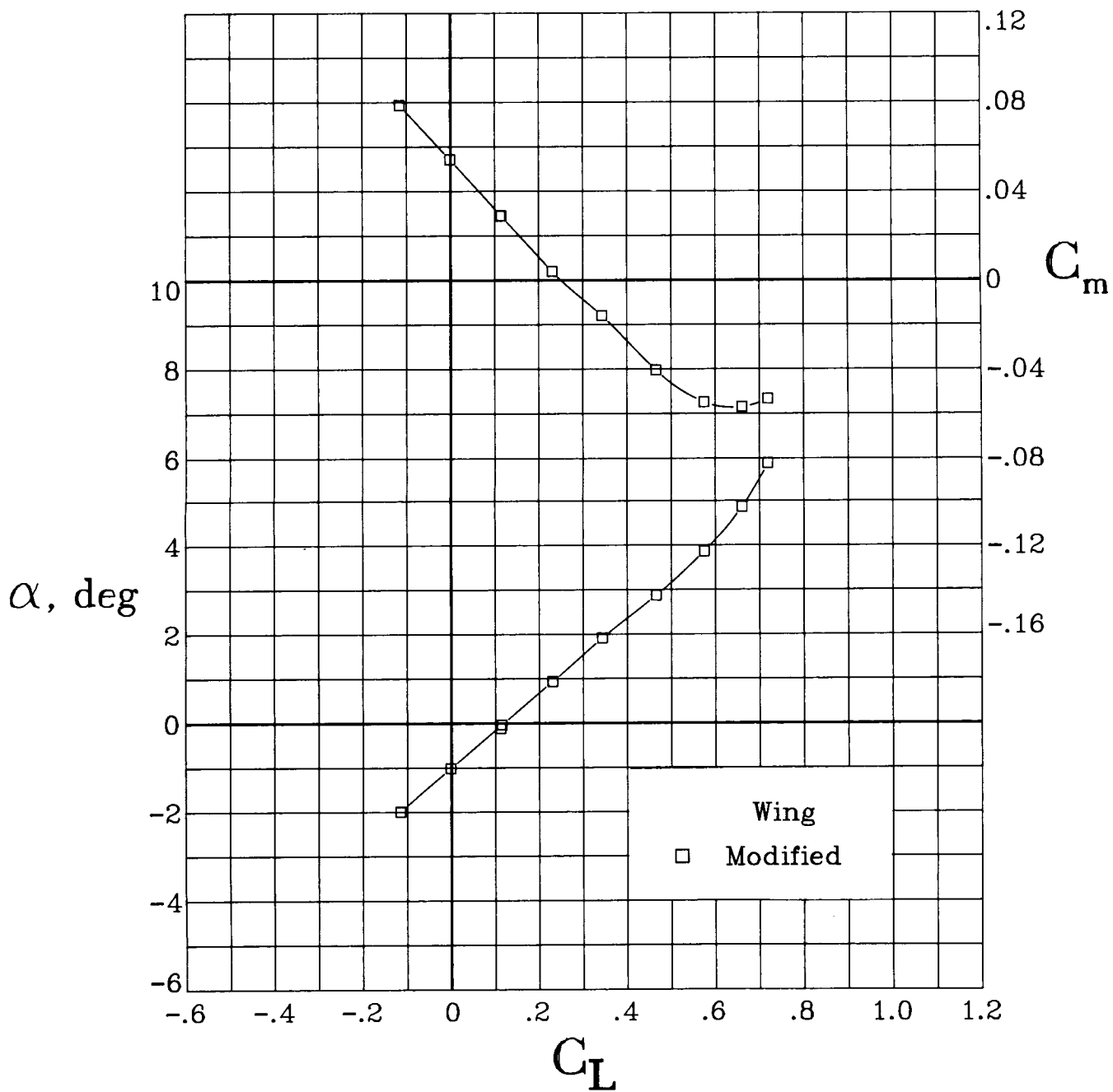
(h) $M = 0.80$.

Figure 8. Continued.



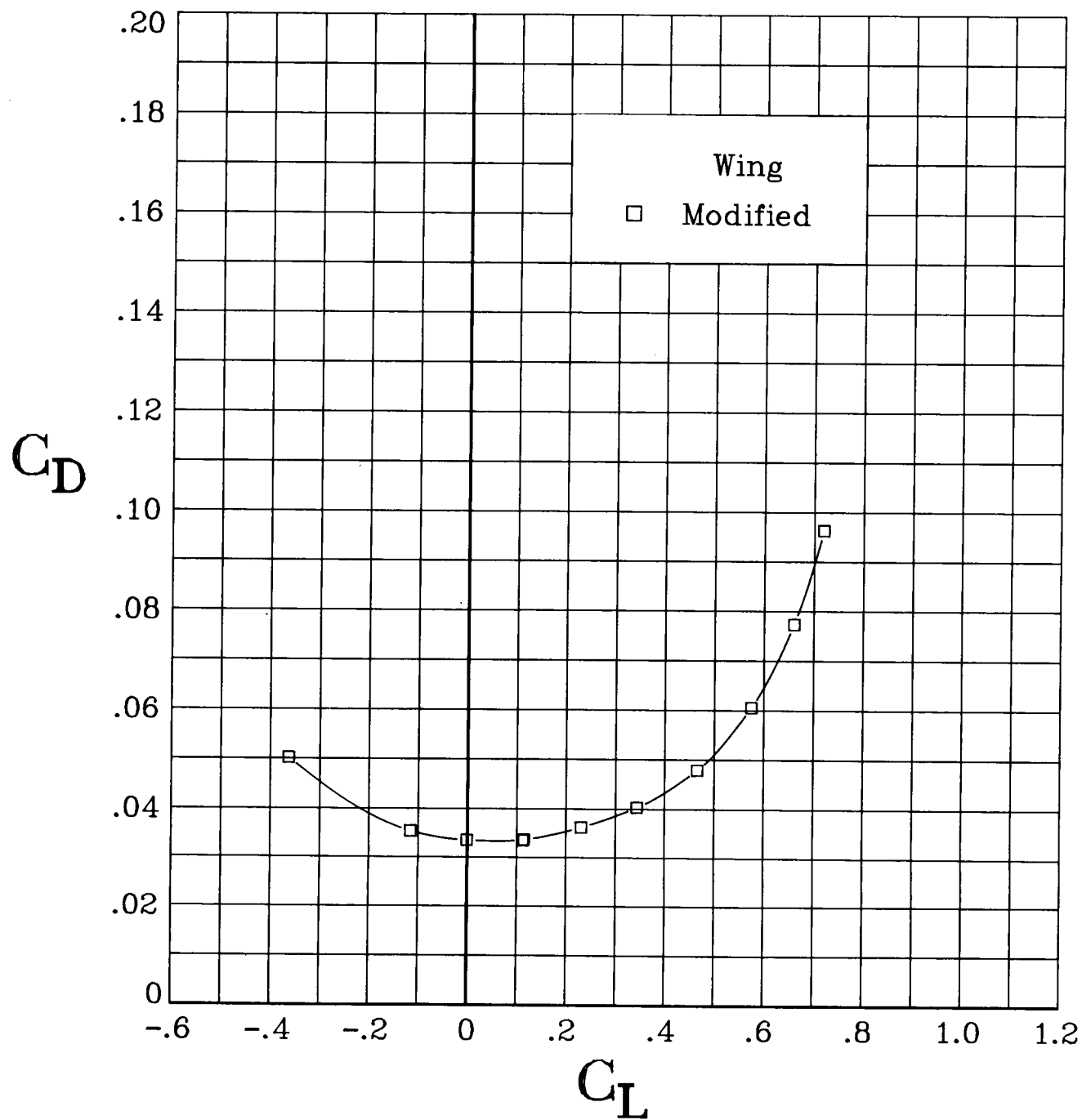
(h) Concluded.

Figure 8. Continued.



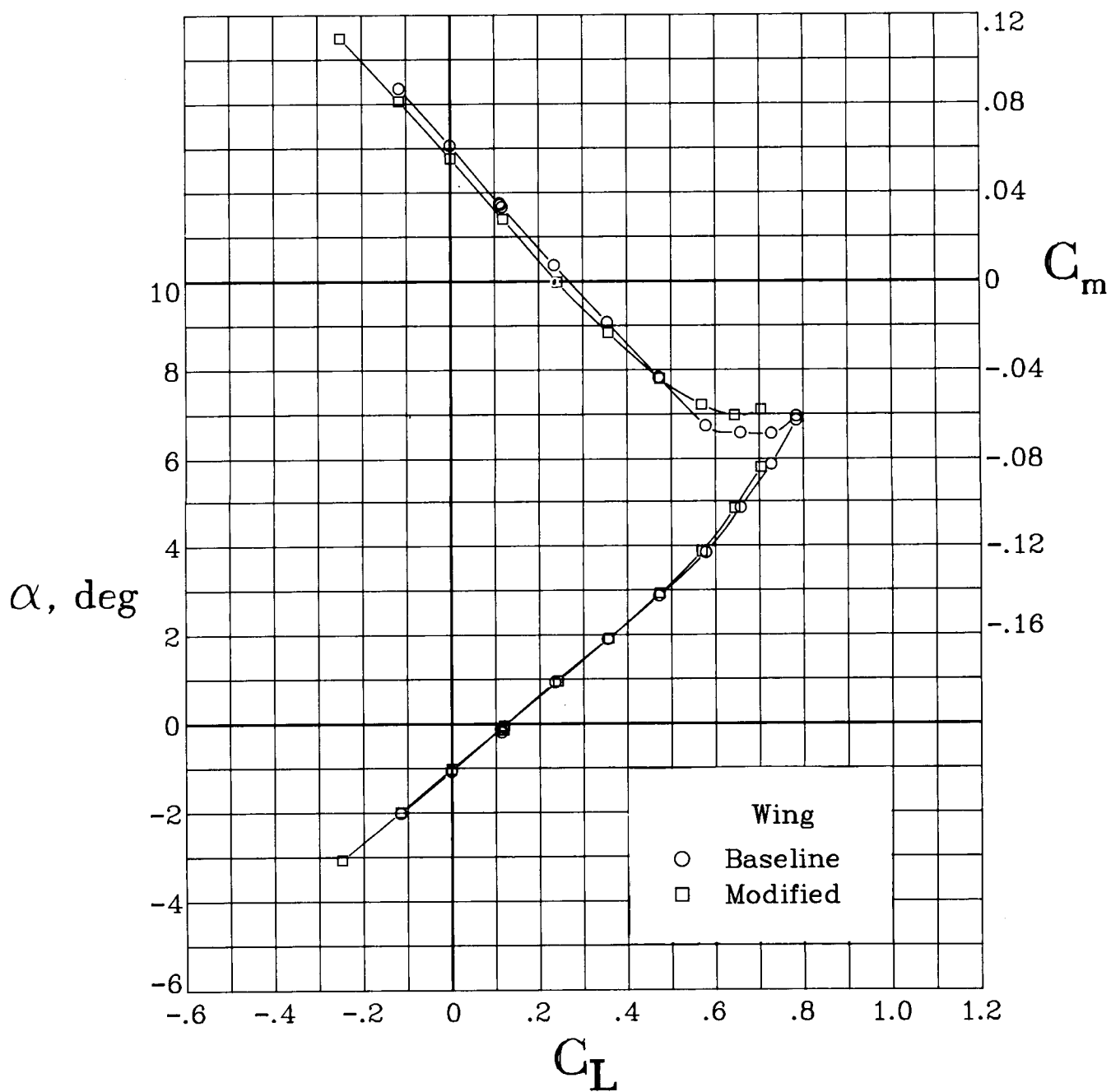
(i) $M = 0.825$.

Figure 8. Continued.



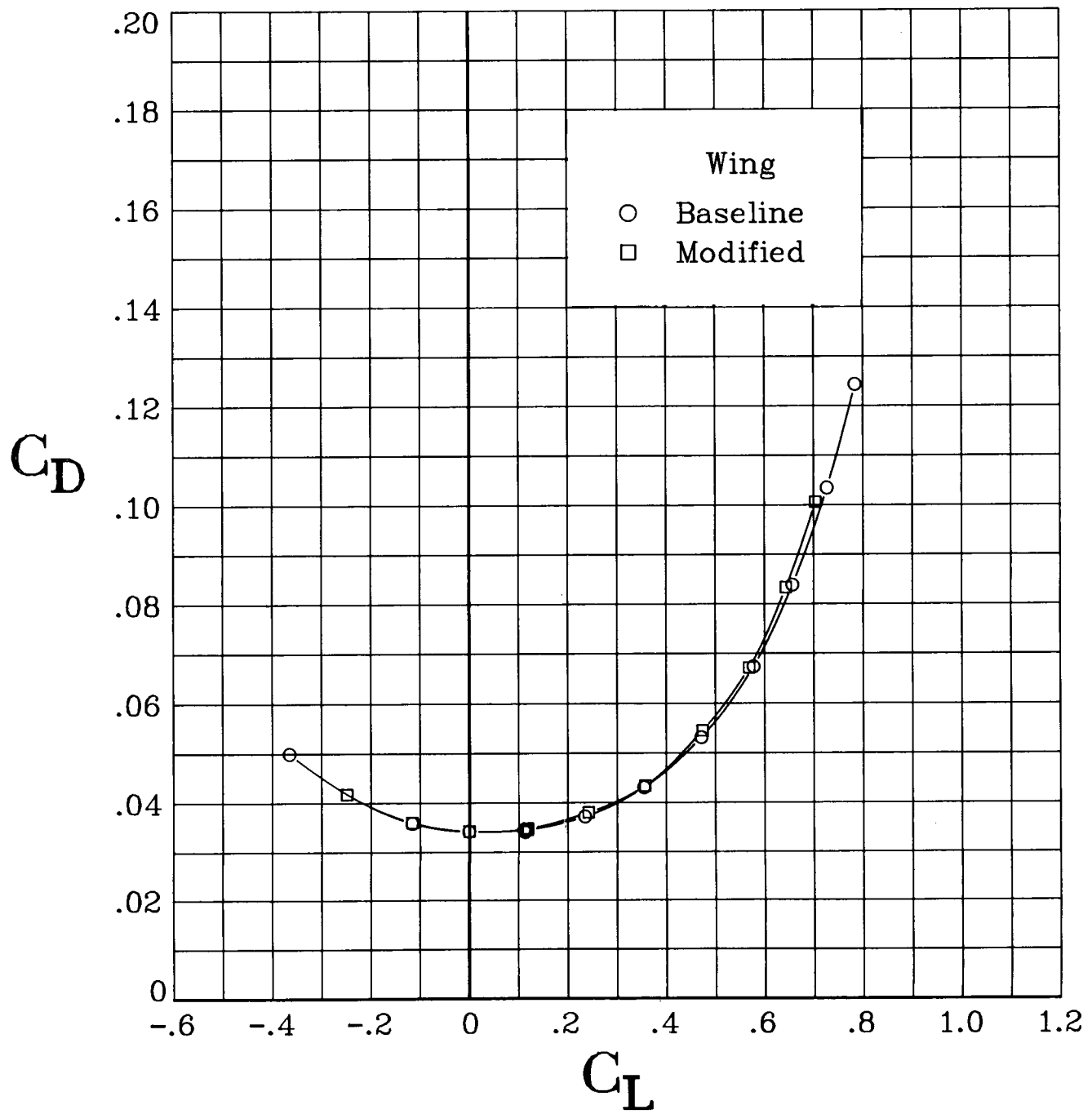
(i) Concluded.

Figure 8. Continued.



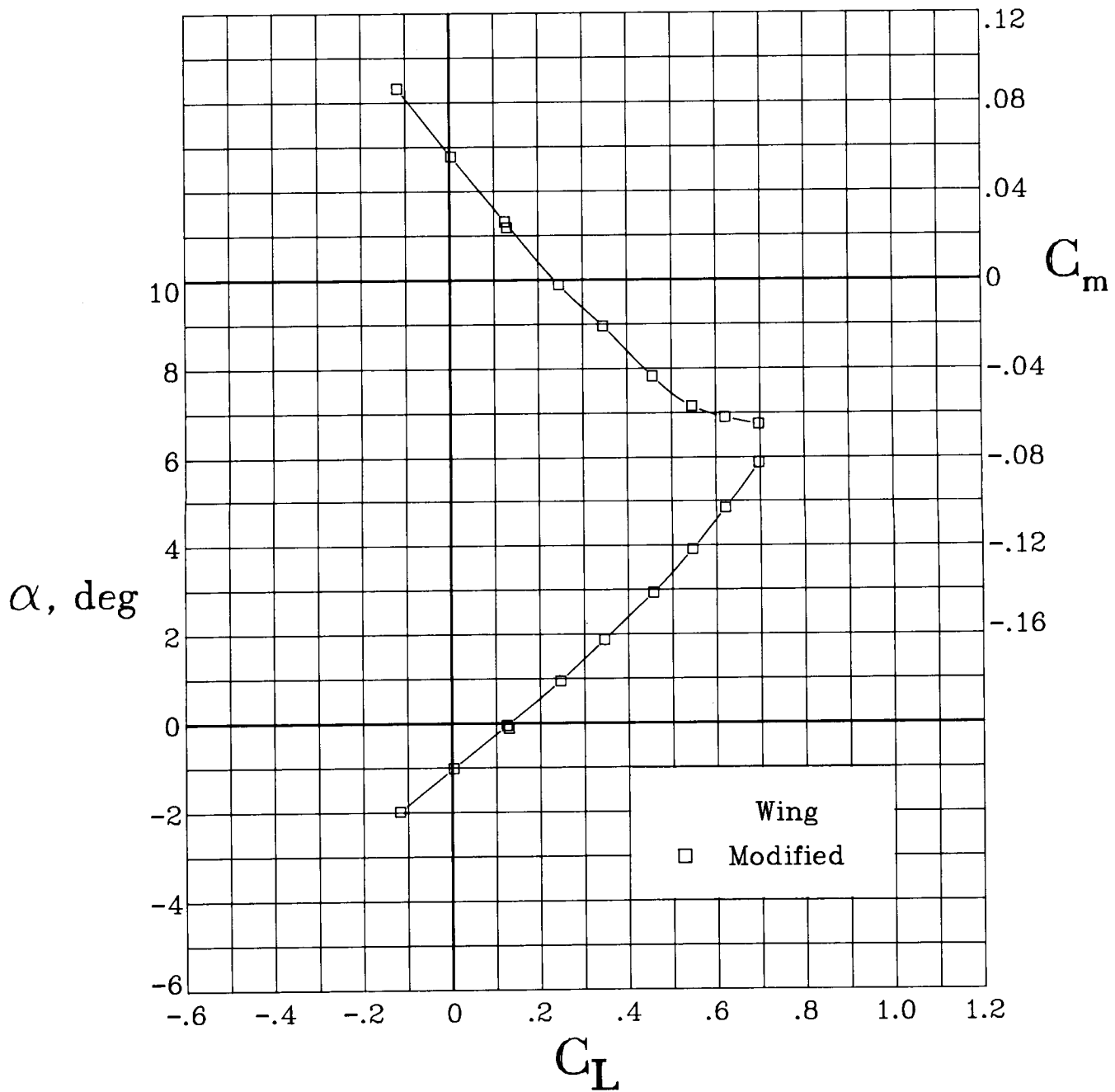
(j) $M = 0.85$.

Figure 8. Continued.



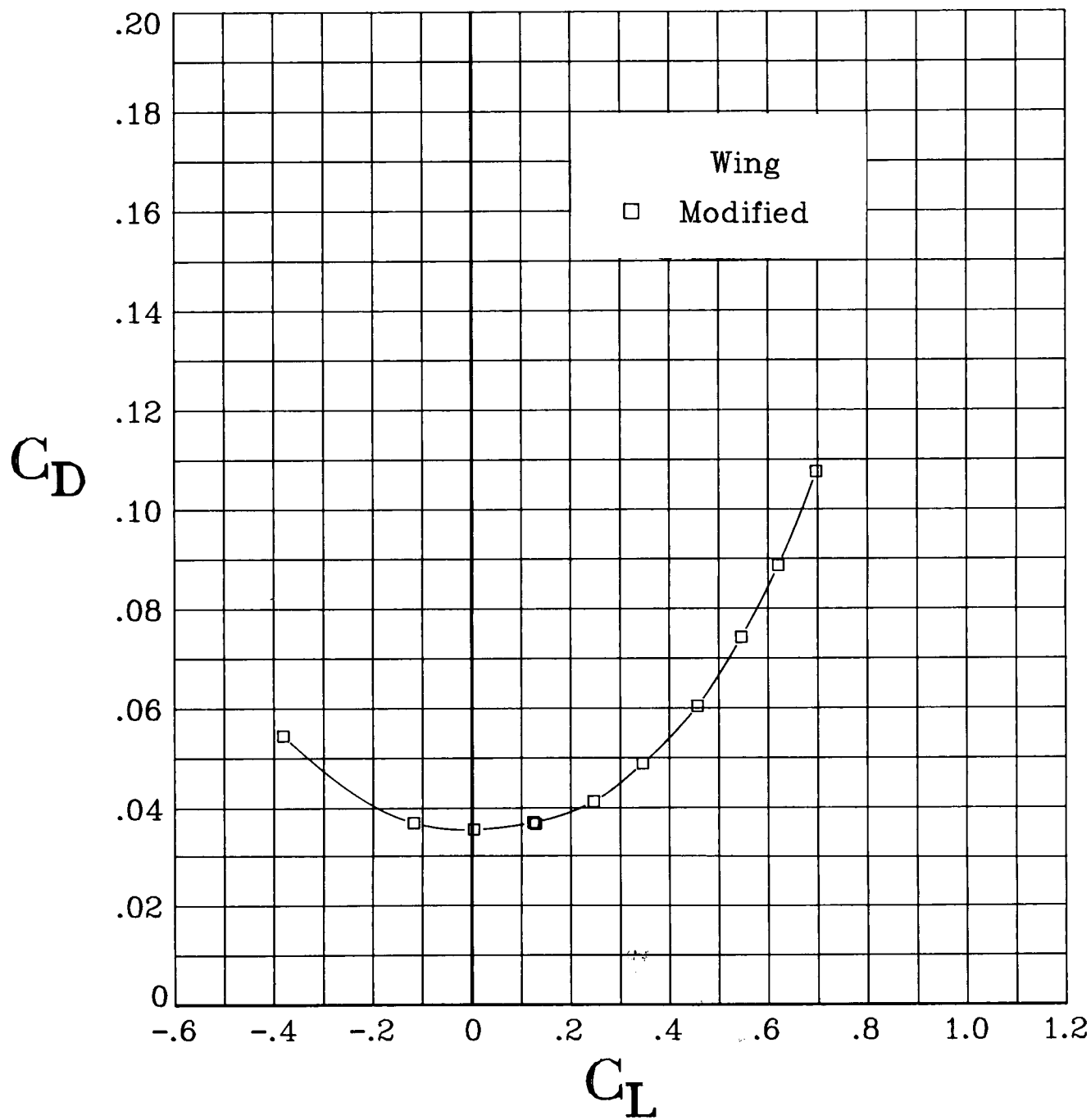
(j) Concluded.

Figure 8. Continued.



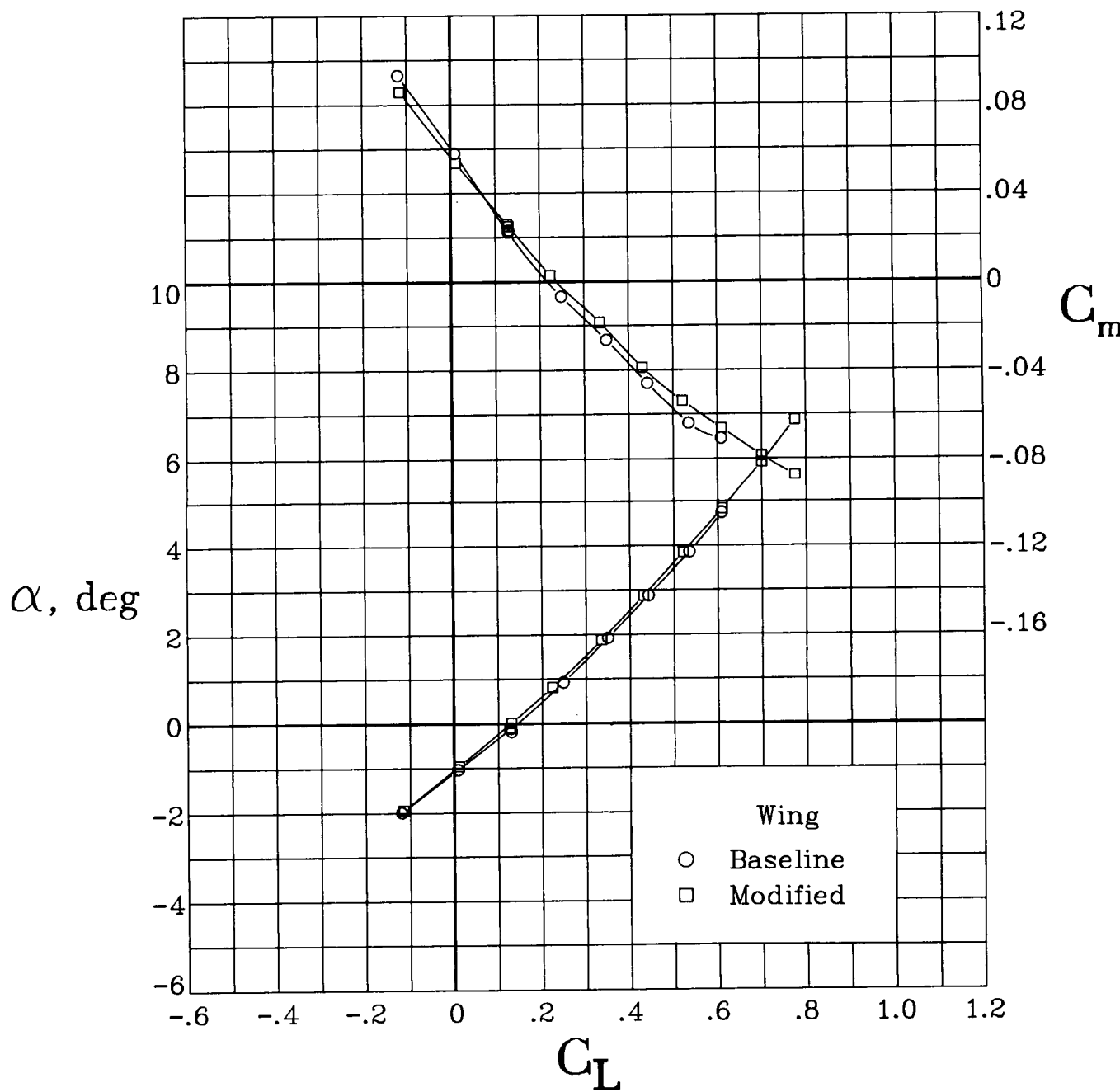
(k) $M = 0.875$.

Figure 8. Continued.



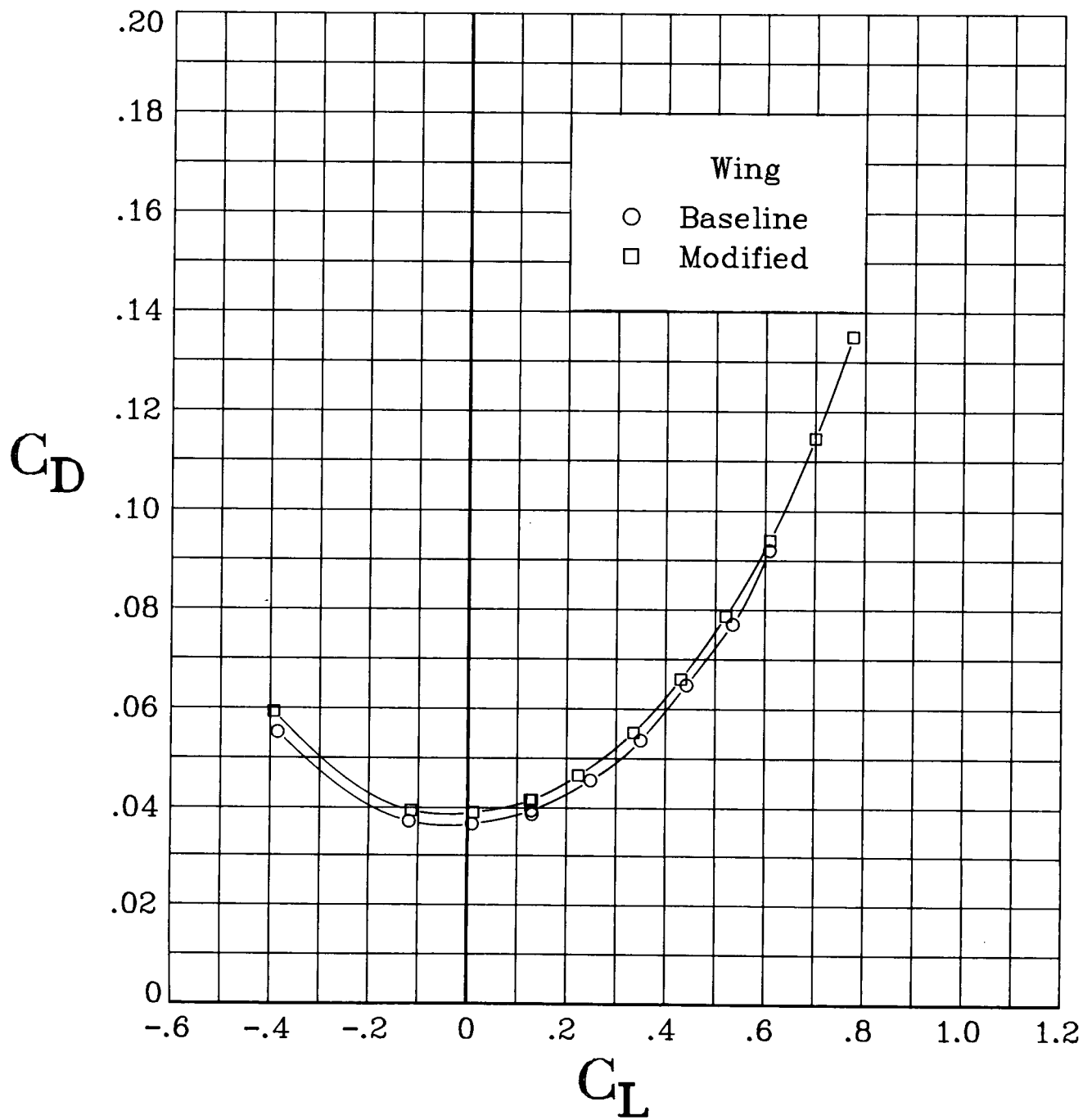
(k) Concluded.

Figure 8. Continued.



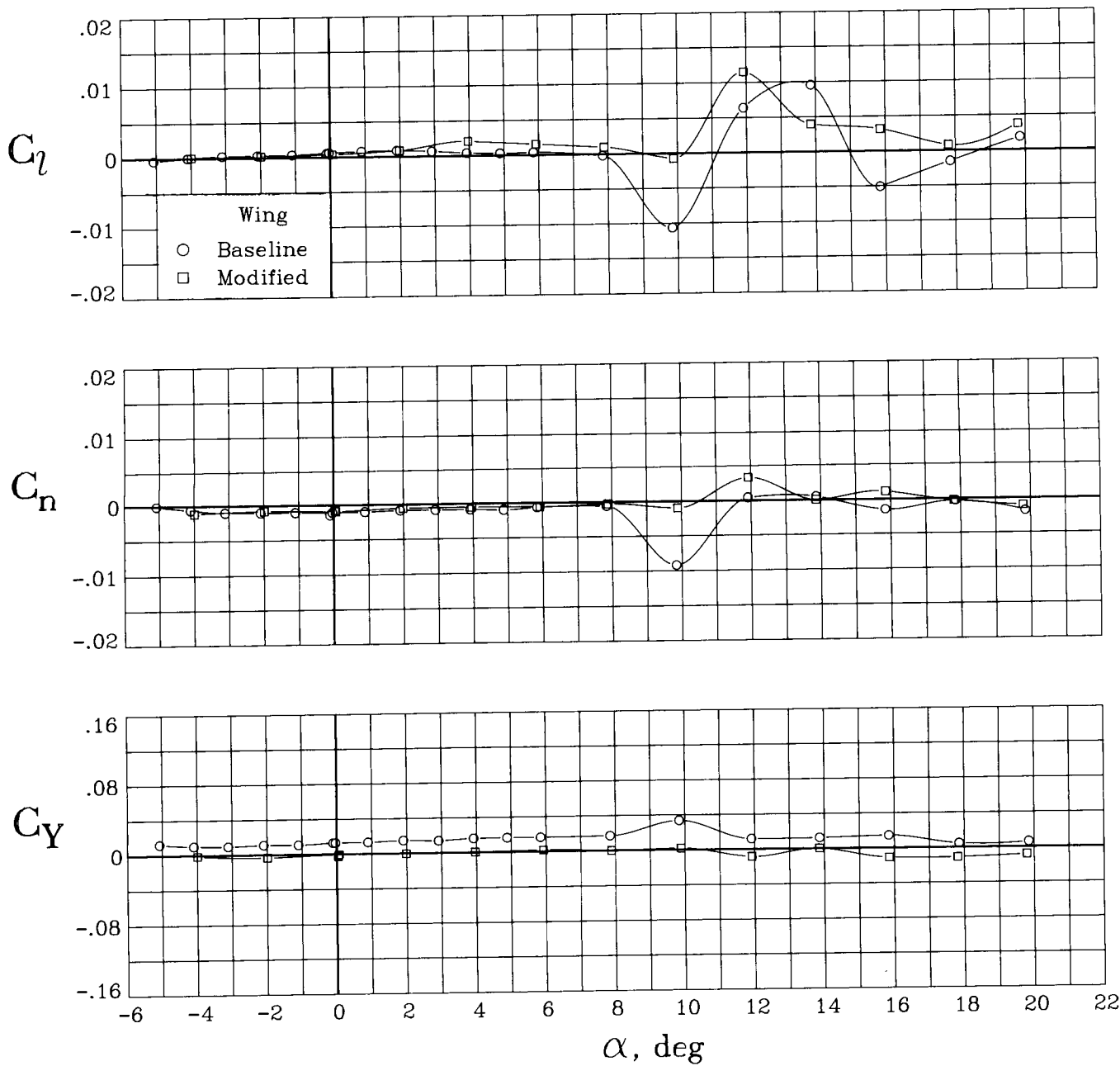
(1) $M = 0.90$.

Figure 8. Continued.



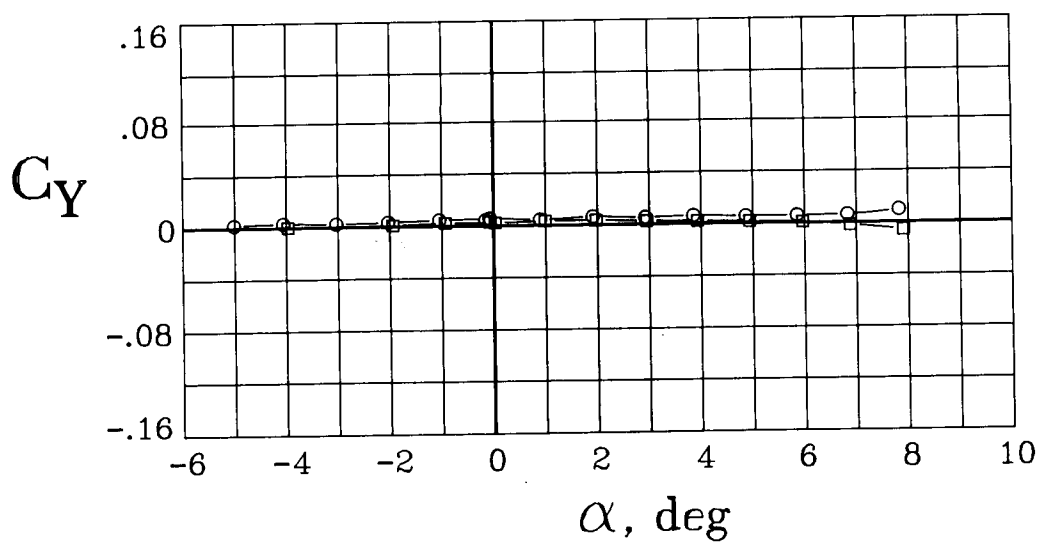
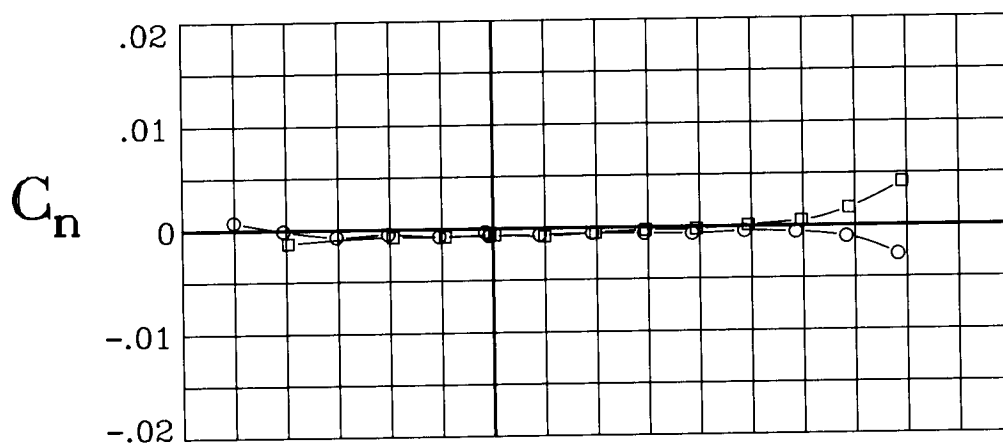
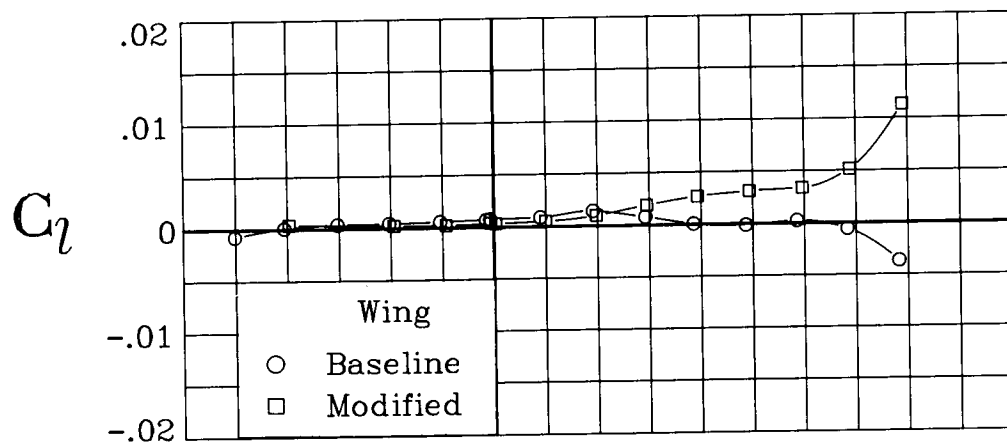
(l) Concluded.

Figure 8. Concluded.



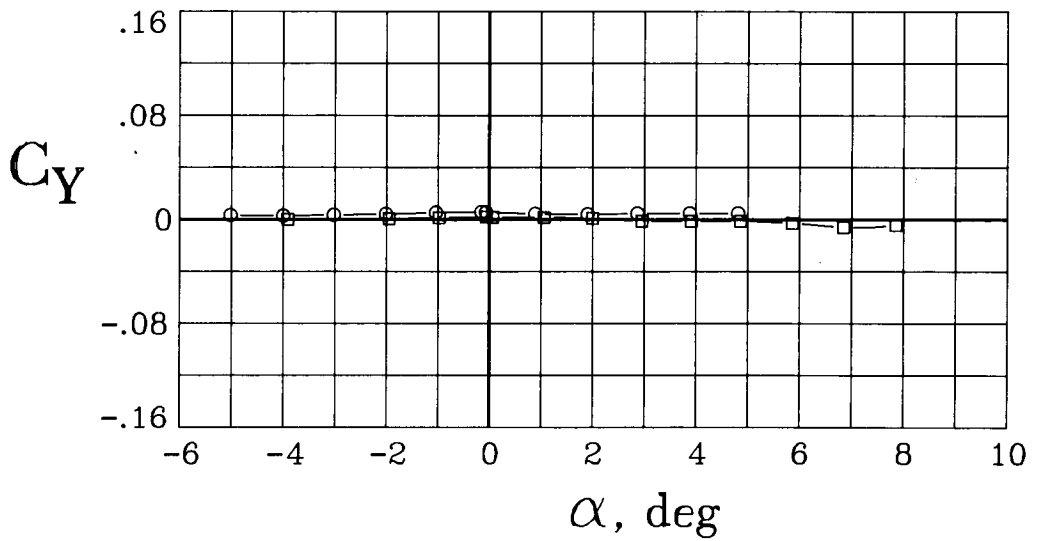
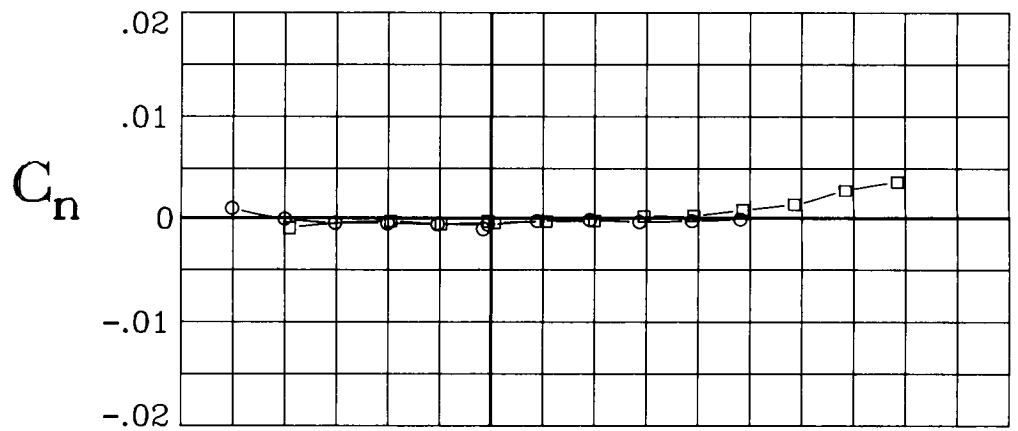
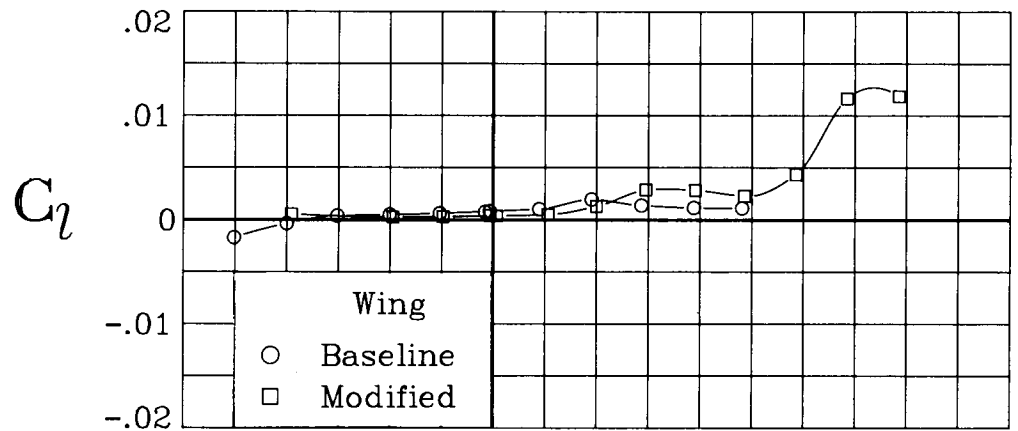
(a) $M = 0.20$.

Figure 9. Lateral-directional aerodynamic characteristics of the baseline and modified wing configurations, with wings swept 20° . $\beta = 0^\circ$.



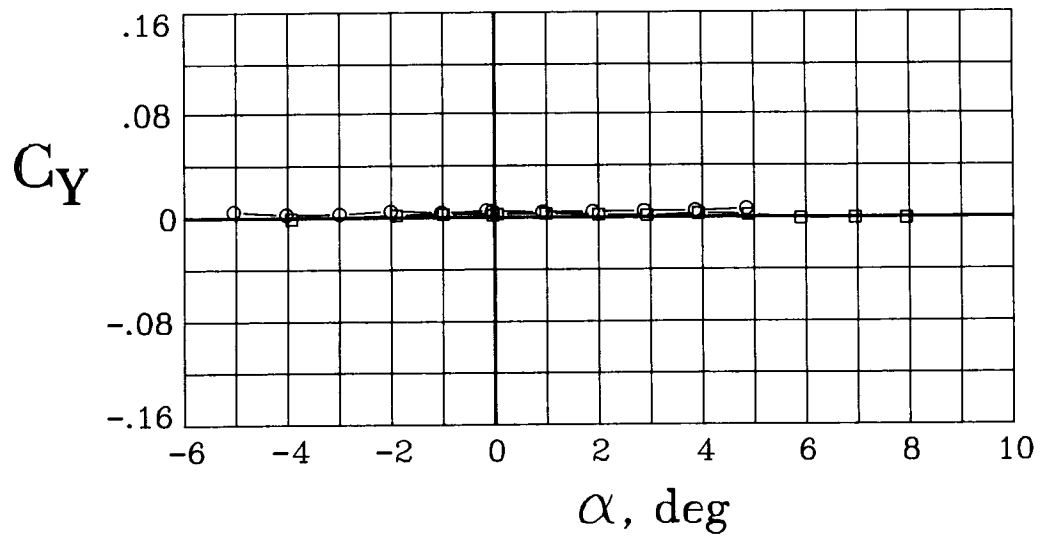
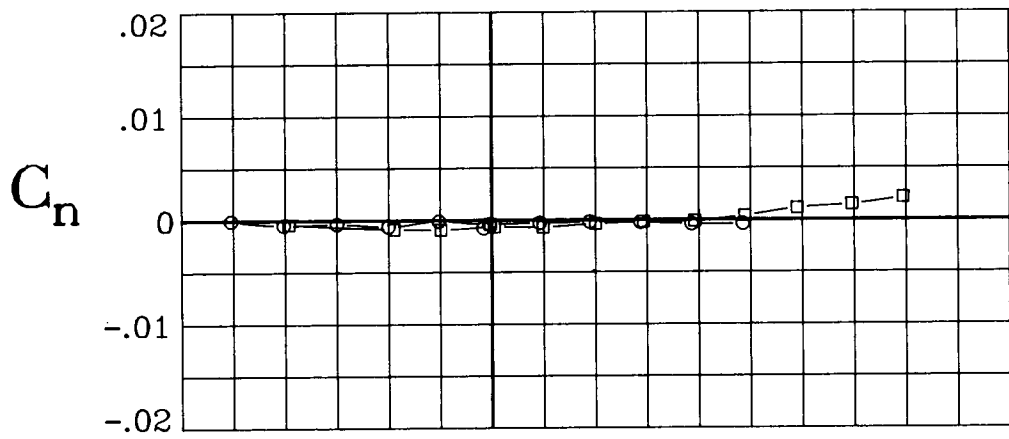
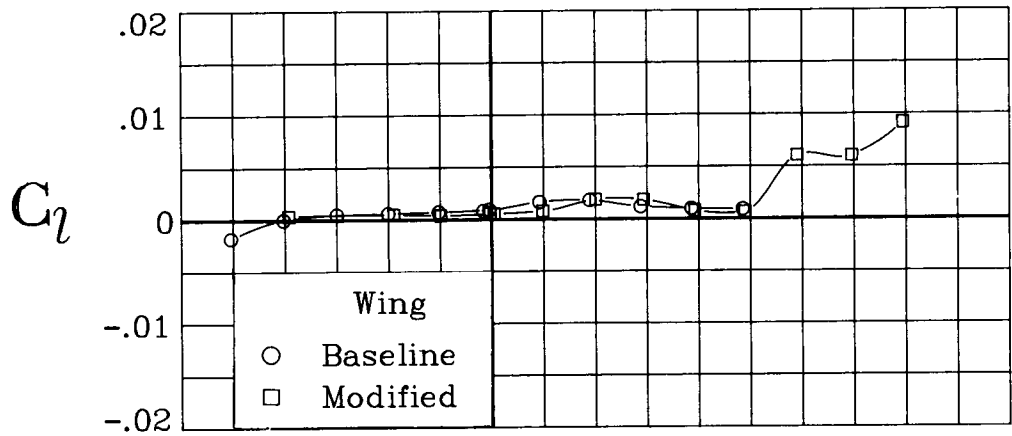
(b) $M = 0.60$.

Figure 9. Continued.



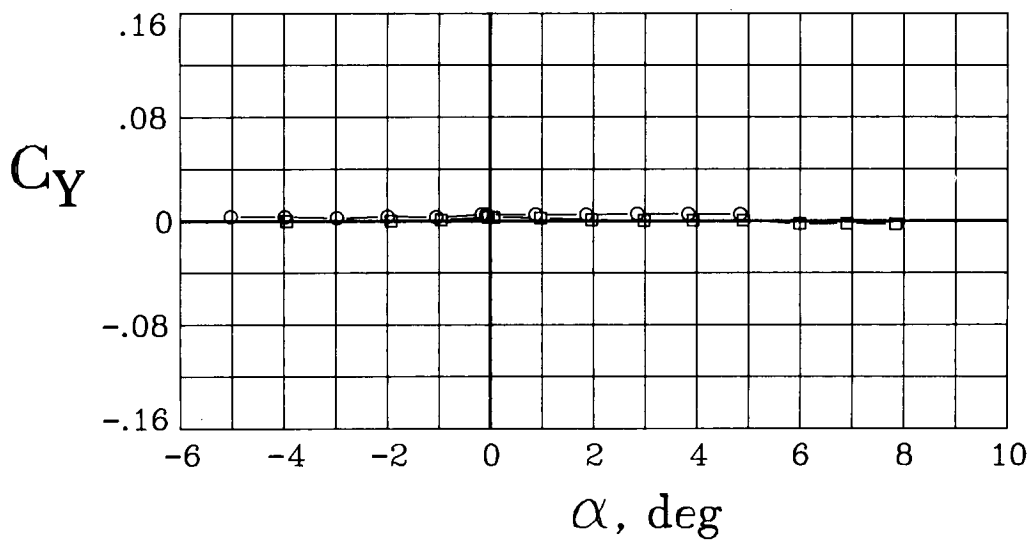
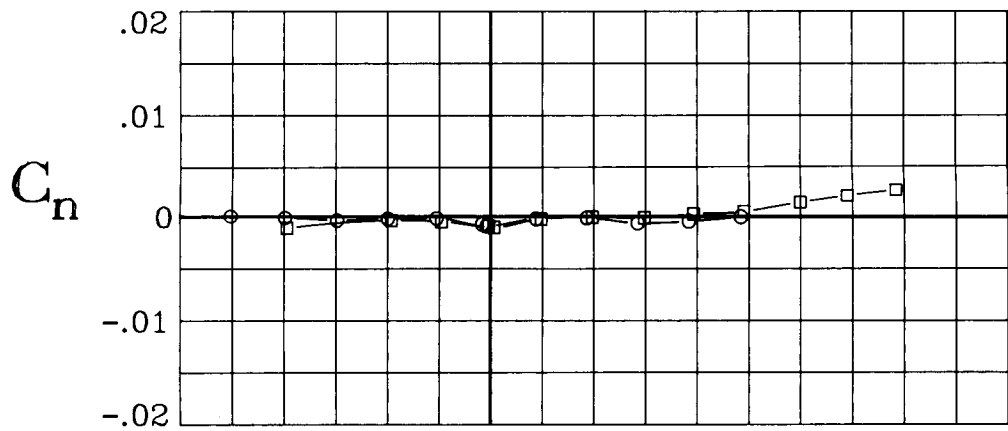
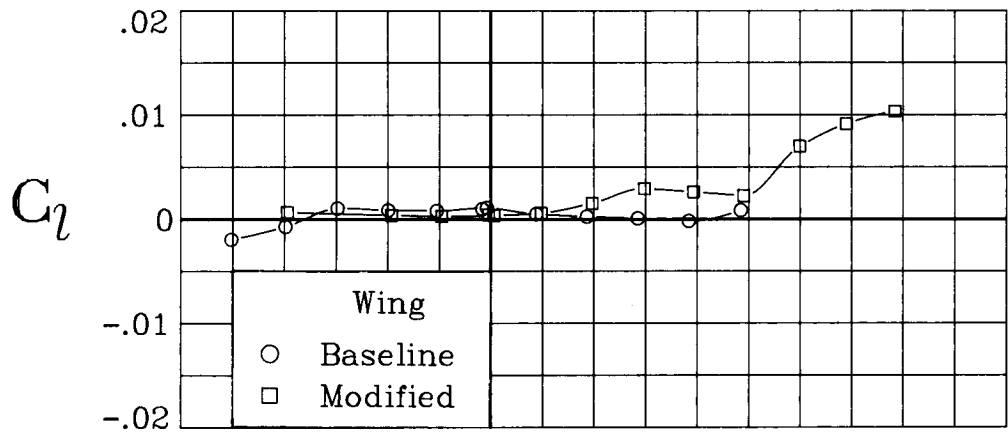
(c) $M = 0.70$.

Figure 9. Continued.



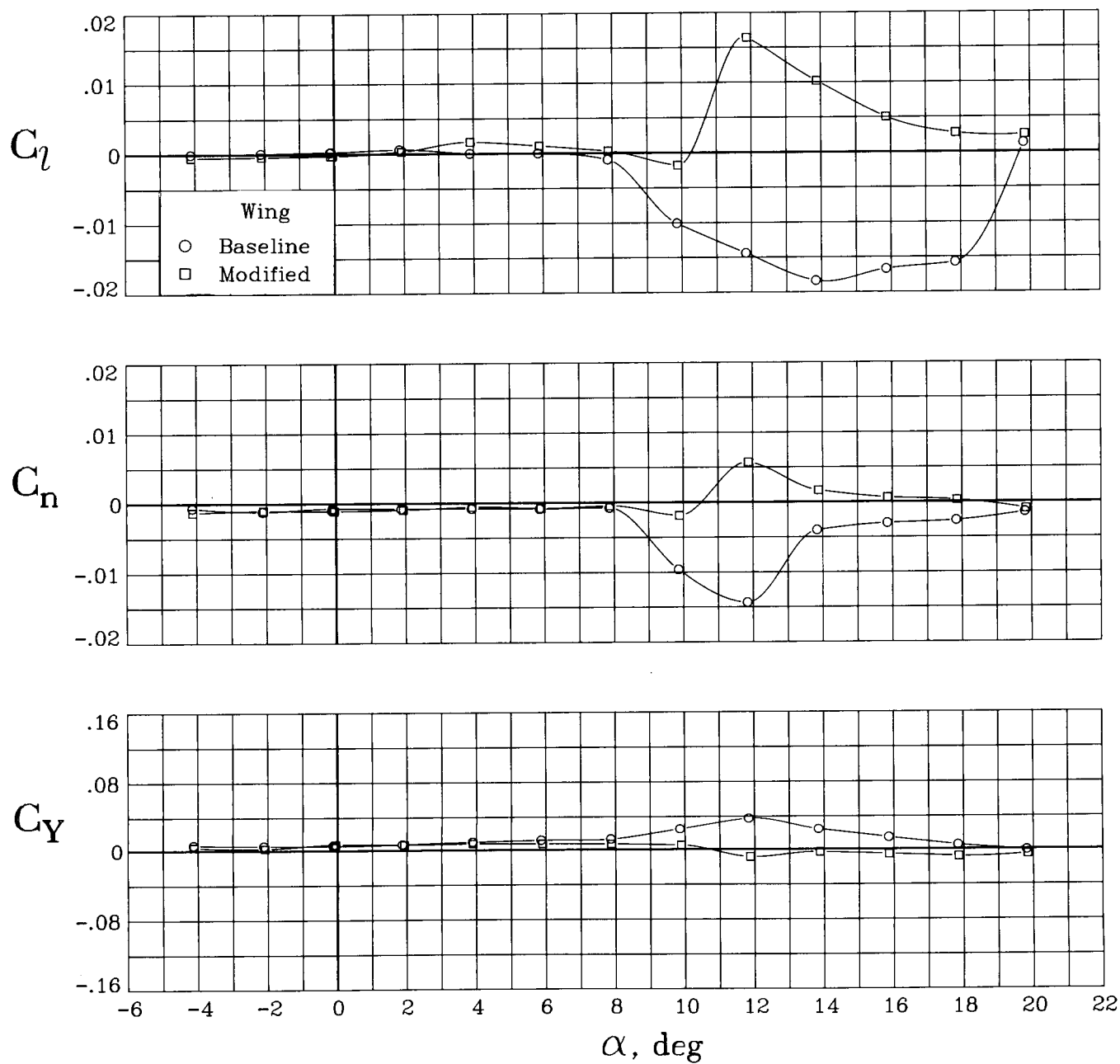
(d) $M = 0.75$.

Figure 9. Continued.



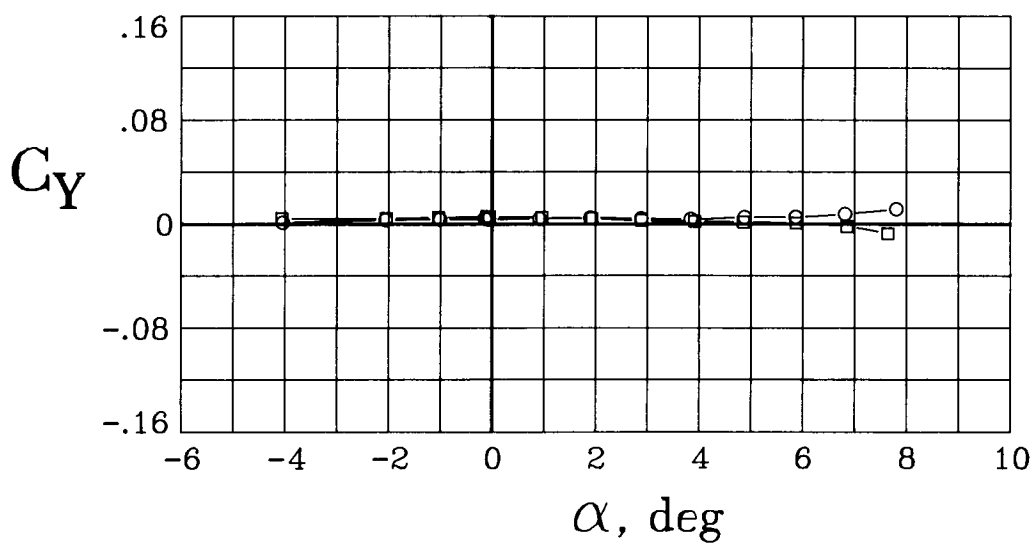
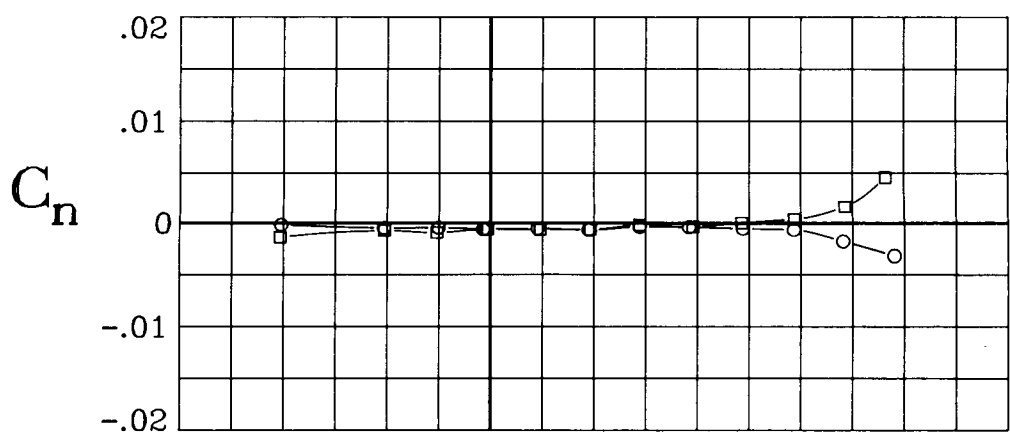
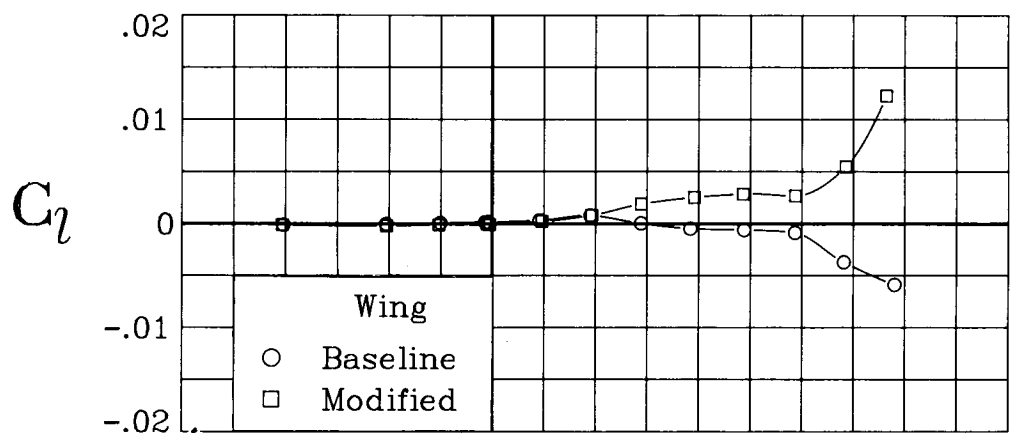
(e) $M = 0.80$.

Figure 9. Concluded.



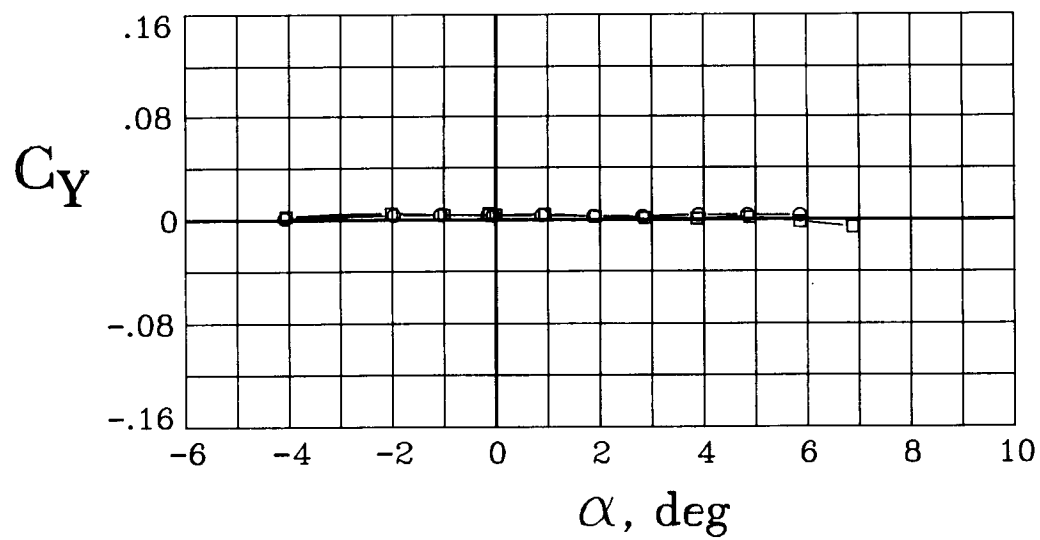
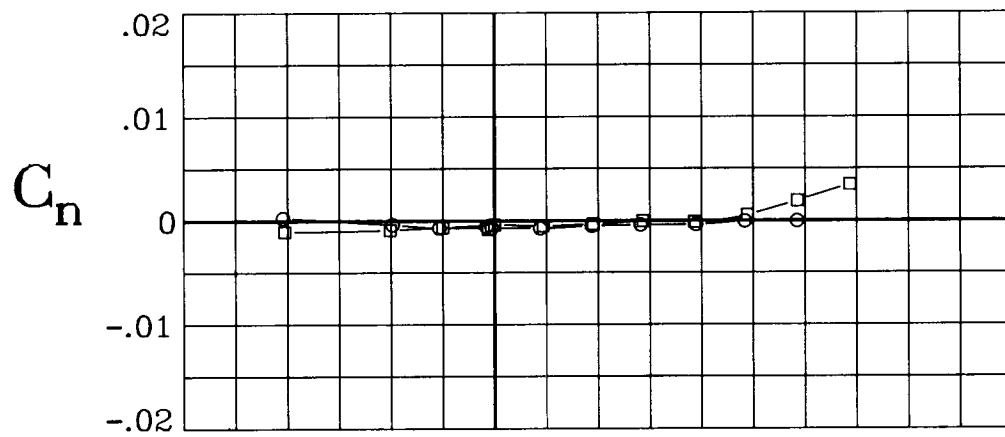
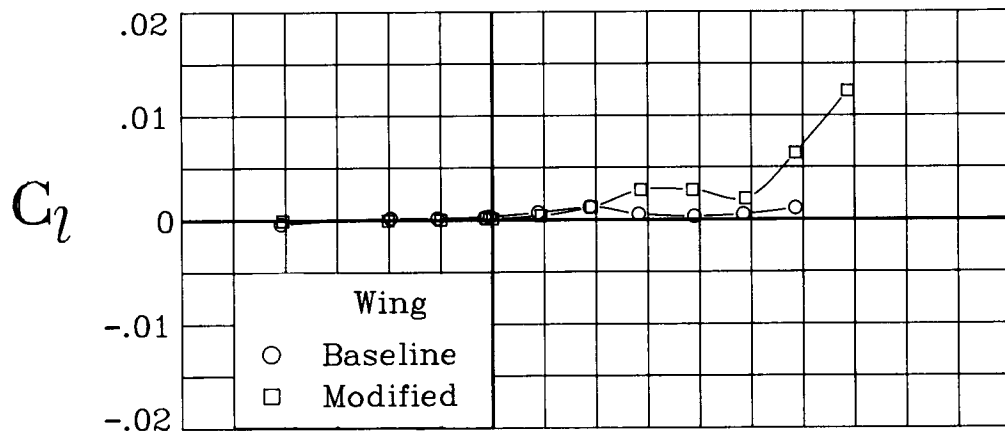
(a) $M = 0.20$.

Figure 10. Lateral-directional aerodynamic characteristics of the baseline and modified wing configurations, with wings swept 25° . $\beta = 0^\circ$.



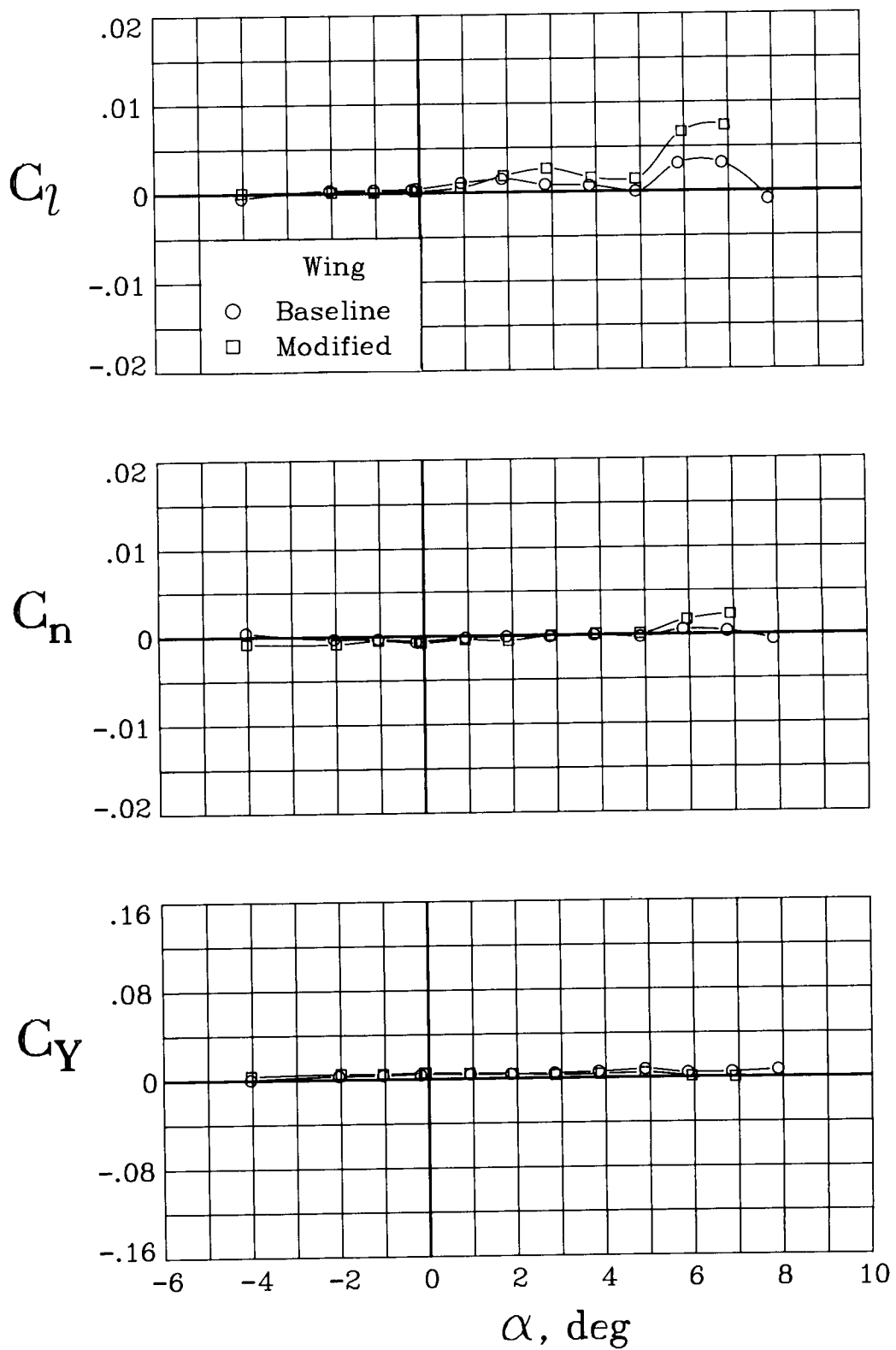
(b) $M = 0.60$.

Figure 10. Continued.



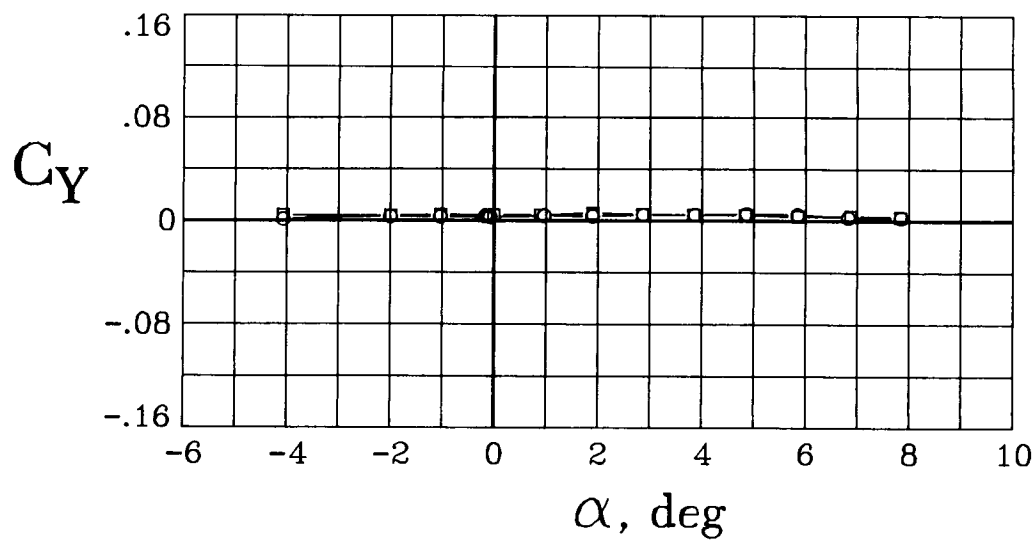
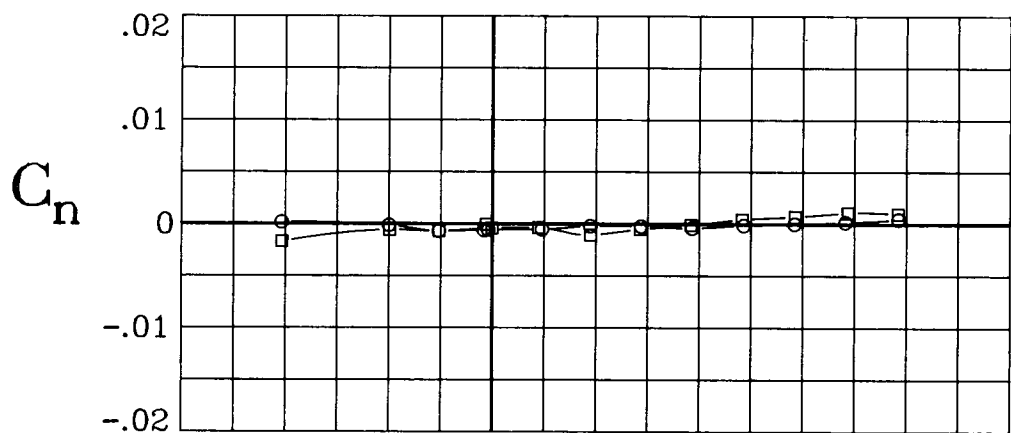
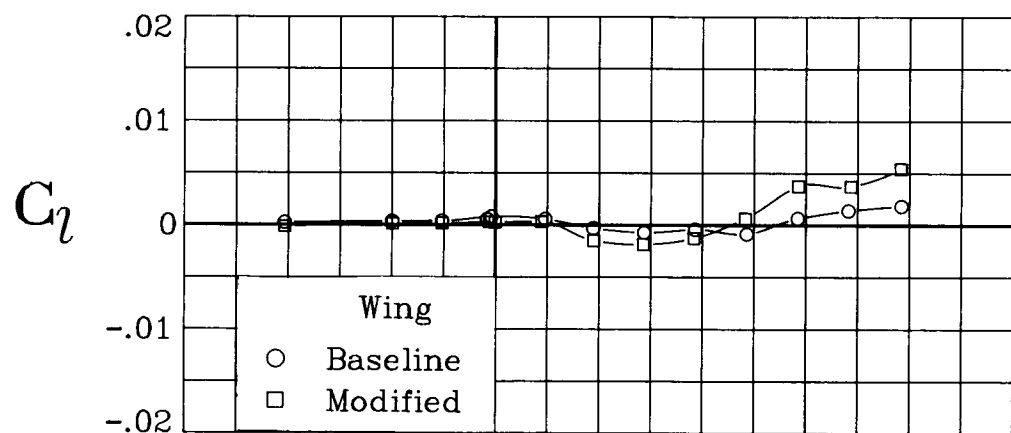
(c) $M = 0.70$.

Figure 10. Continued.



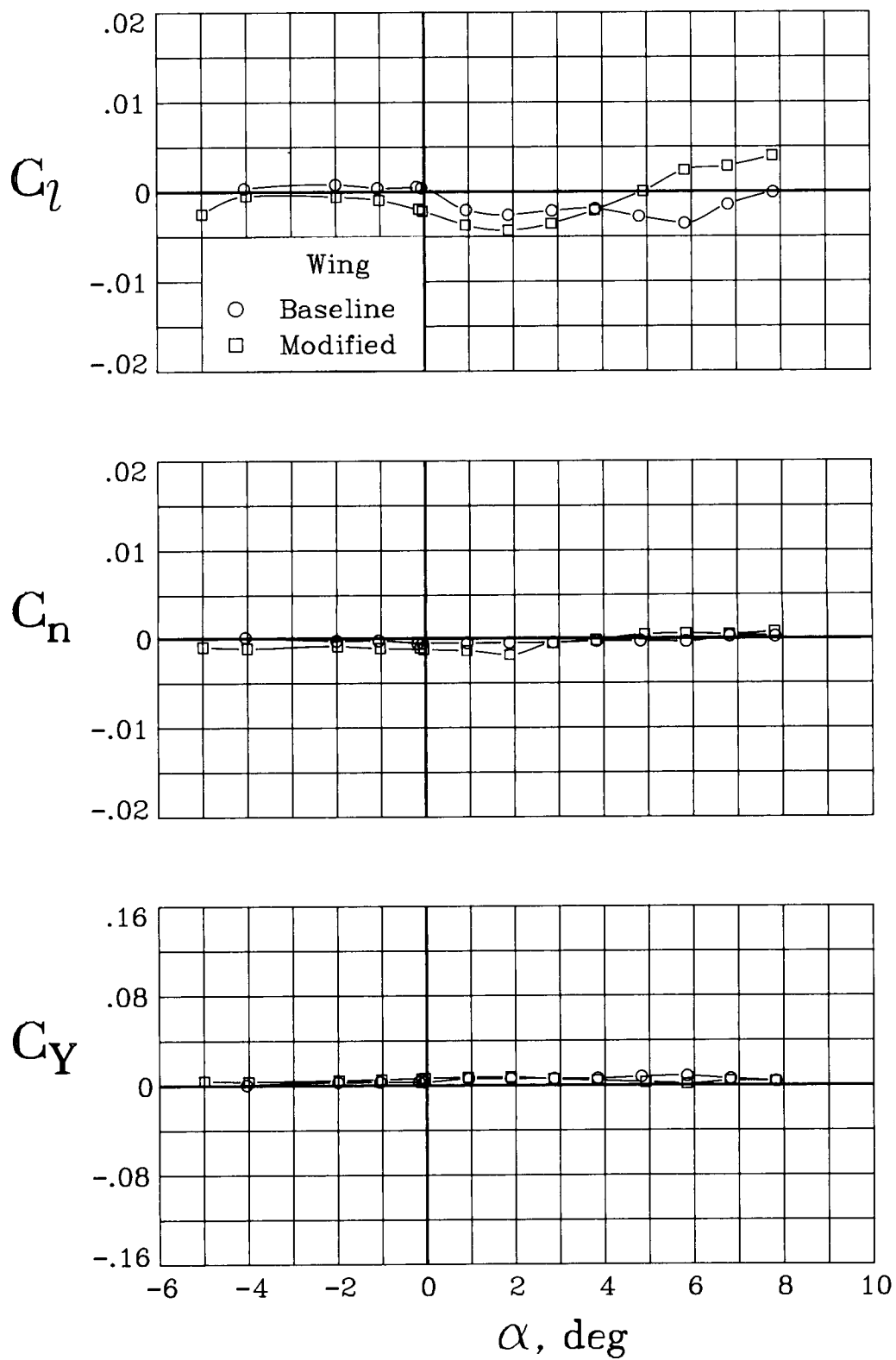
(d) $M = 0.75$.

Figure 10. Continued.



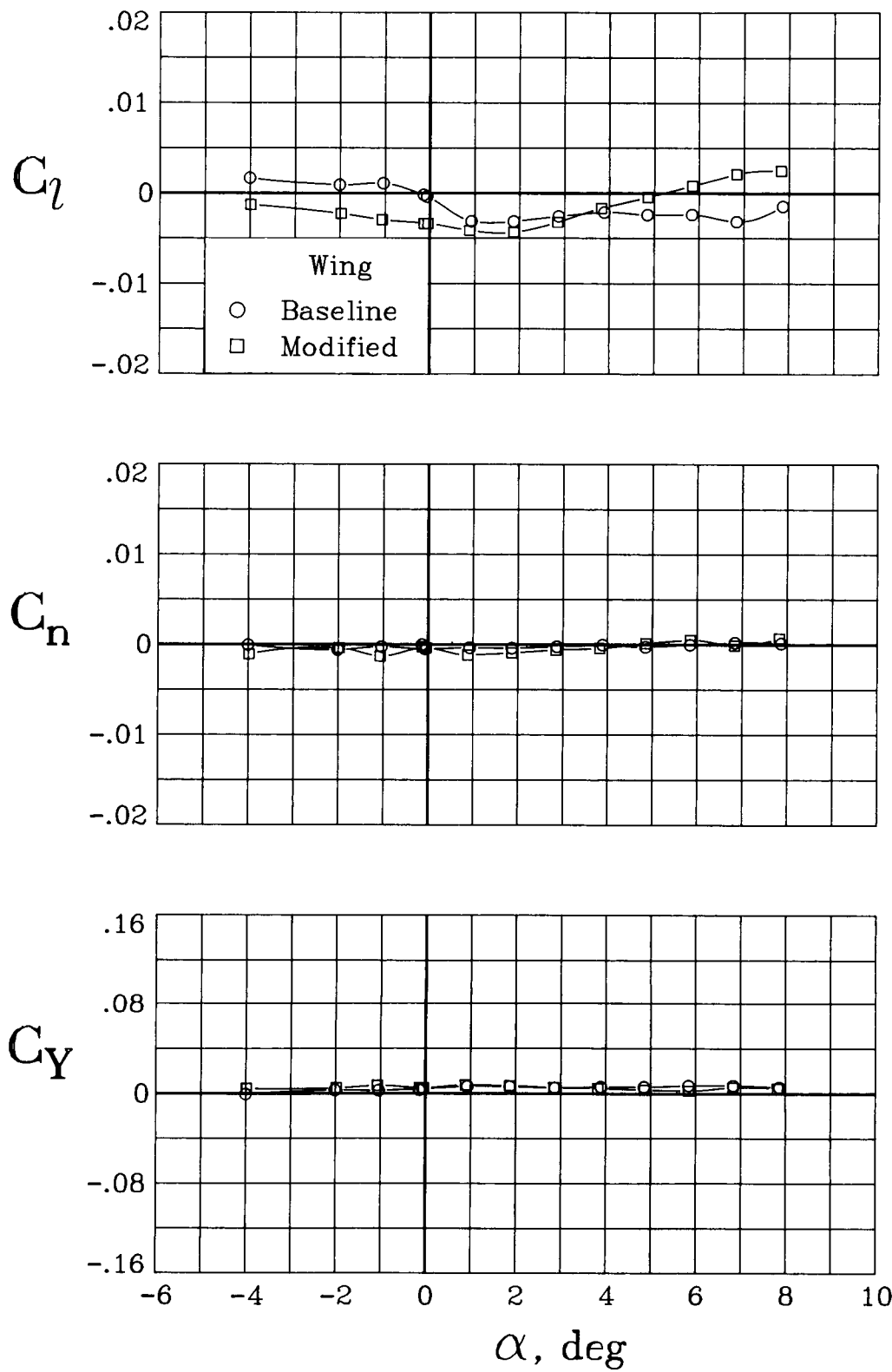
(e) $M = 0.80$.

Figure 10. Continued.



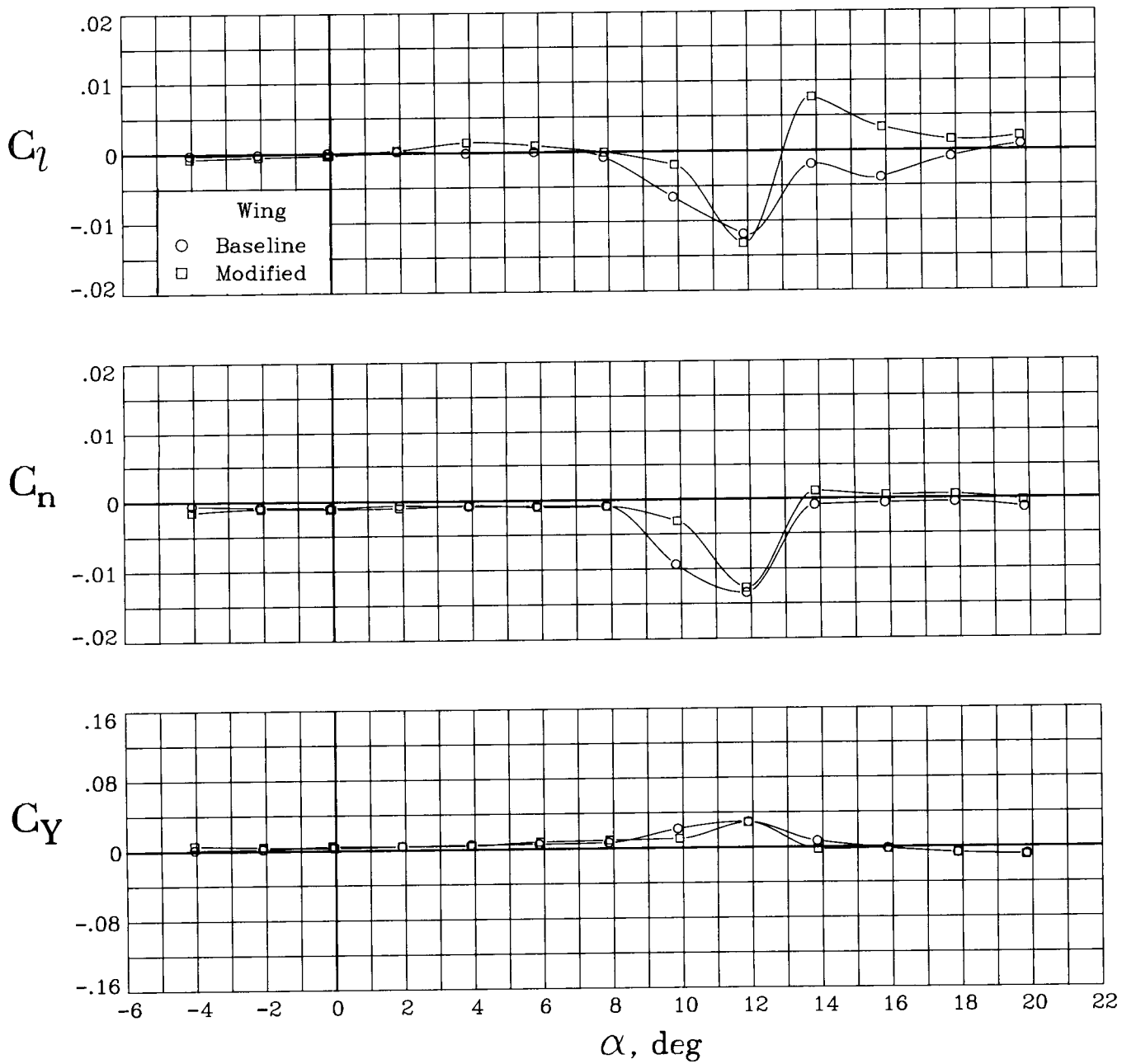
(f) $M = 0.85$.

Figure 10. Continued.



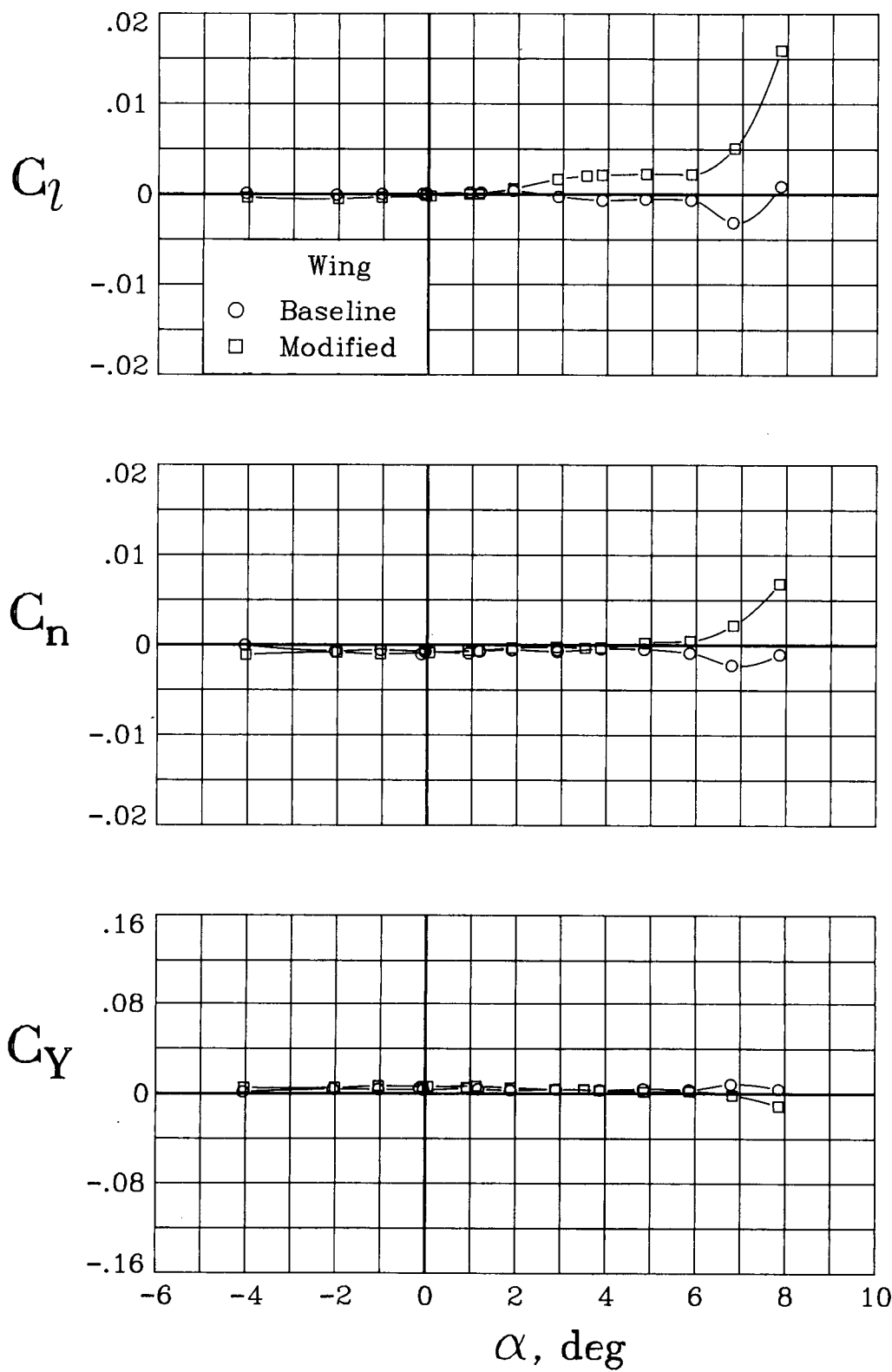
(g) $M = 0.875$.

Figure 10. Concluded.



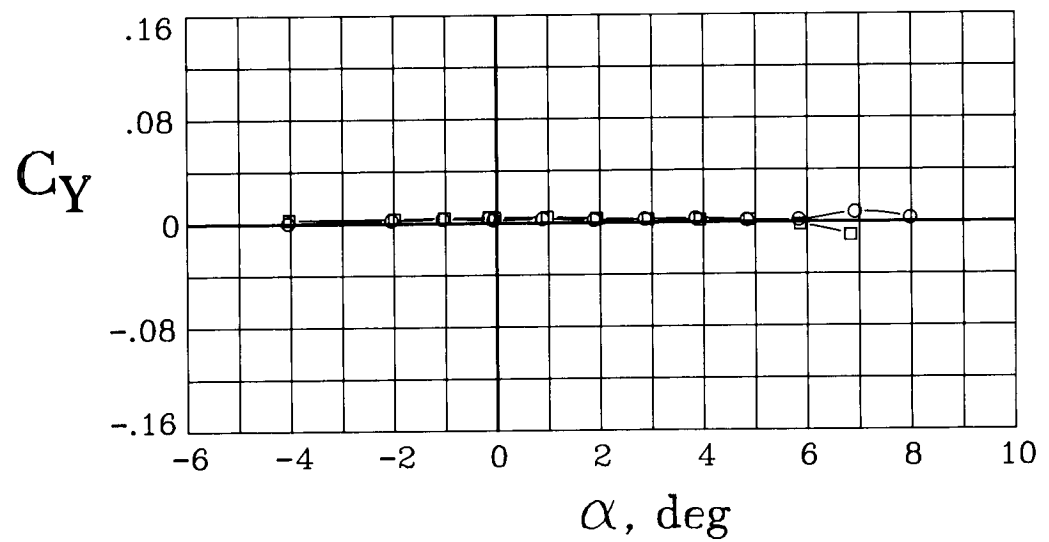
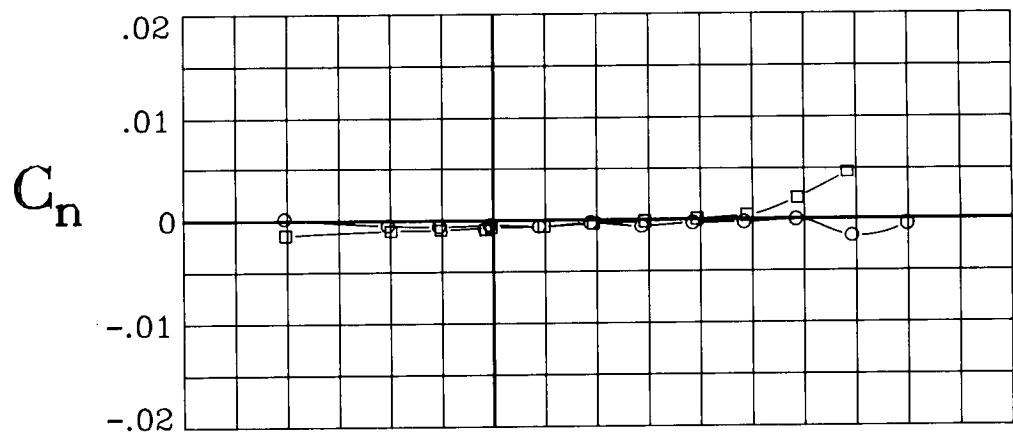
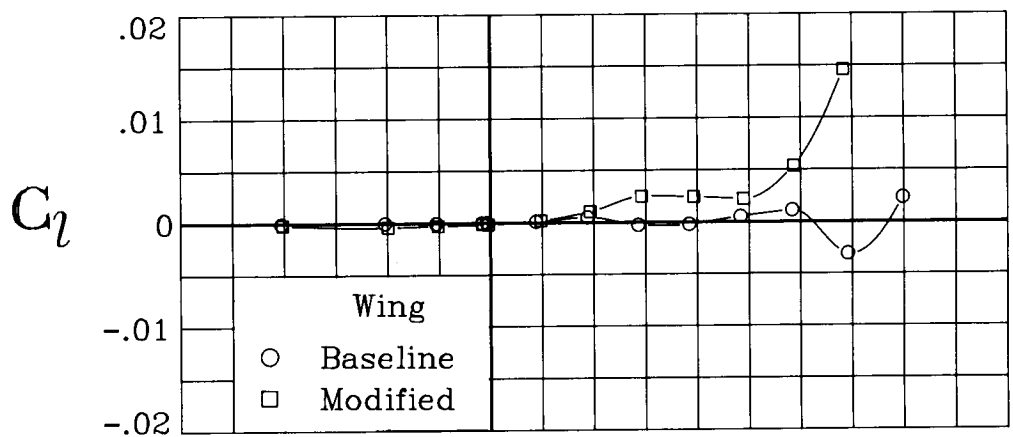
(a) $M = 0.20$.

Figure 11. Lateral-directional aerodynamic characteristics of the baseline and modified wing configurations, with wings swept 30° . $\beta = 0^\circ$.



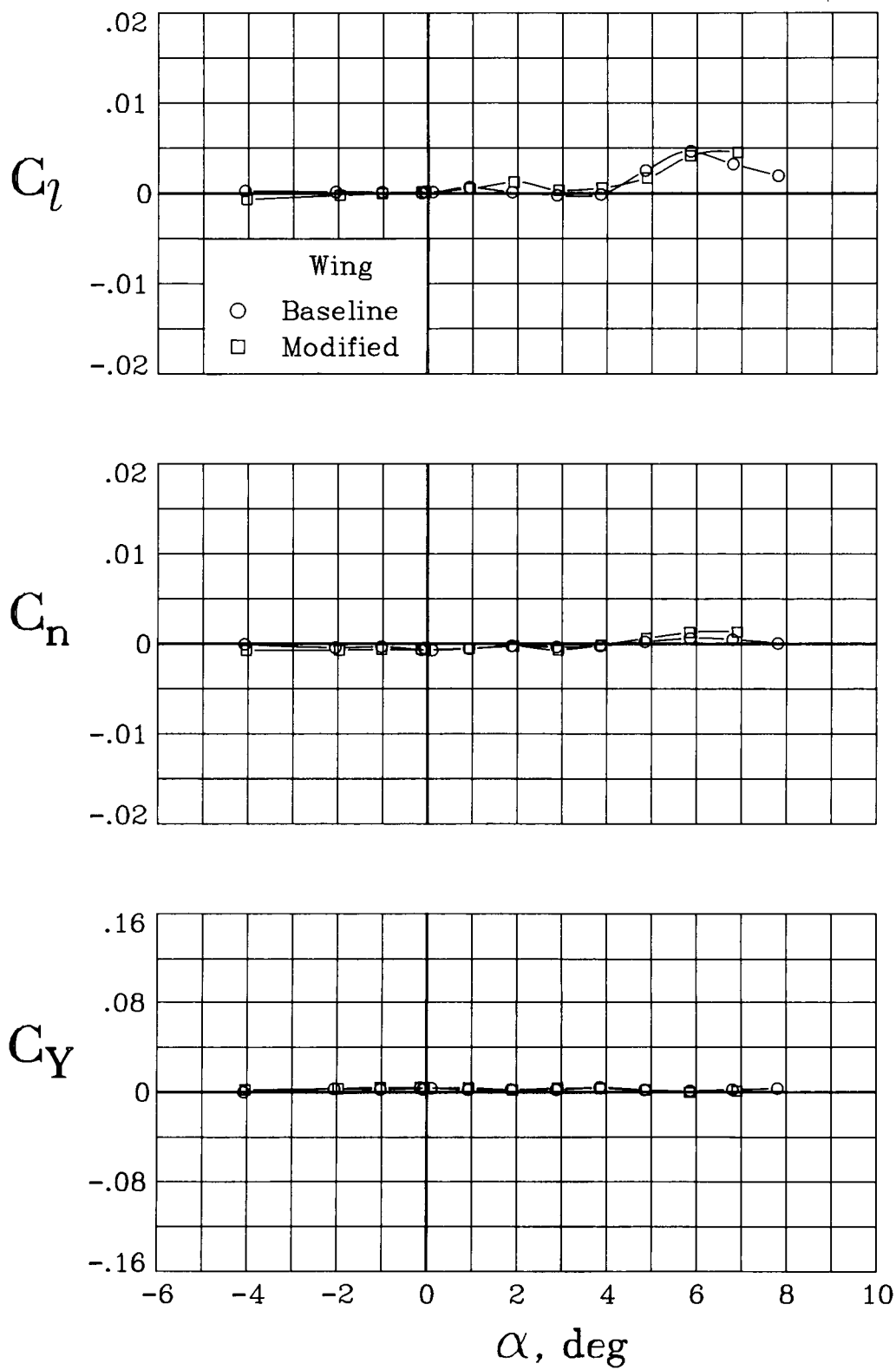
(b) $M = 0.60$.

Figure 11. Continued.



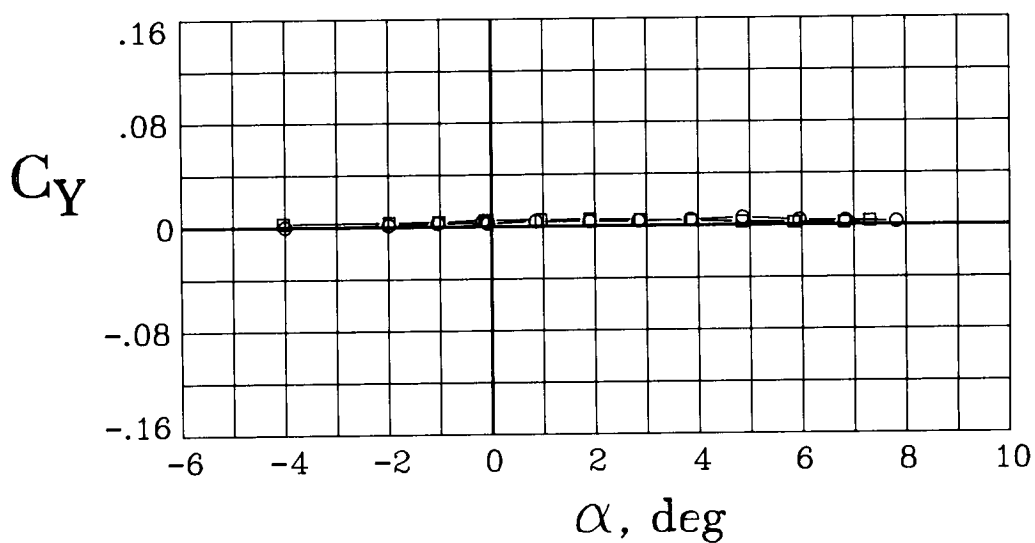
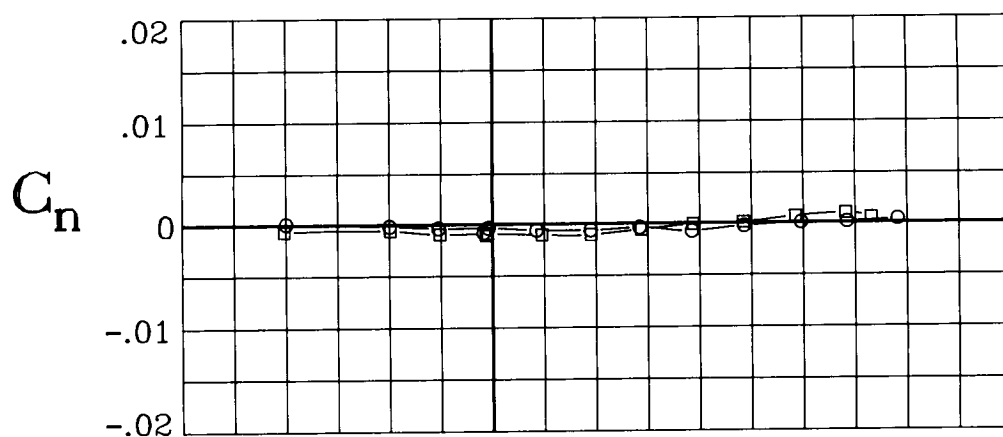
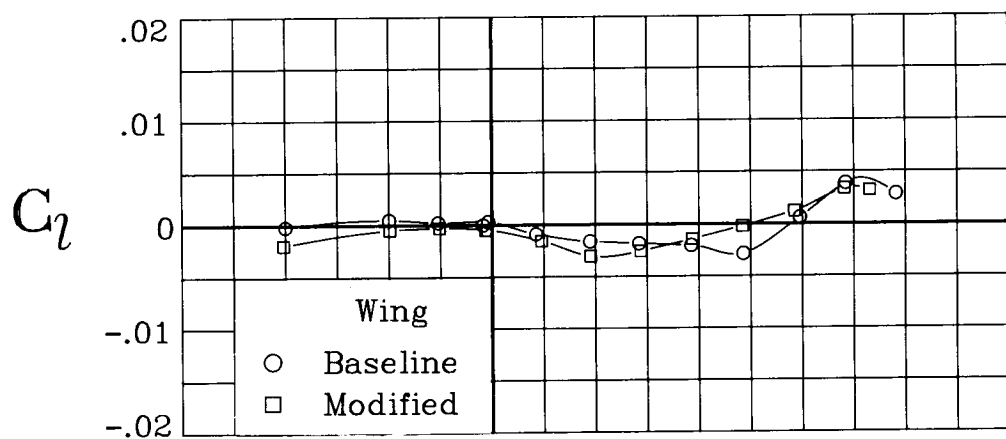
(c) $M = 0.70$.

Figure 11. Continued.



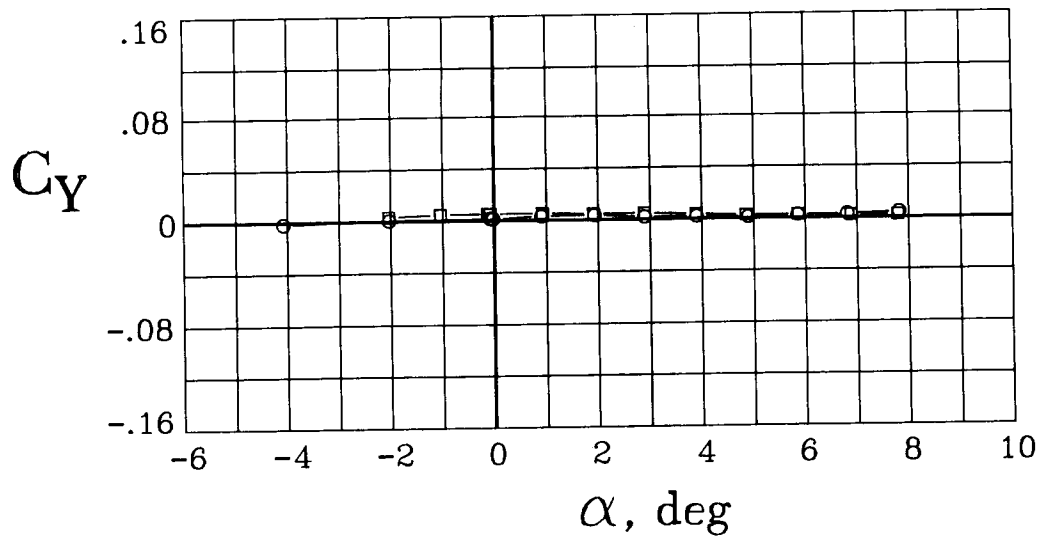
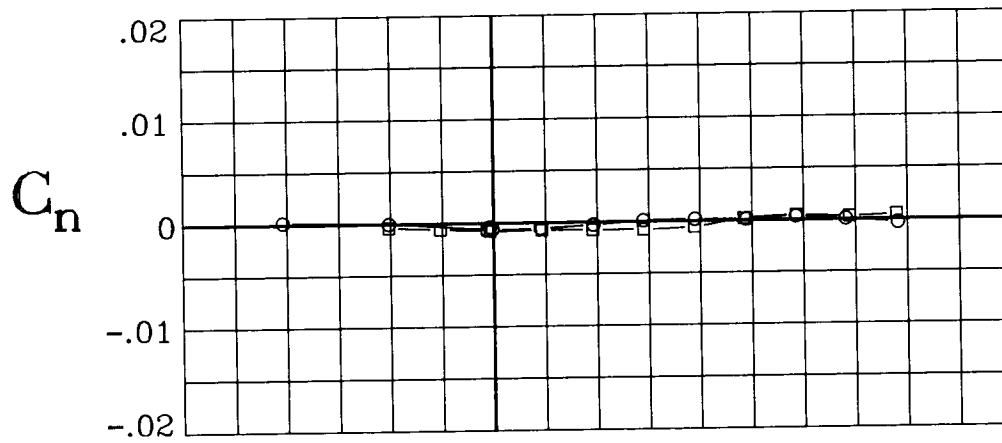
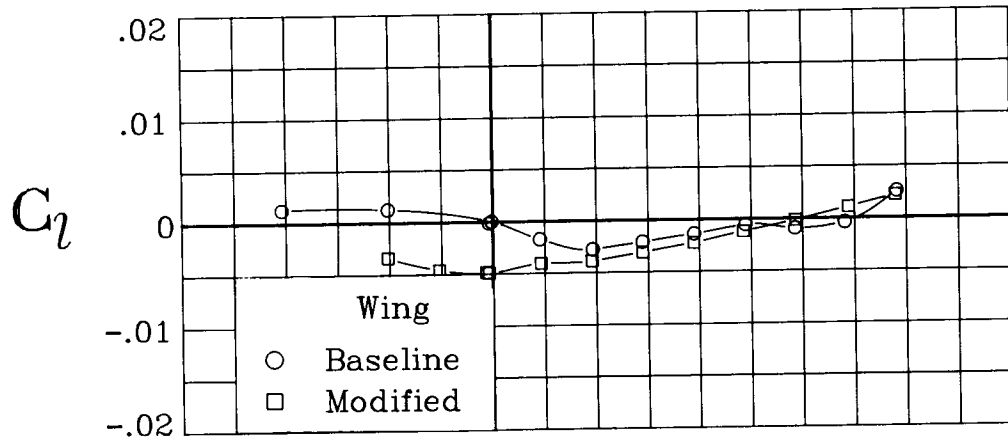
(d) $M = 0.80$.

Figure 11. Continued.



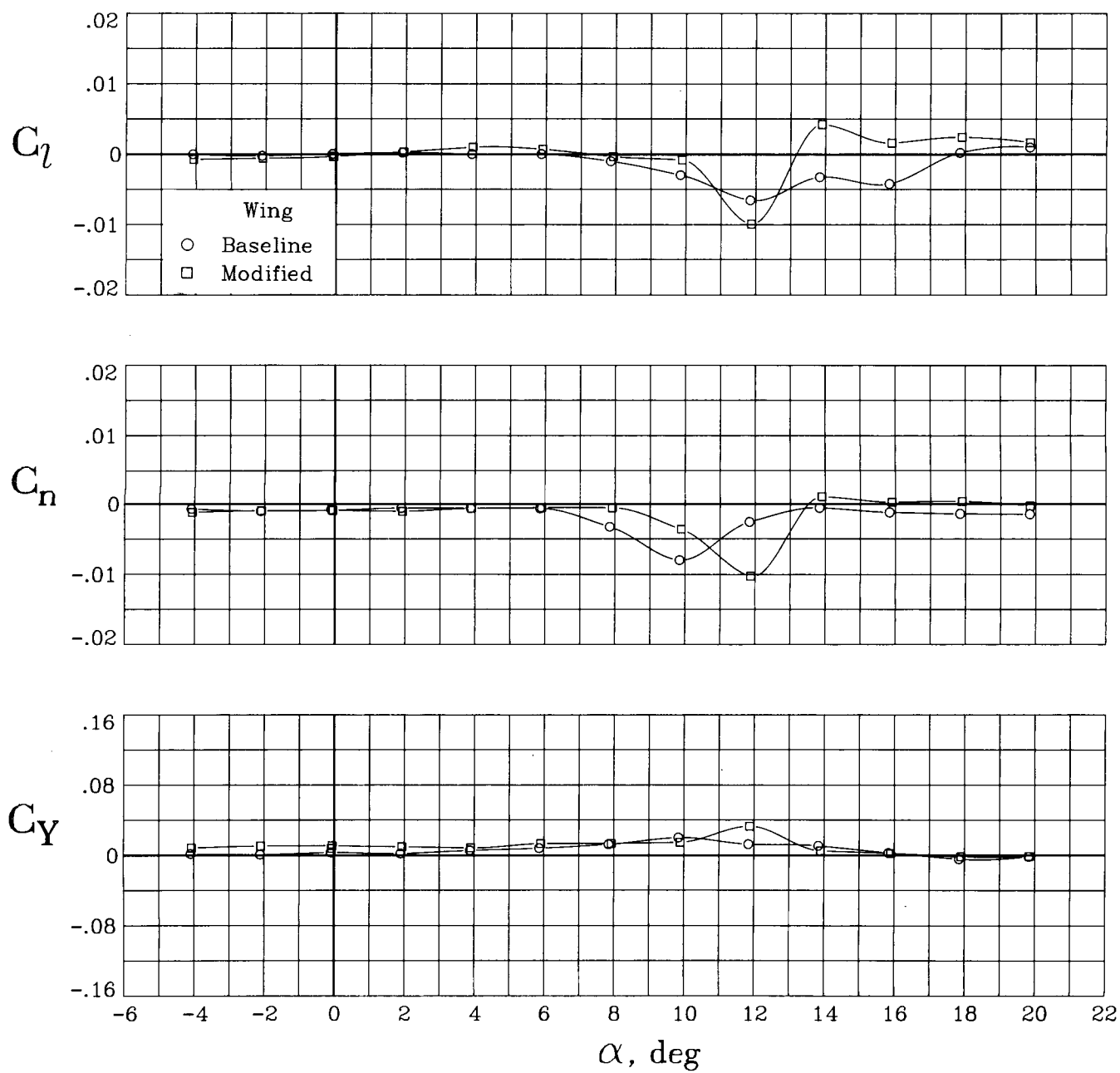
(e) $M = 0.85$.

Figure 11. Continued.



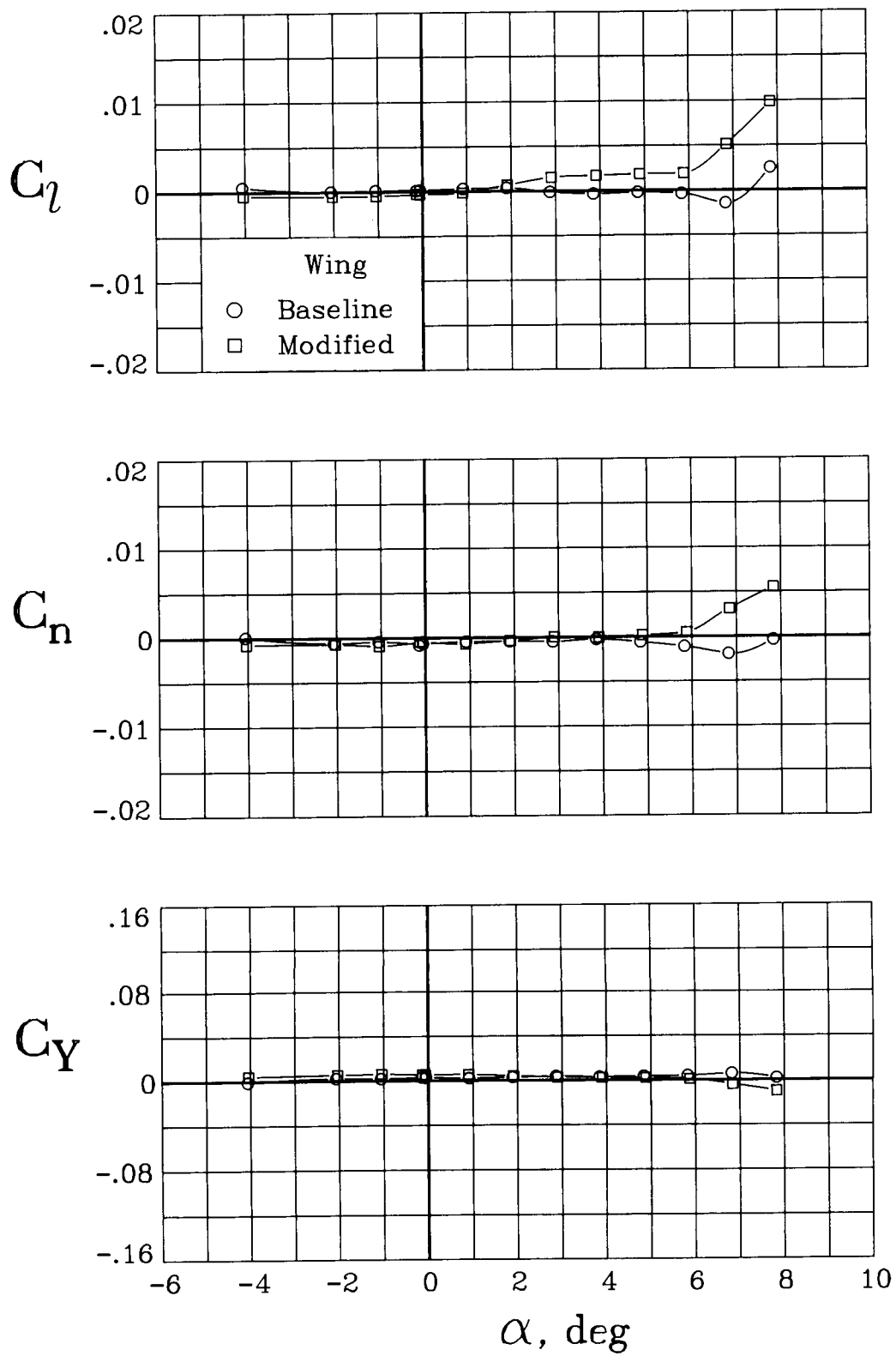
(f) $M = 0.90$.

Figure 11. Concluded.



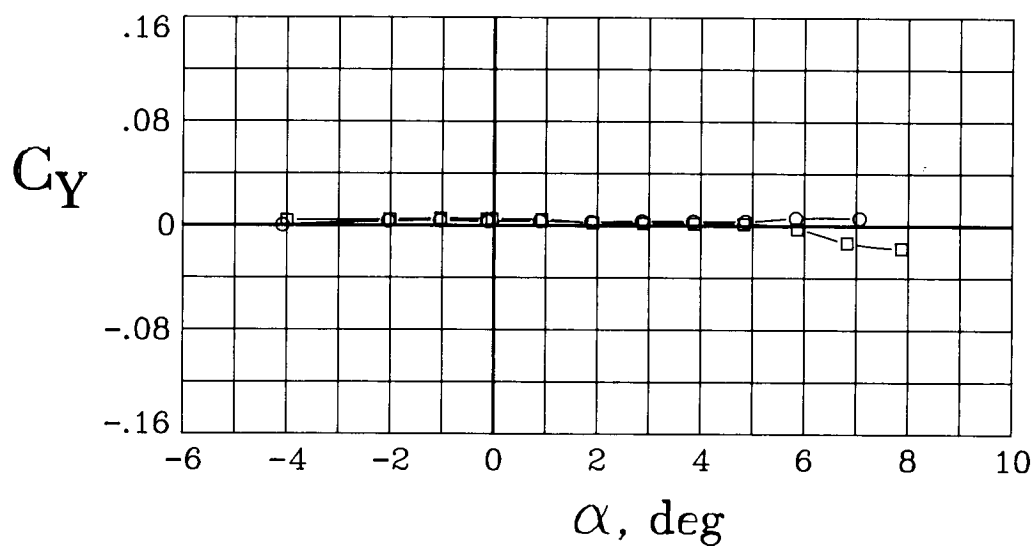
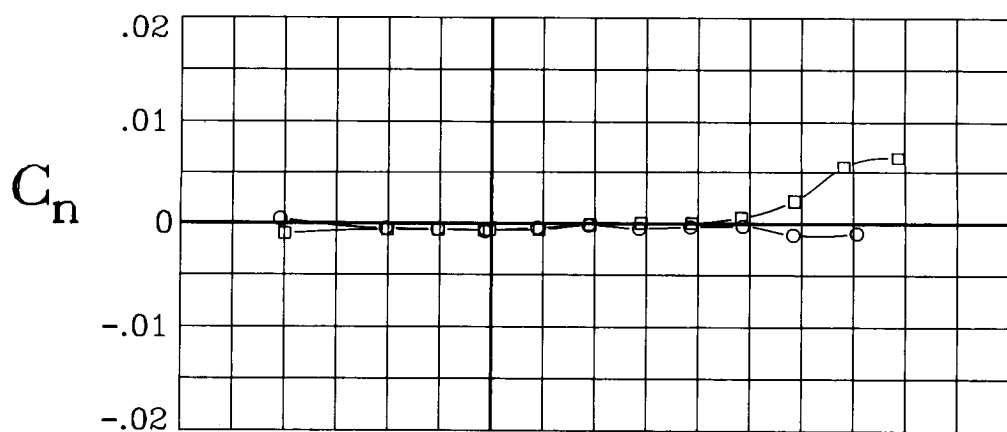
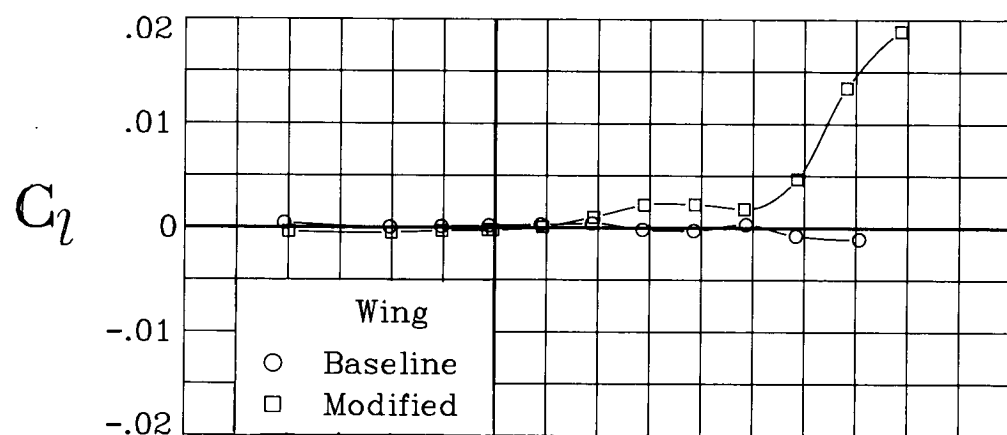
(a) $M = 0.20$.

Figure 12. Lateral-directional aerodynamic characteristics of the baseline and modified wing configurations, with wings swept 35° . $\beta = 0^\circ$.



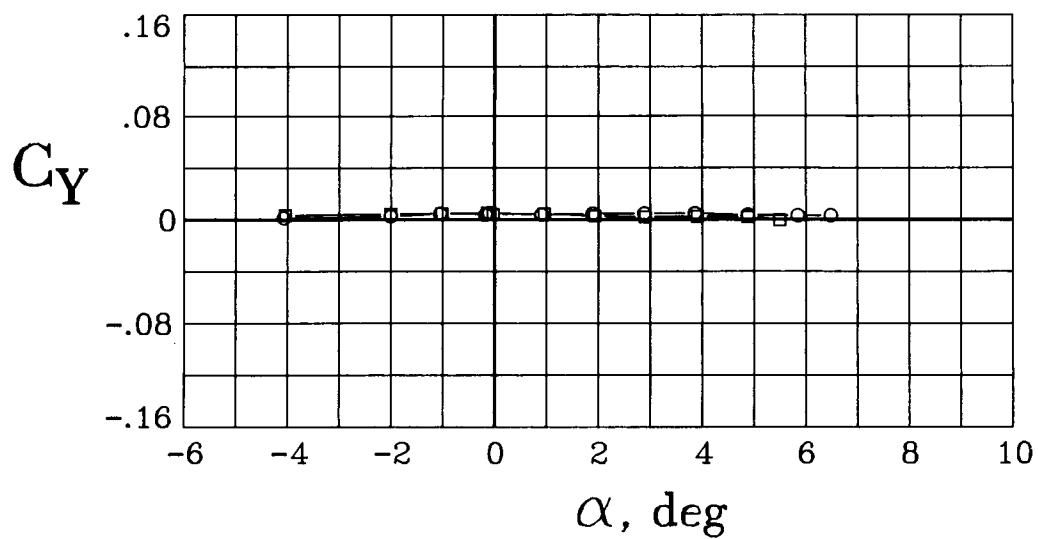
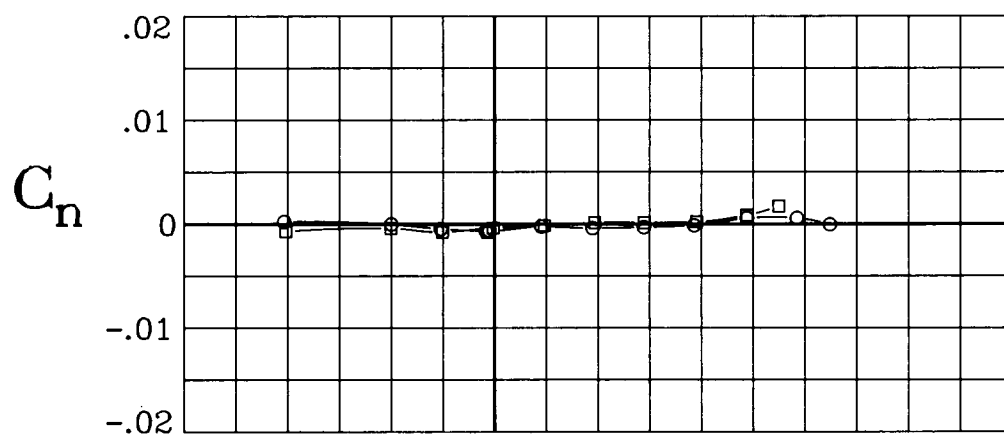
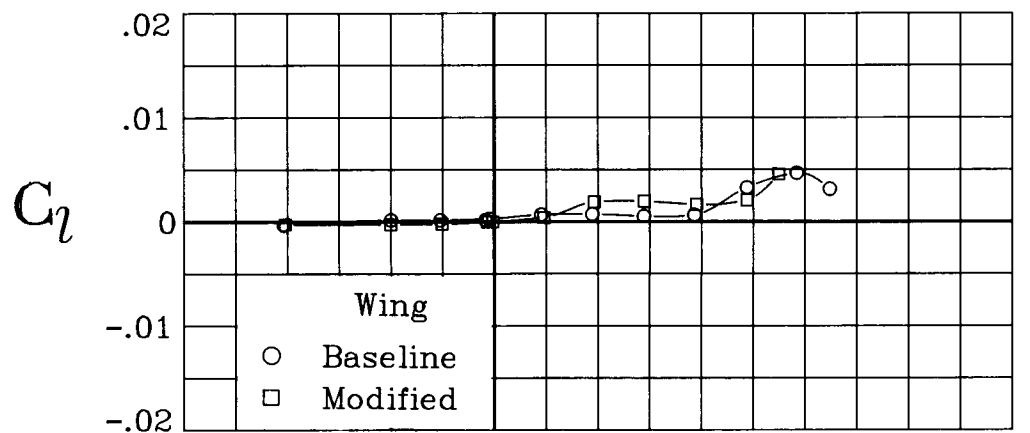
(b) $M = 0.60$.

Figure 12. Continued.



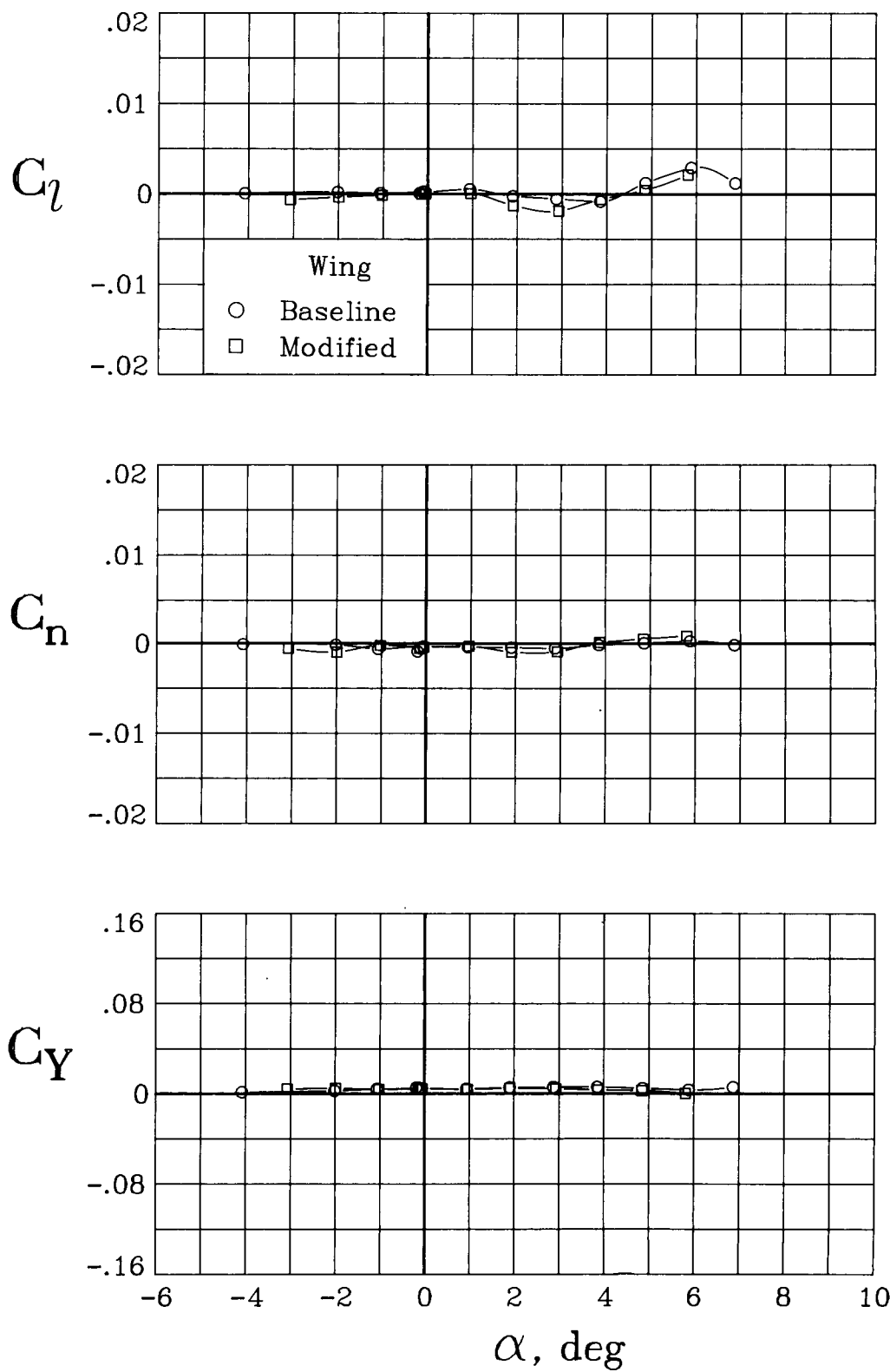
(c) $M = 0.70$.

Figure 12. Continued.



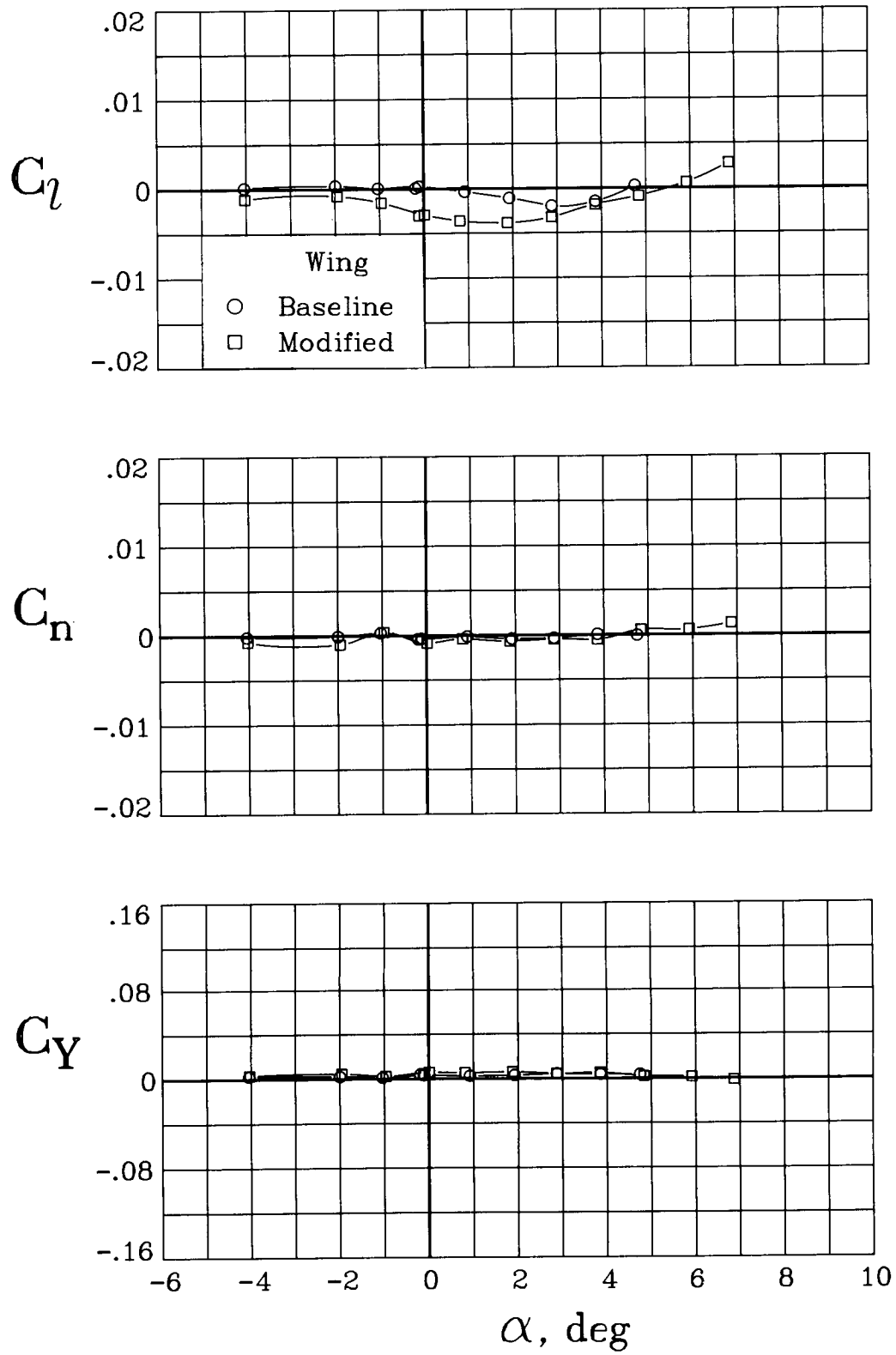
(d) $M = 0.80$.

Figure 12. Continued.



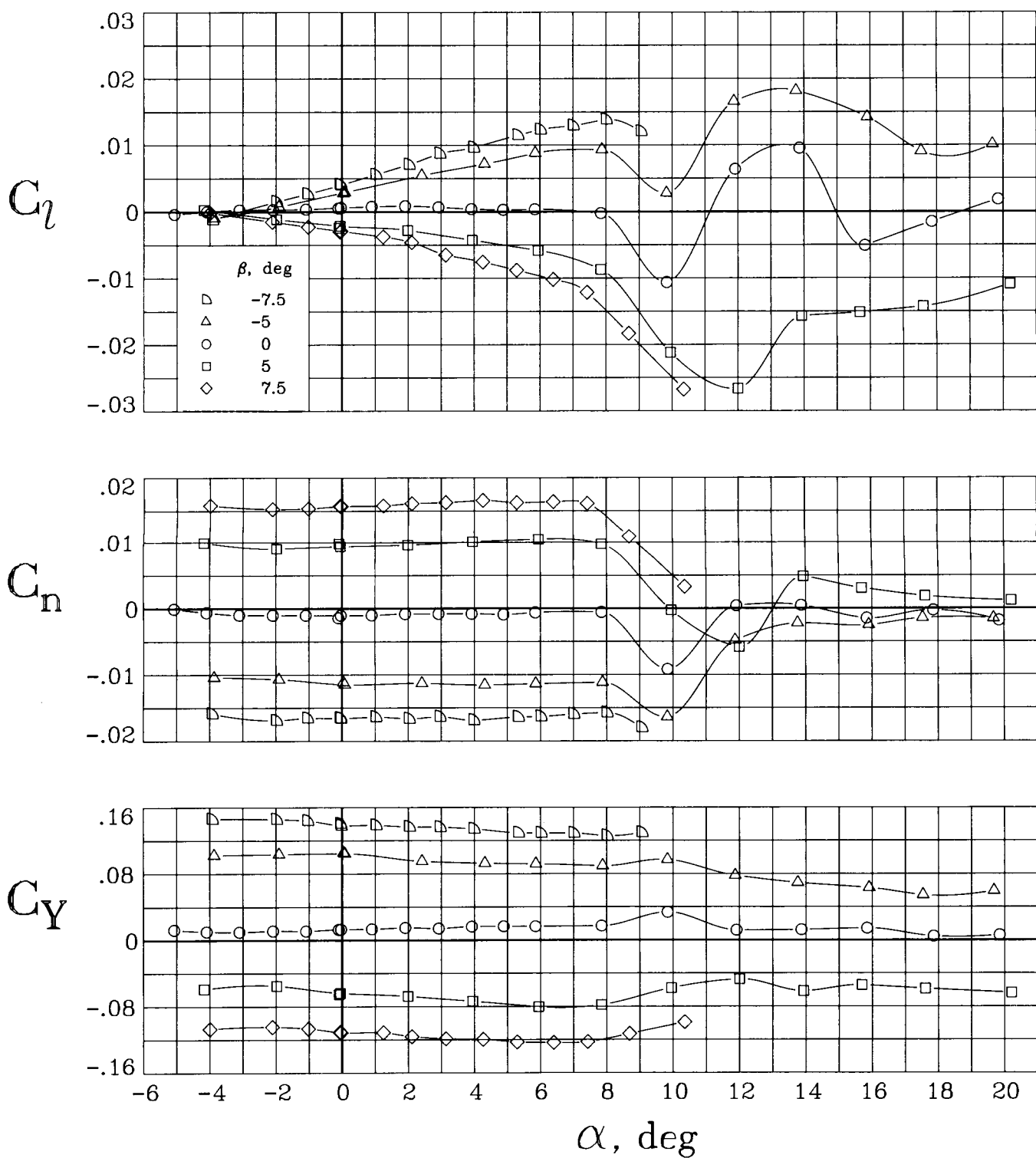
(e) $M = 0.85$.

Figure 12. Continued.



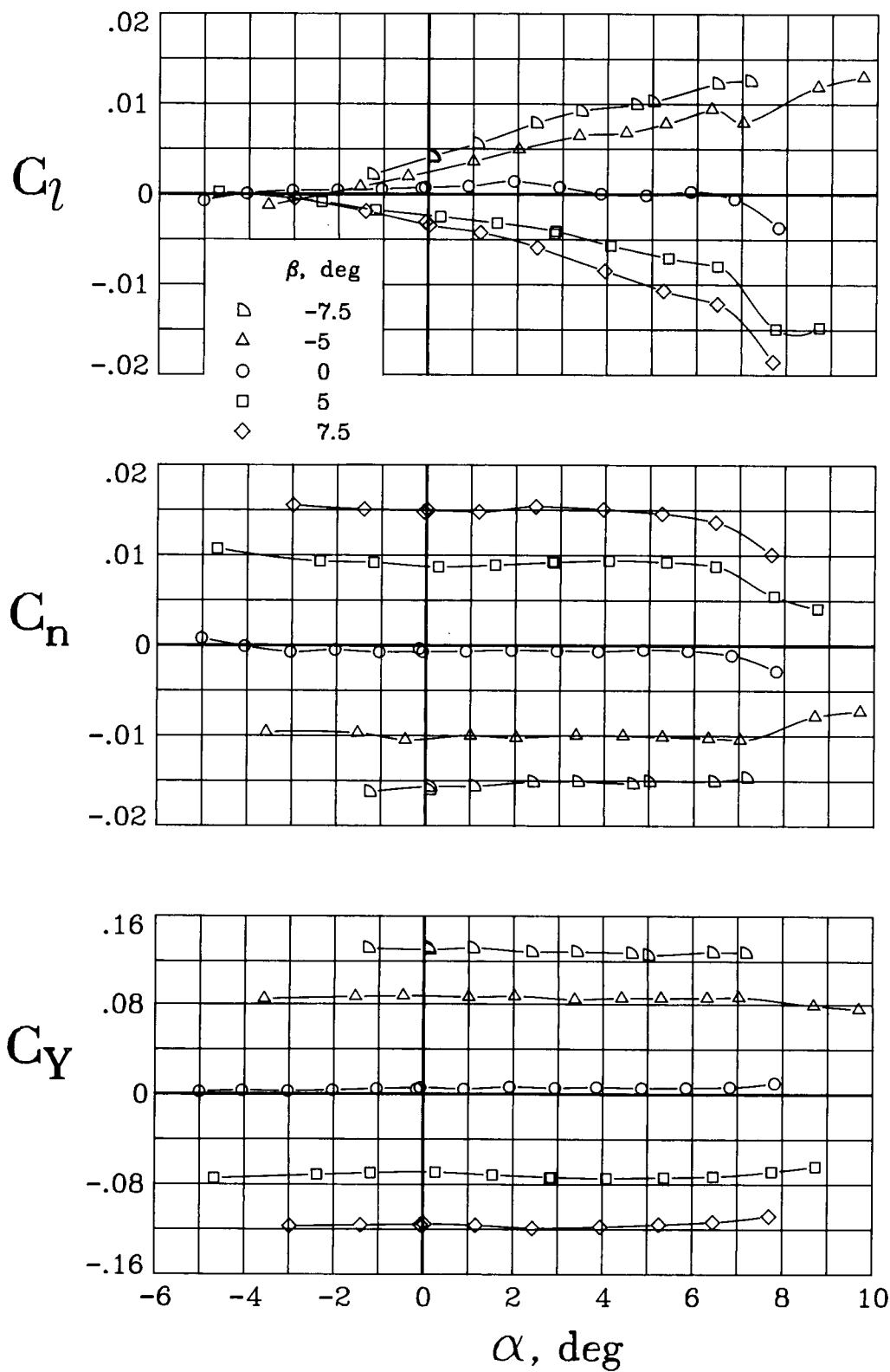
(f) $M = 0.90$.

Figure 12. Concluded.



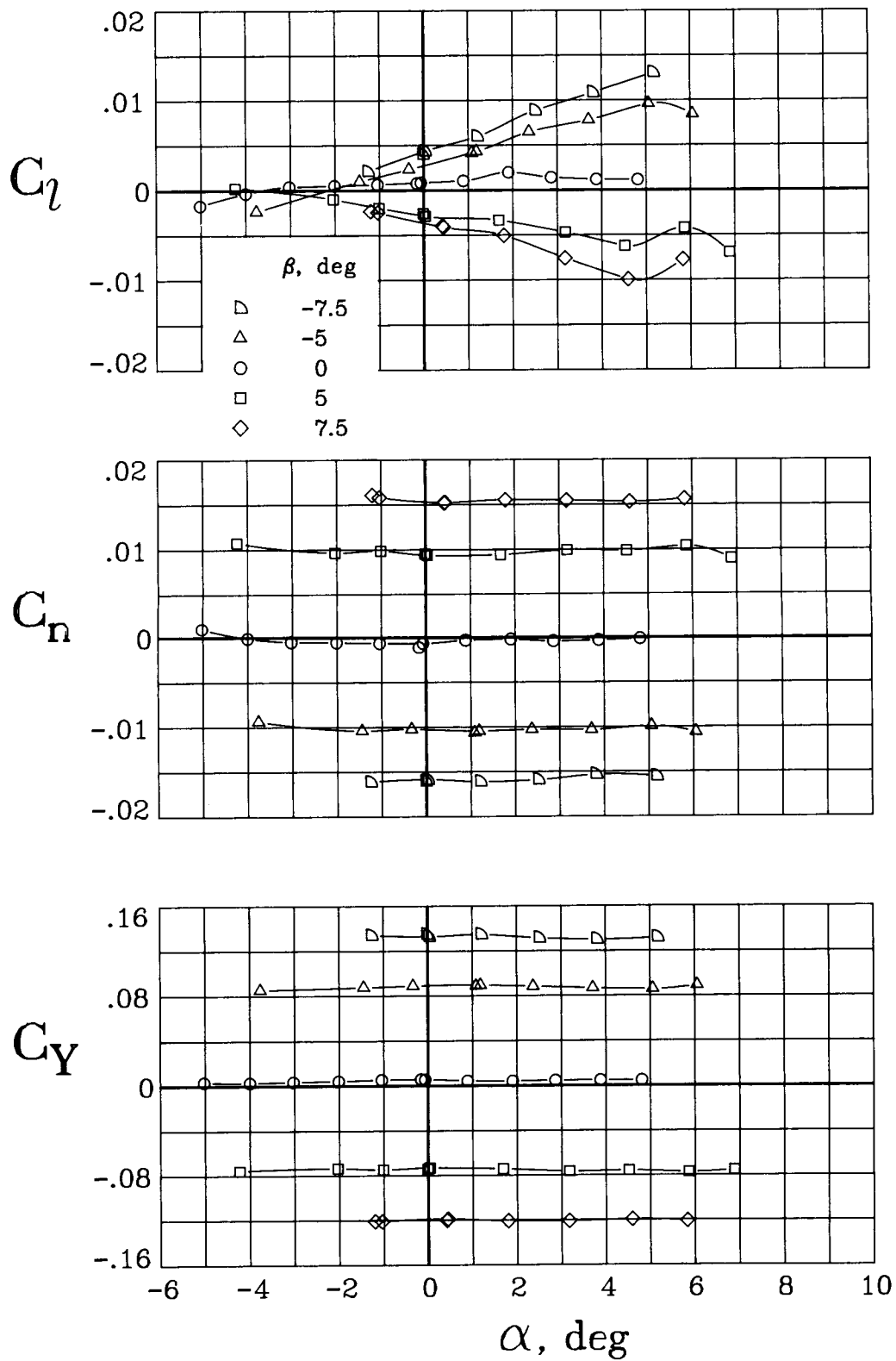
(a) $M = 0.20$.

Figure 13. Lateral-directional aerodynamic characteristics of the baseline wing configuration for a range of sideslip angles. $\Lambda = 20^\circ$.



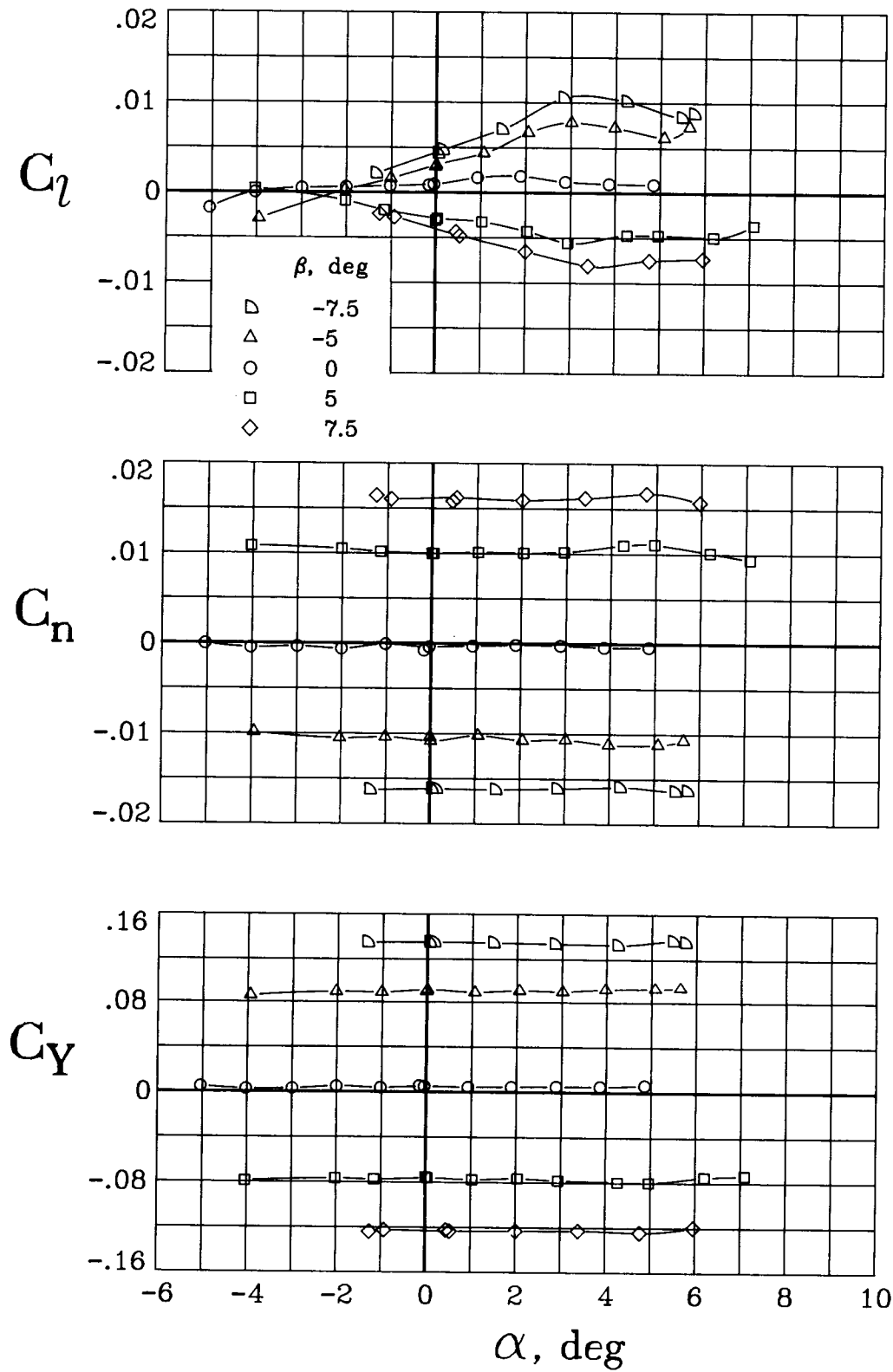
(b) $M = 0.60$.

Figure 13. Continued.



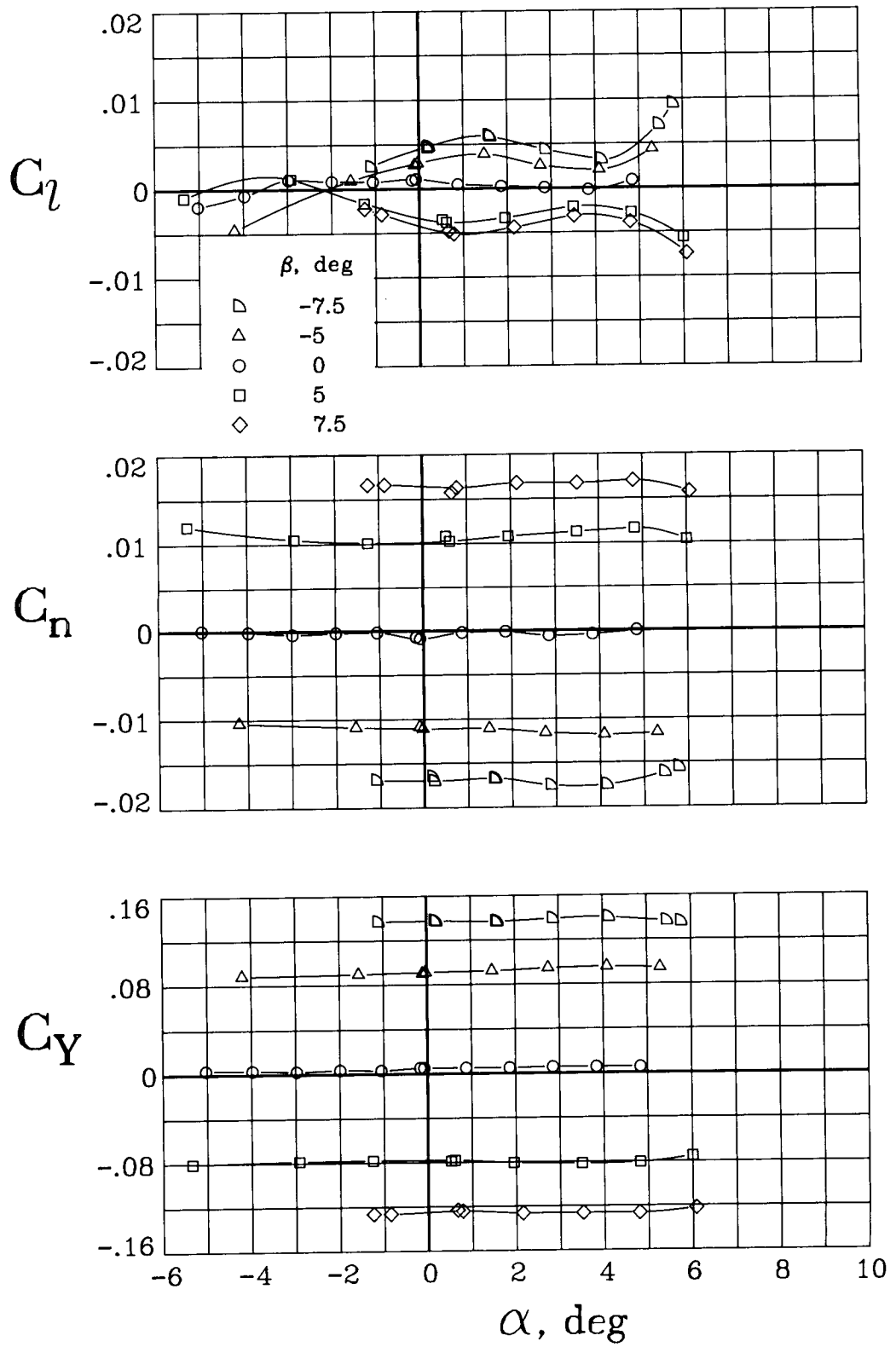
(c) $M = 0.70$.

Figure 13. Continued.



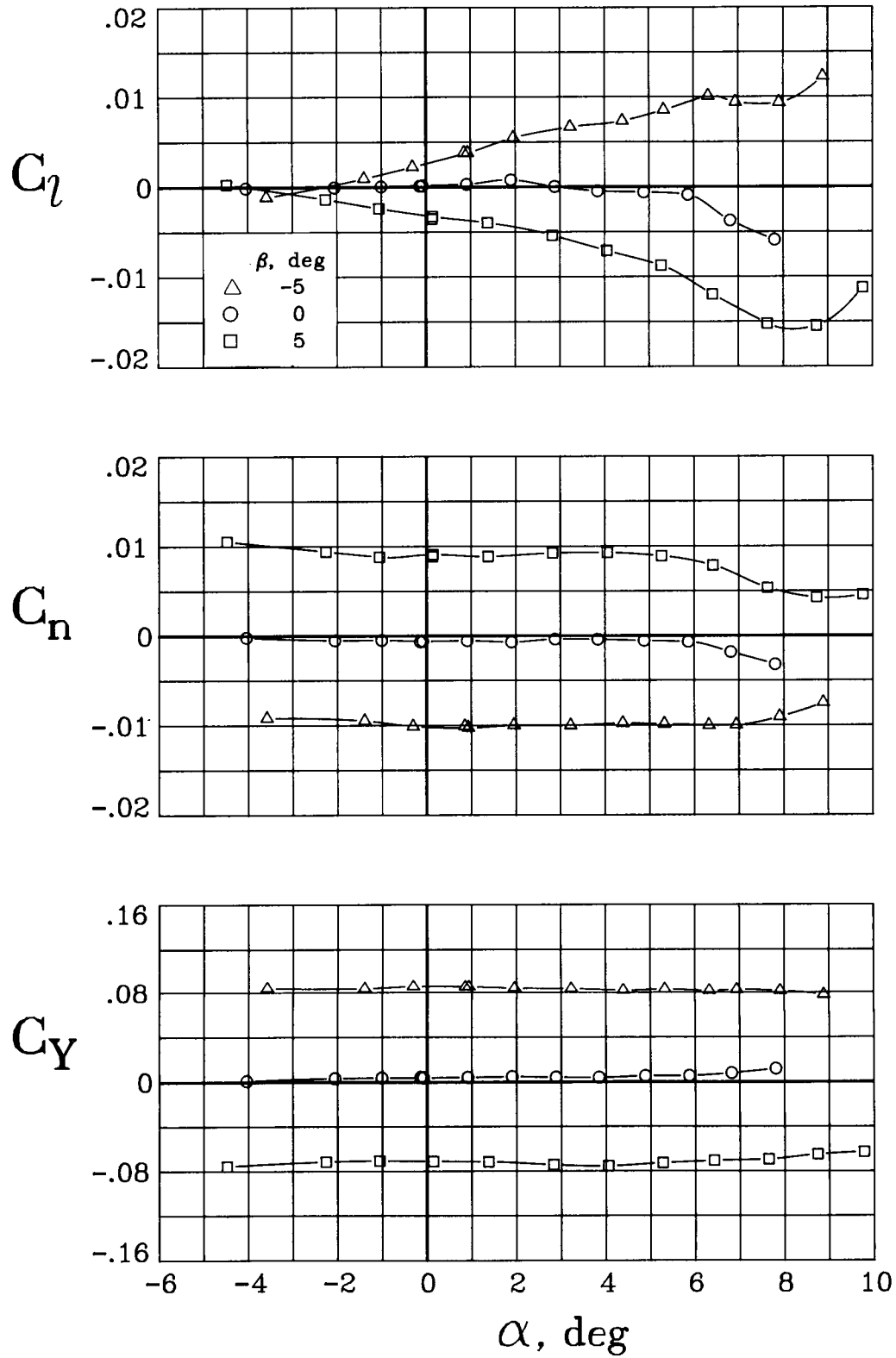
(d) $M = 0.75$.

Figure 13. Continued.



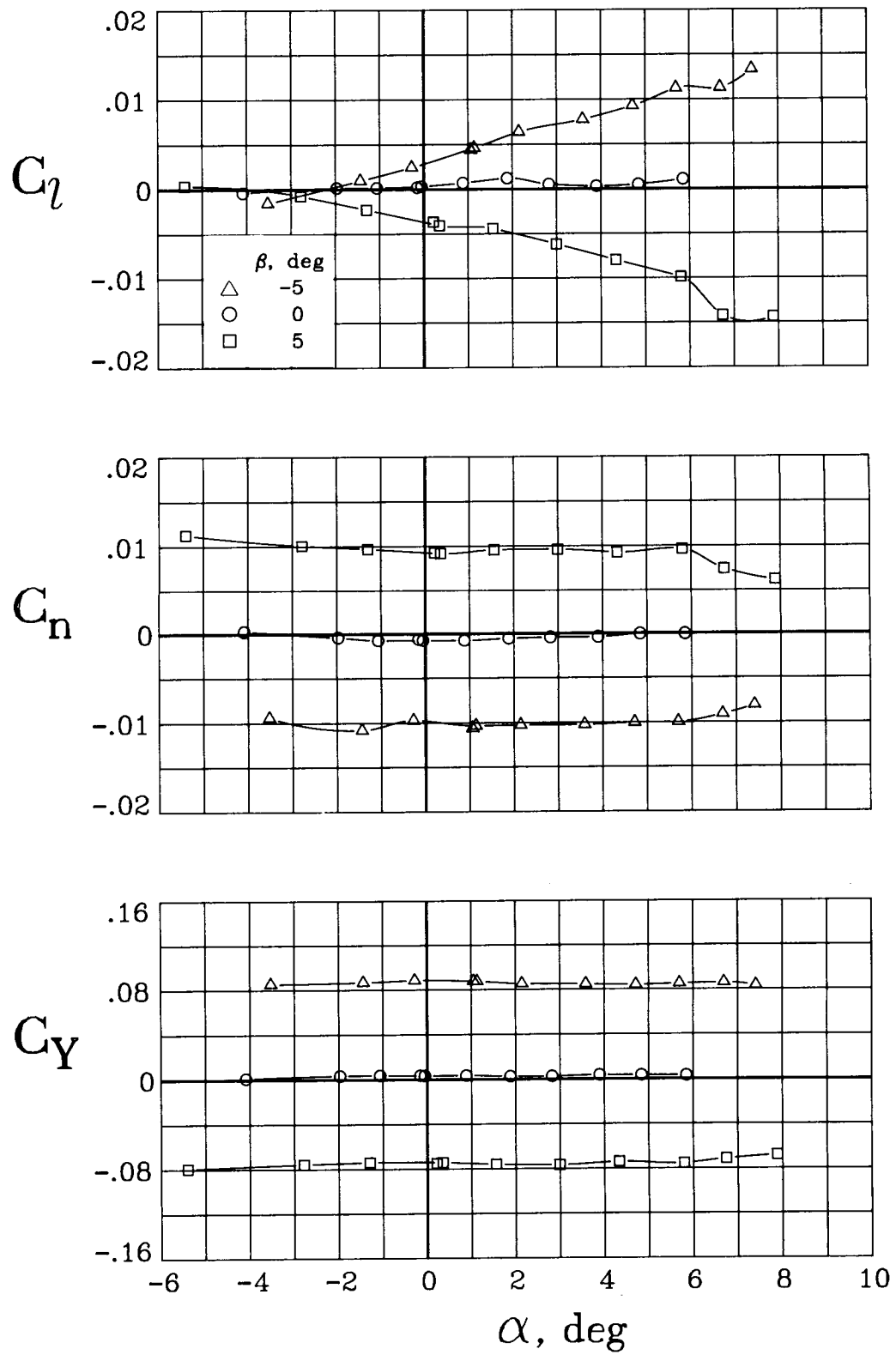
(e) $M = 0.80$.

Figure 13. Concluded.



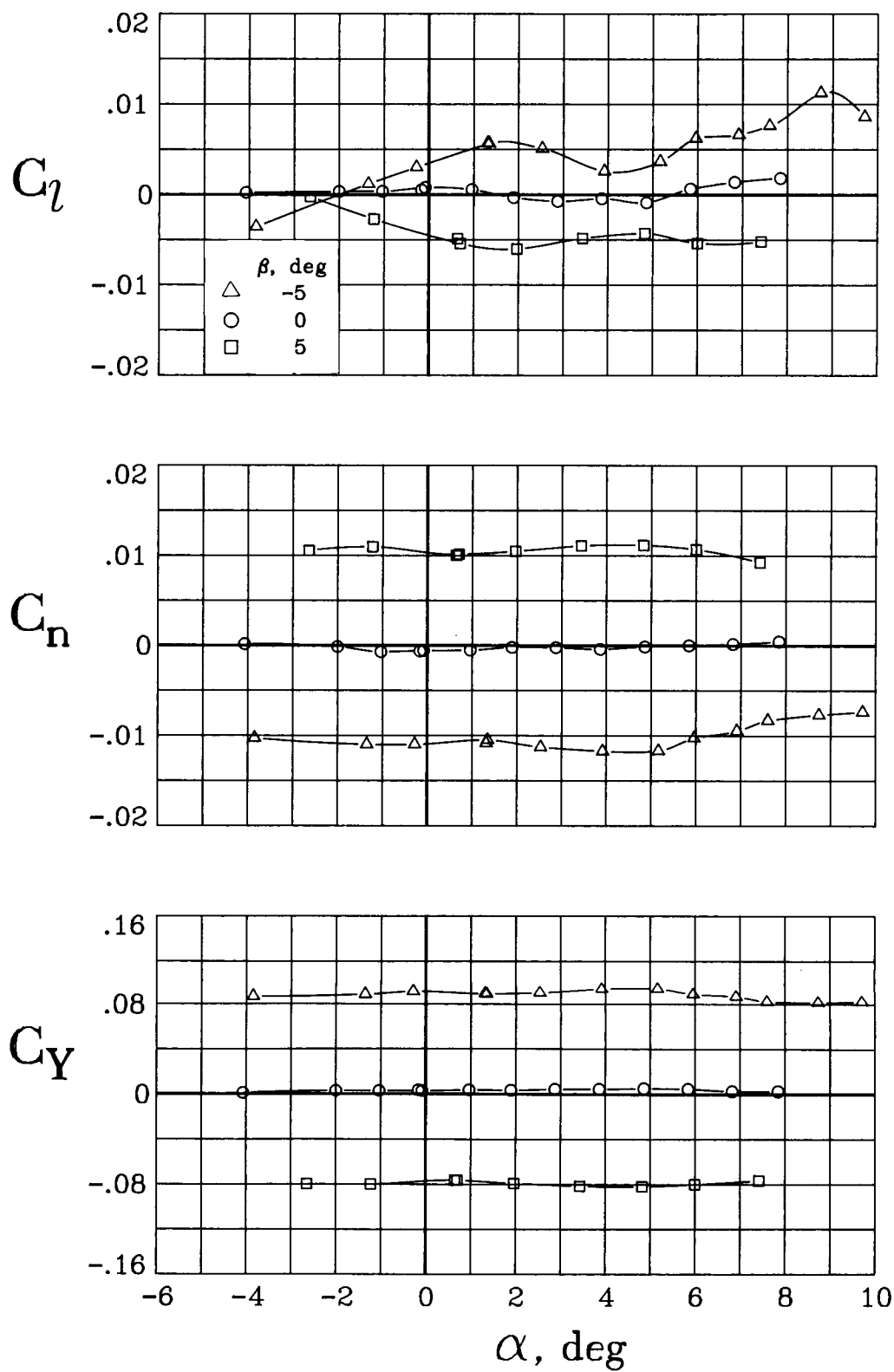
(a) $M = 0.60$

Figure 14. Lateral-directional aerodynamic characteristics of the baseline wing configuration for a range of sideslip angles. $\Lambda = 25^\circ$.



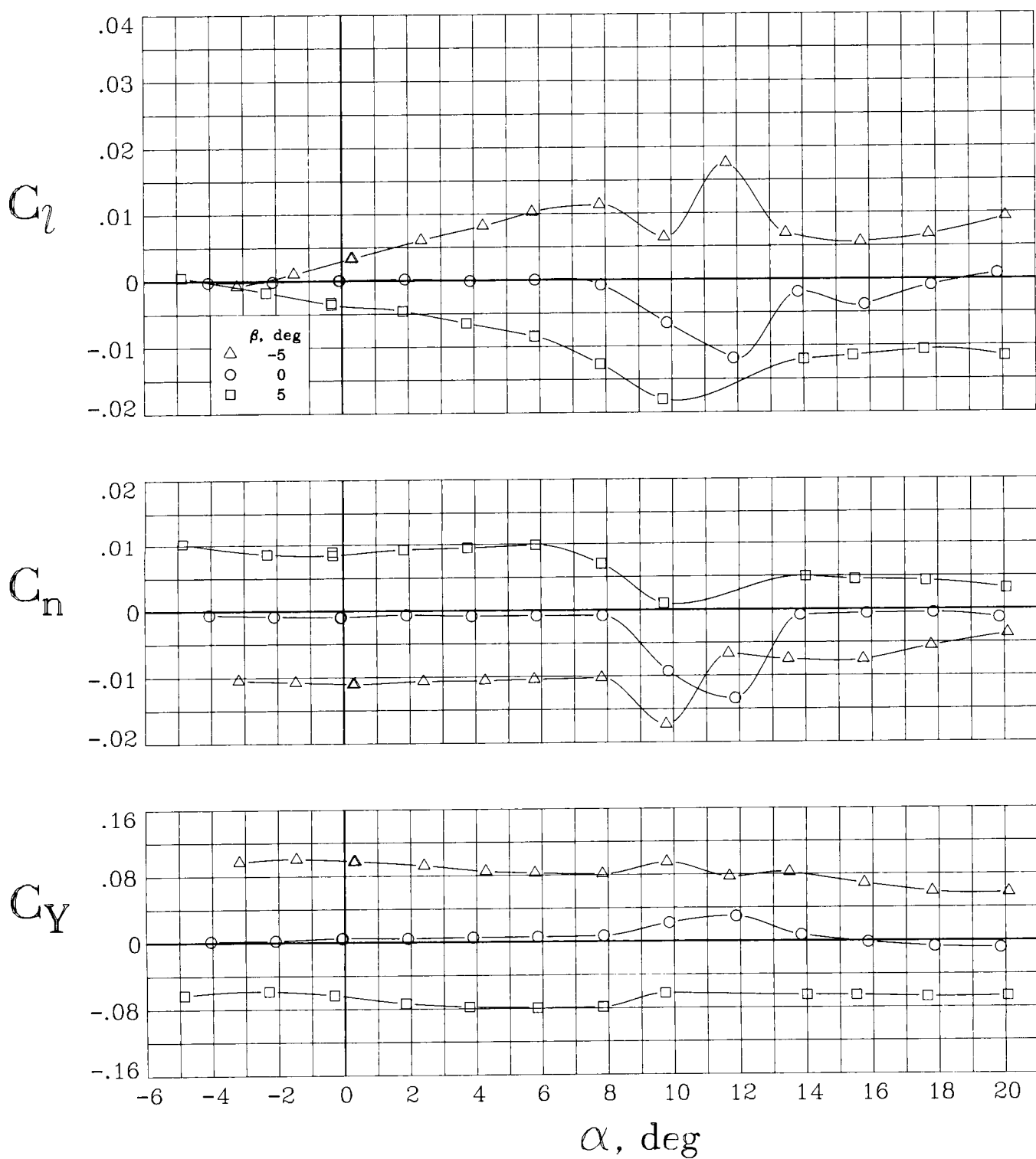
(b) $M = 0.70$.

Figure 14. Continued.



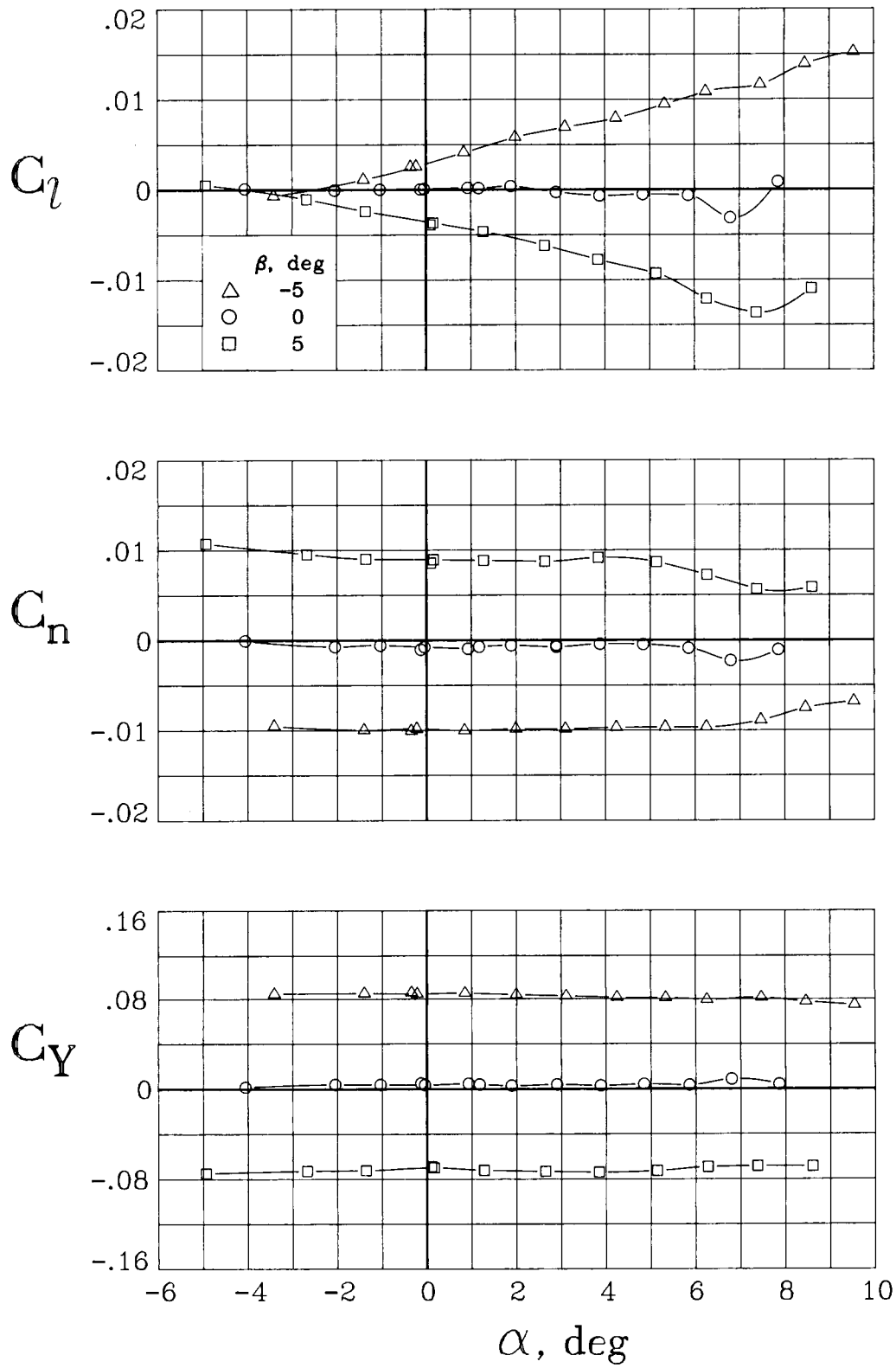
(c) $M = 0.80$.

Figure 14. Concluded.

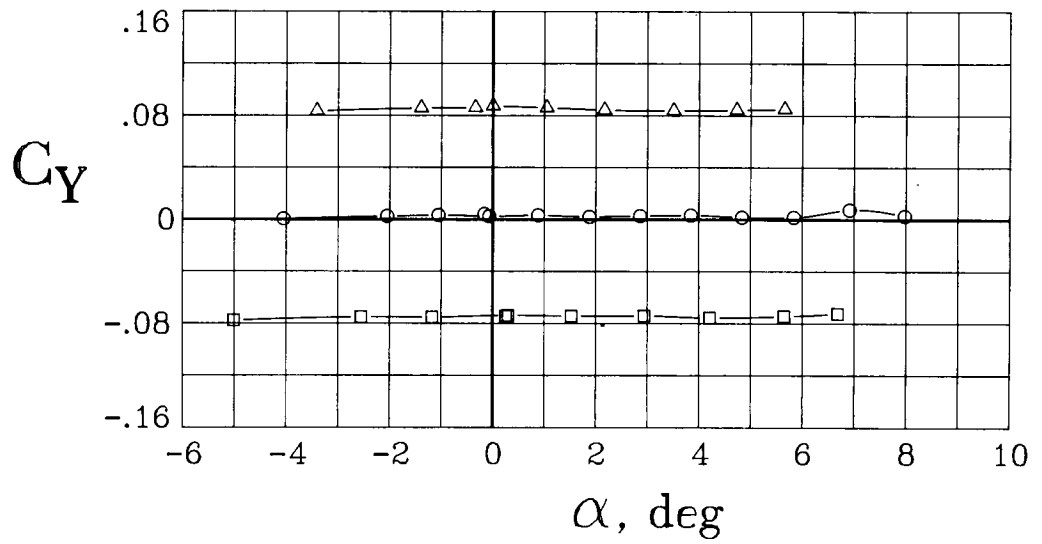
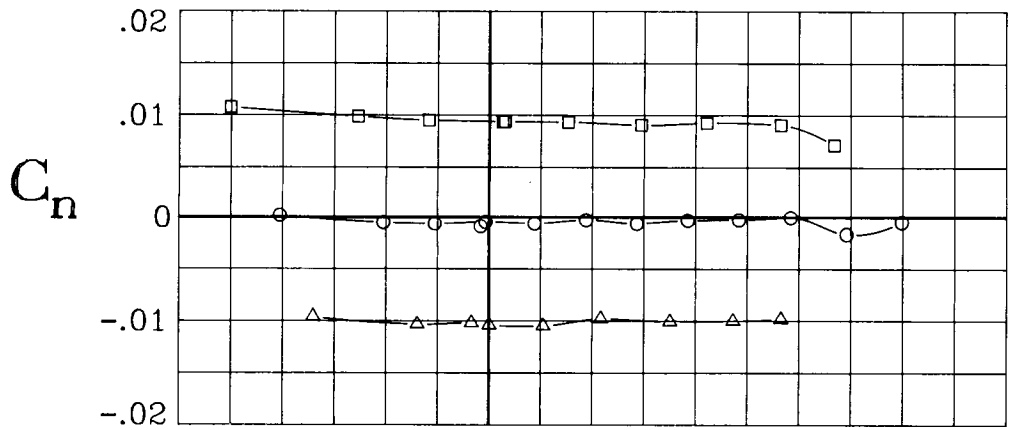
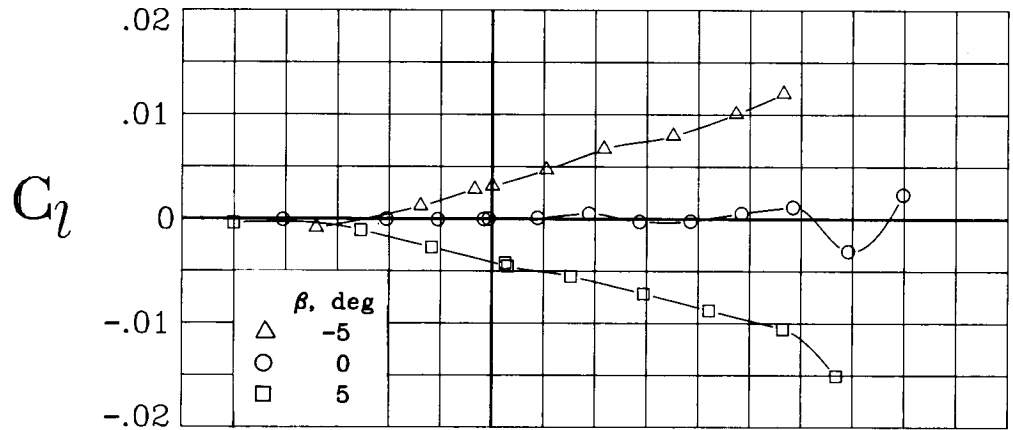


(a) $M = 0.20$.

Figure 15. Lateral-directional aerodynamic characteristics of the baseline wing configuration for a range of sideslip angles. $\Lambda = 30^\circ$.

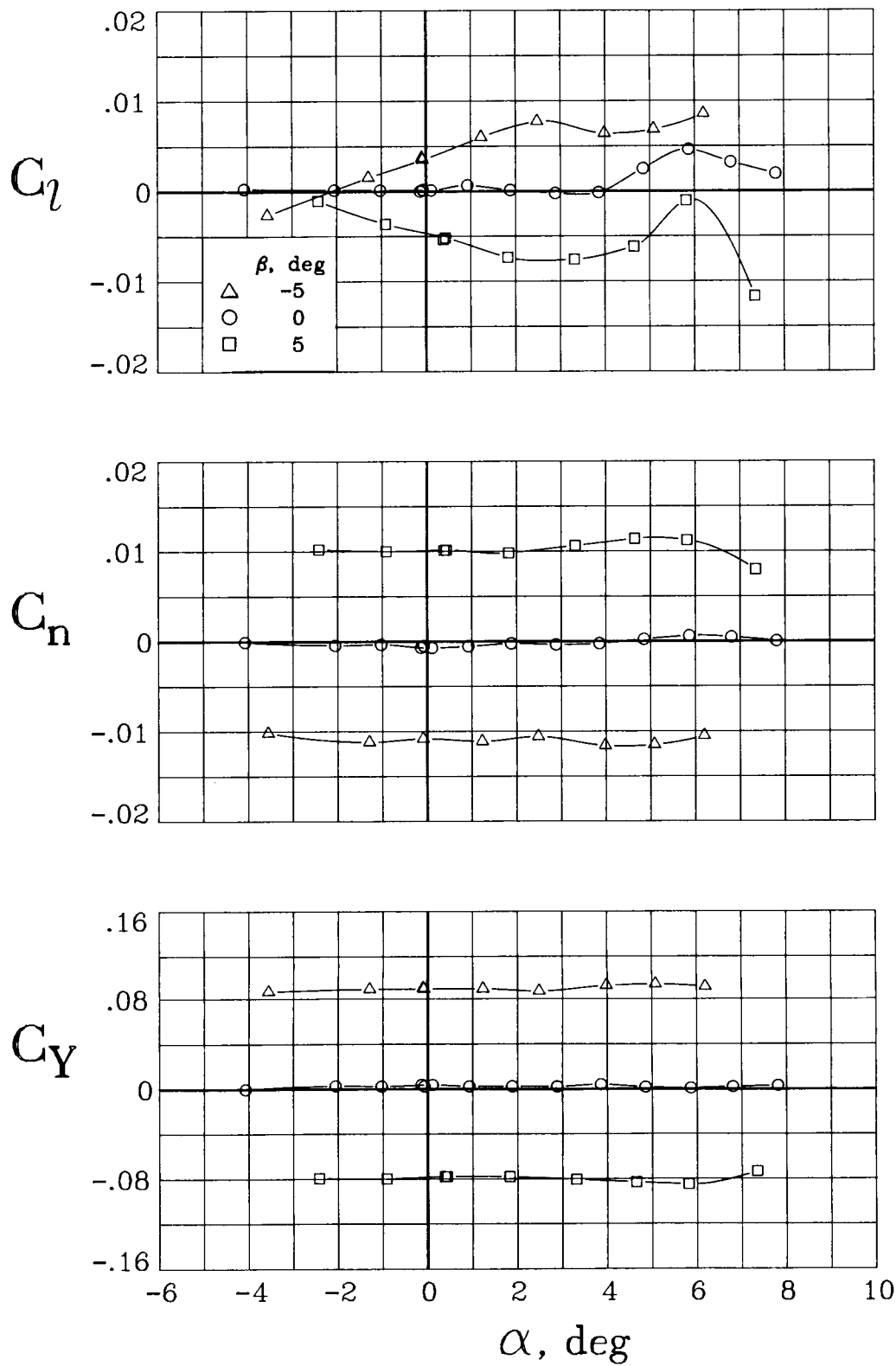


(b) $M = 0.60$.
 Figure 15. Continued.



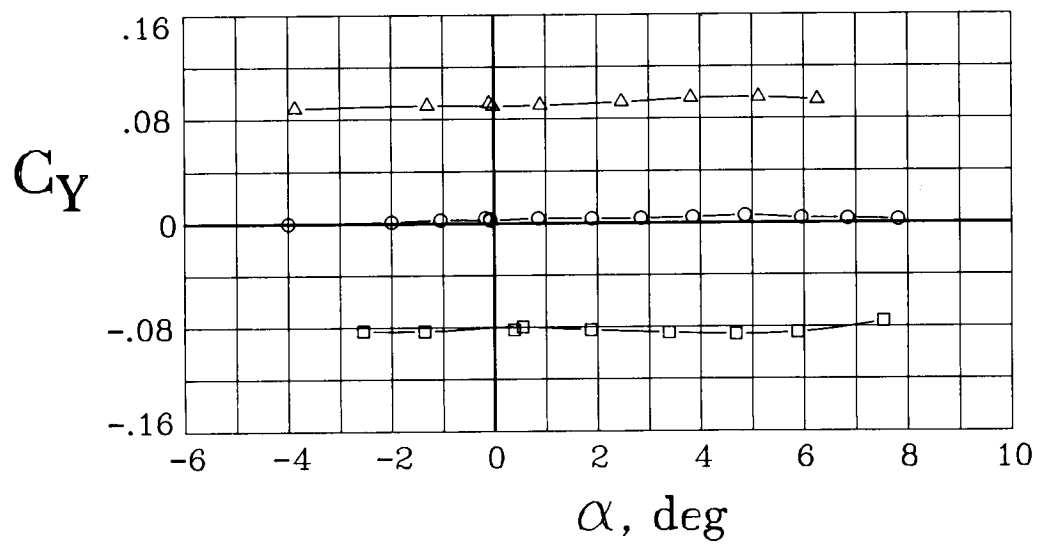
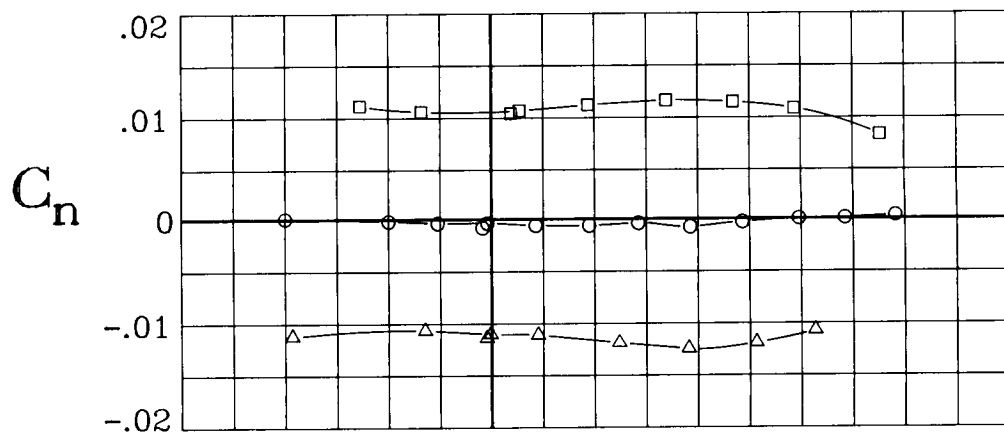
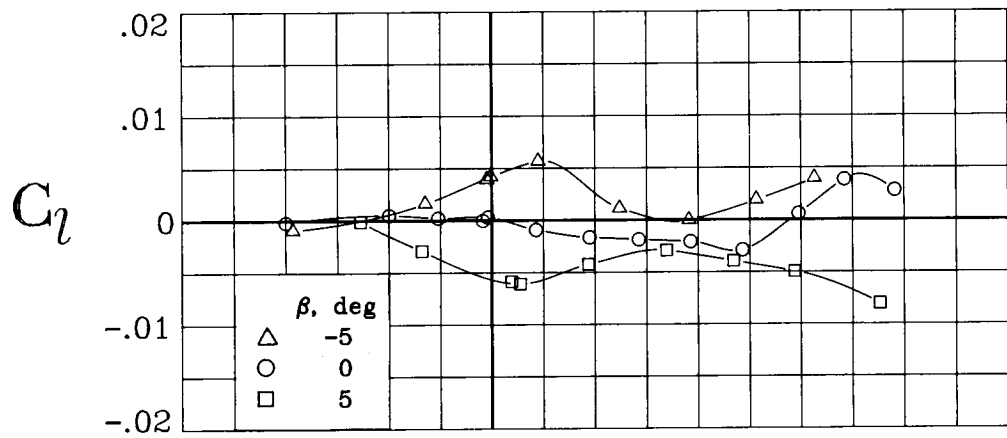
(c) $M = 0.70$.

Figure 15. Continued.



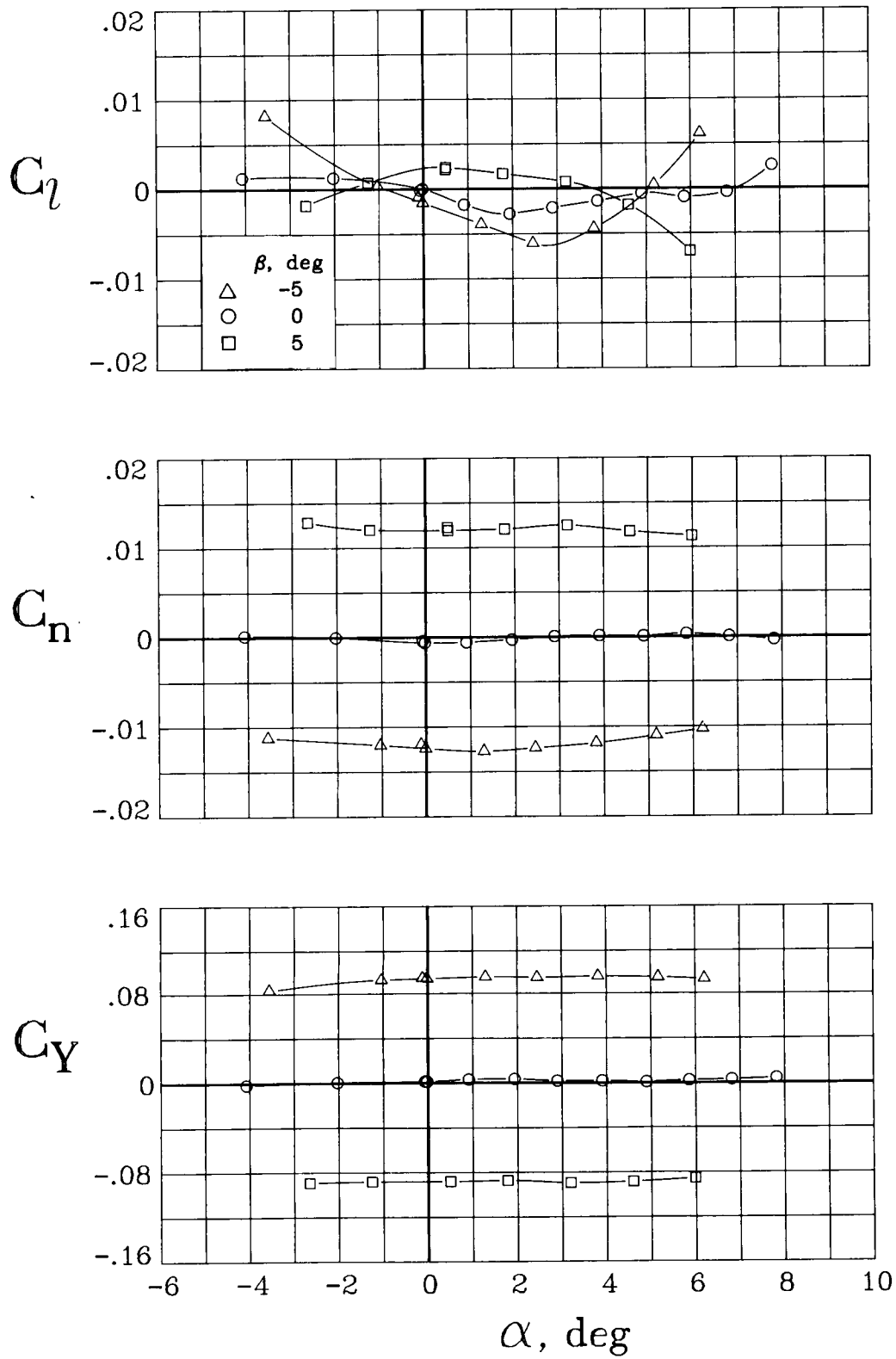
(d) $M = 0.80$.

Figure 15. Continued.



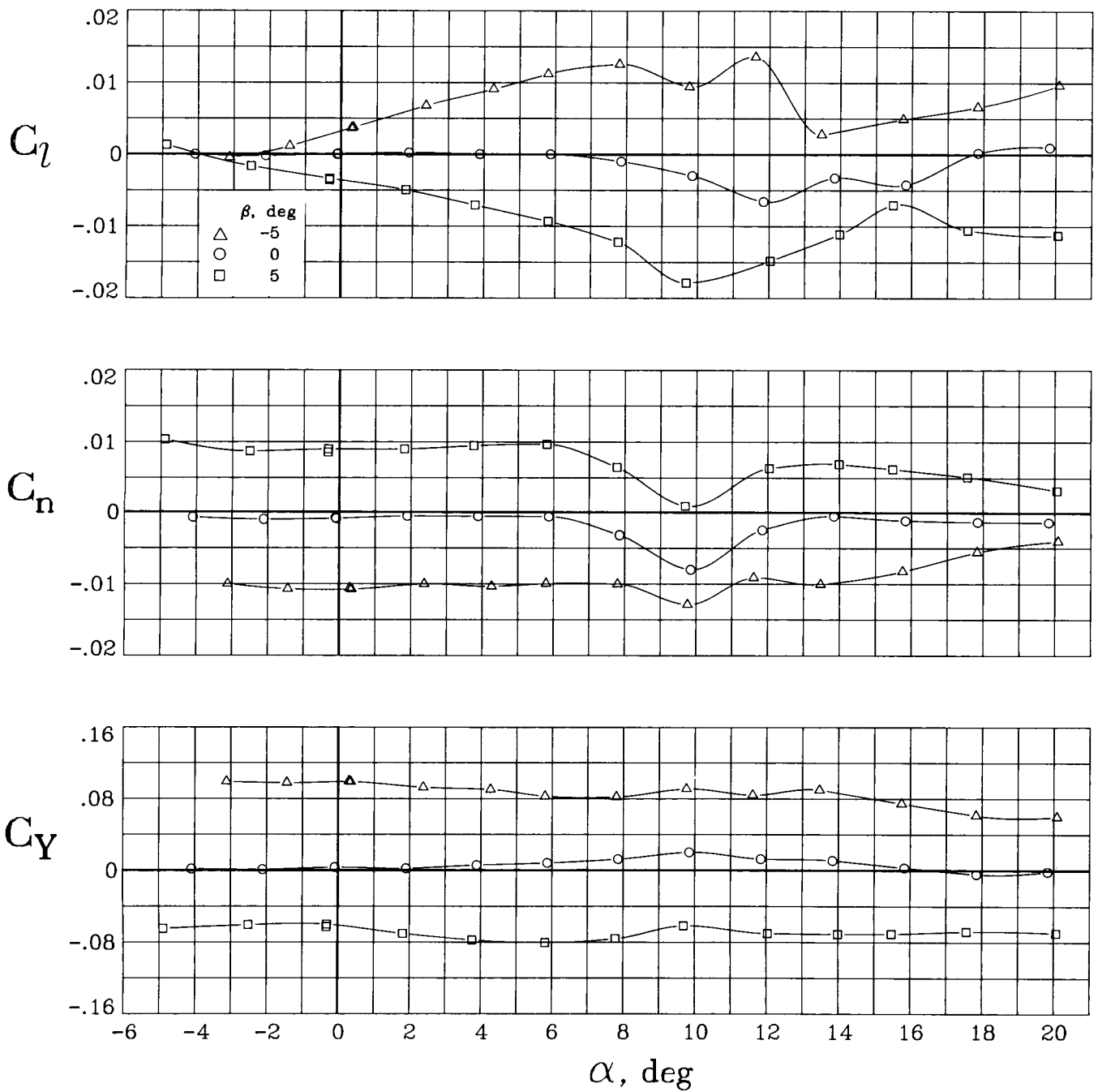
(e) $M = 0.85$.

Figure 15. Continued.



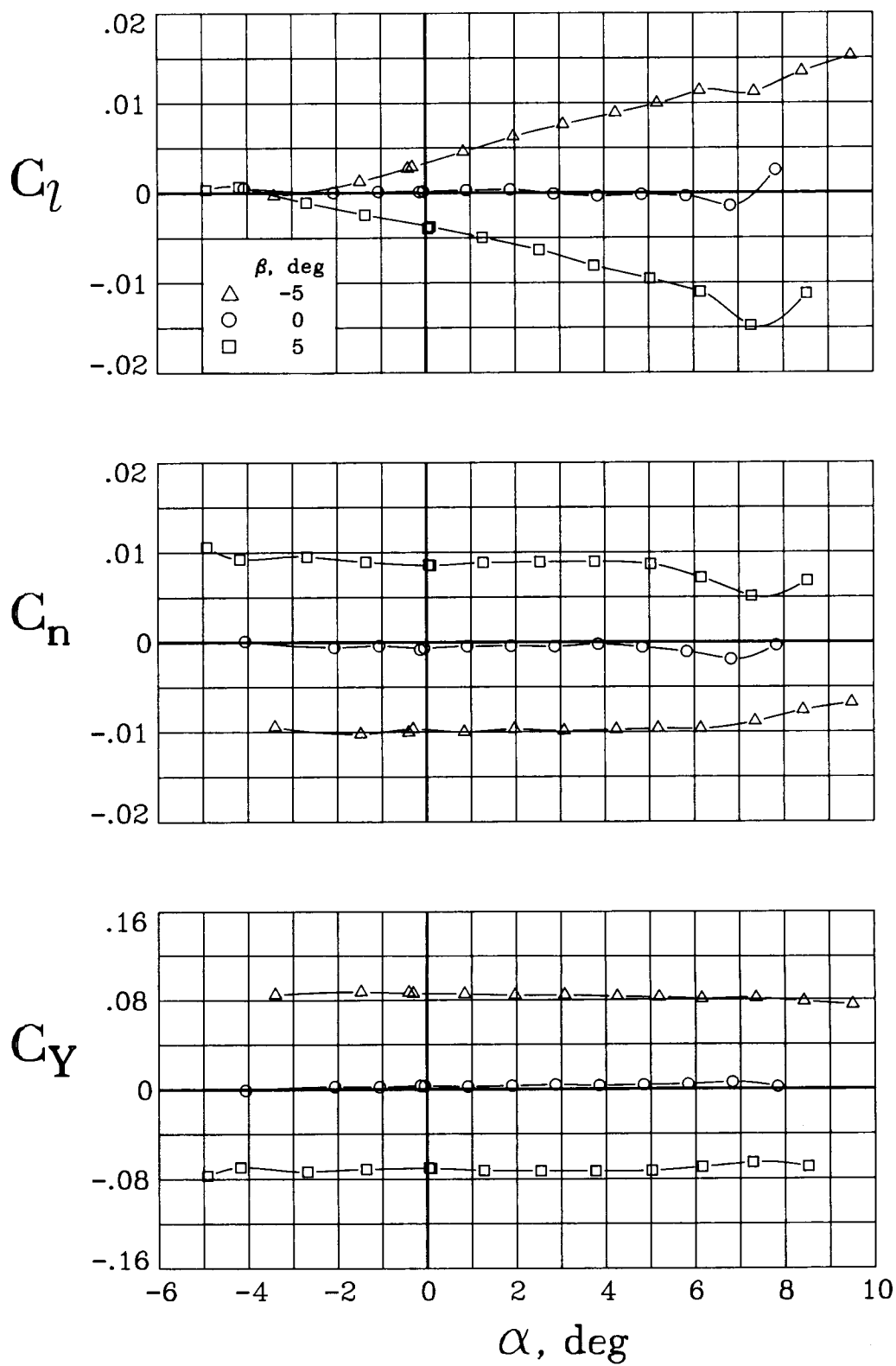
(f) $M = 0.90$.

Figure 15. Concluded.



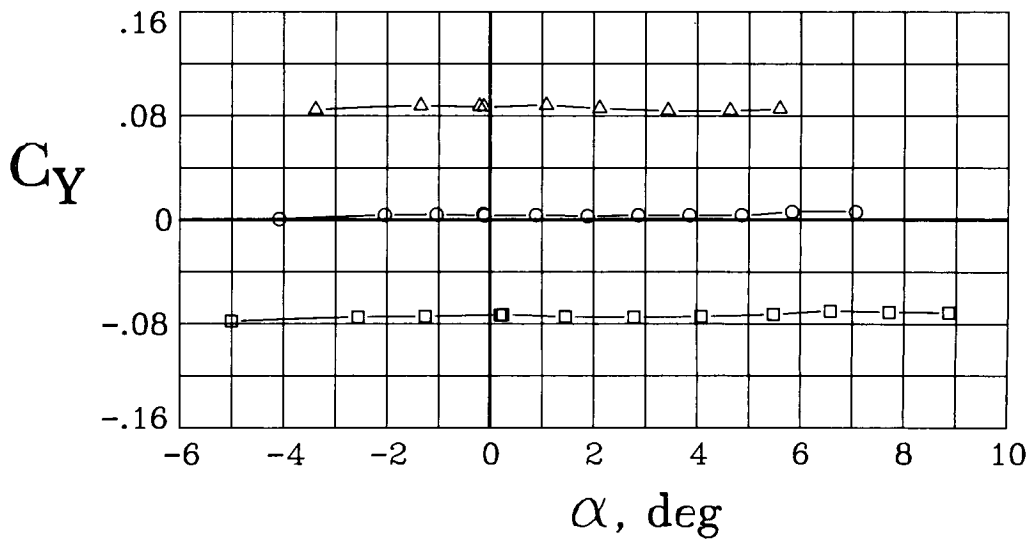
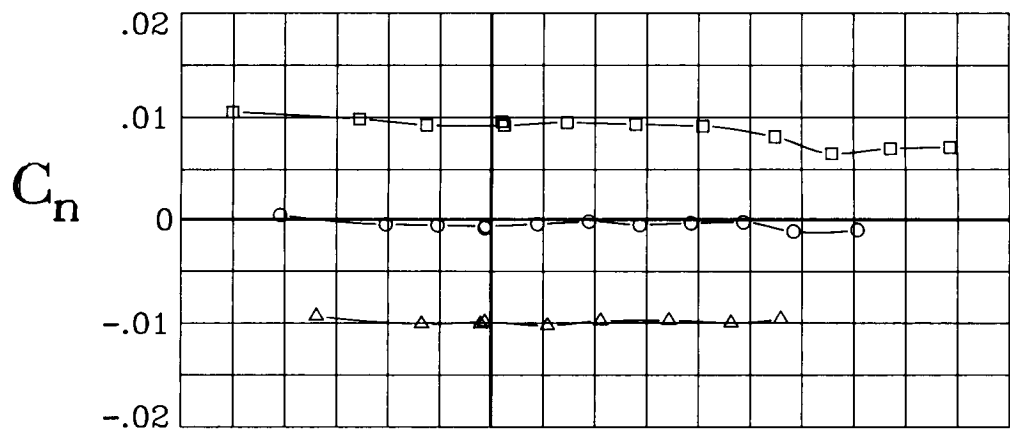
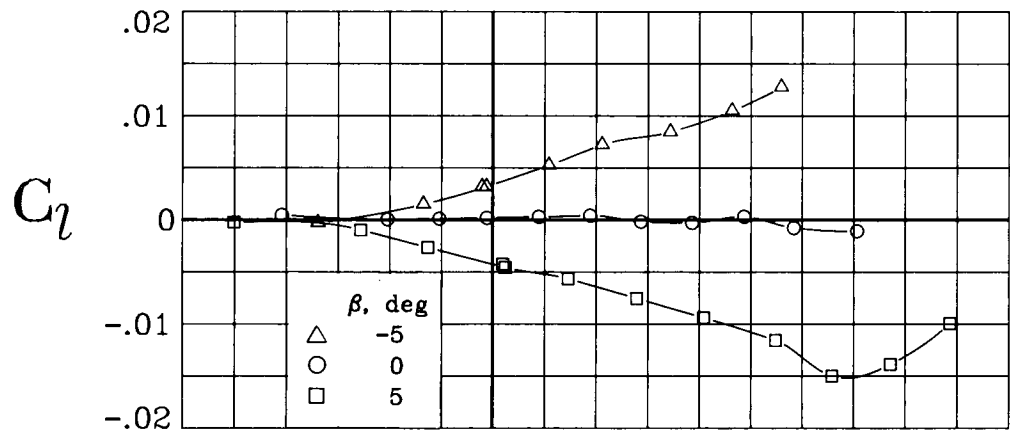
(a) $M = 0.20$.

Figure 16. Lateral-directional aerodynamic characteristics of the baseline wing configuration for a range of sideslip angles. $\Lambda = 35^\circ$.



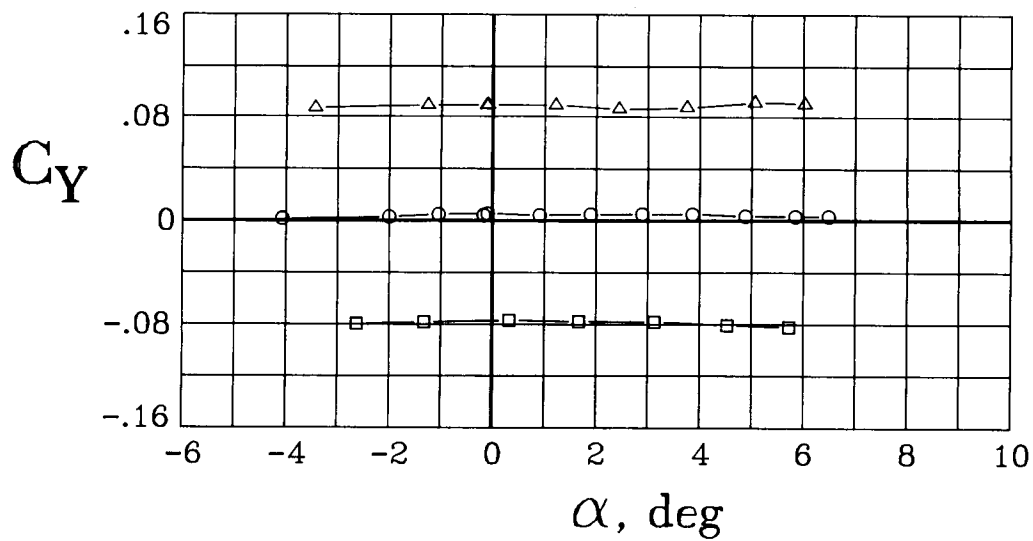
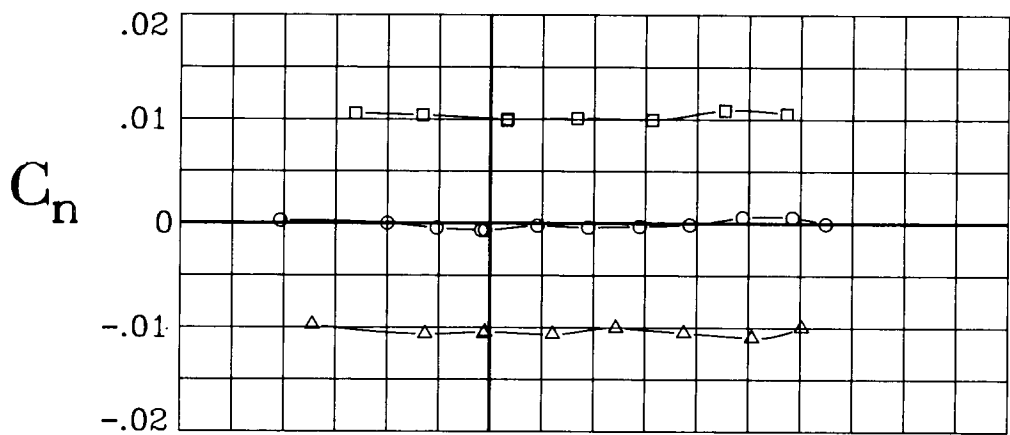
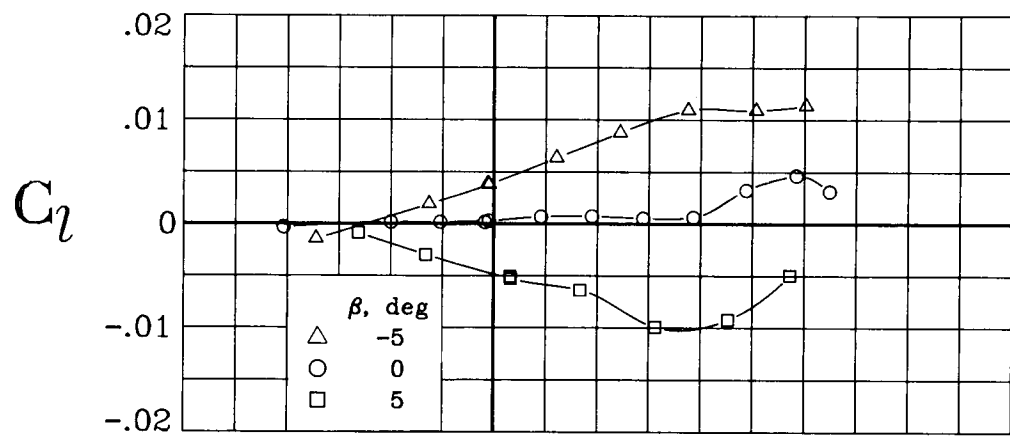
(b) $M = 0.60$.

Figure 16. Continued.



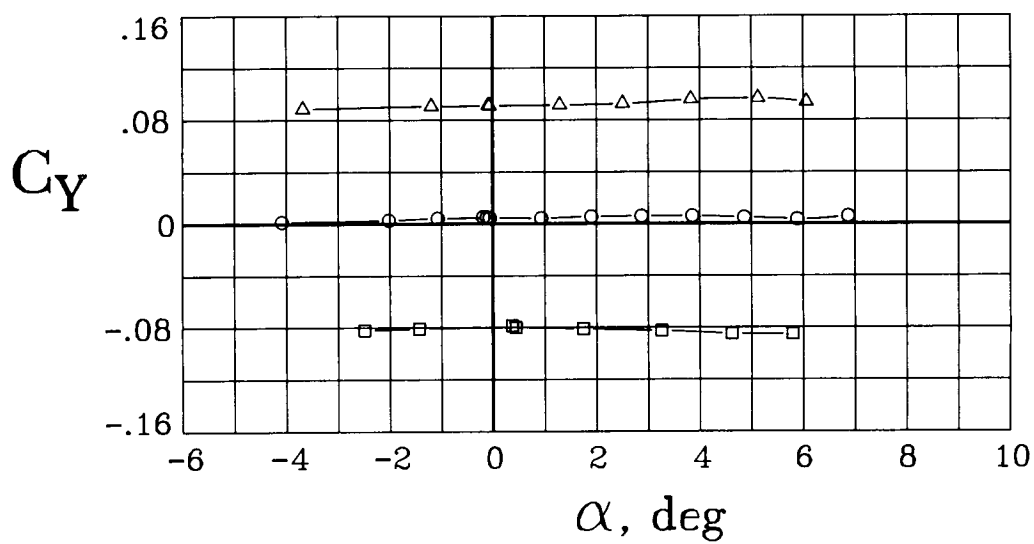
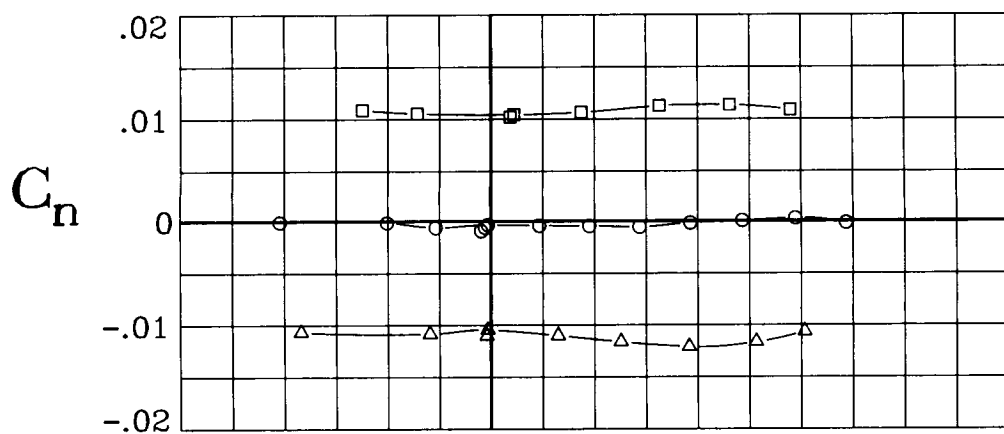
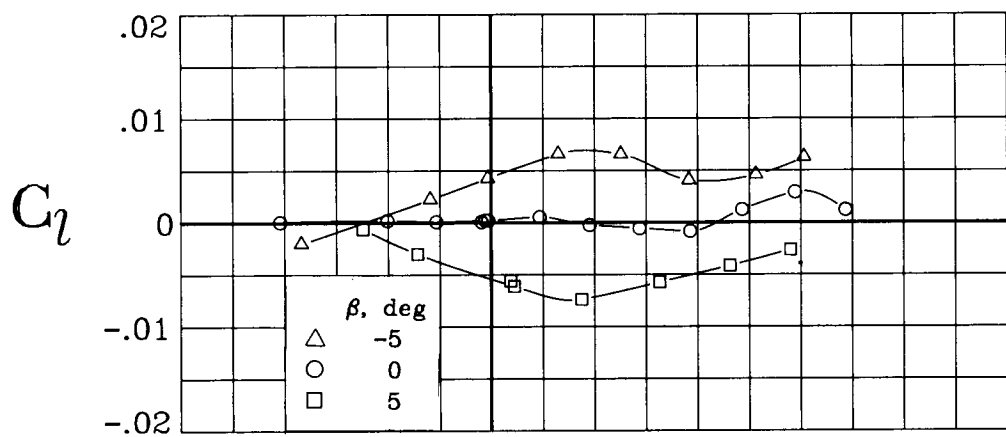
(c) $M = 0.70$.

Figure 16. Continued.



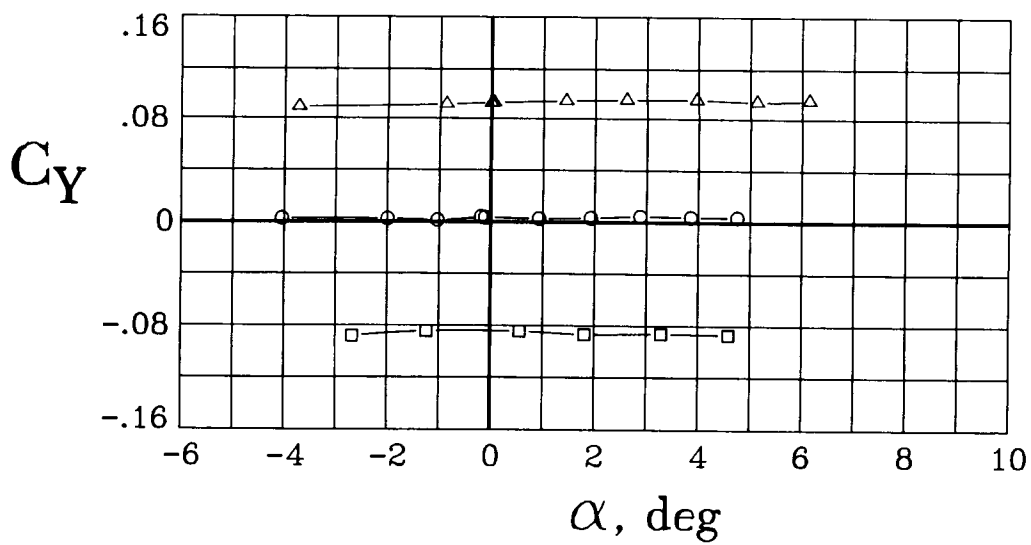
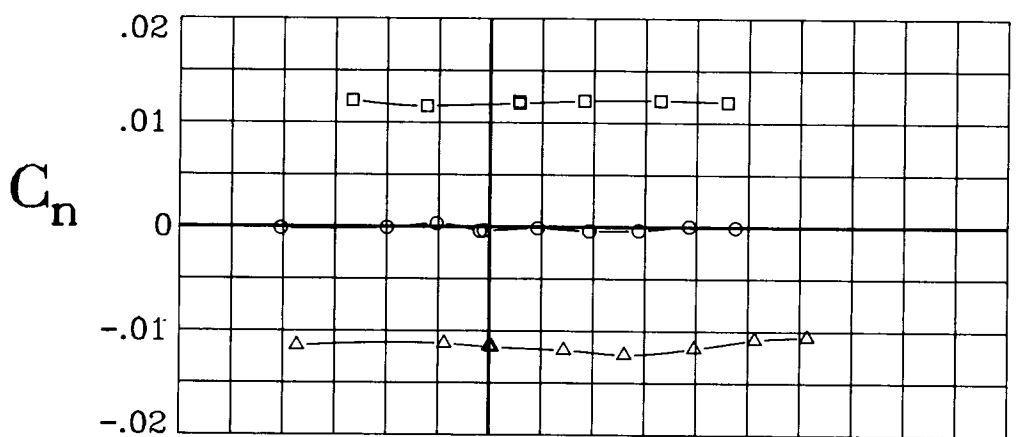
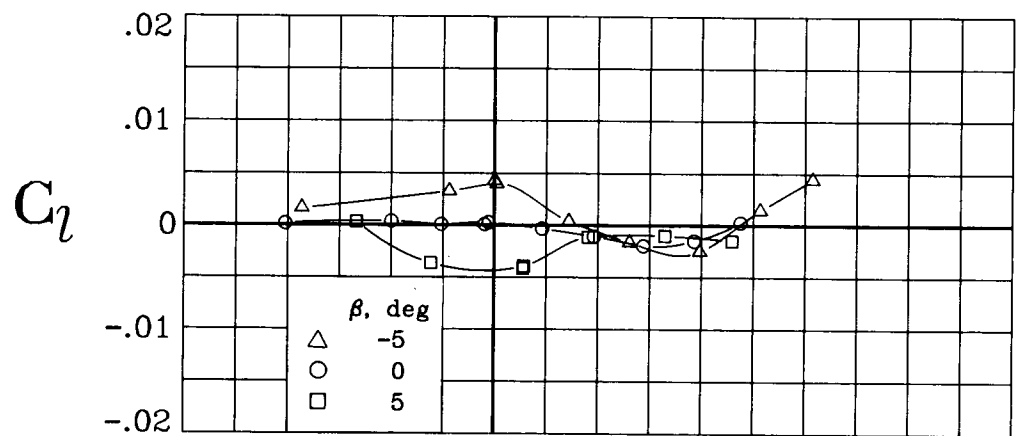
(d) $M = 0.80$.

Figure 16. Continued.



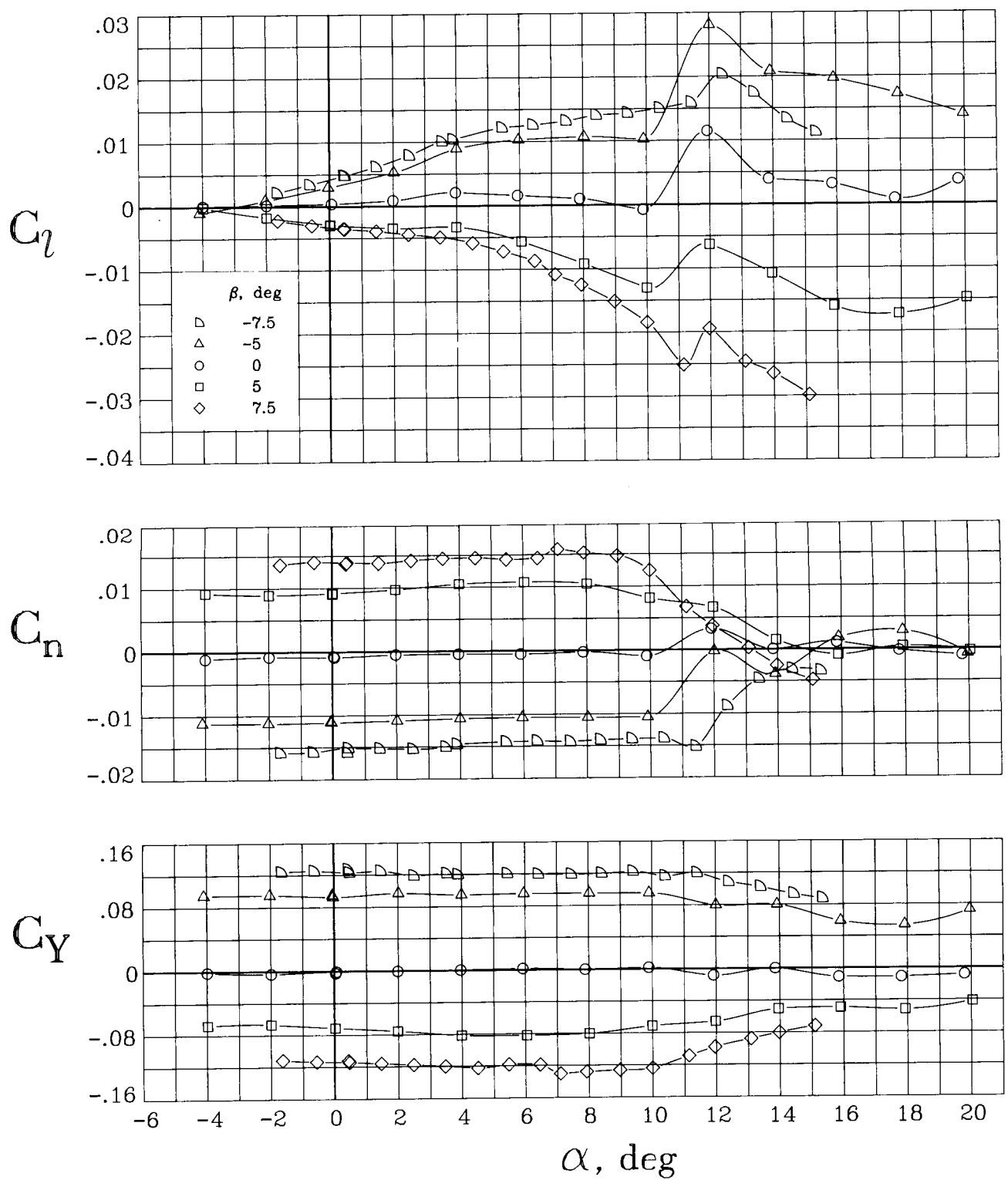
(e) $M = 0.85$.

Figure 16. Continued.



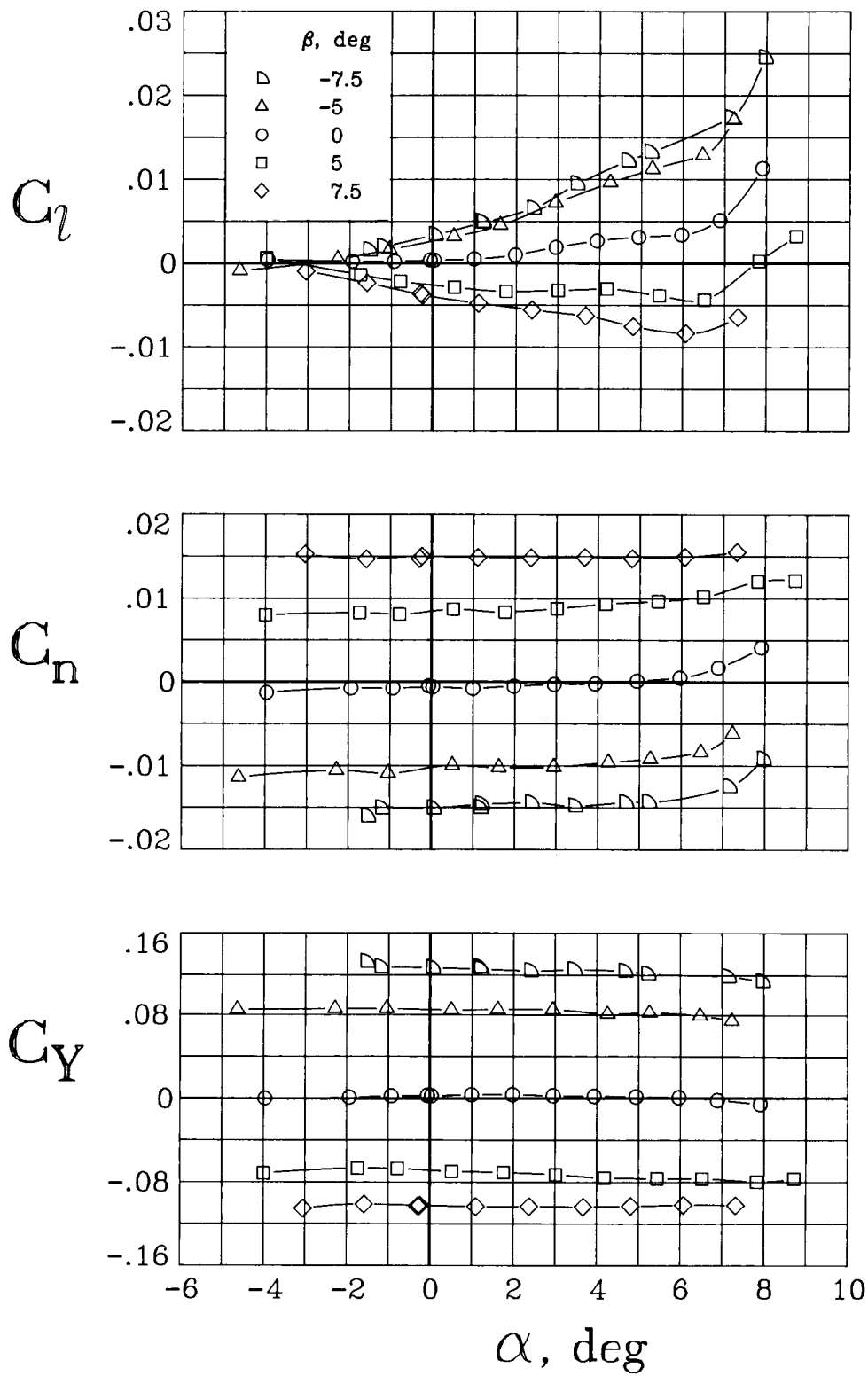
(f) $M = 0.90$.

Figure 16. Concluded.



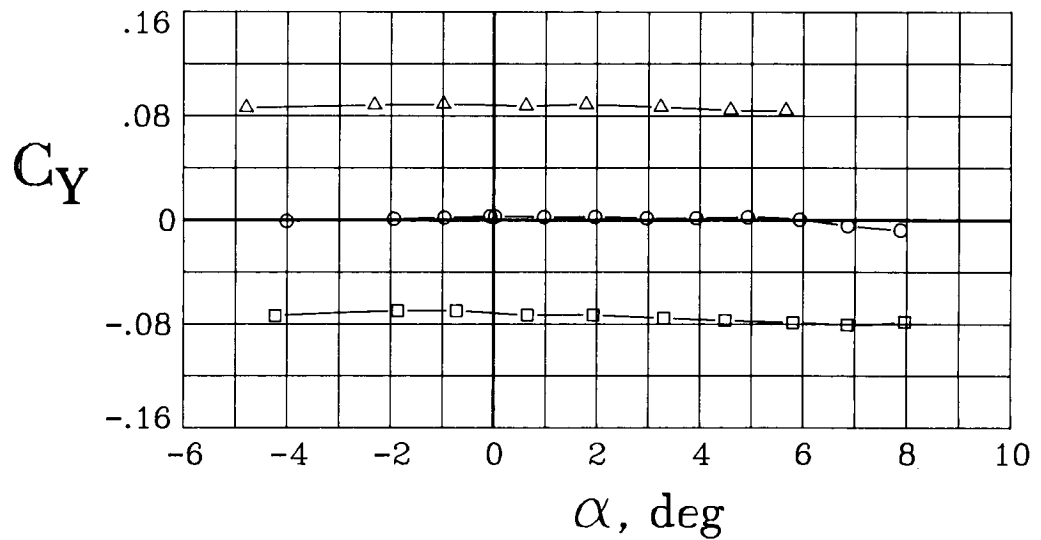
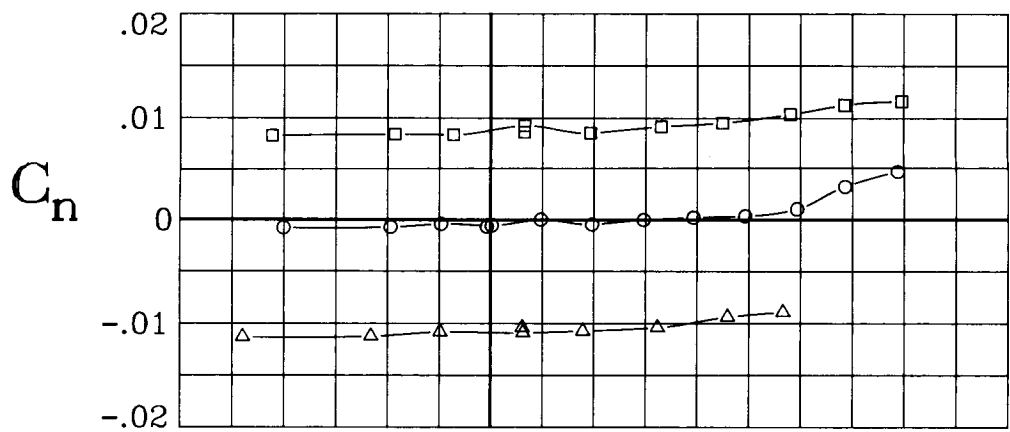
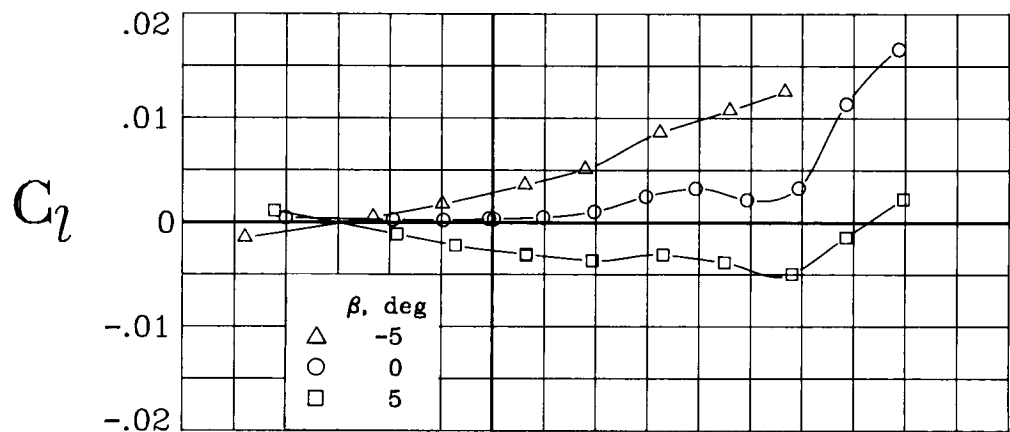
(a) $M = 0.20$.

Figure 17. Lateral-directional aerodynamic characteristics of the modified wing configuration for a range of sideslip angles. $\Lambda = 20^\circ$.



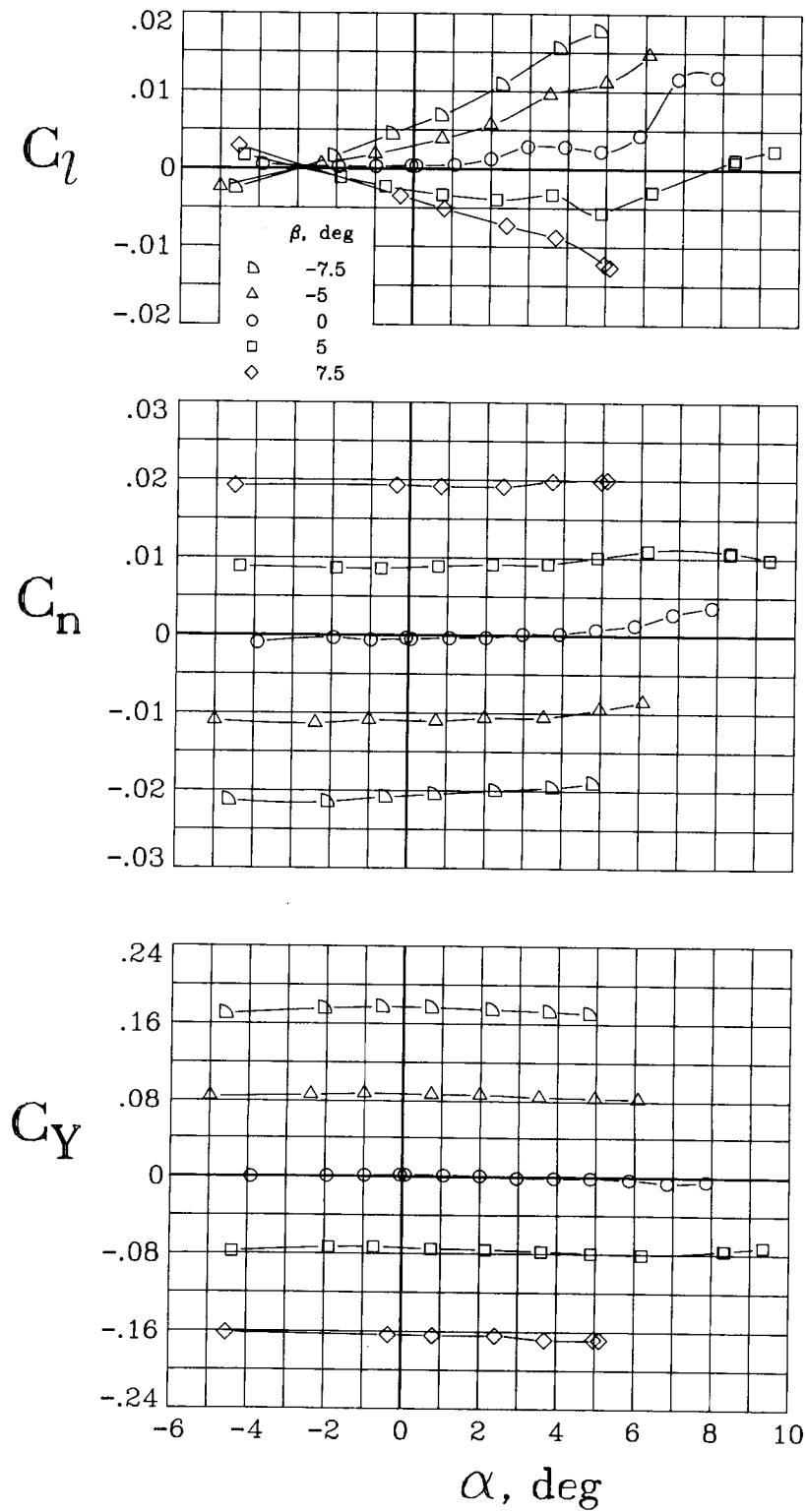
(b) $M = 0.60$.

Figure 17. Continued.



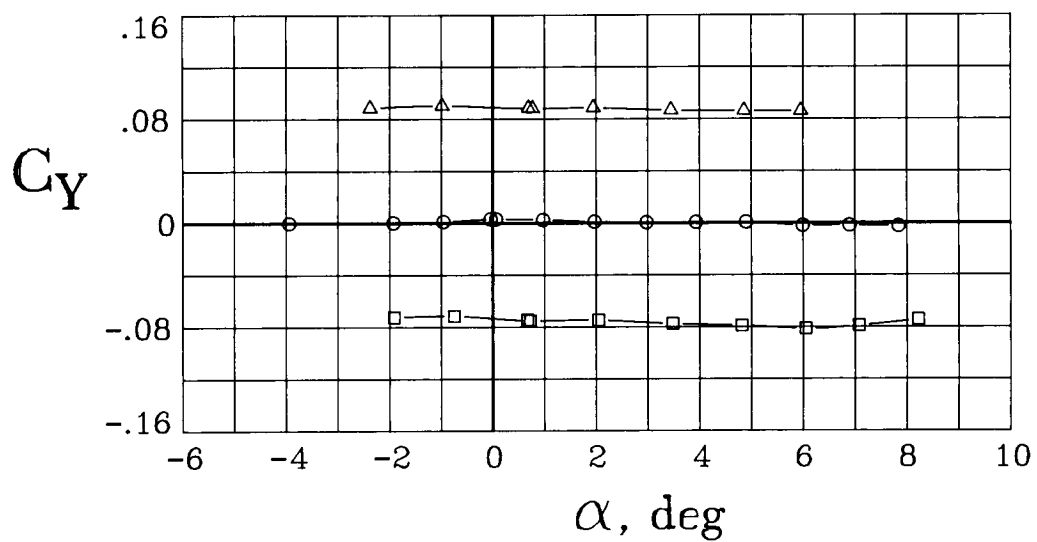
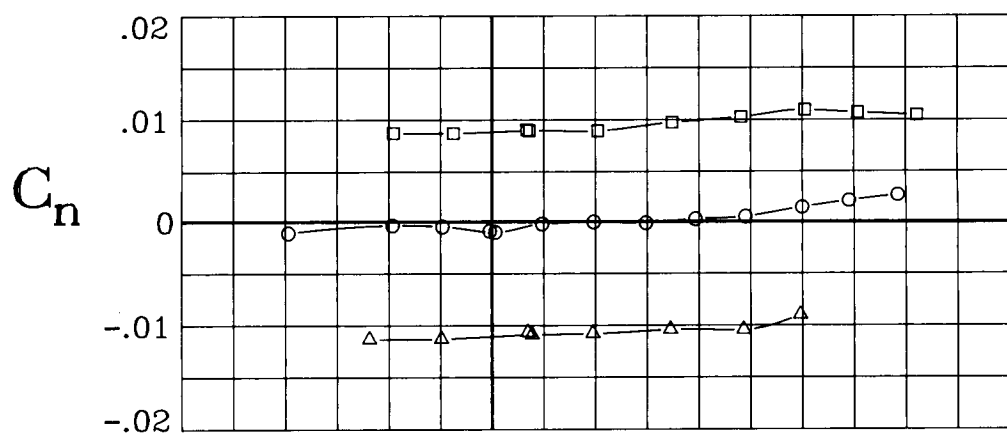
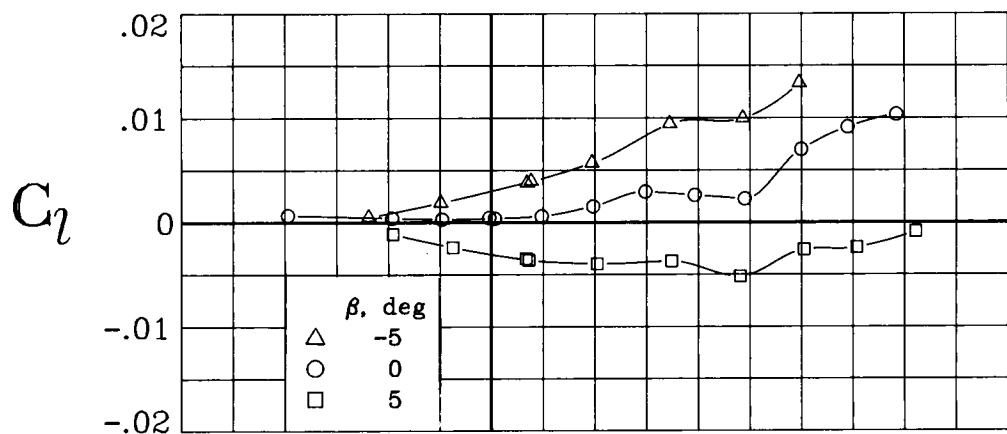
(c) $M = 0.675$.

Figure 17. Continued.



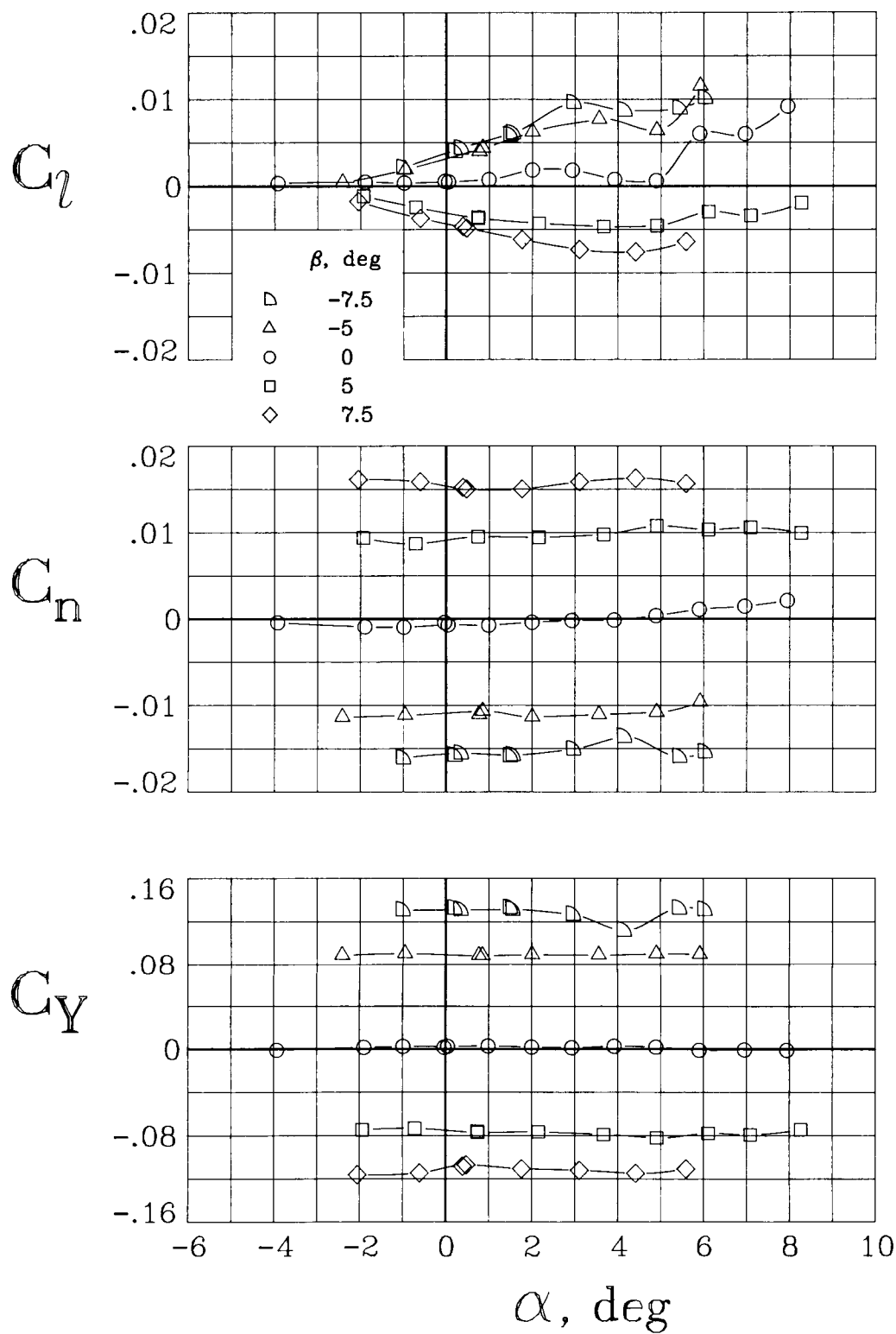
(d) $M = 0.70$.

Figure 17. Continued.



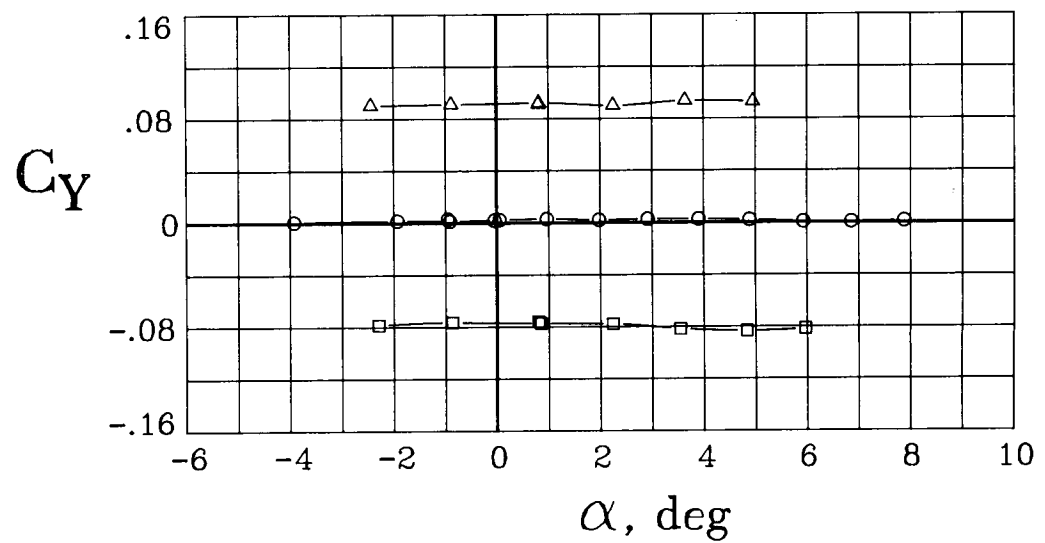
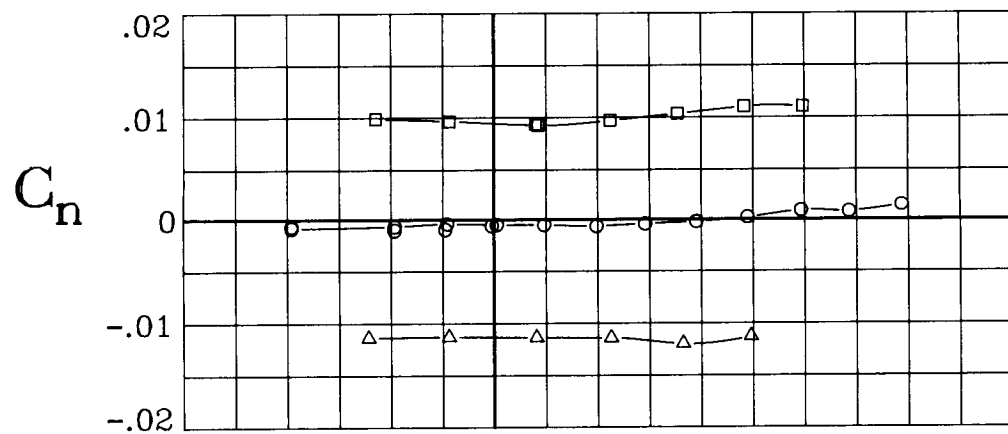
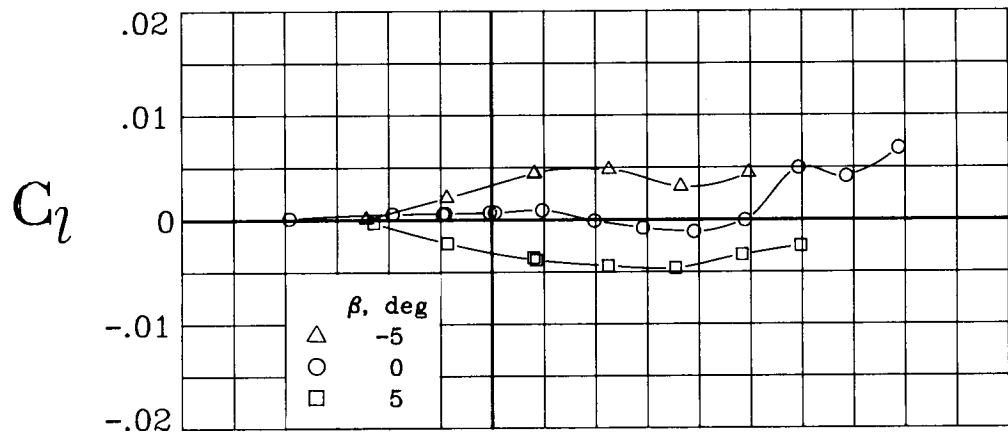
(e) $M = 0.725$.

Figure 17. Continued.



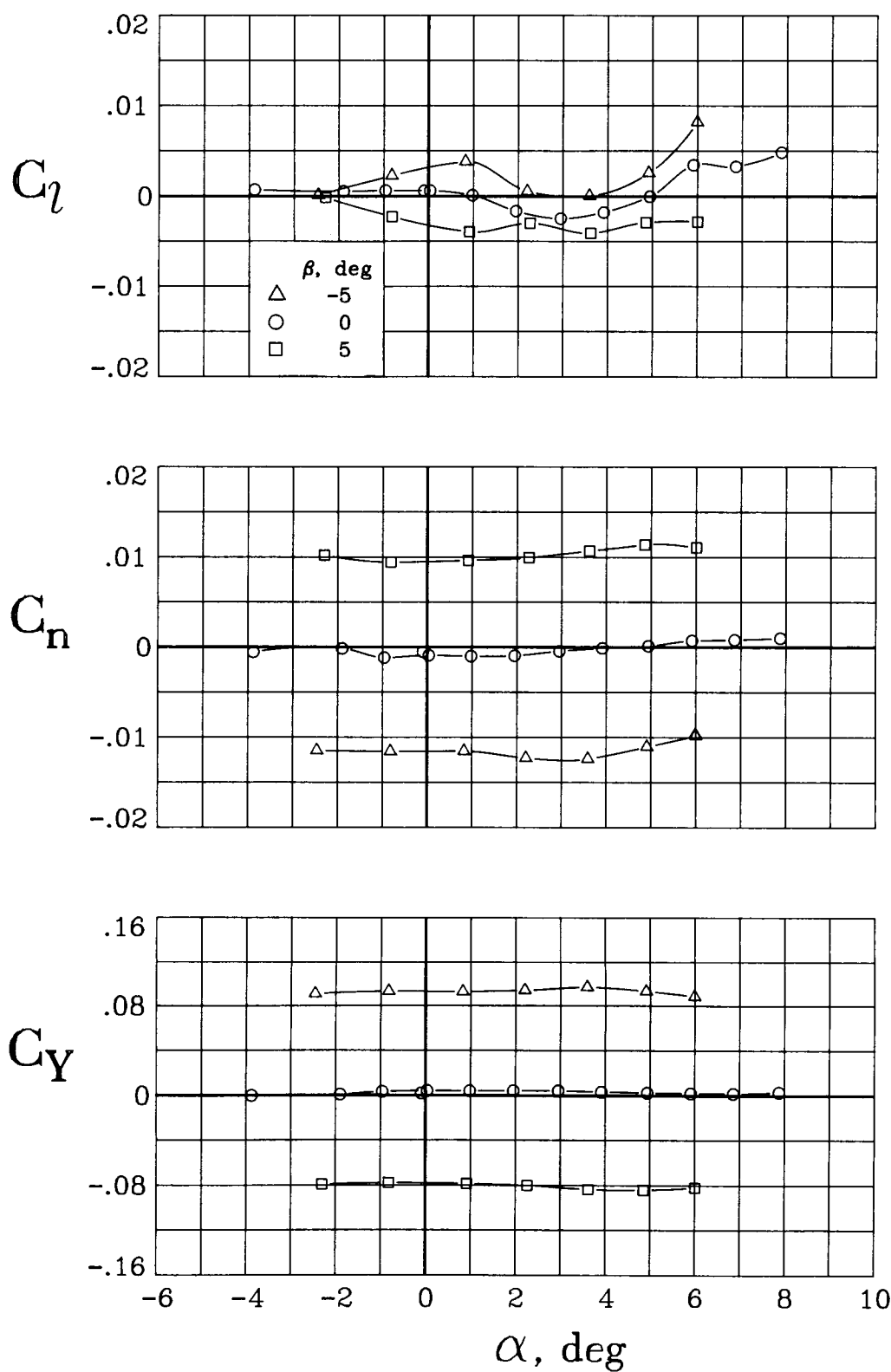
(f) $M = 0.75$.

Figure 17. Continued.



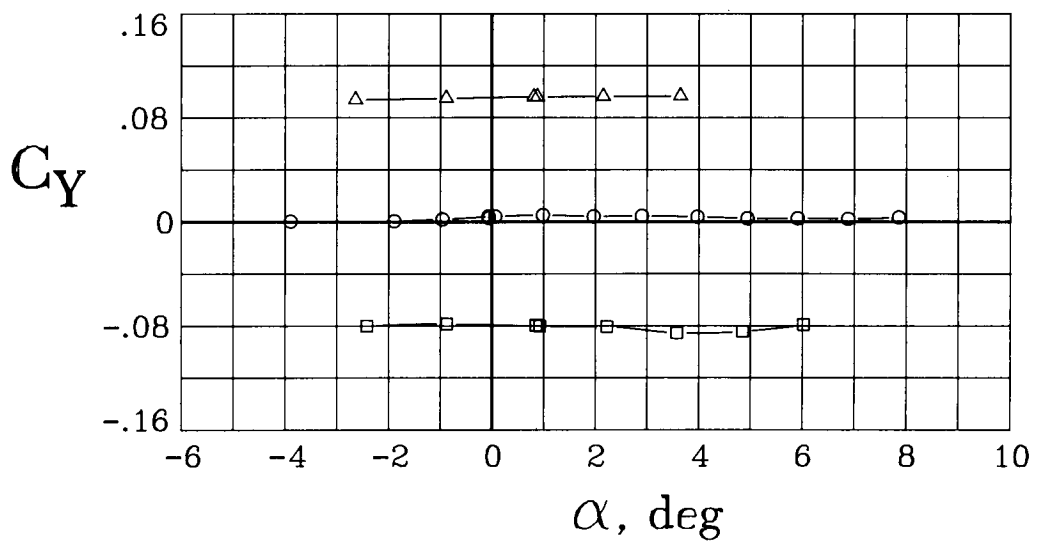
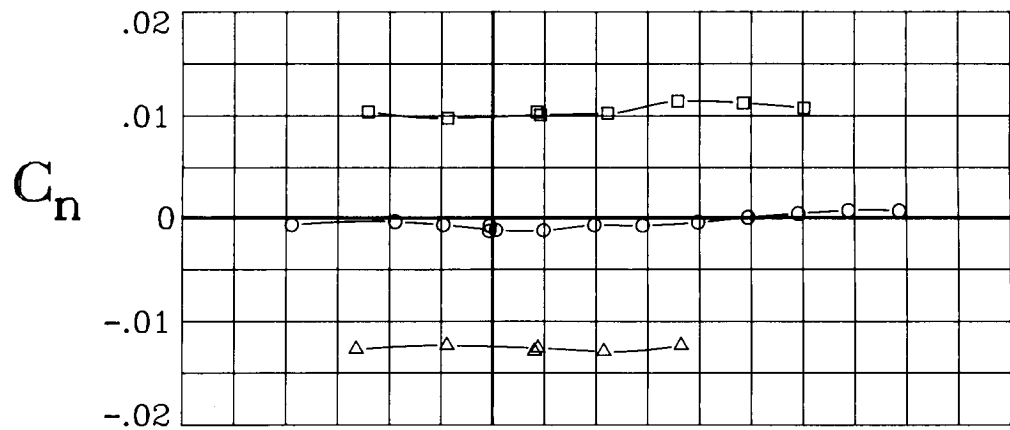
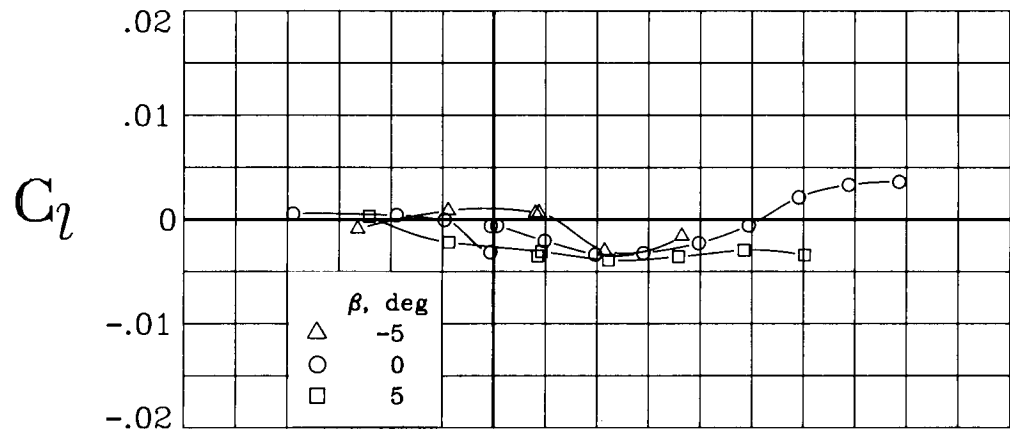
(g) $M = 0.775$.

Figure 17. Continued.



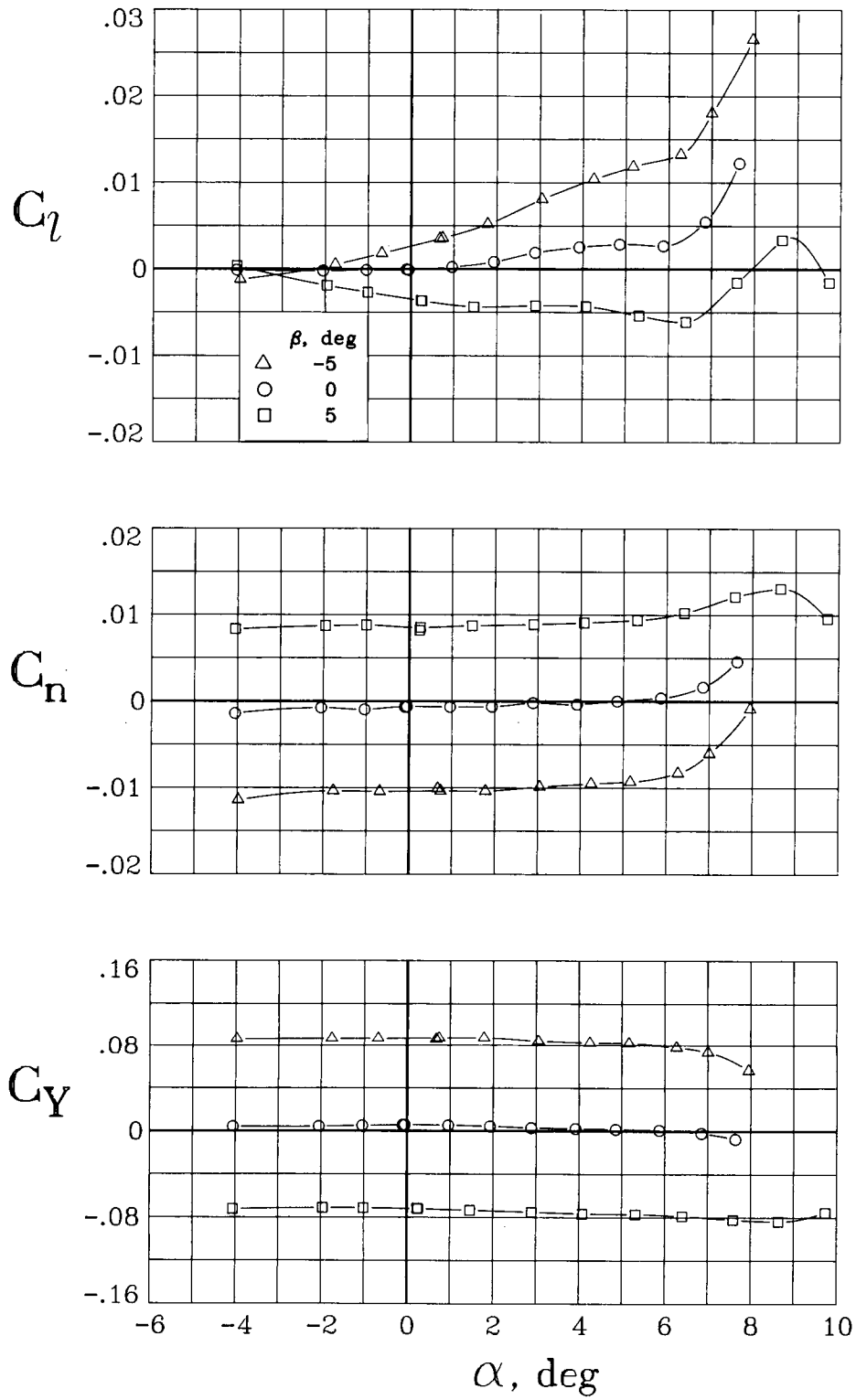
(h) $M = 0.80$.

Figure 17. Continued.



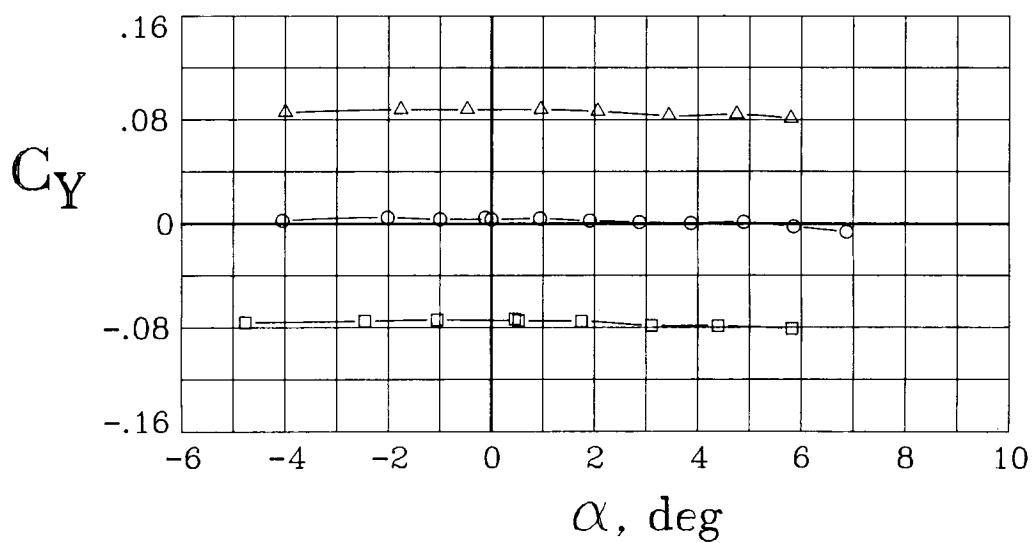
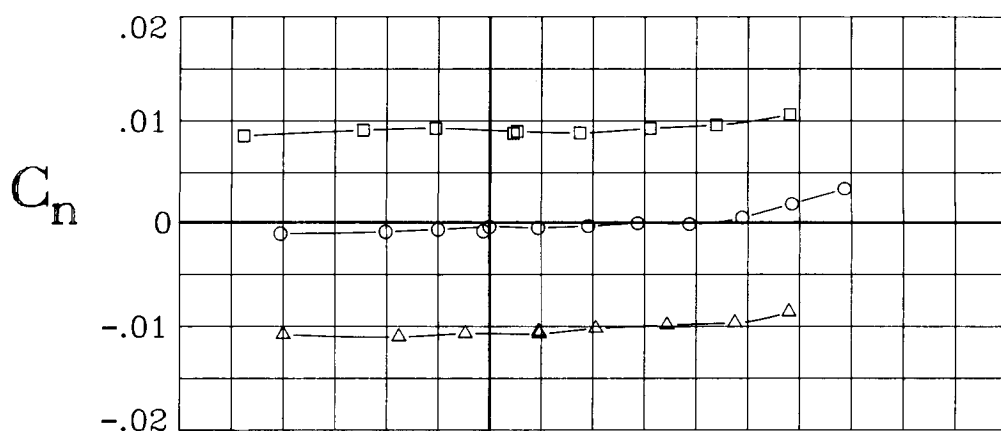
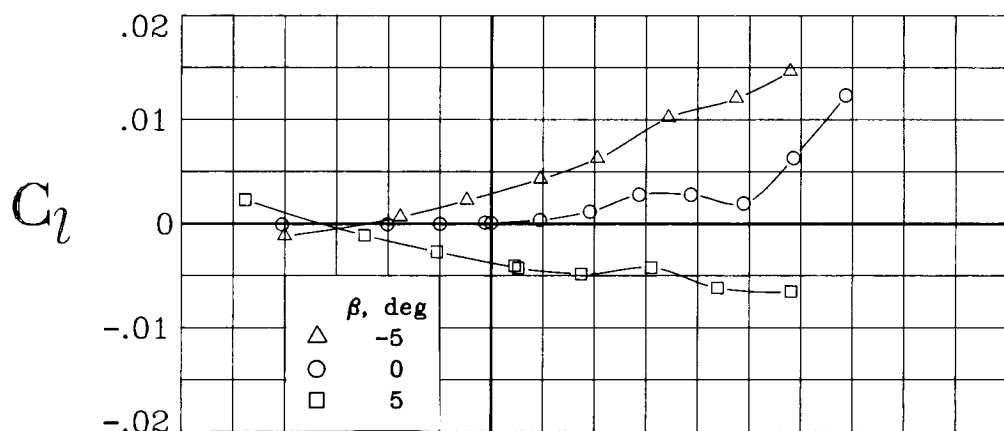
(i) $M = 0.825$.

Figure 17. Concluded.



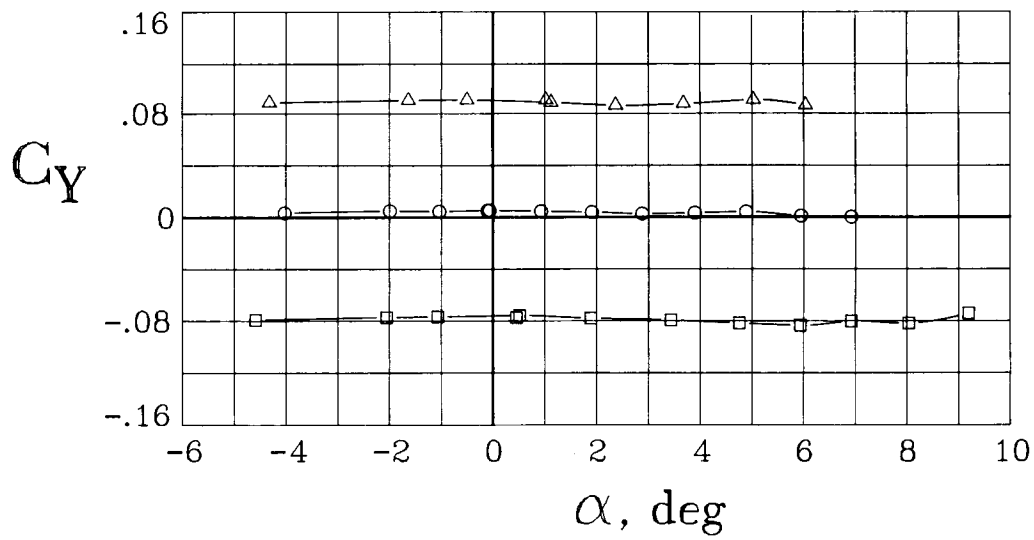
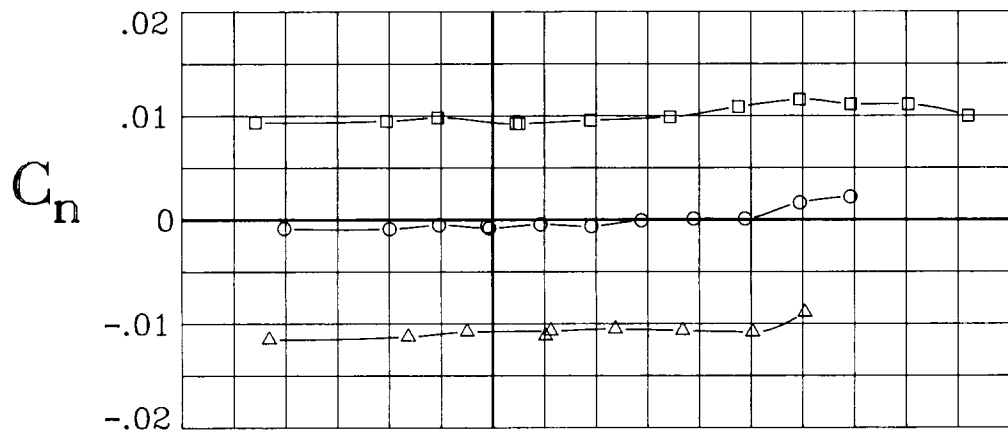
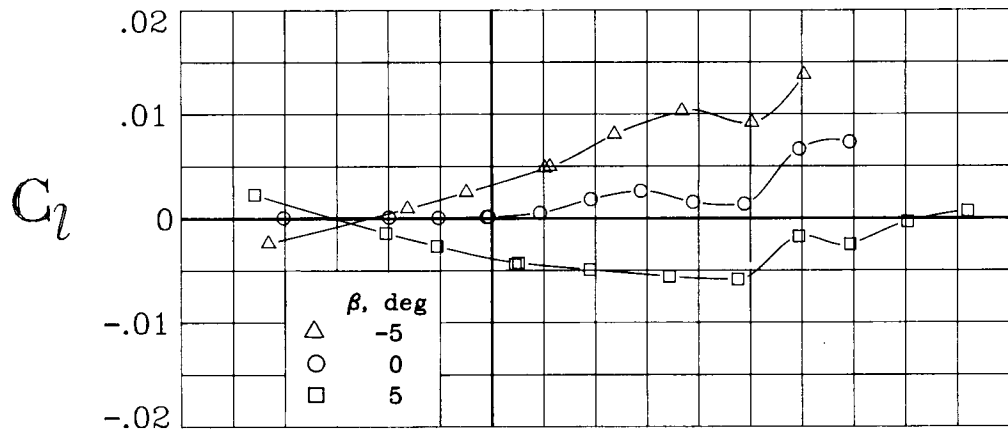
(a) $M = 0.60$.

Figure 18. Lateral-directional aerodynamic characteristics of the modified wing configuration for a range of sideslip angles. $\Lambda = 25^\circ$.



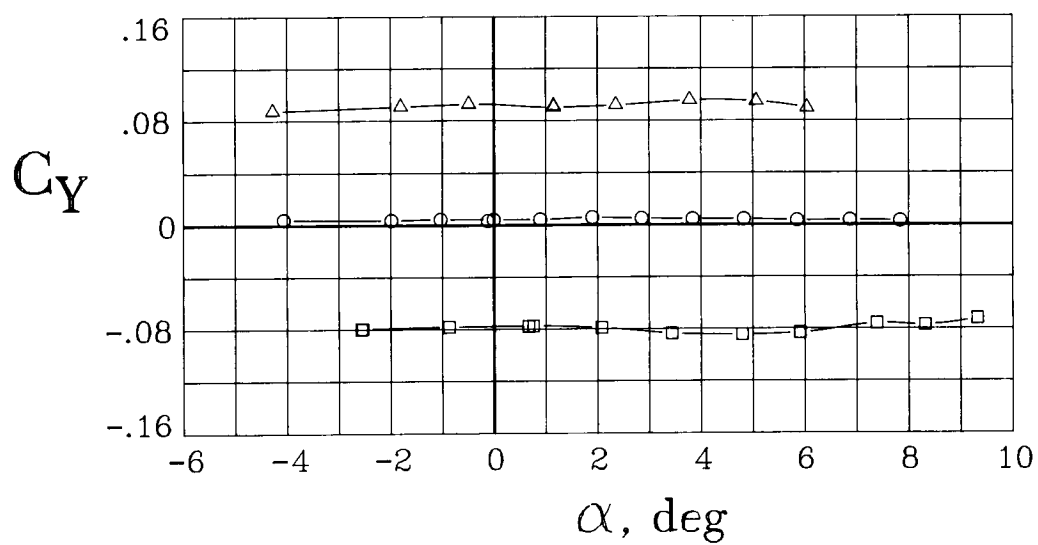
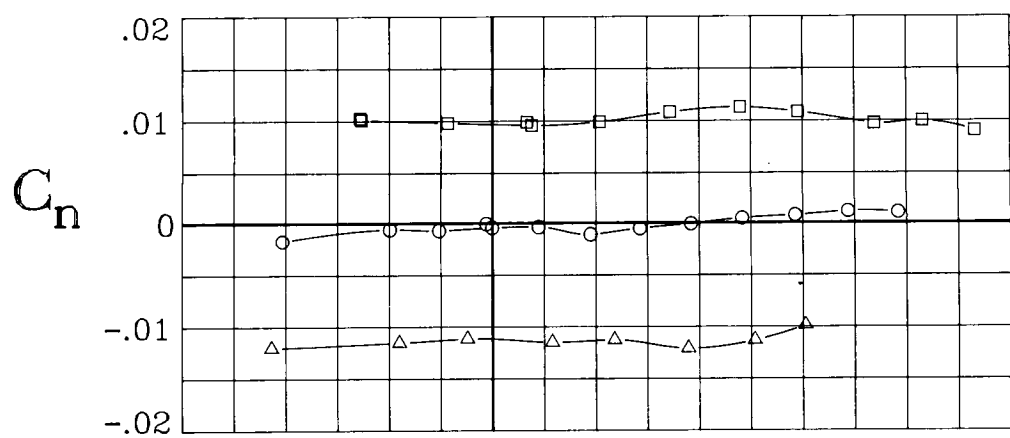
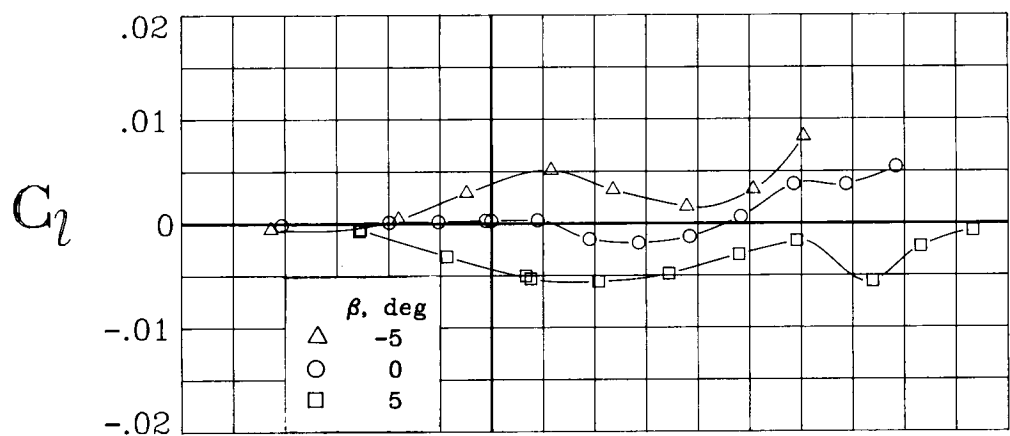
(b) $M = 0.70$.

Figure 18. Continued.



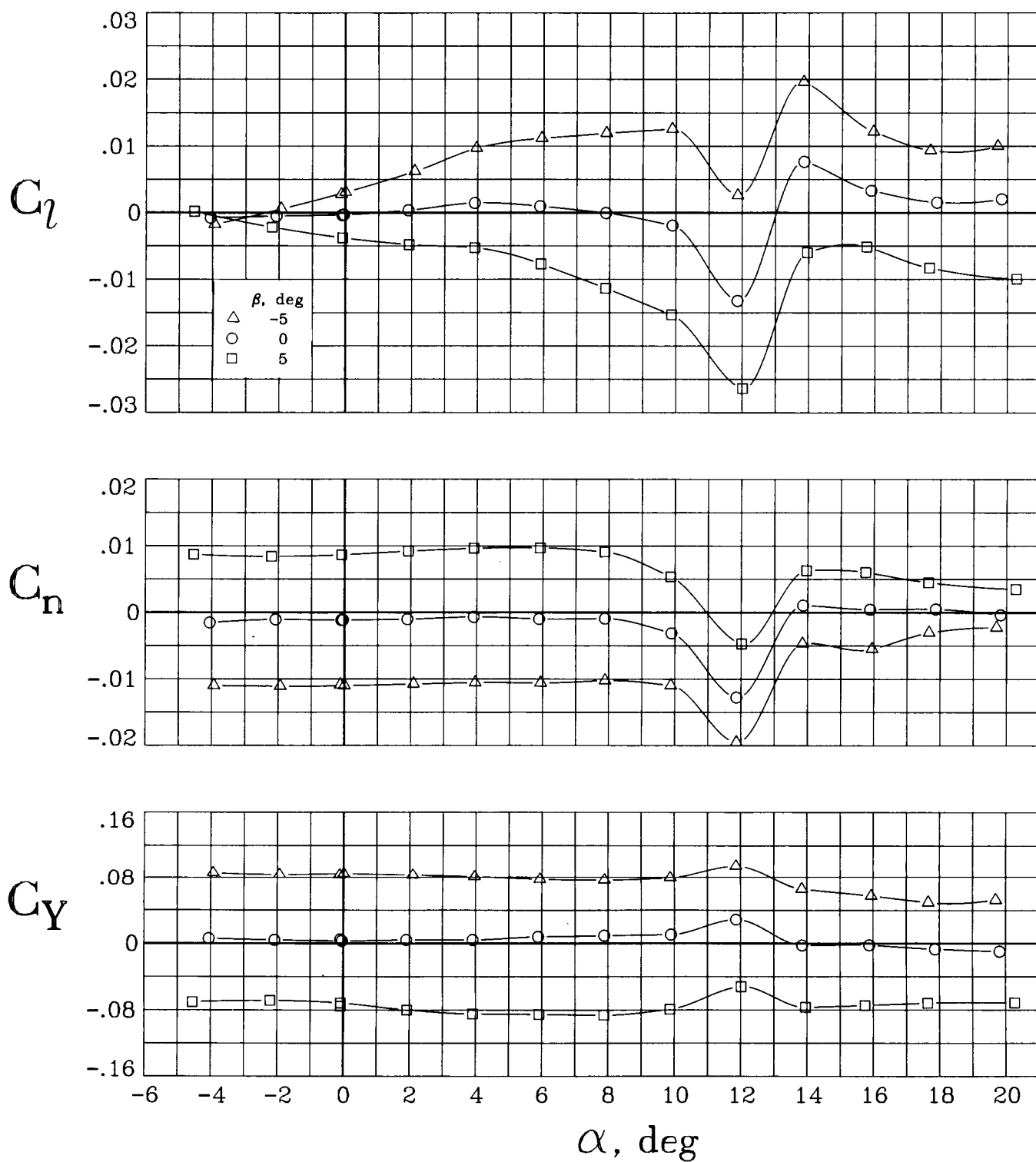
(c) $M = 0.75$.

Figure 18. Continued.



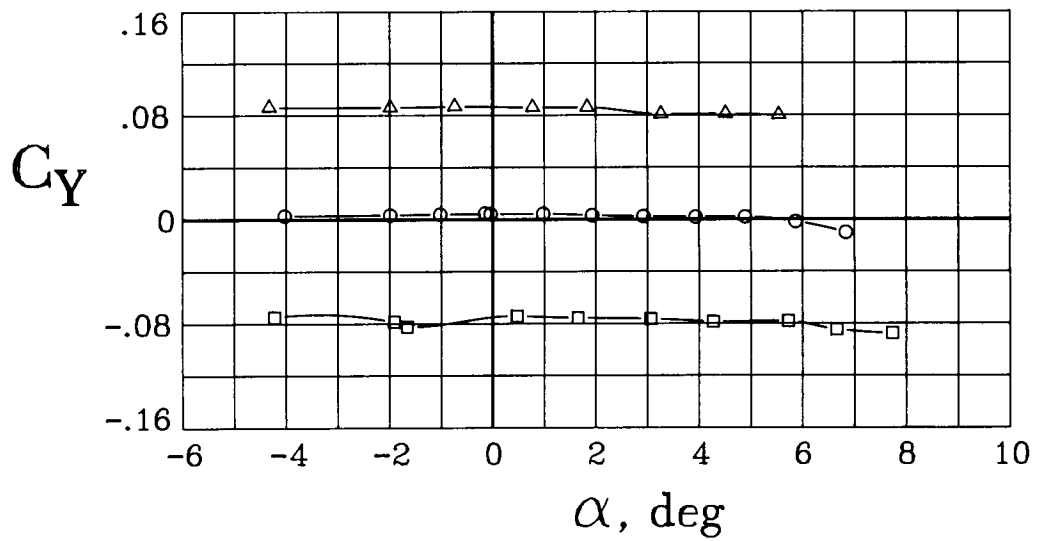
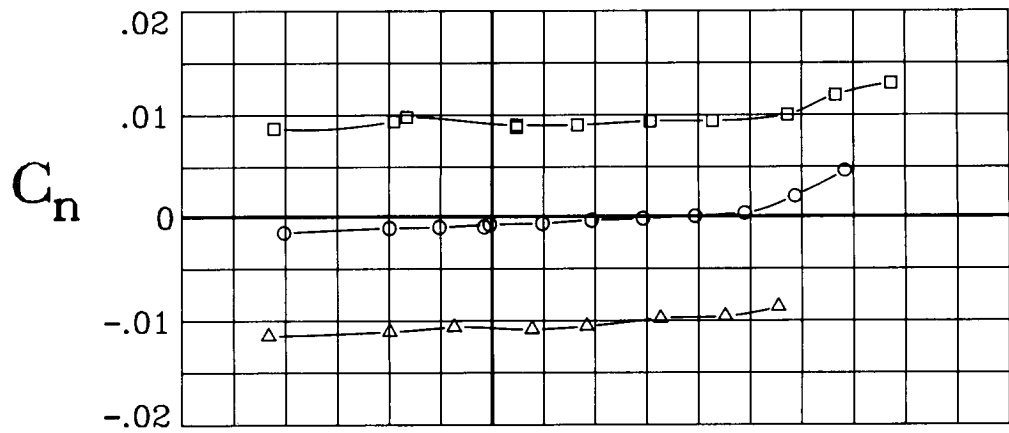
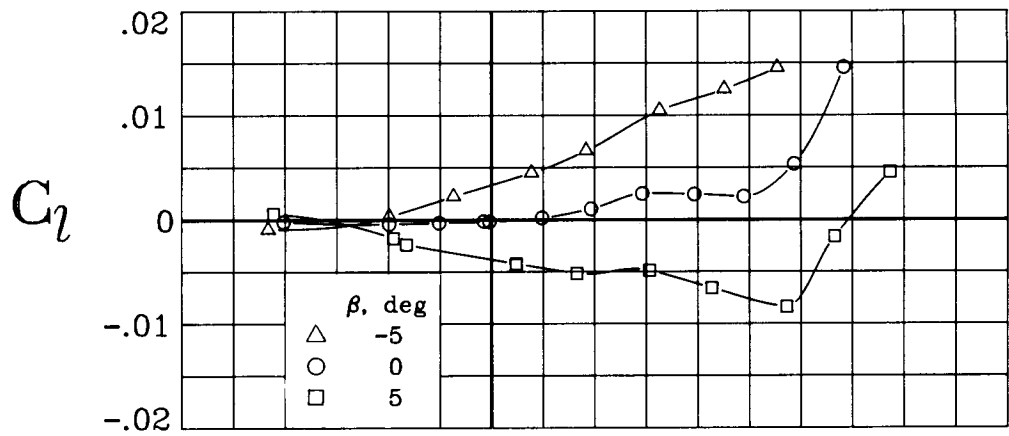
(d) $M = 0.80$.

Figure 18. Concluded.



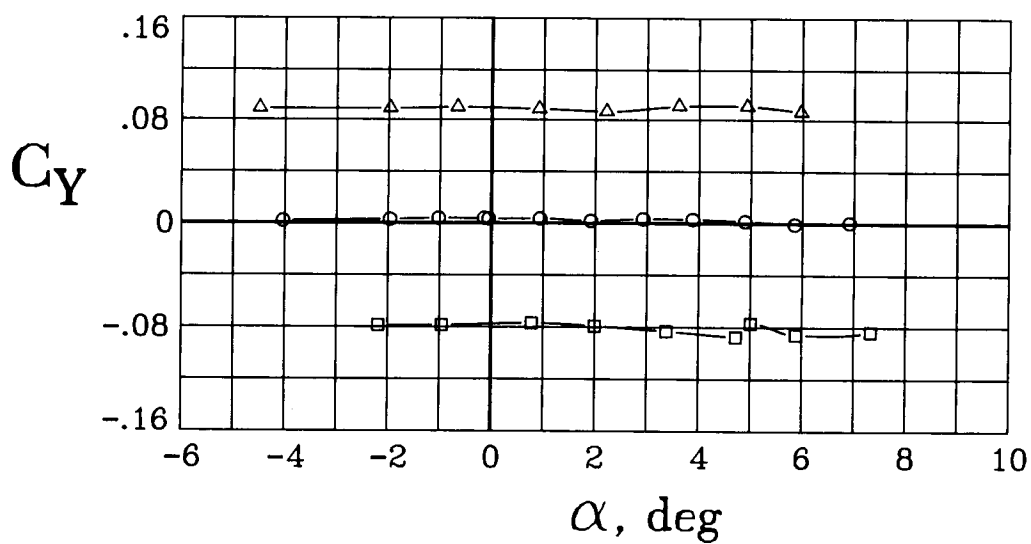
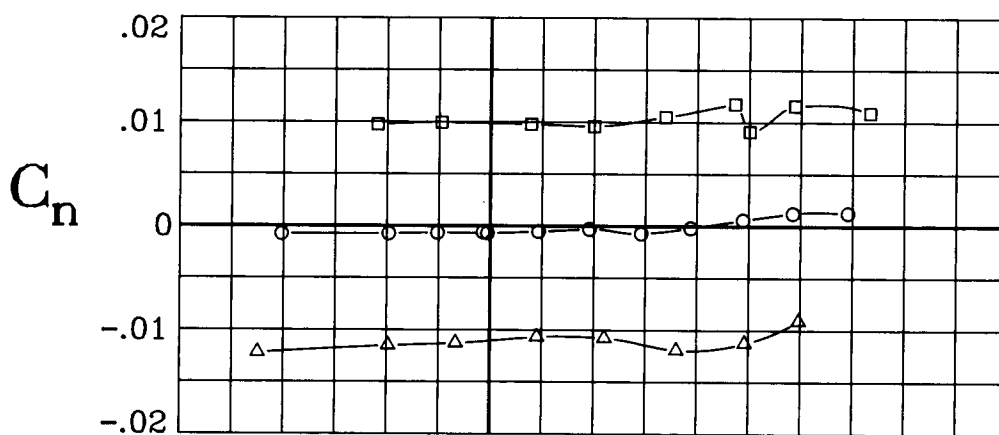
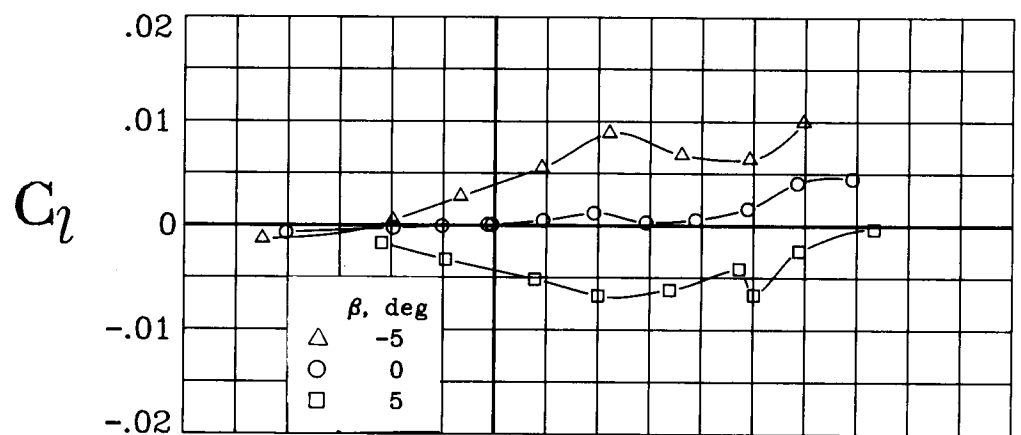
(a) $M = 0.20$.

Figure 19. Lateral-directional aerodynamic characteristics of the modified wing configuration for a range of sideslip angles. $\Lambda = 30^\circ$.



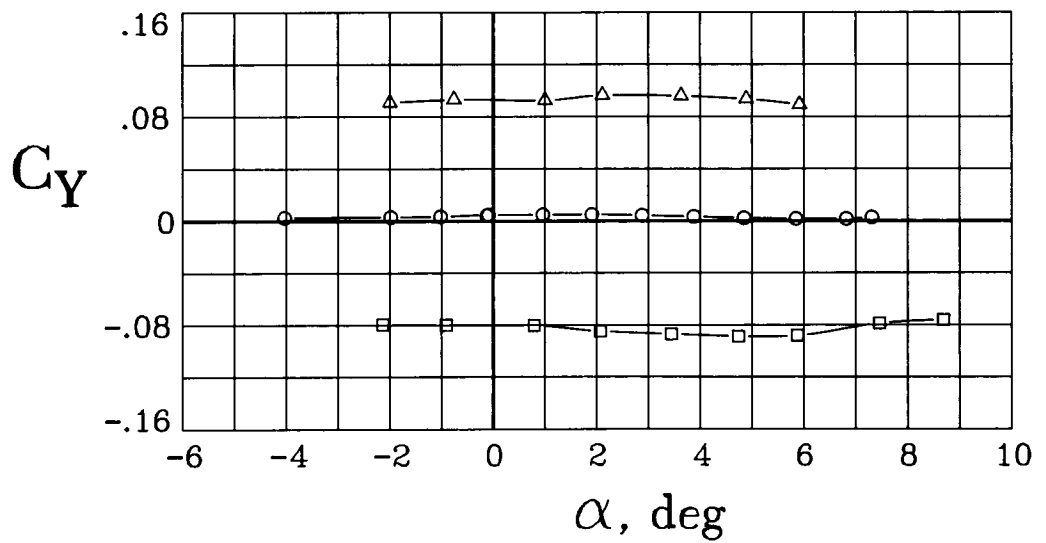
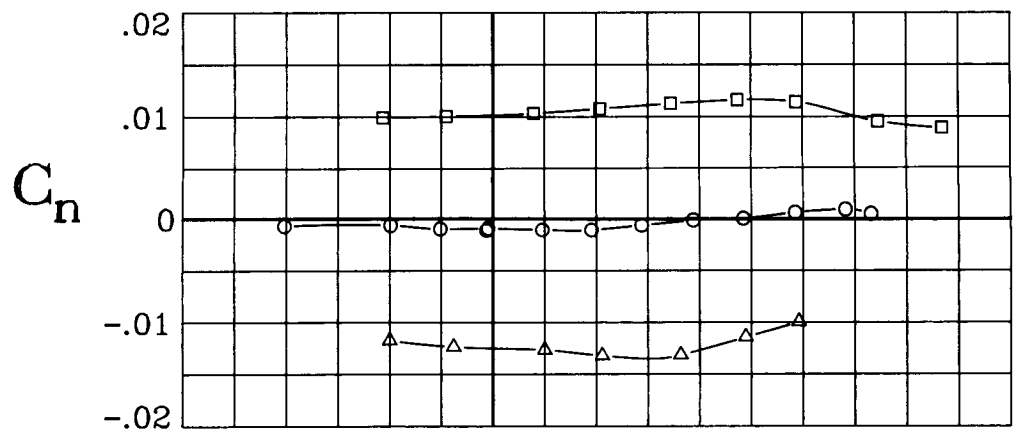
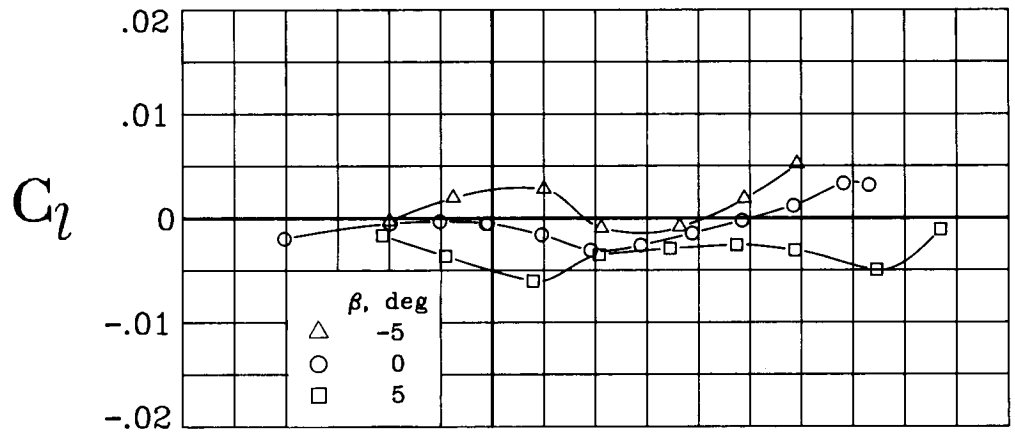
(b) $M = 0.70$.

Figure 19. Continued.



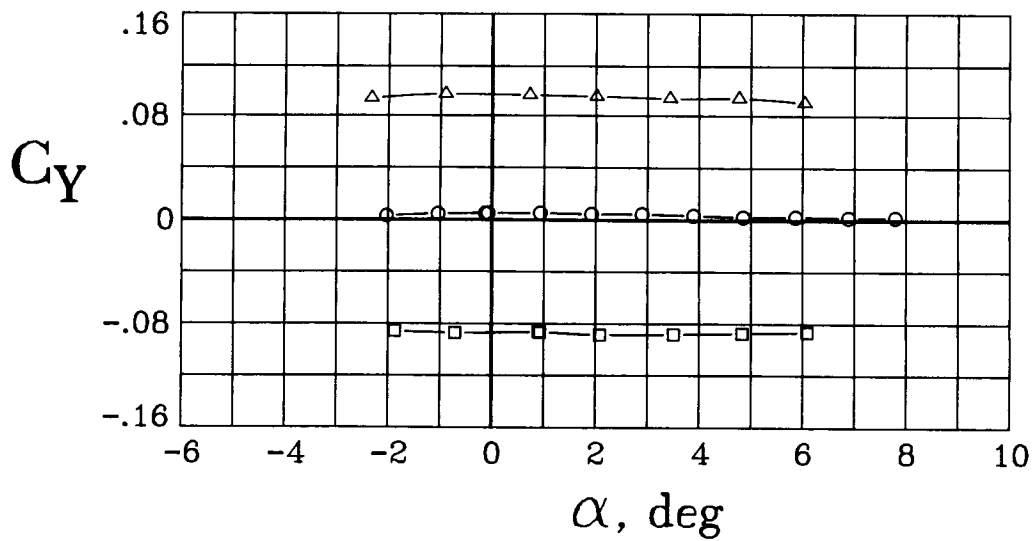
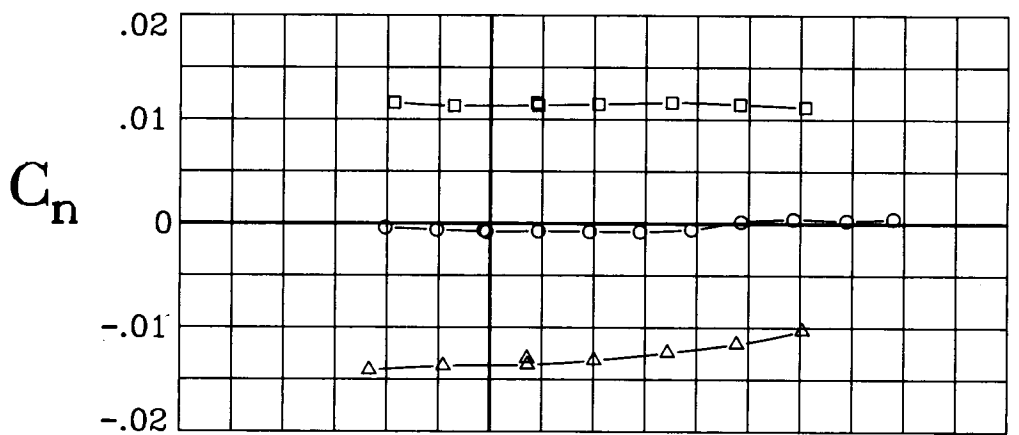
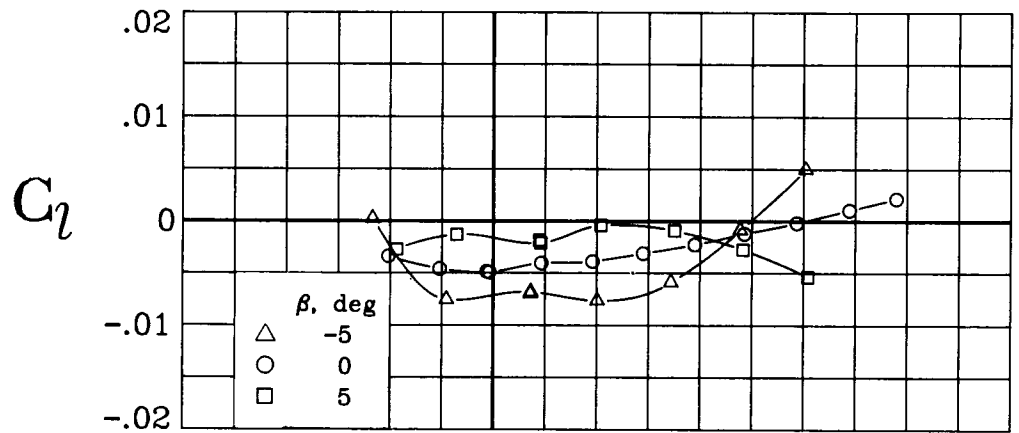
(c) $M = 0.80$.

Figure 19. Continued.



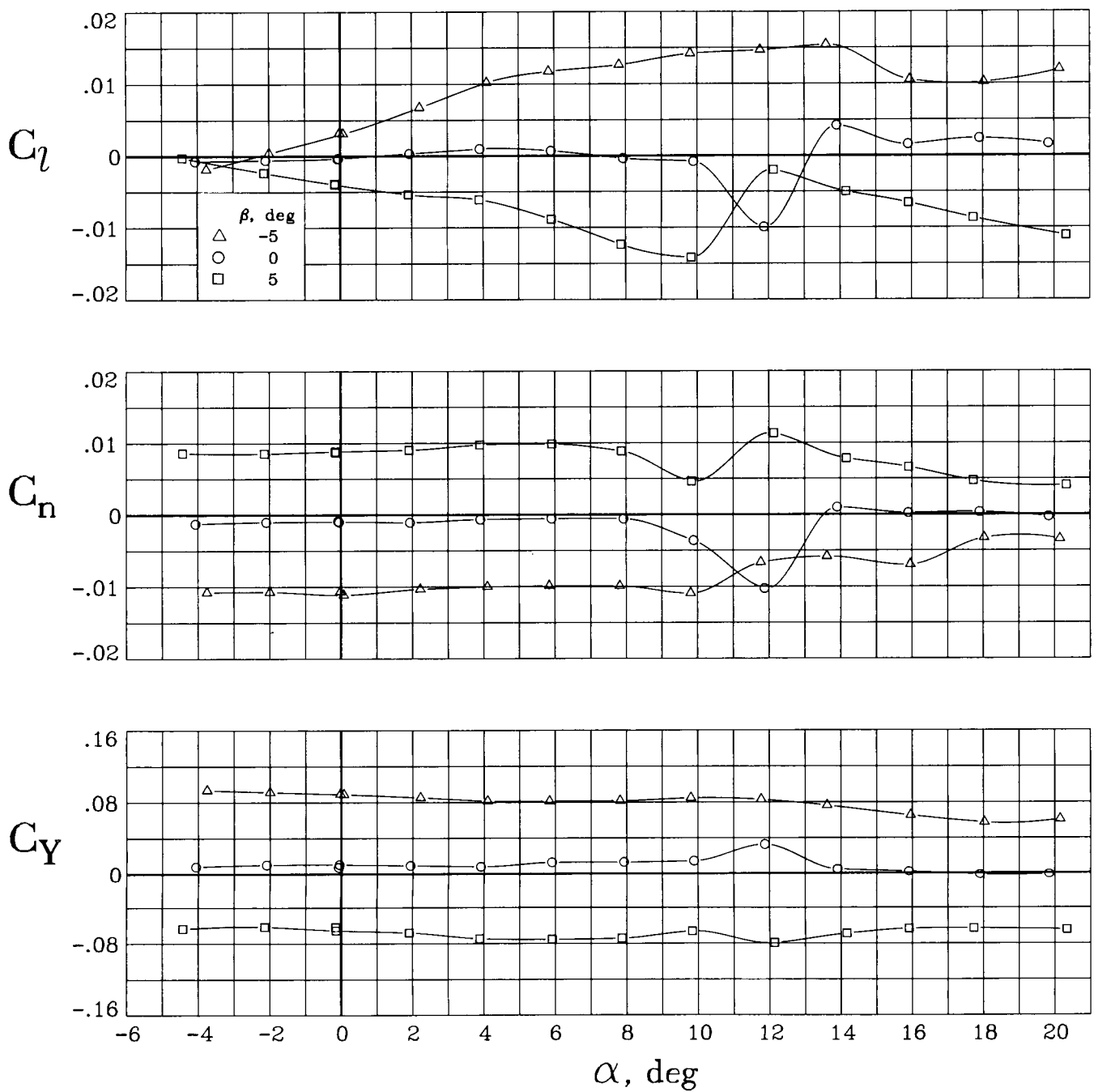
(d) $M = 0.85$.

Figure 19. Continued.



(e) $M = 0.90$.

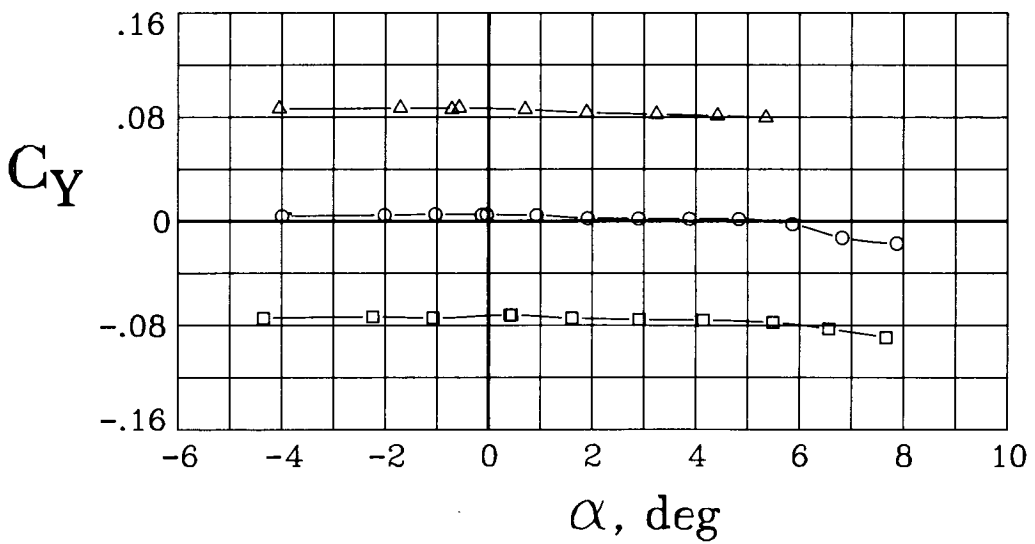
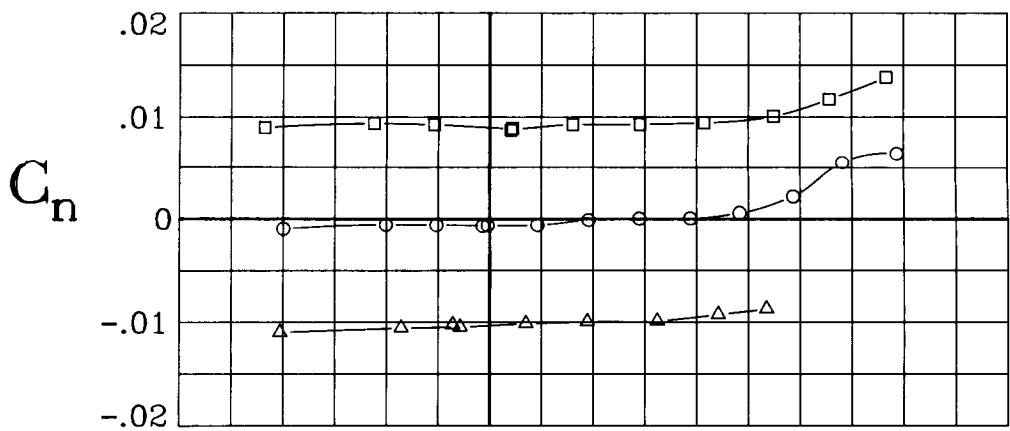
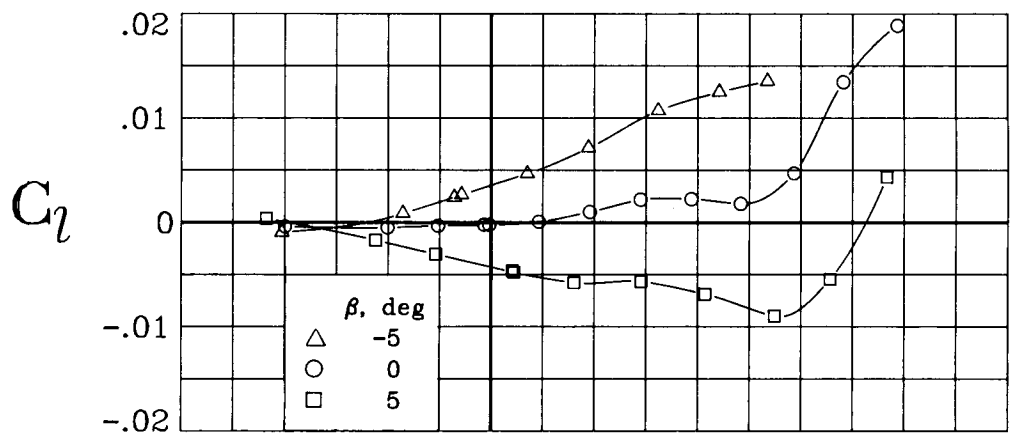
Figure 19. Concluded.



(a) $M = 0.20$.

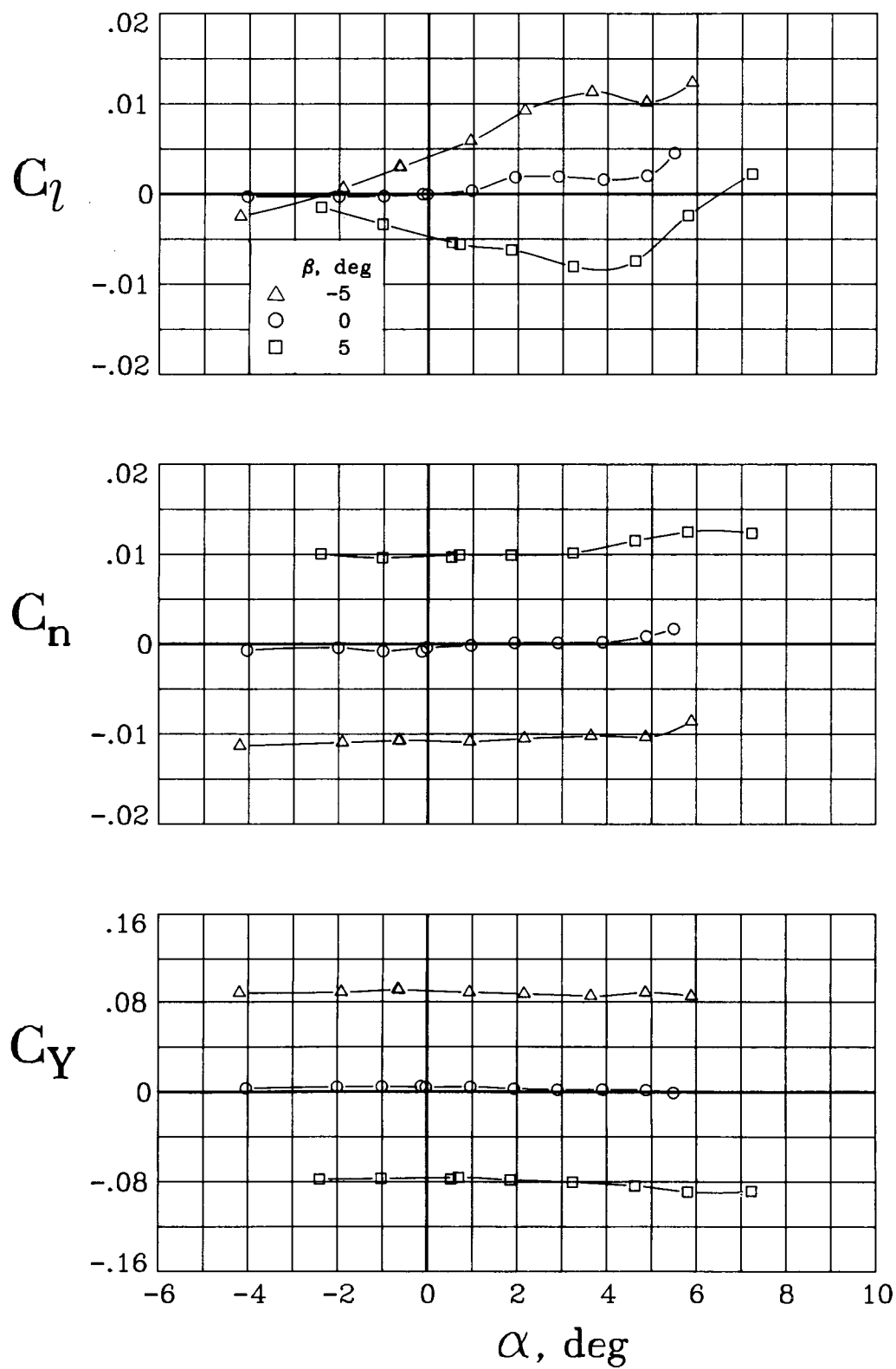
Figure 20. Lateral-directional aerodynamic characteristics of the modified wing configuration for a range of sideslip angles. $\Lambda = 35^\circ$.

PRECEDING PAGE BLANK NOT FILMED



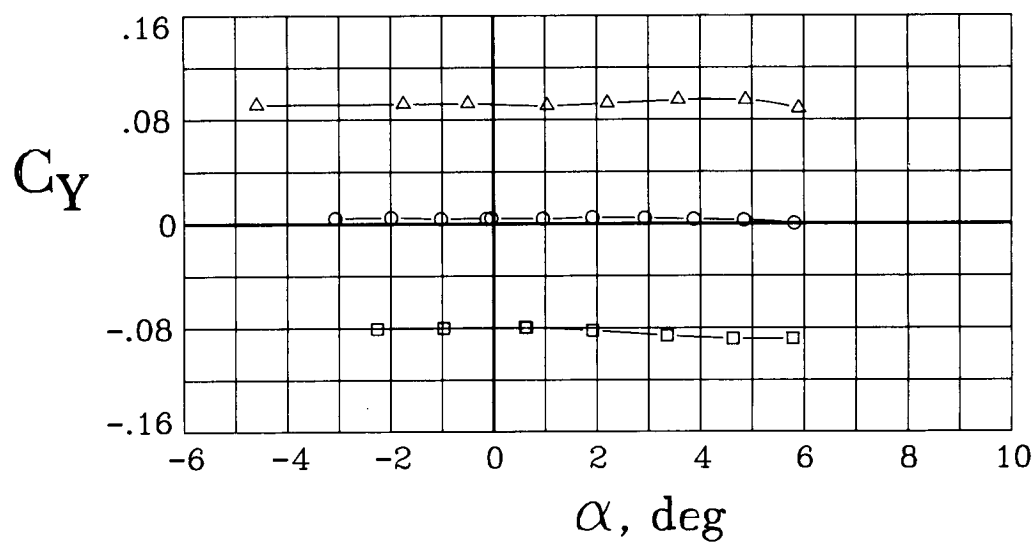
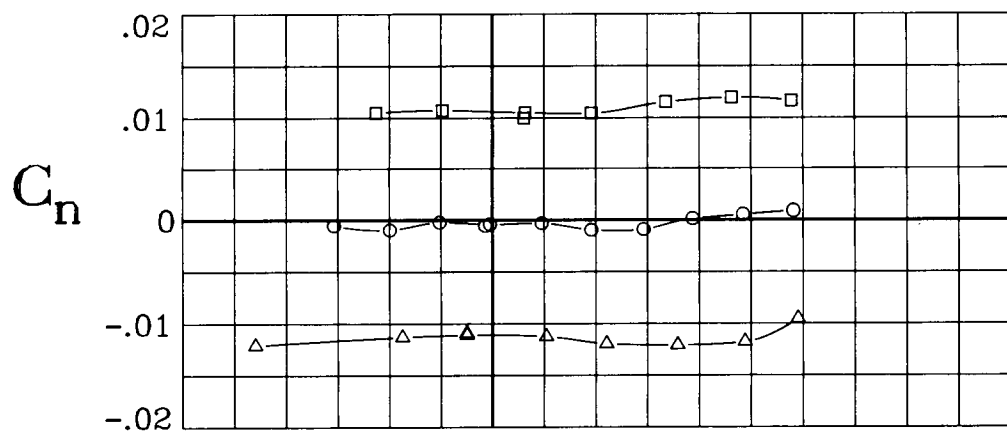
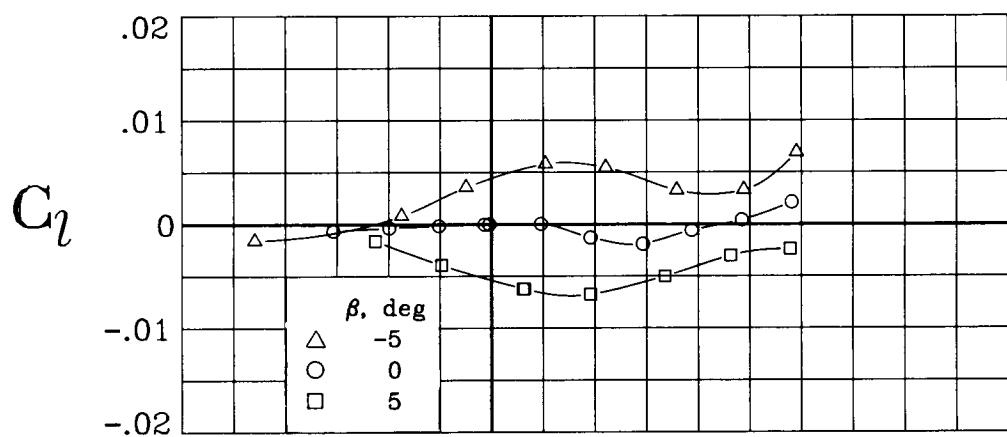
(b) $M = 0.70$.

Figure 20. Continued.



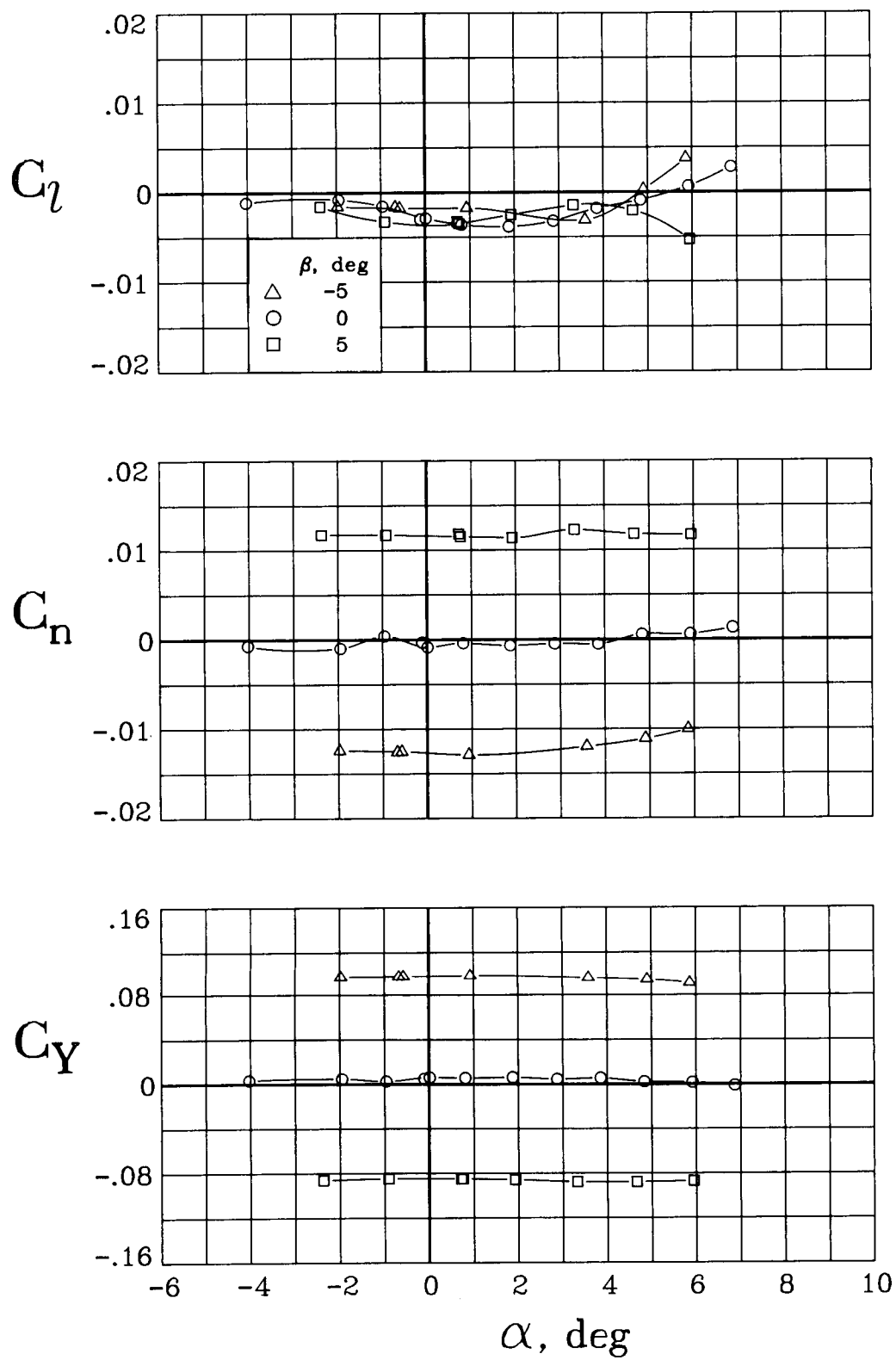
(c) $M = 0.80$.

Figure 20. Continued.



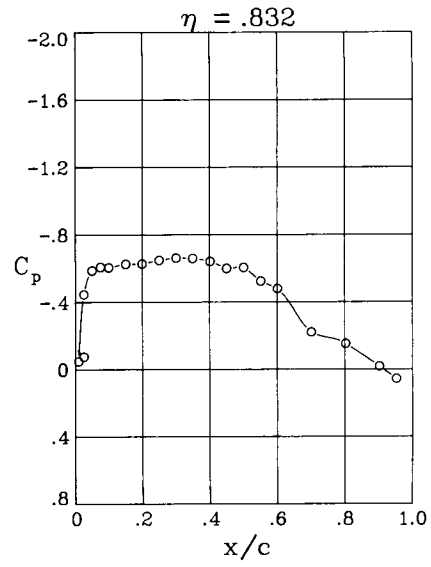
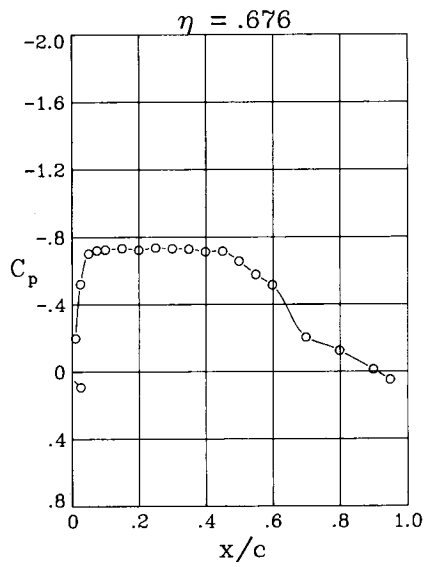
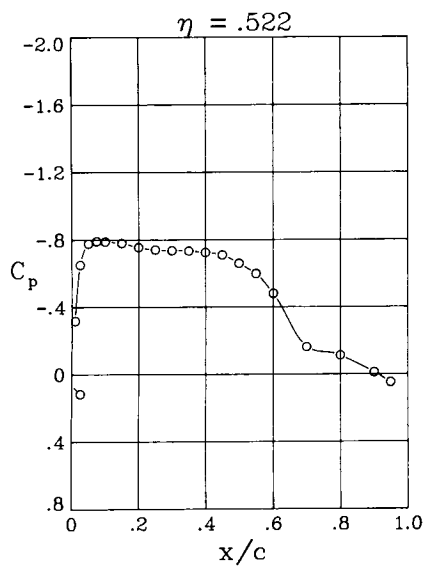
(d) $M = 0.85$.

Figure 20. Continued.

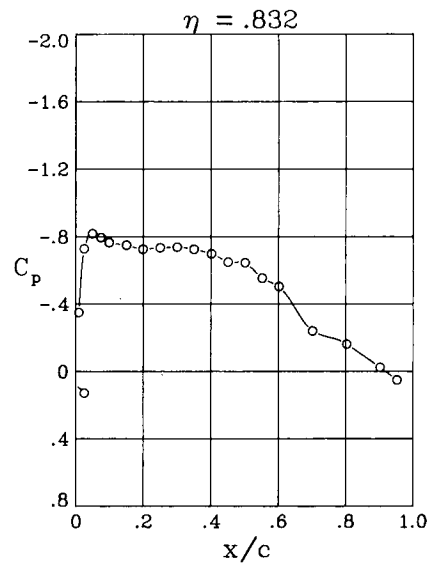
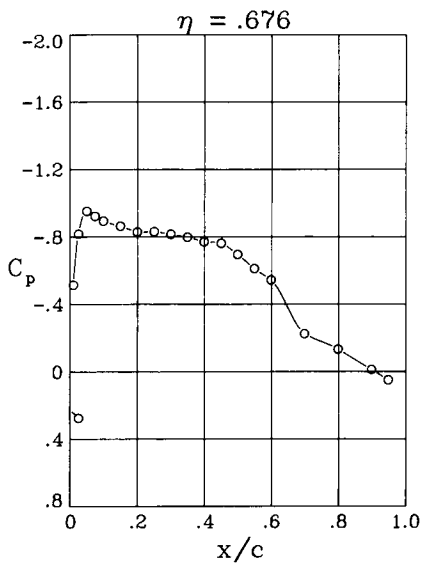
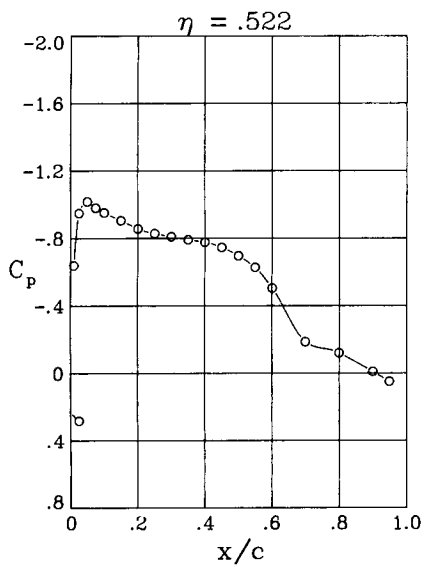


(e) $M = 0.90$.

Figure 20. Concluded.



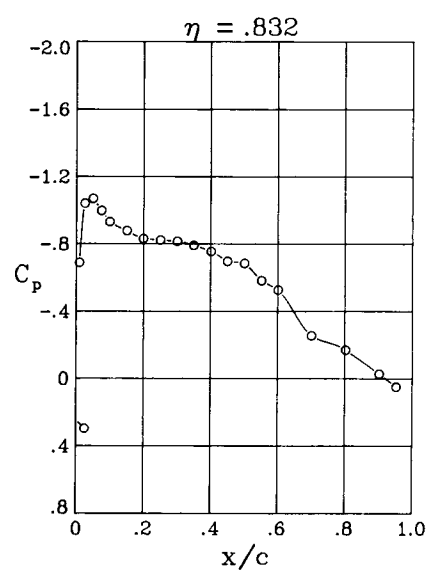
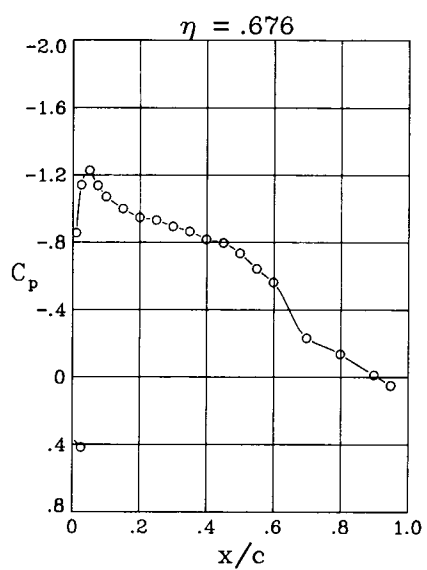
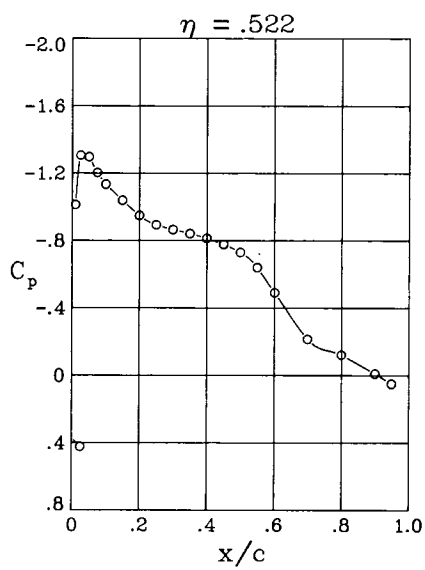
$\alpha = 1.98^\circ$



$\alpha = 2.95^\circ$

(a) $M = 0.60$.

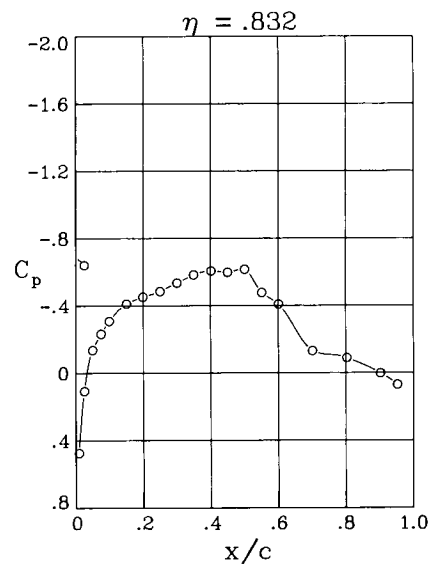
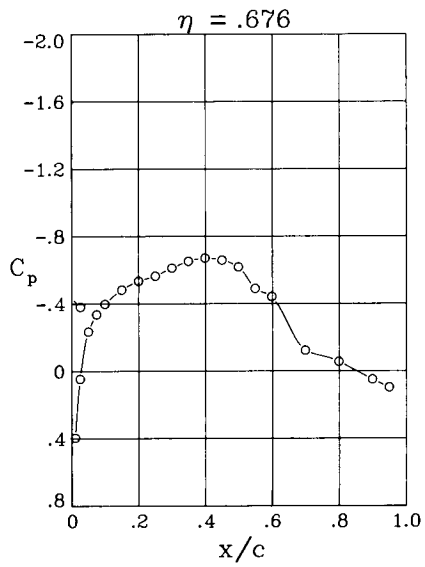
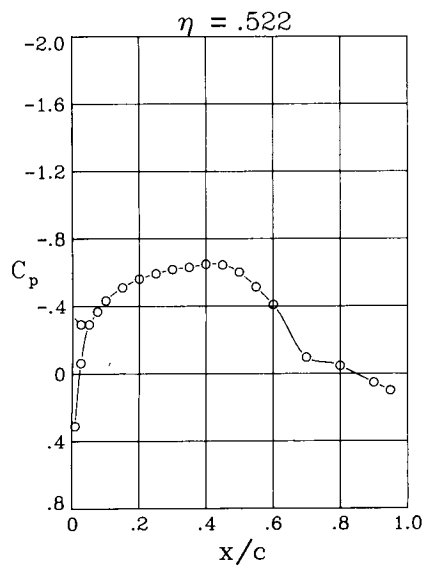
Figure 21. Wing pressure distributions for wing B swept 20° .



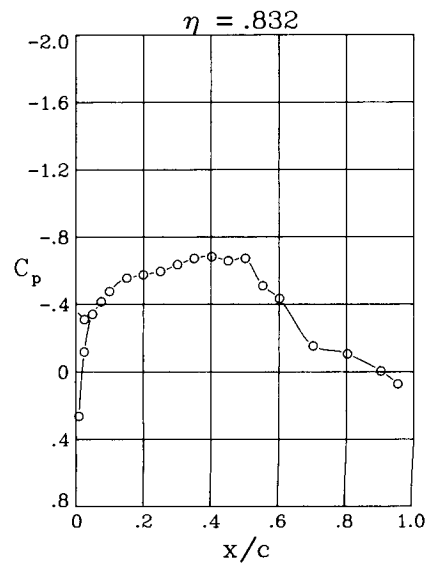
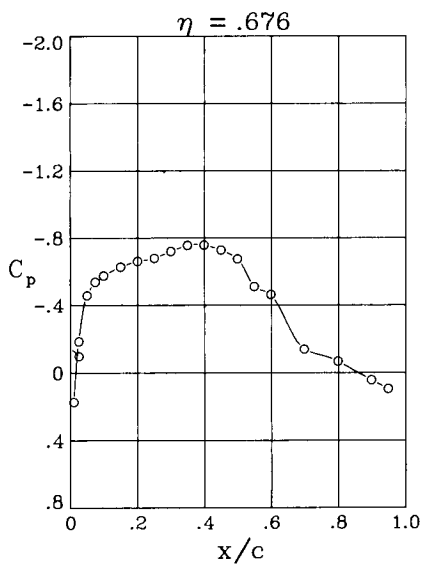
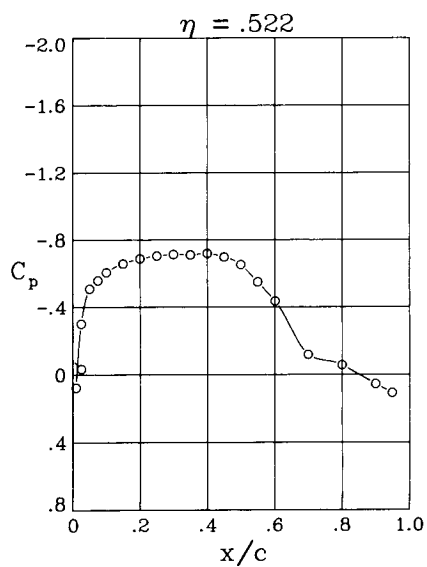
$\alpha = 3.94^\circ$

(a) Concluded.

Figure 21. Continued.



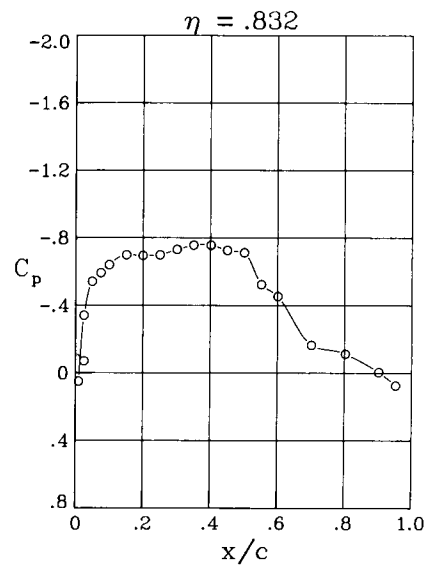
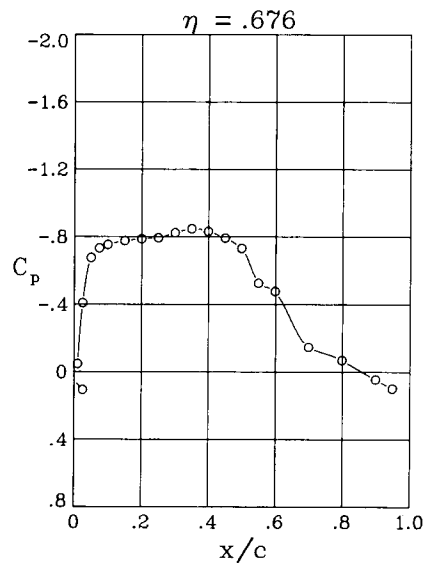
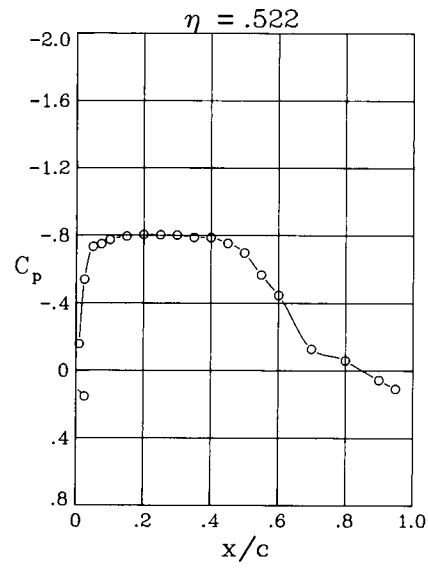
$\alpha = 0.06^\circ$



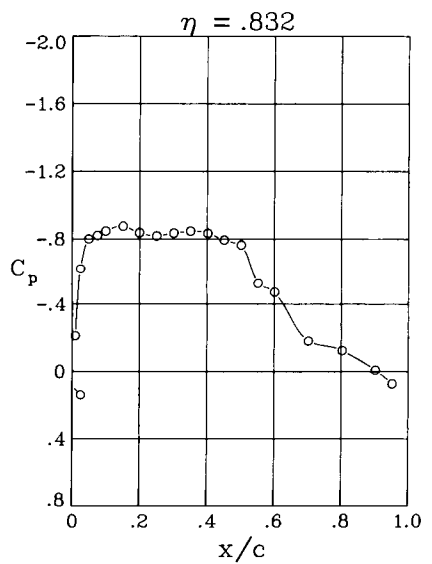
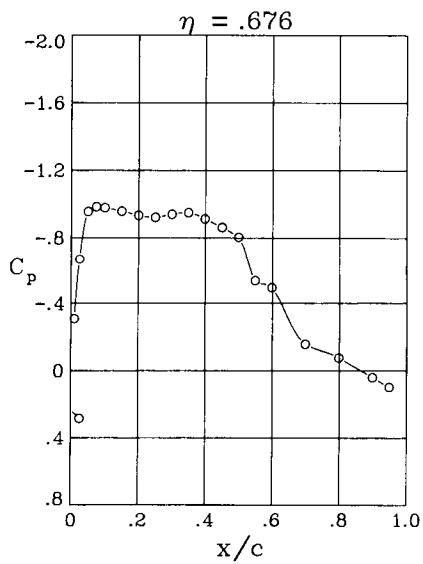
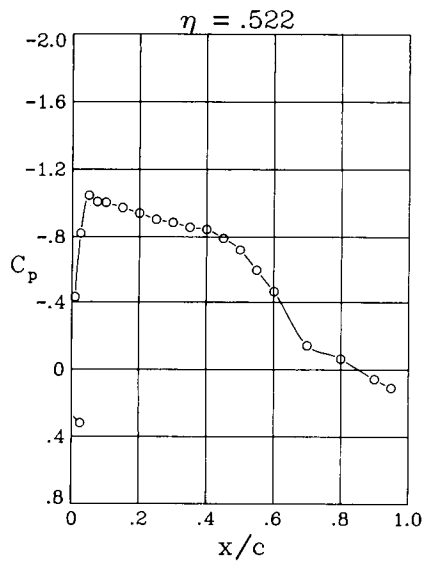
$\alpha = 1.06^\circ$

(b) $M = 0.70$.

Figure 21. Continued.



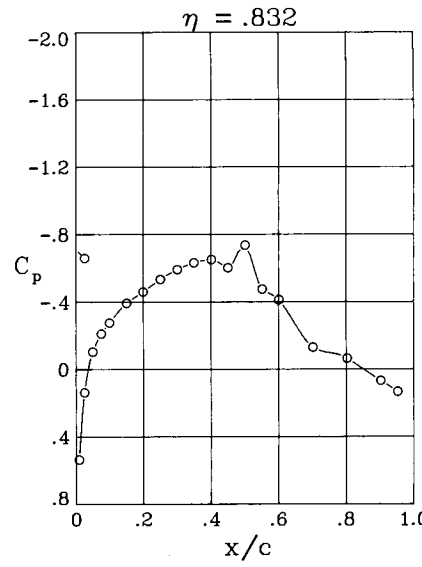
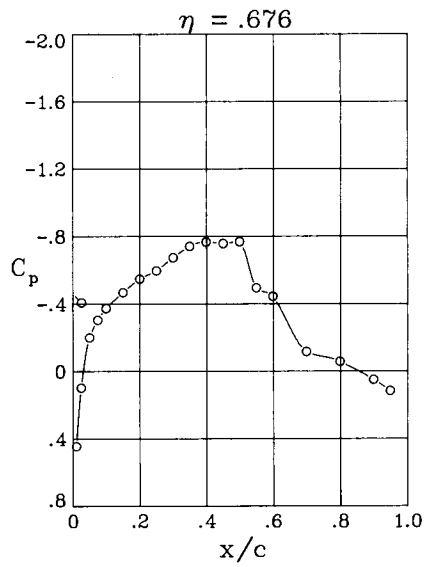
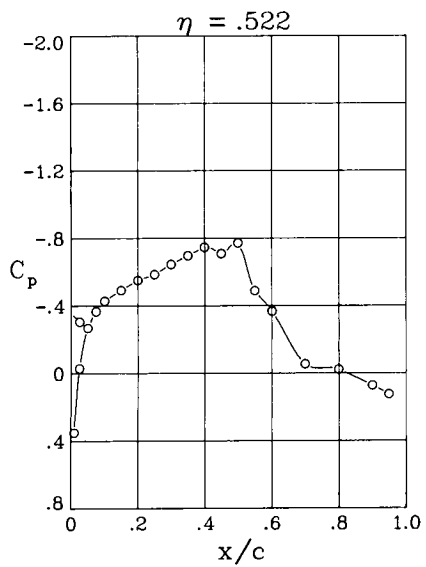
$\alpha = 2.00^\circ$



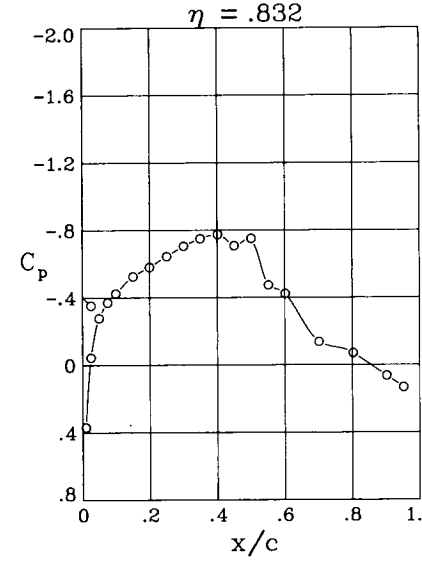
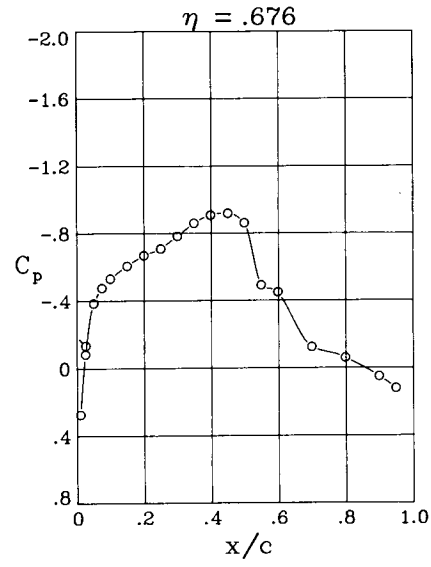
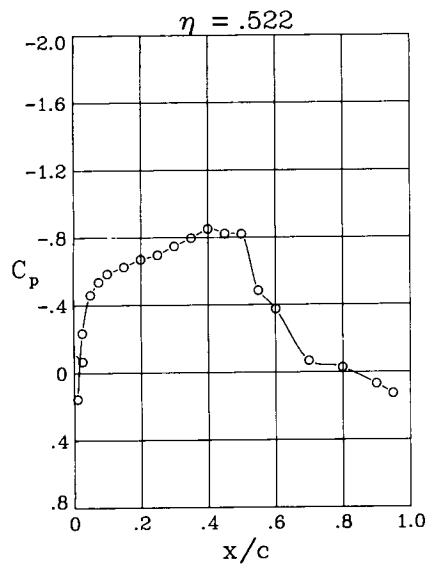
$\alpha = 2.95^\circ$

(b) Concluded.

Figure 21. Continued.



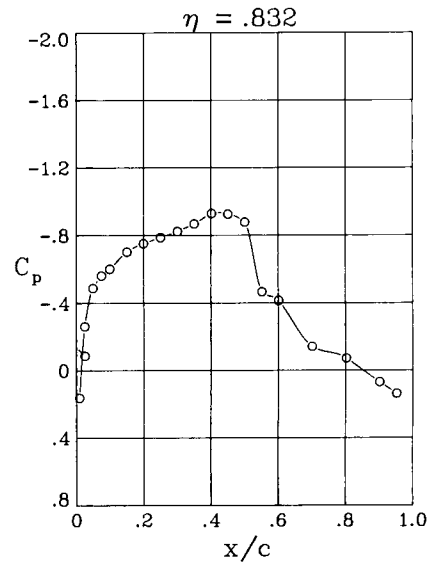
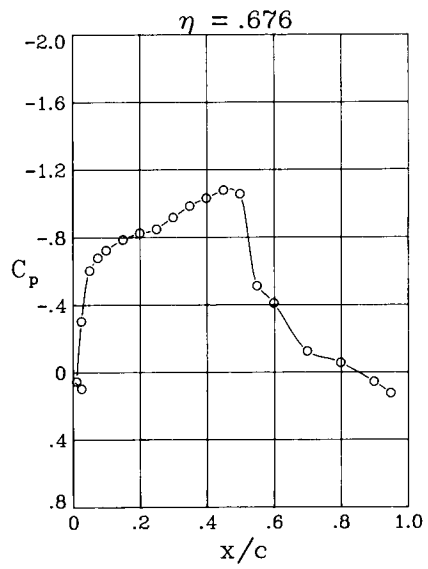
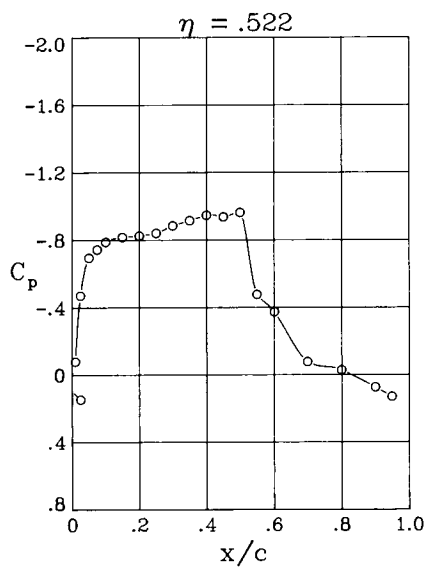
$\alpha = 0.50^\circ$



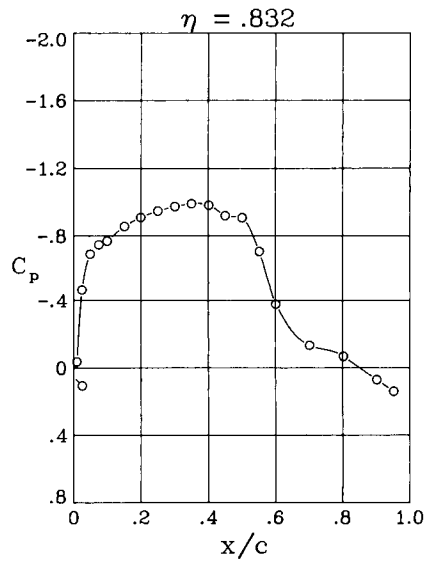
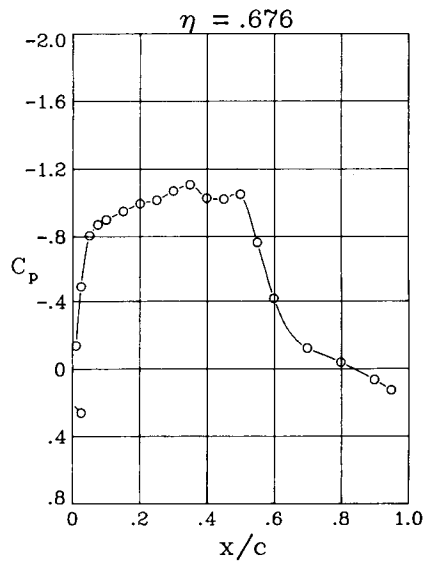
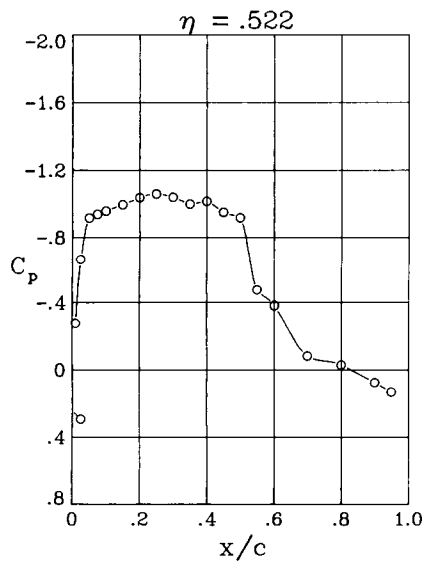
$\alpha = 0.99^\circ$

(c) $M = 0.75$.

Figure 21. Continued.



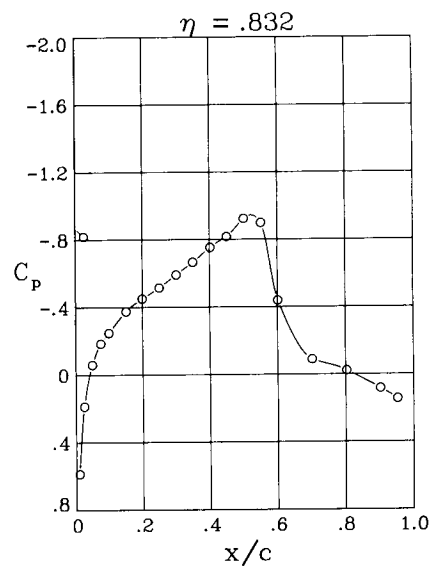
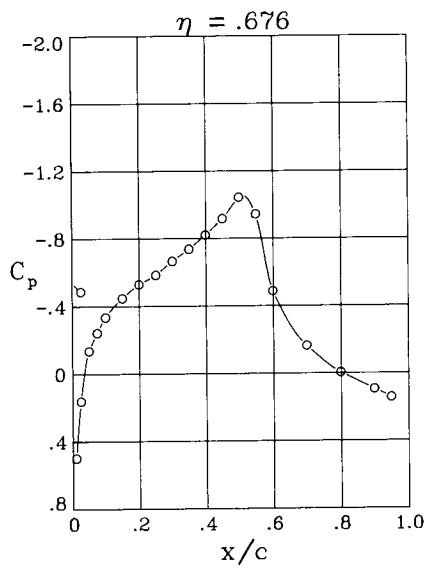
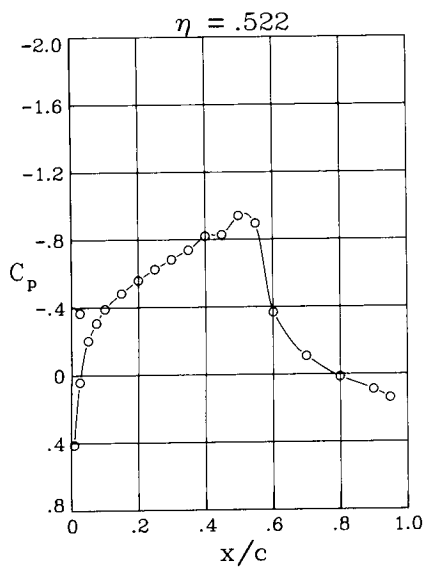
$\alpha = 2.00^\circ$



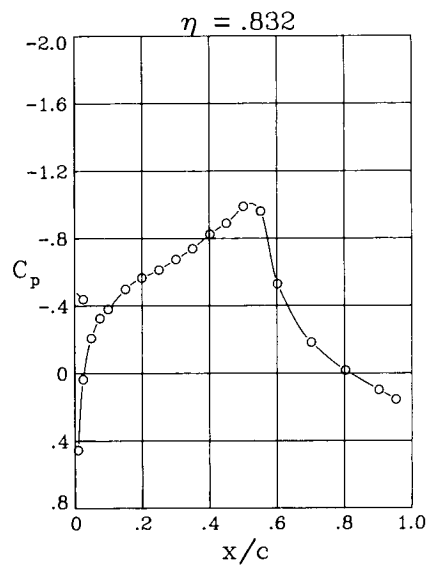
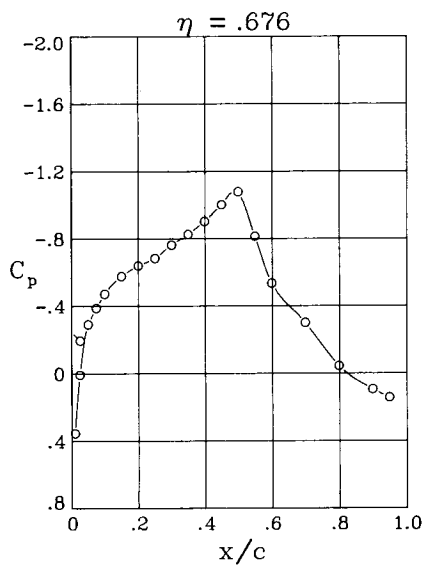
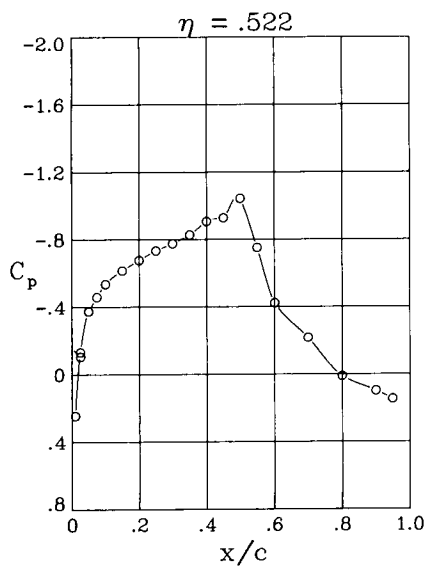
$\alpha = 2.93^\circ$

(c) Concluded.

Figure 21. Continued.



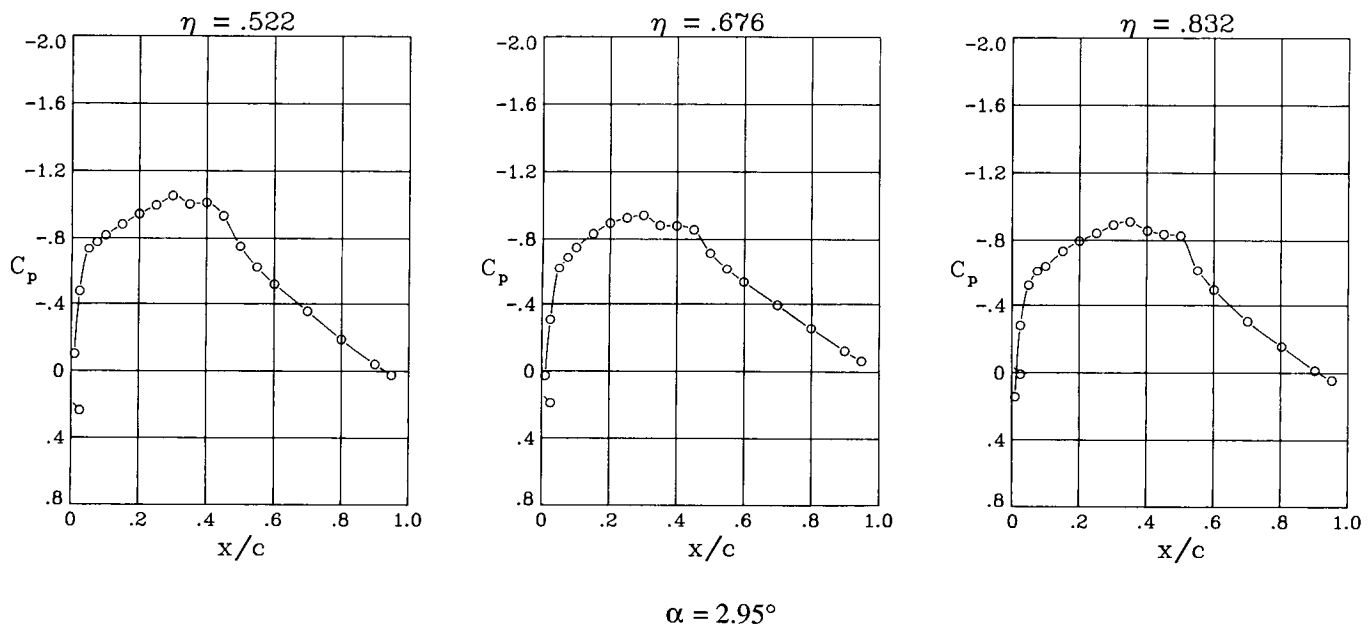
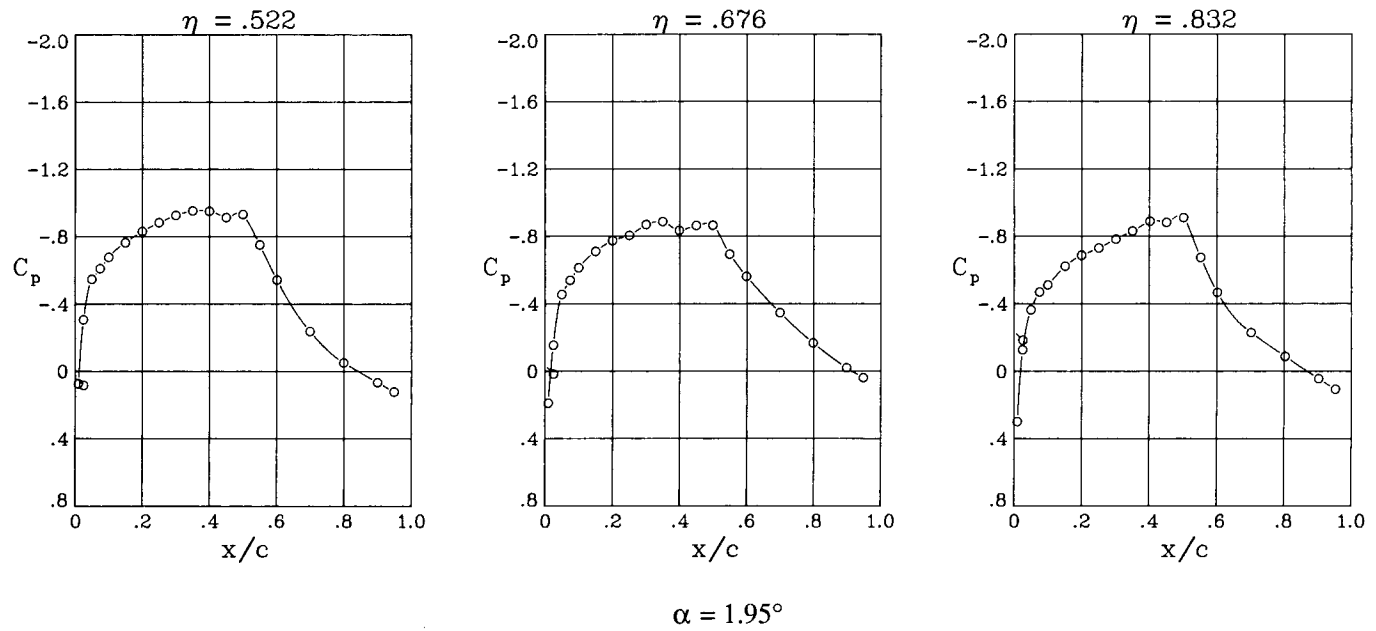
$\alpha = 0.03^\circ$



$\alpha = 0.98^\circ$

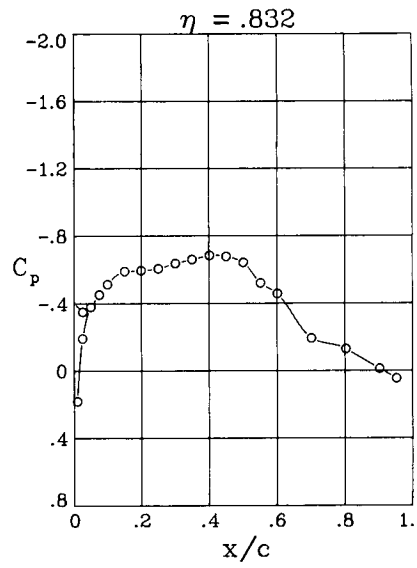
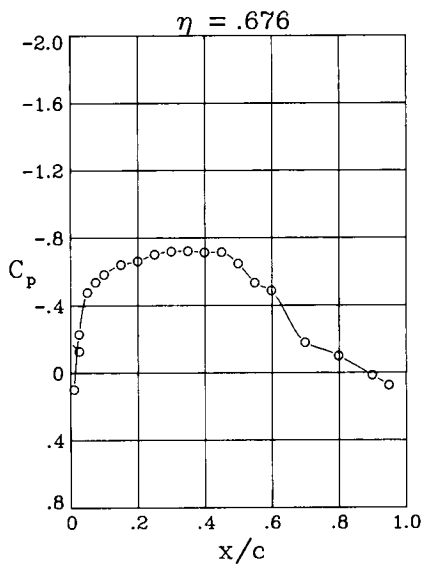
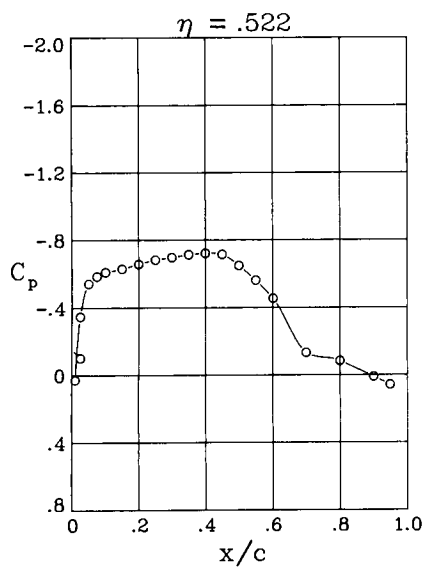
(d) $M = 0.80$.

Figure 21. Continued.

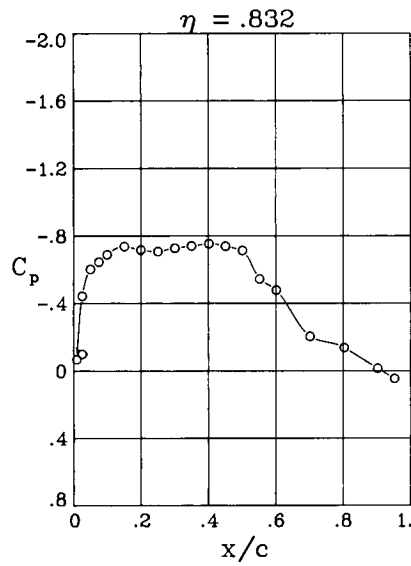
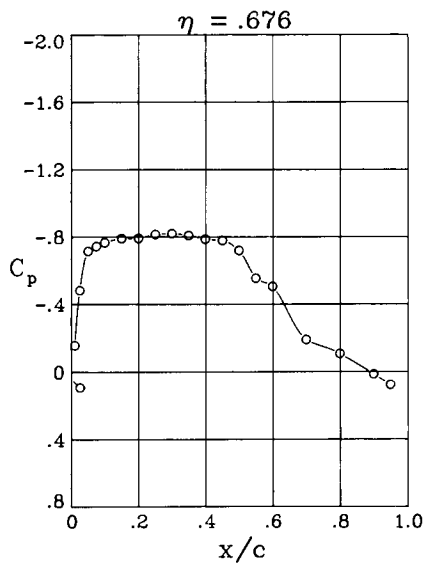
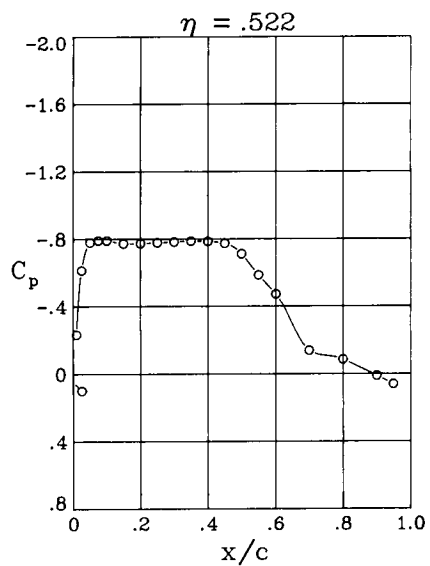


(d) Concluded.

Figure 21. Concluded.



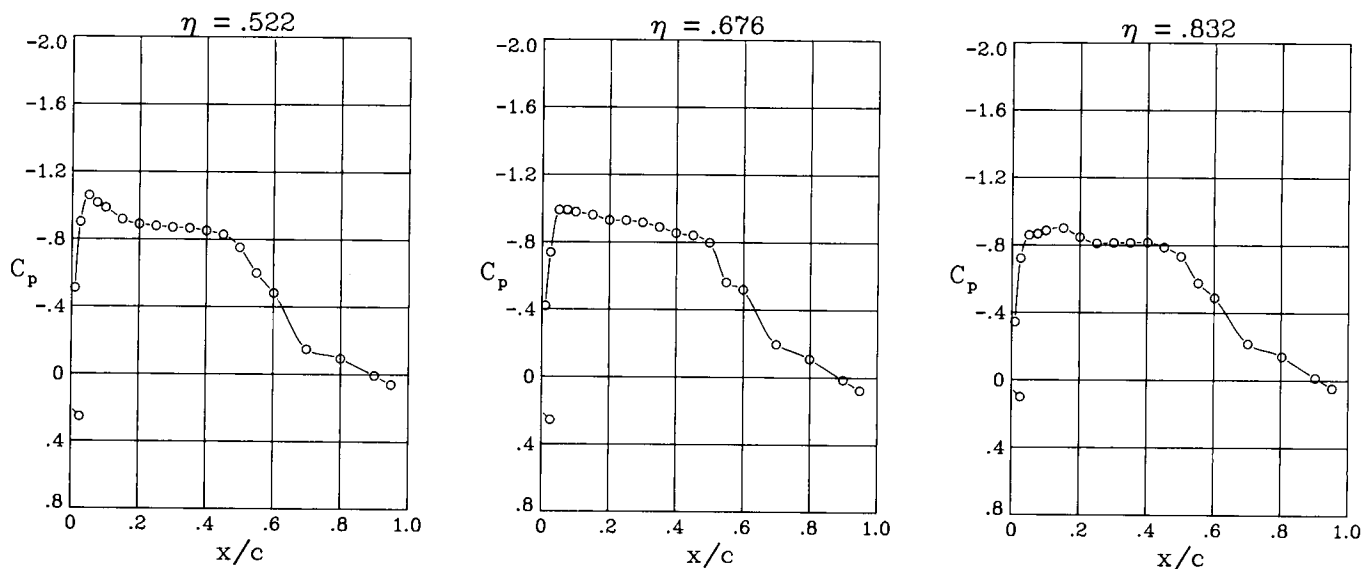
$\alpha = 0.94^\circ$



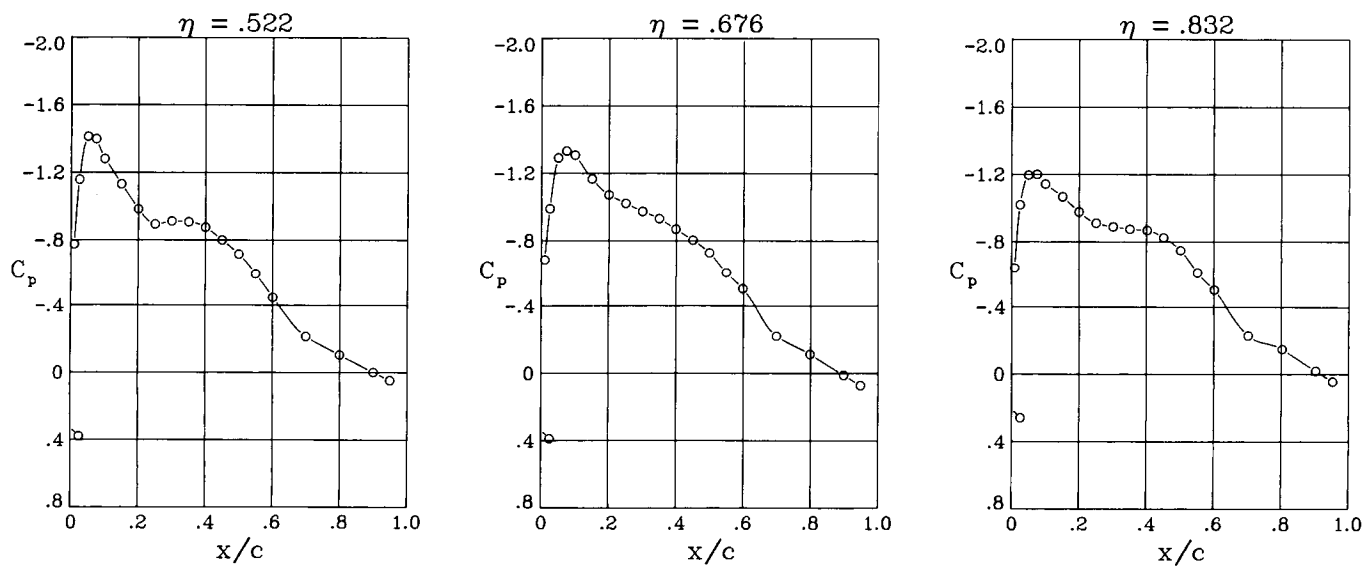
$\alpha = 1.91^\circ$

(a) $M = 0.70$.

Figure 22. Wing pressure distributions for wing B swept 25° .



$\alpha = 2.87^\circ$

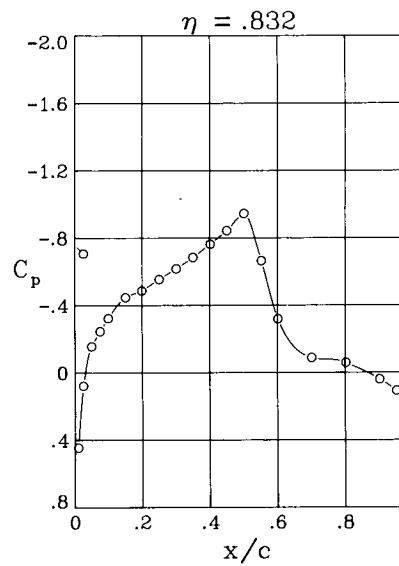
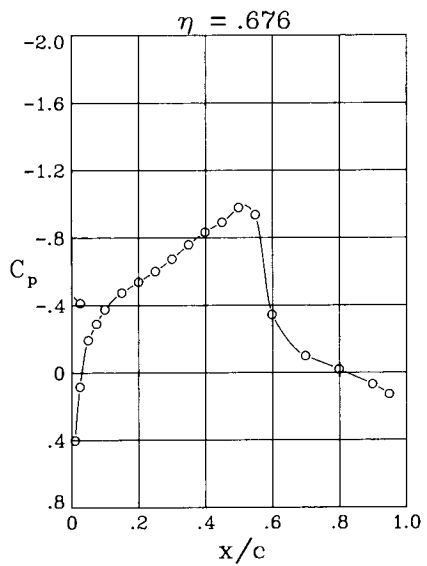
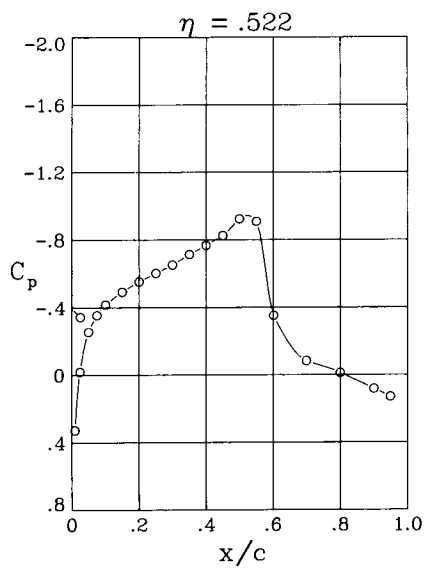


$\alpha = 3.87^\circ$

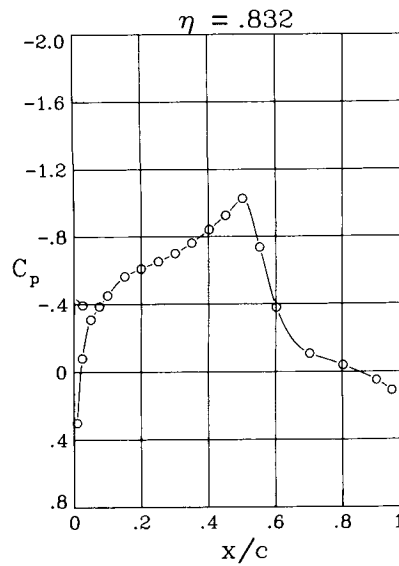
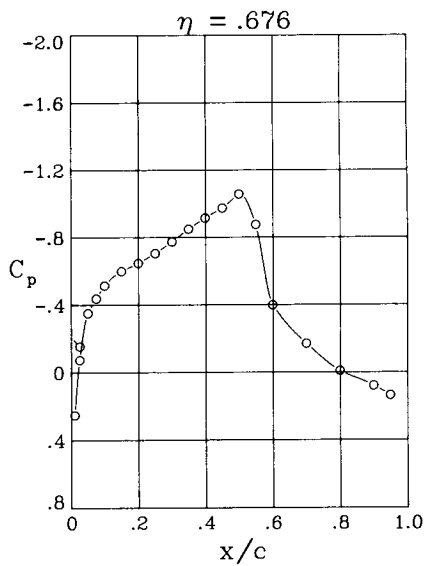
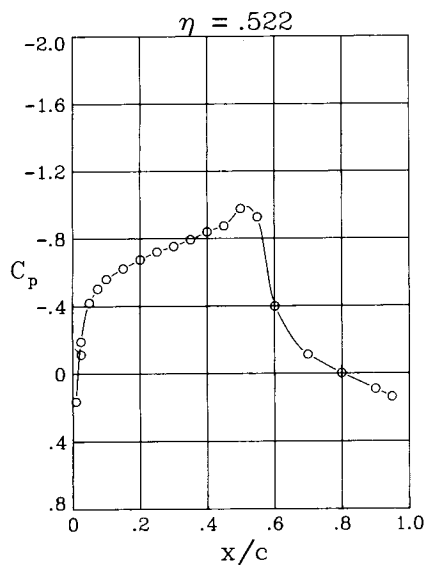
(a) Concluded.

Figure 22. Continued.

C-3



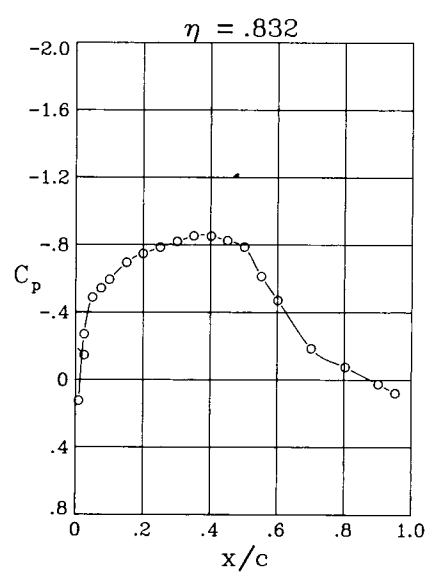
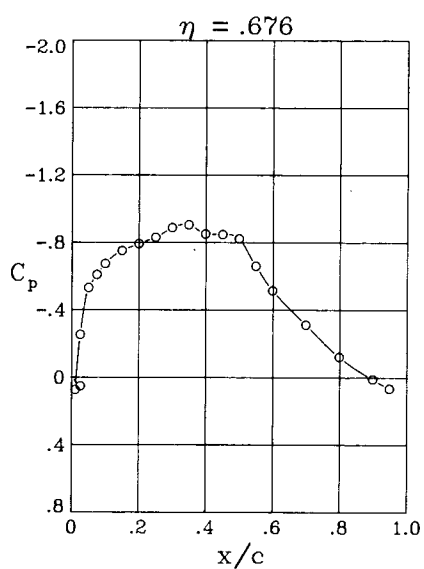
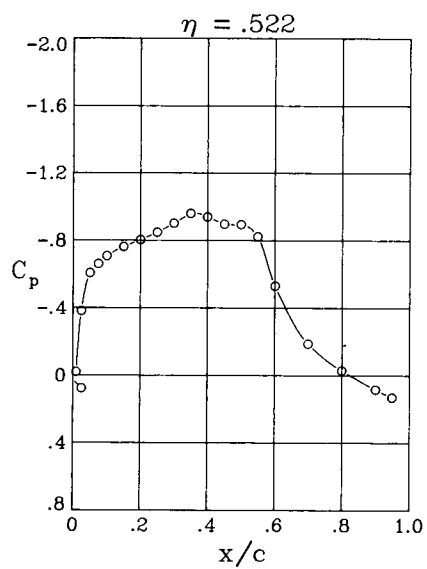
$\alpha = -0.01^\circ$



$\alpha = 0.89^\circ$

(b) $M = 0.80$.

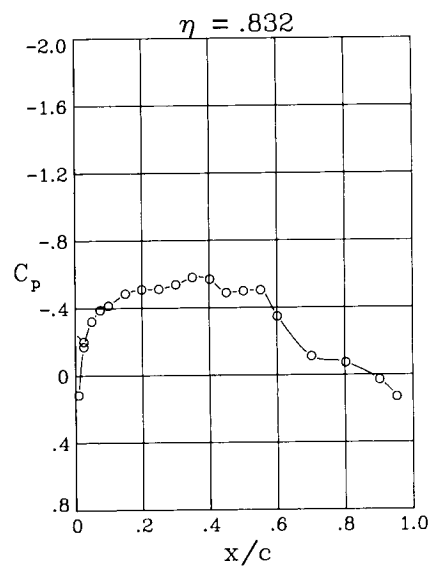
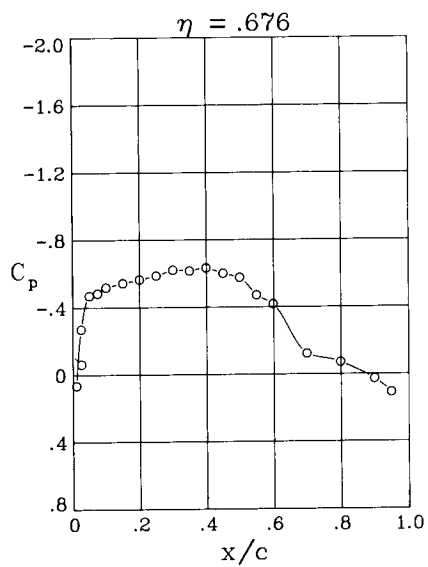
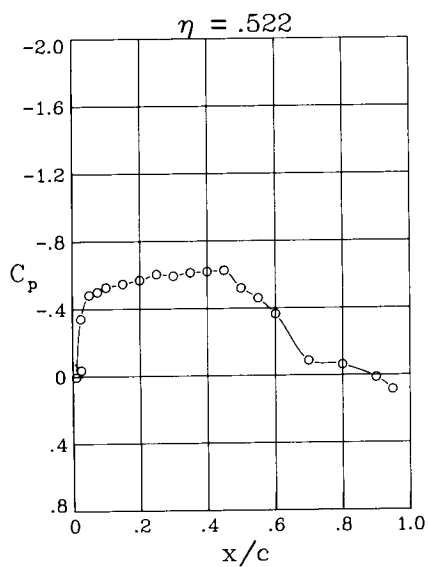
Figure 22. Continued.



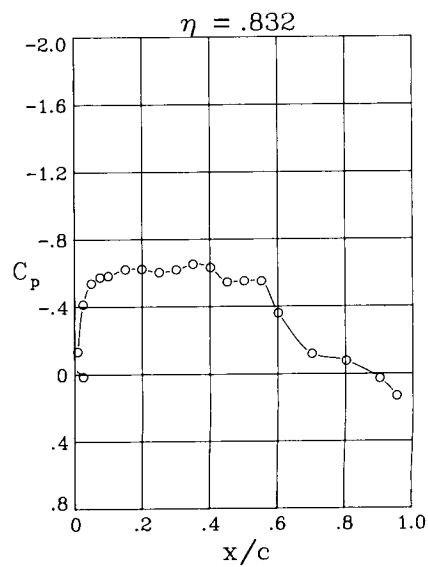
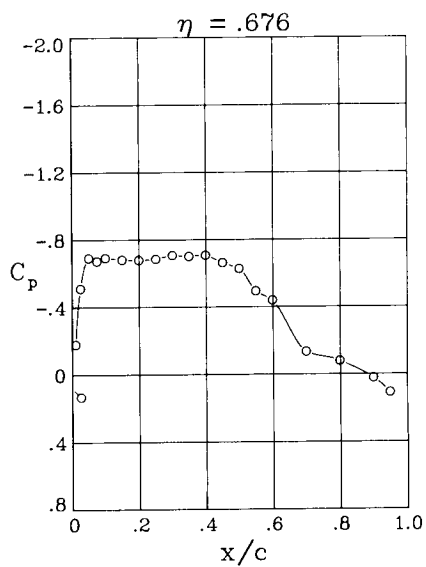
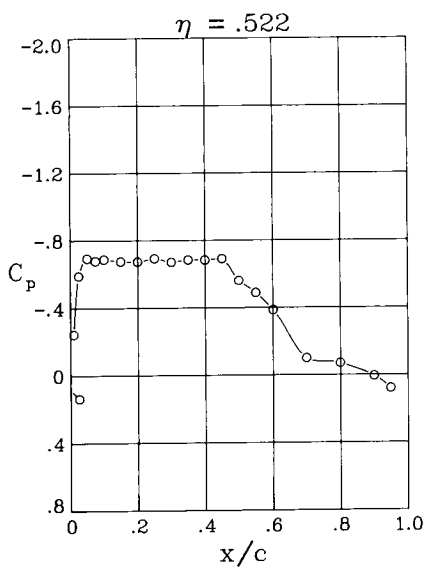
$\alpha = 1.90^\circ$

(b) Concluded.

Figure 22. Concluded.



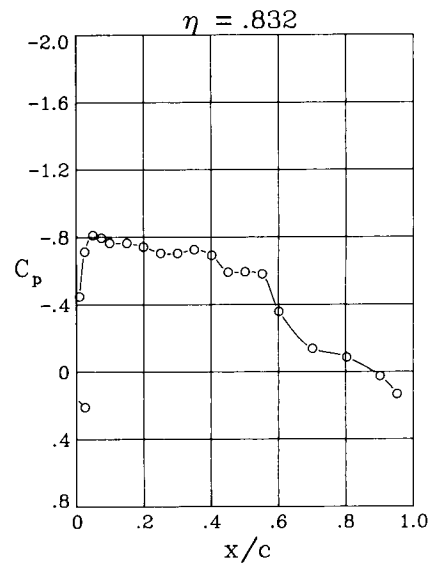
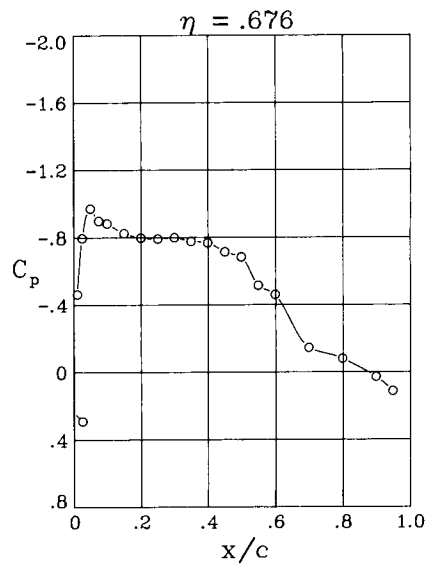
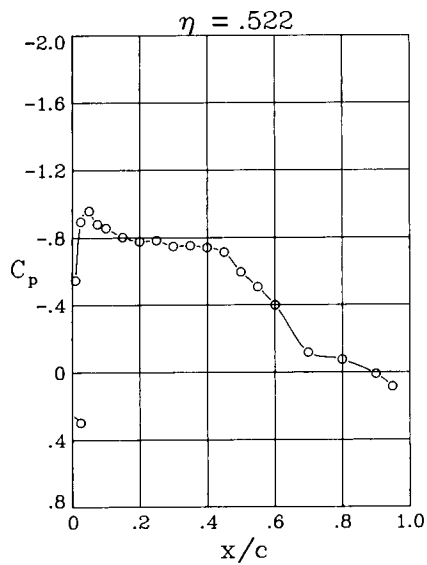
$\alpha = 0.98^\circ$



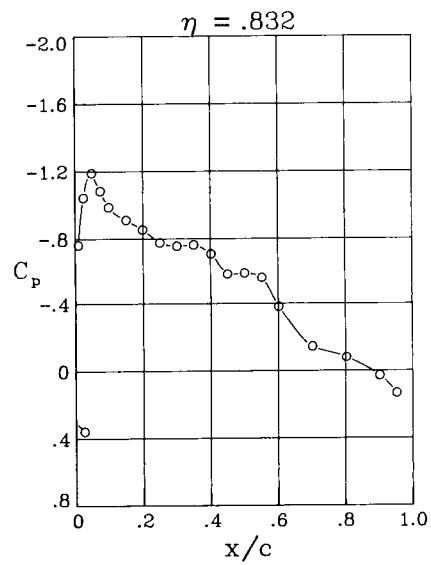
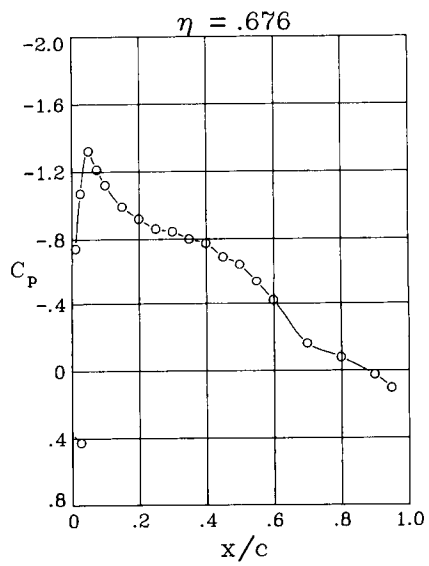
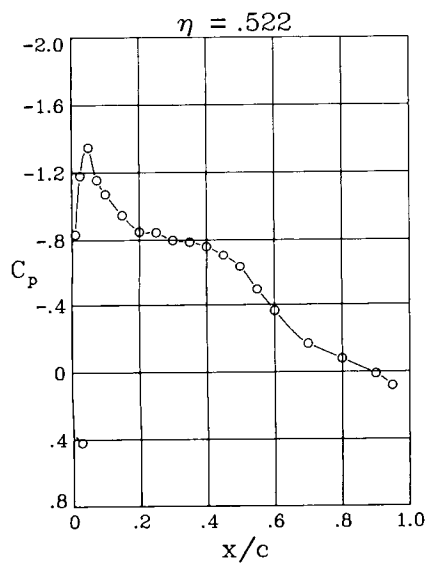
$\alpha = 1.93^\circ$

(a) $M = 0.70$.

Figure 23. Wing pressure distributions for wing B swept 30° .



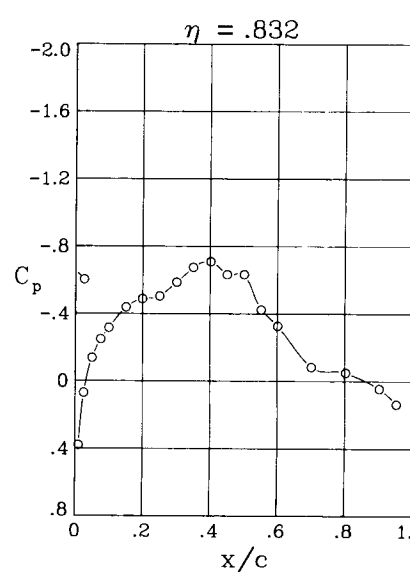
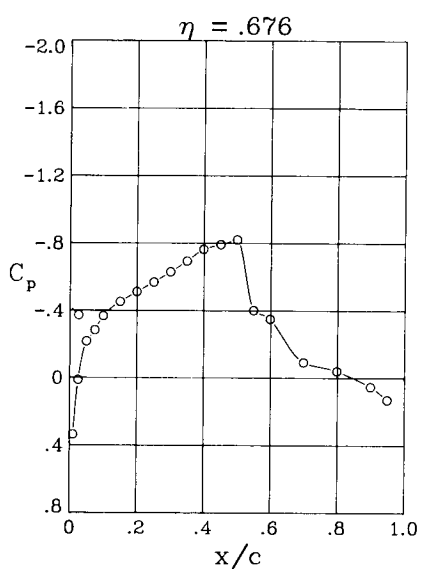
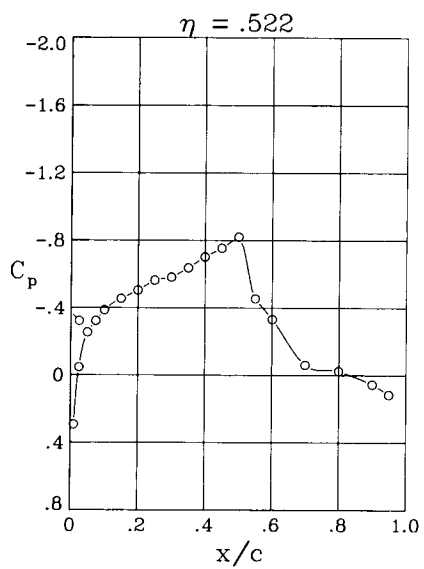
$\alpha = 2.92^\circ$



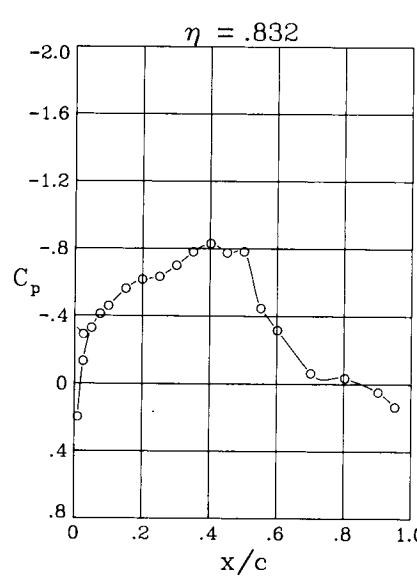
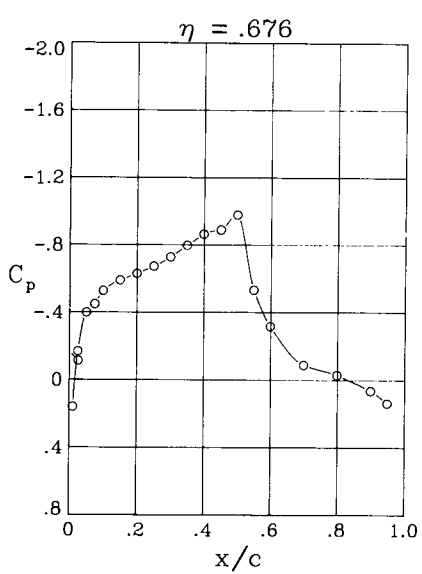
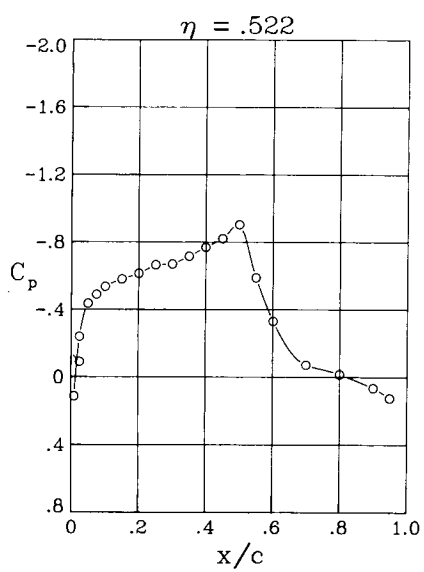
$\alpha = 3.93^\circ$

(a) Concluded.

Figure 23. Continued.



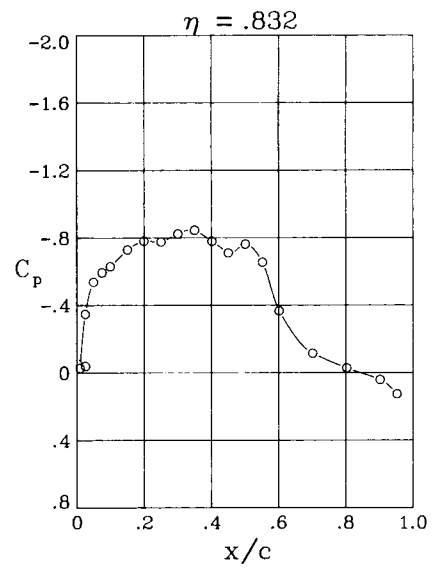
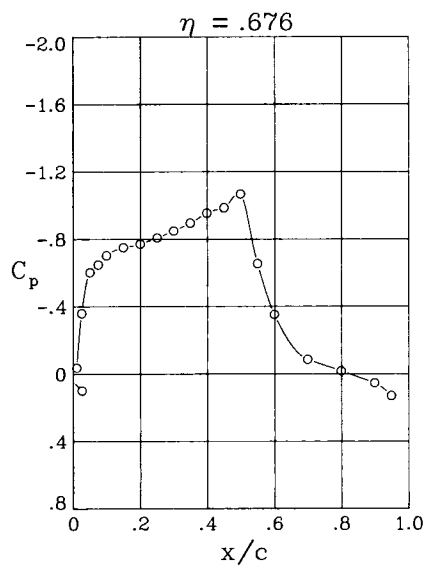
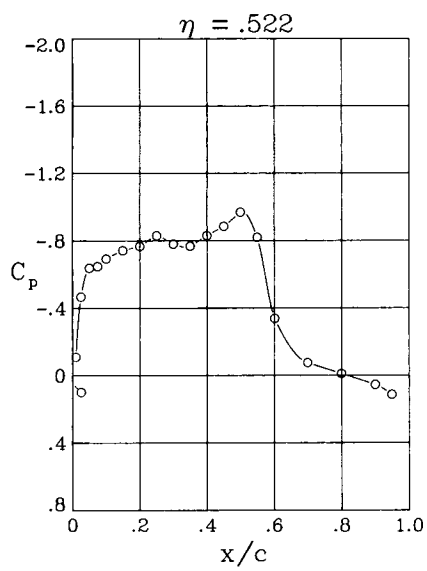
$\alpha = -0.05^\circ$



$\alpha = 0.94^\circ$

(b) $M = 0.80$.

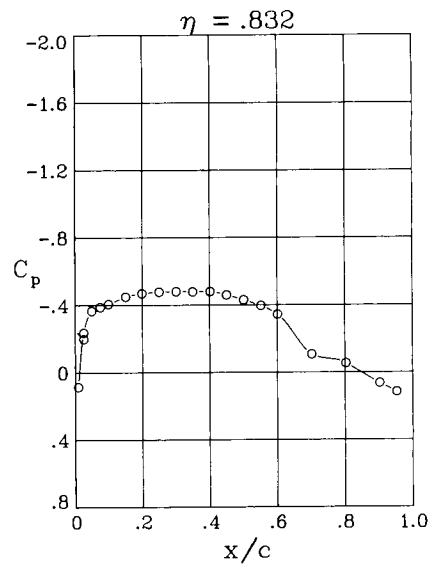
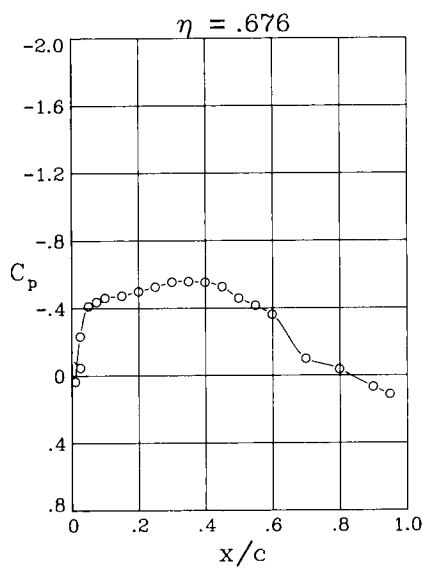
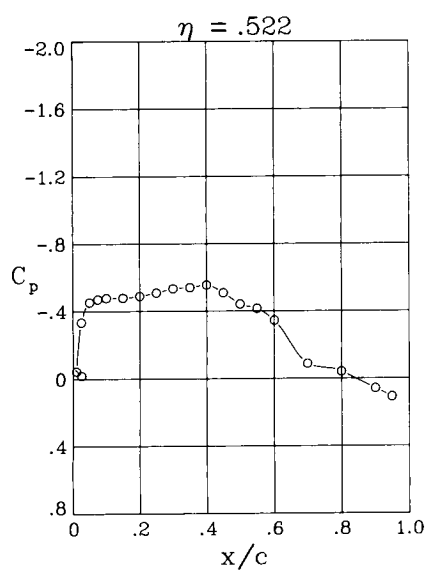
Figure 23. Continued.



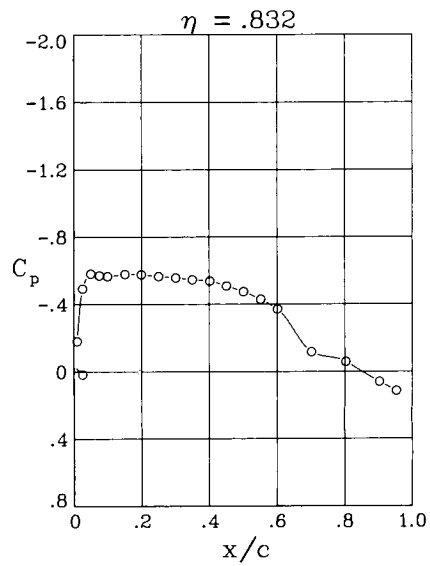
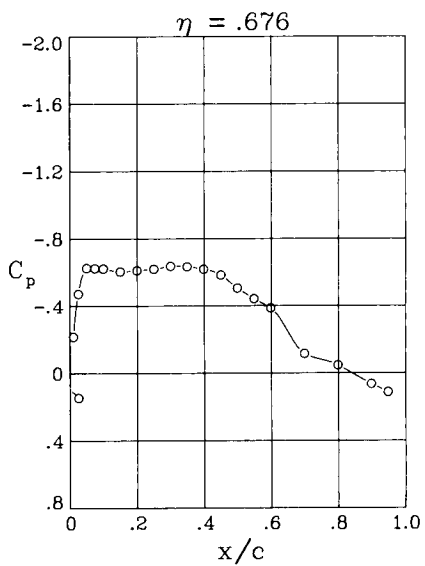
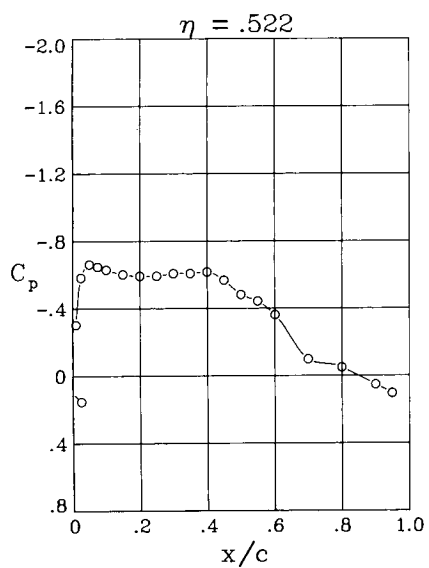
$\alpha = 1.92^\circ$

(b) Concluded.

Figure 23. Concluded.



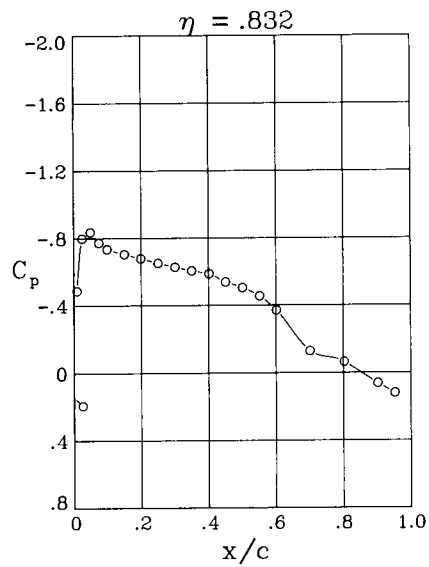
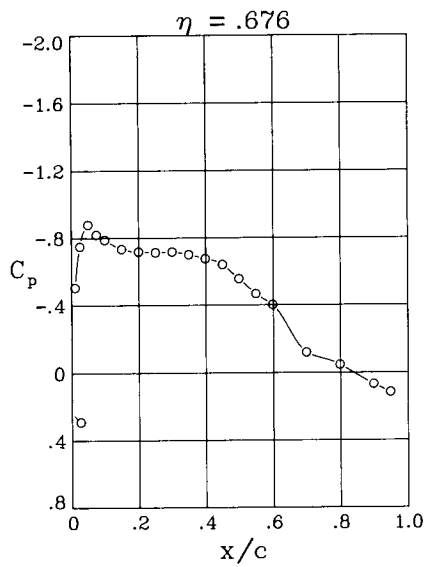
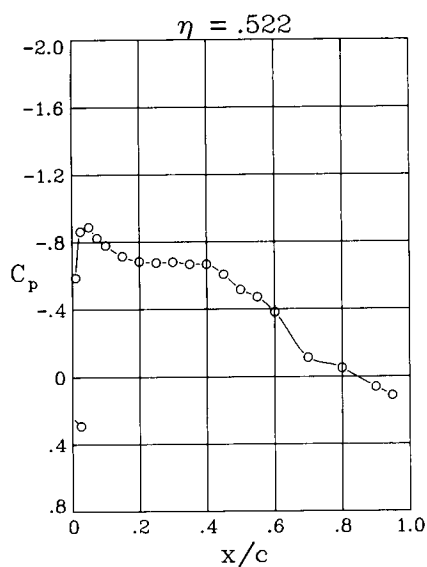
$\alpha = 0.92^\circ$



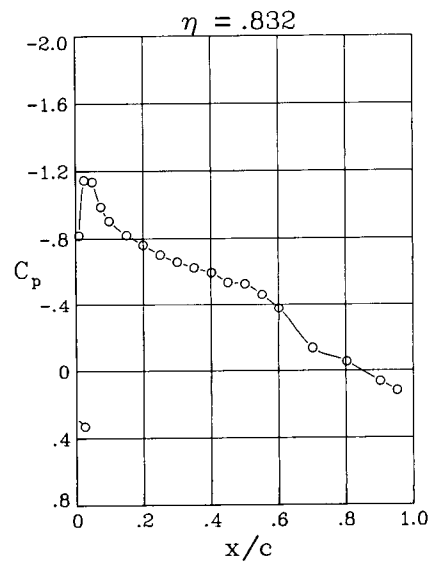
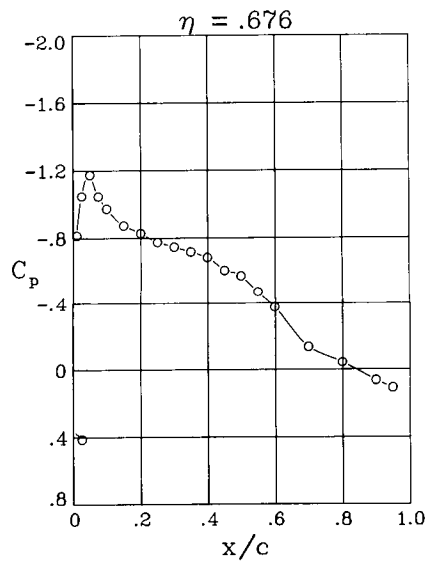
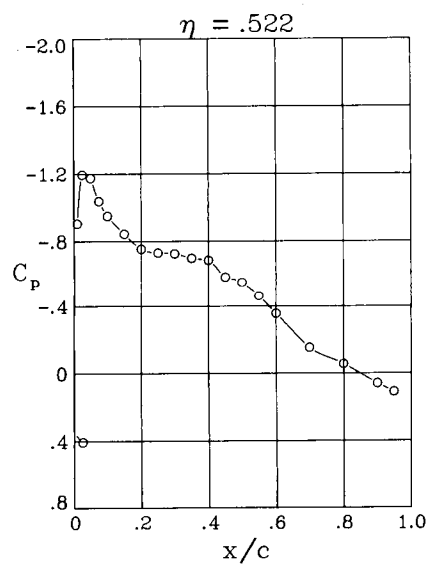
$\alpha = 1.91^\circ$

(a) $M = 0.70$.

Figure 24. Wing pressure distributions for wing B swept 35° .



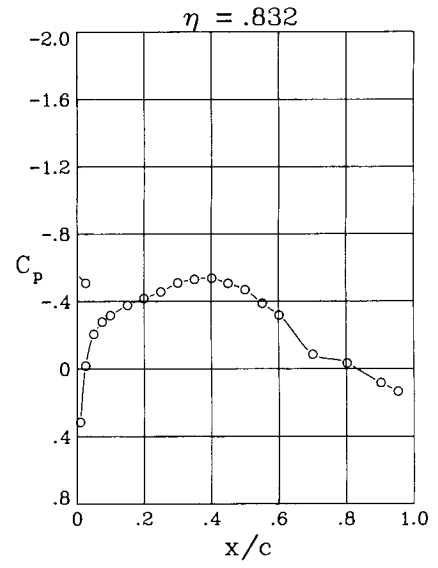
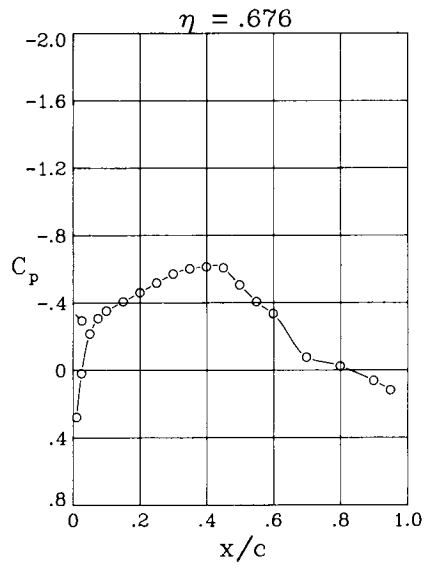
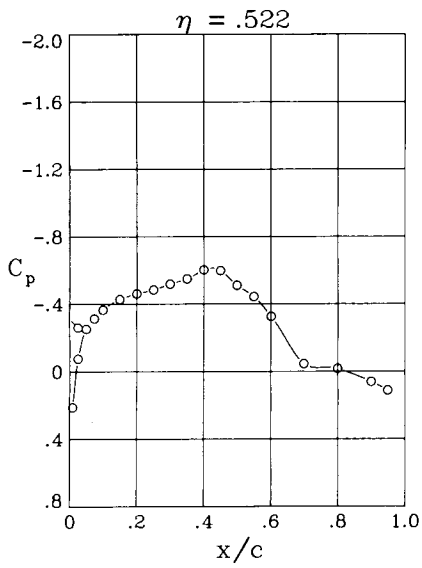
$\alpha = 2.90^\circ$



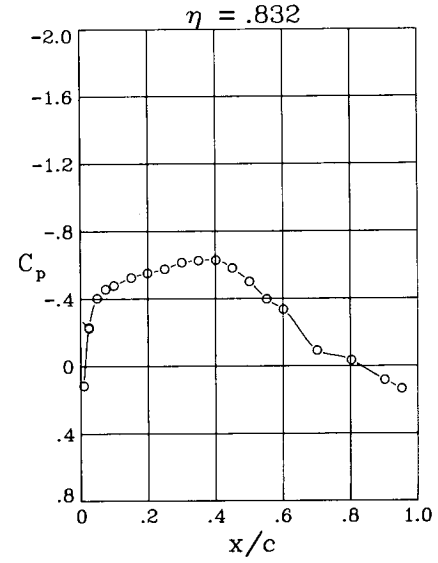
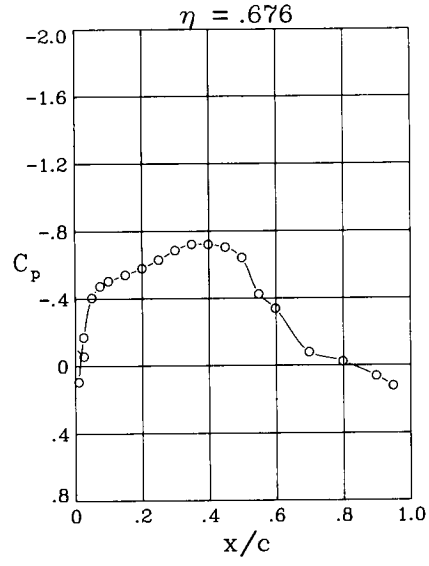
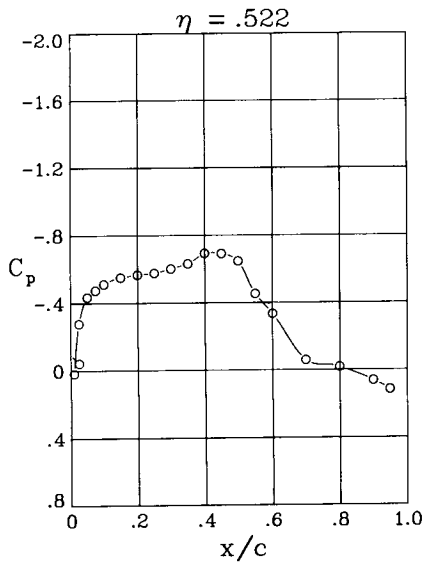
$\alpha = 3.88^\circ$

(a) Concluded.

Figure 24. Continued.



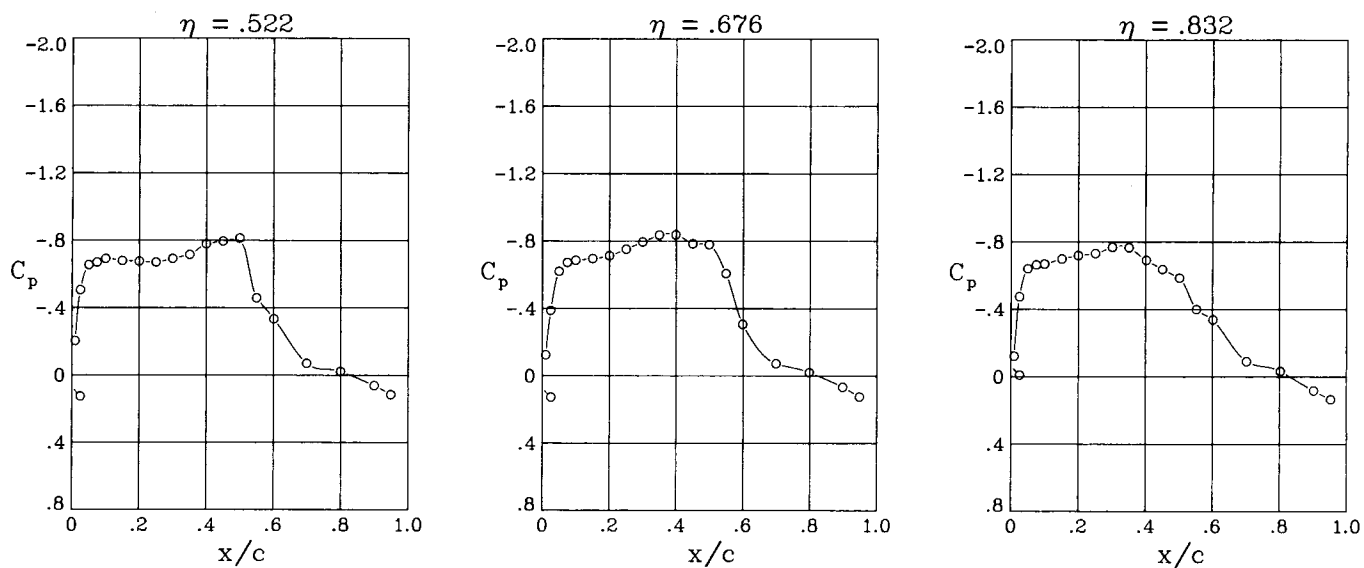
$\alpha = -0.03^\circ$



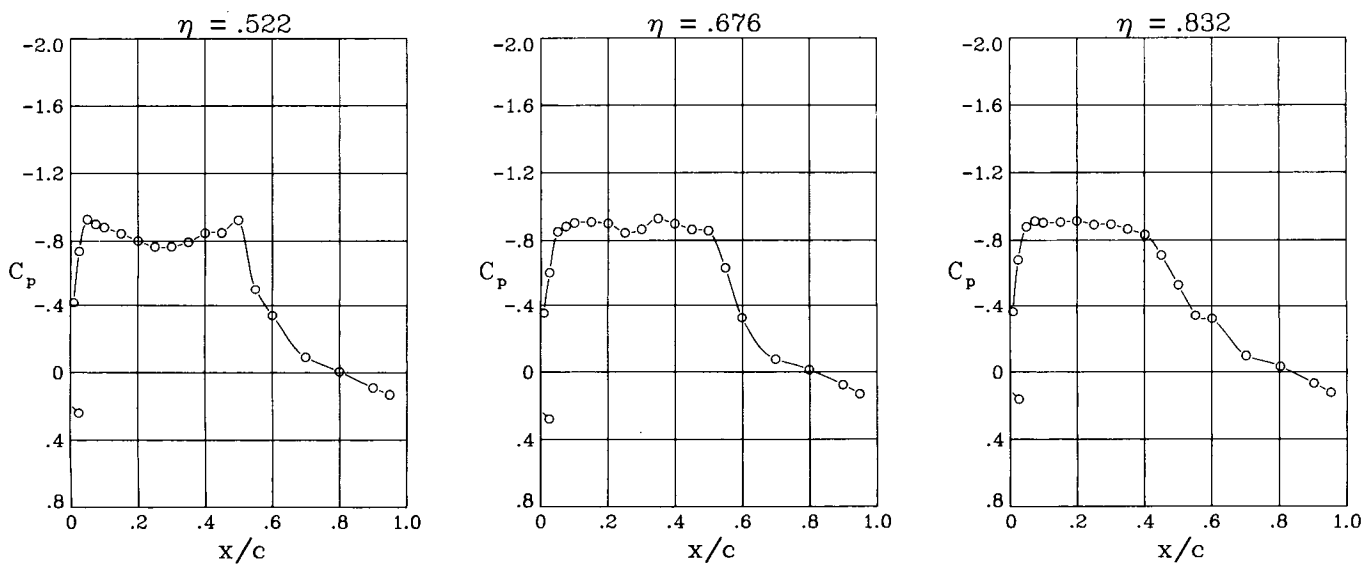
$\alpha = 0.96^\circ$

(b) $M = 0.80$.

Figure 24. Continued.



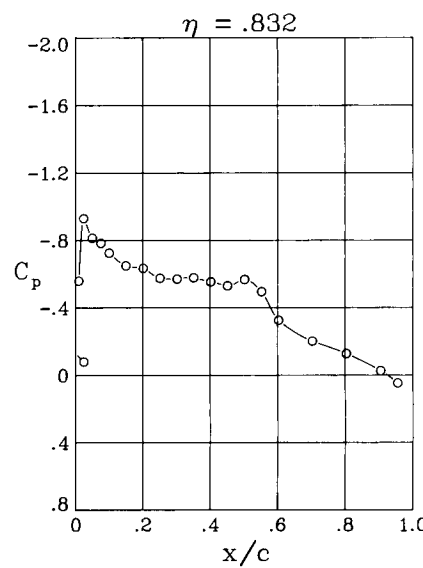
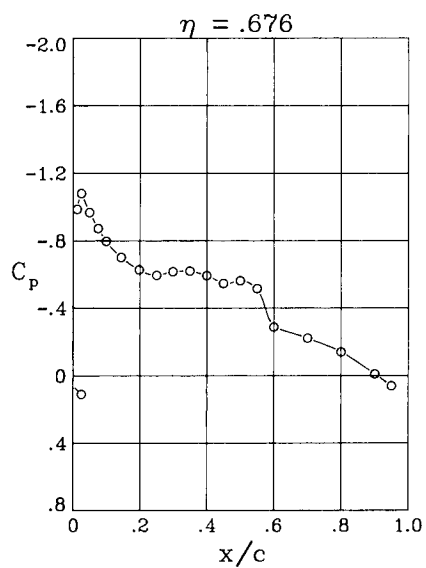
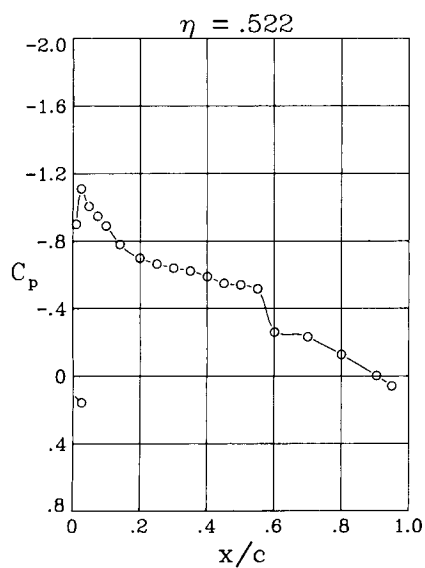
$\alpha = 1.93^\circ$



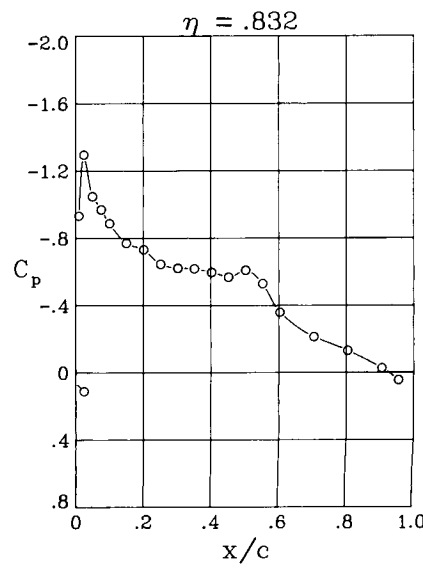
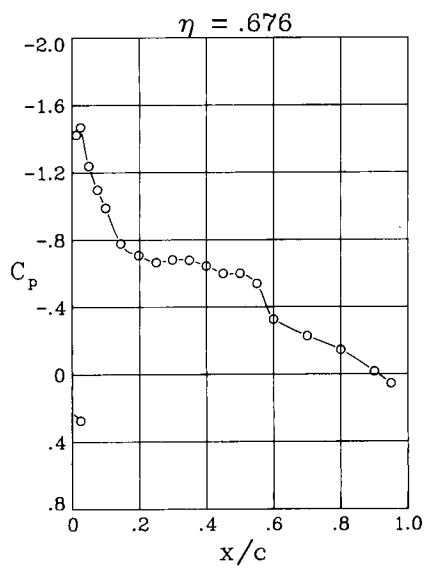
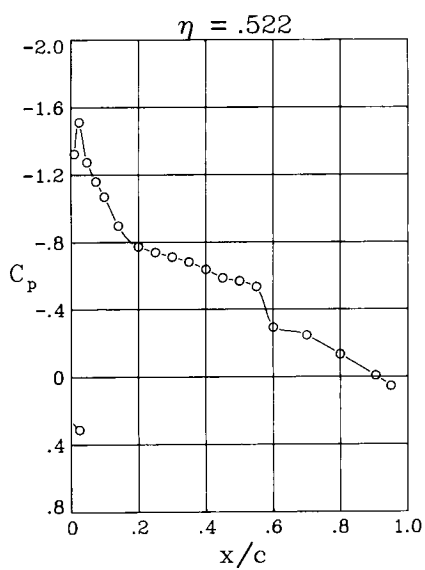
$\alpha = 2.90^\circ$

(b) Concluded.

Figure 24. Concluded.



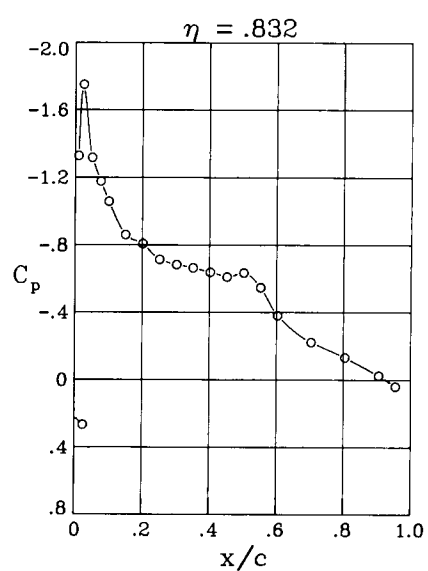
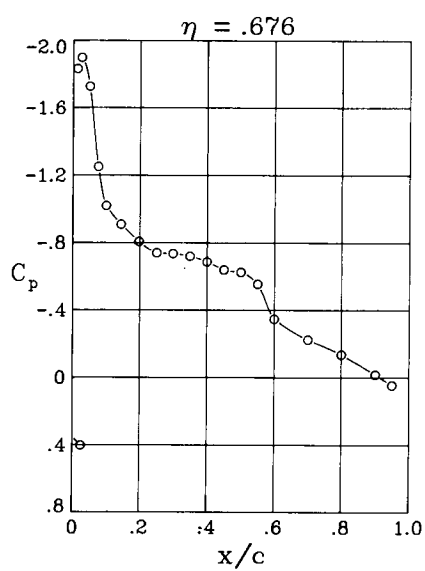
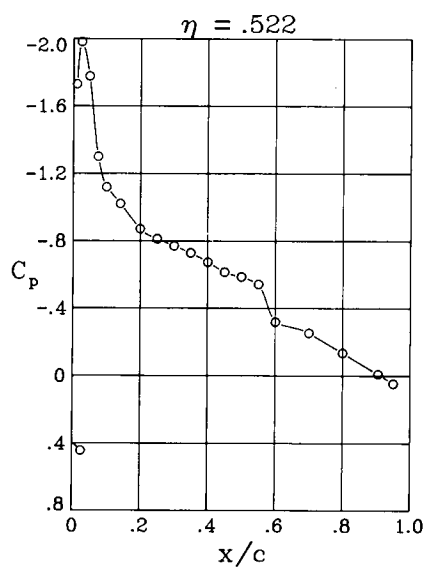
$\alpha = 1.98^\circ$



$\alpha = 2.95^\circ$

(a) $M = 0.60$.

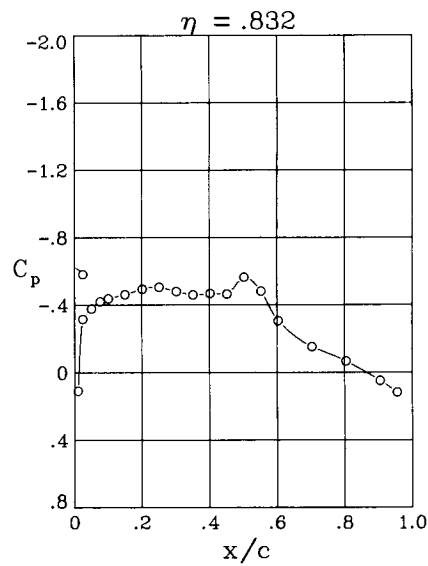
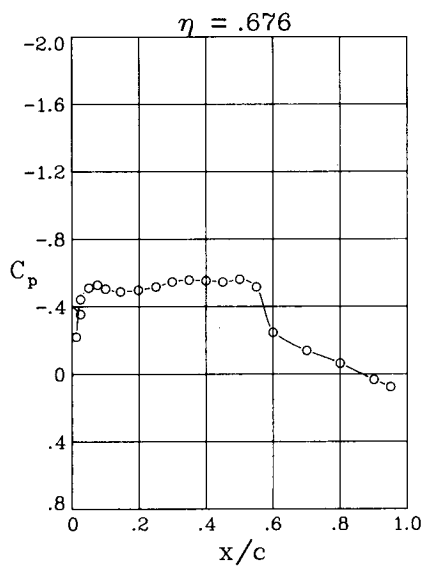
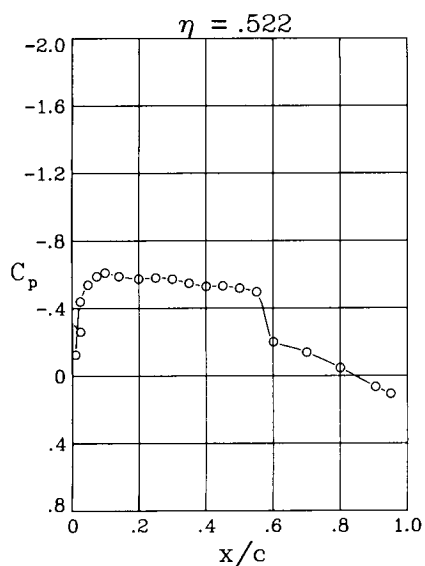
Figure 25. Wing pressure distributions for wing C swept 20° .



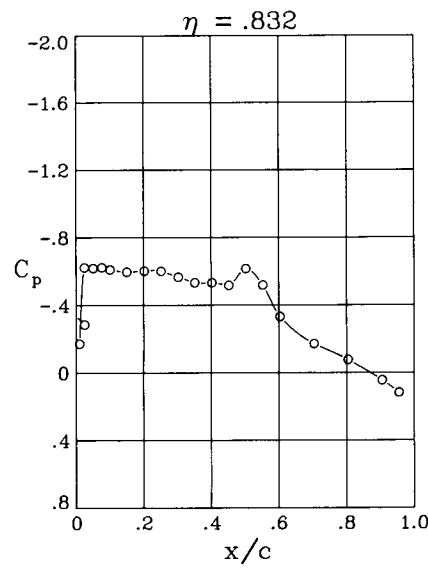
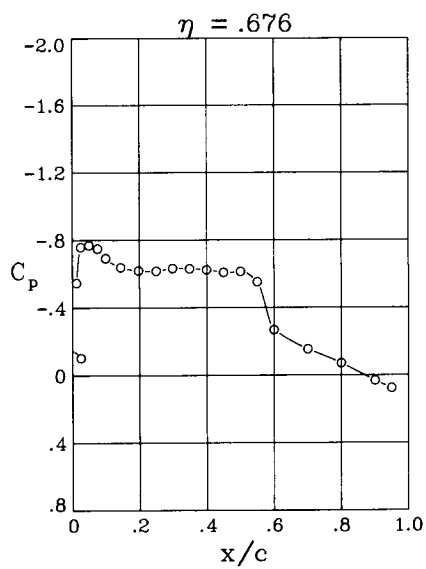
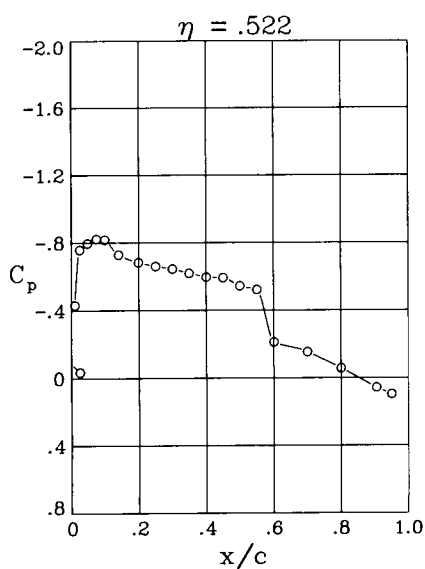
$$\alpha = 3.94^\circ$$

(a) Concluded.

Figure 25. Continued.



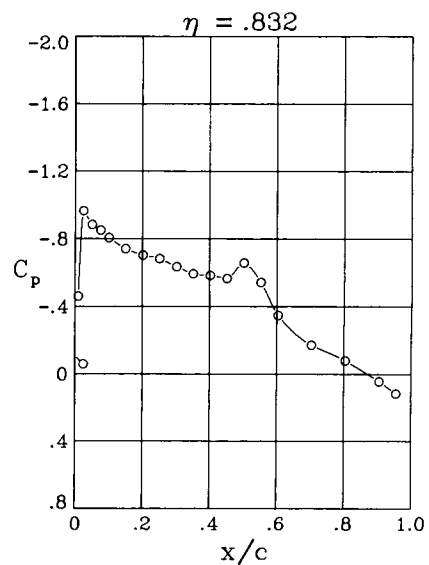
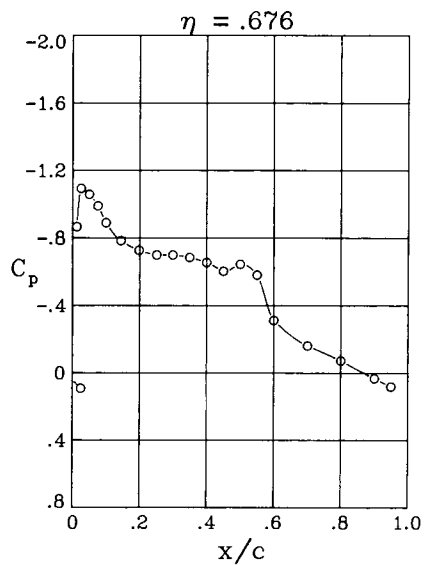
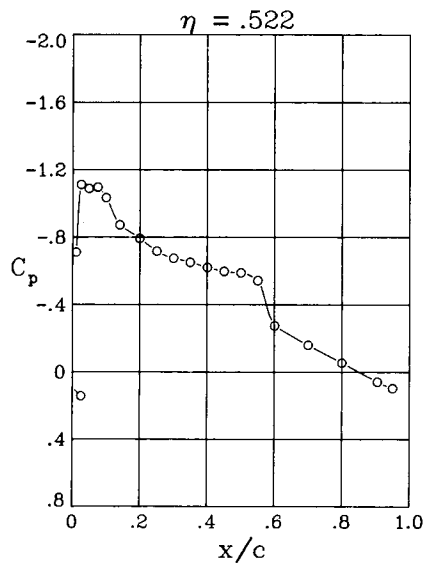
$\alpha = 0.06^\circ$



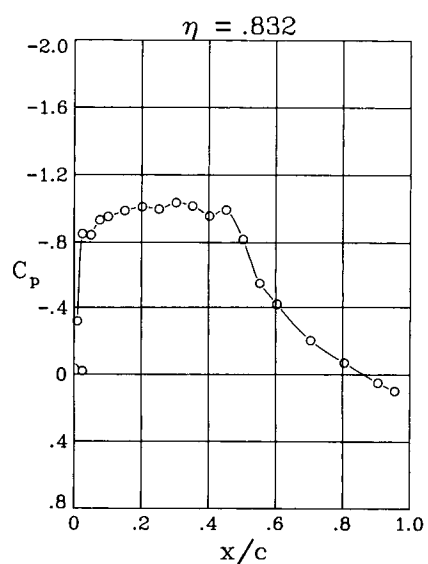
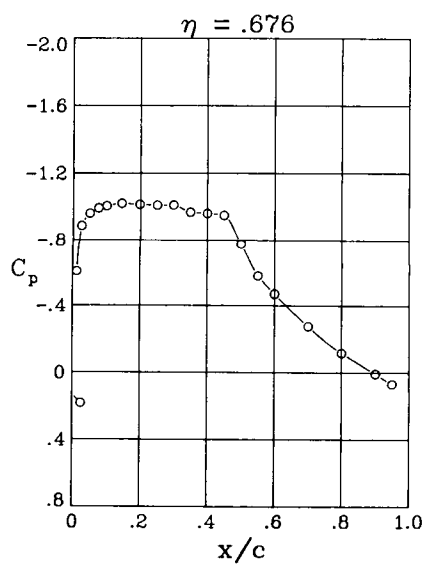
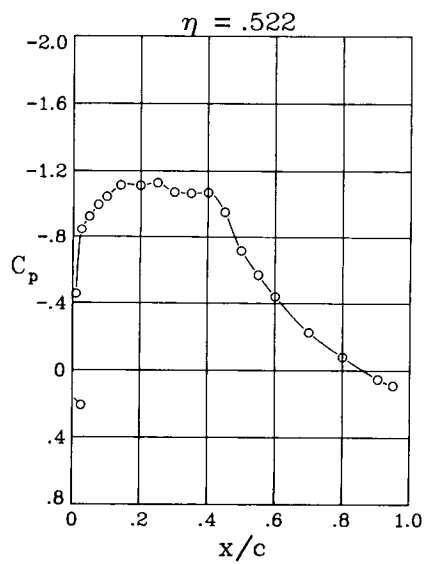
$\alpha = 1.06^\circ$

(b) $M = 0.70$.

Figure 25. Continued.



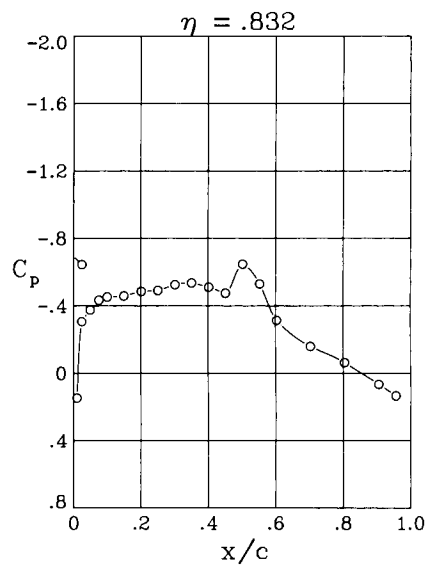
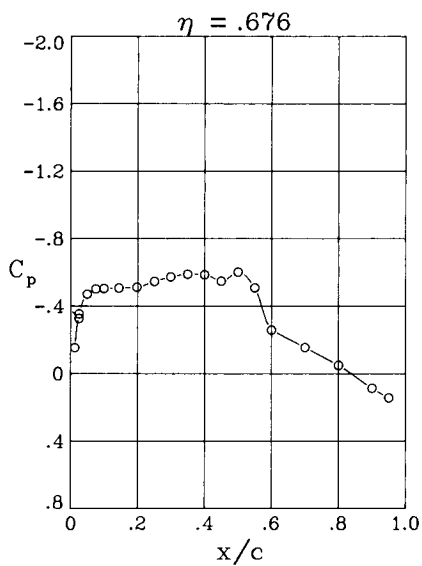
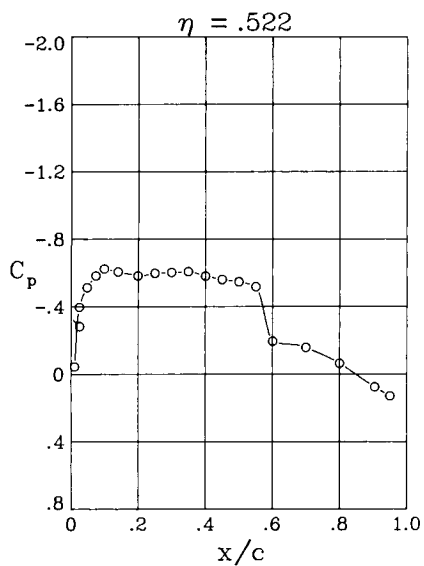
$\alpha = 2.00^\circ$



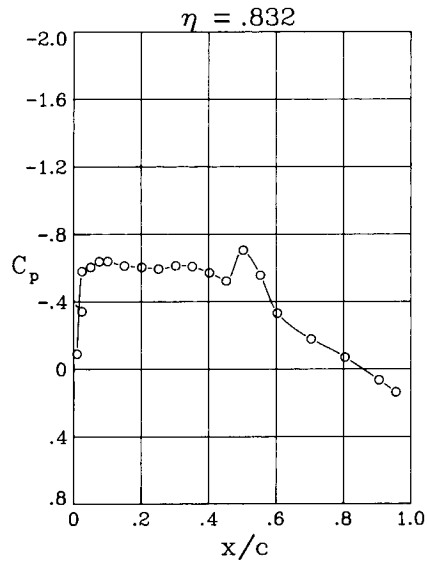
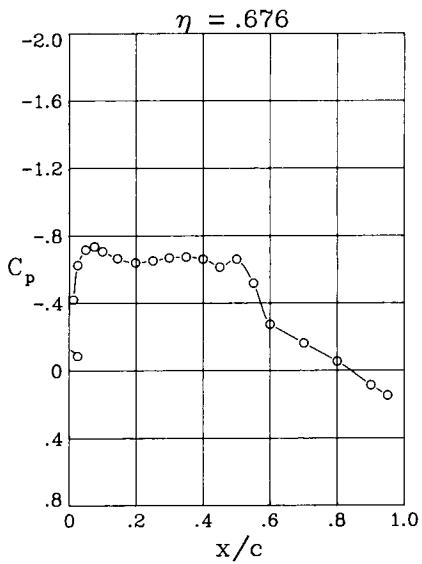
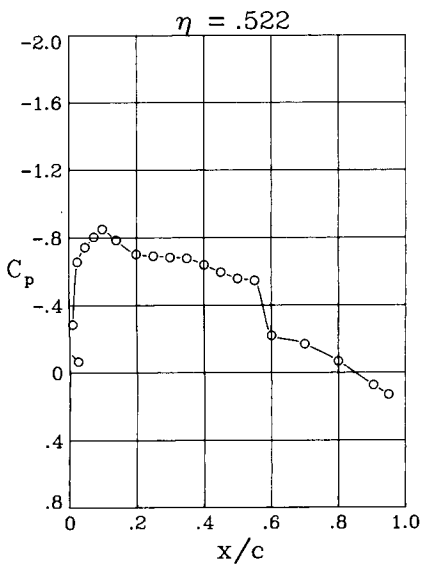
$\alpha = 2.95^\circ$

(b) Concluded.

Figure 25. Continued.



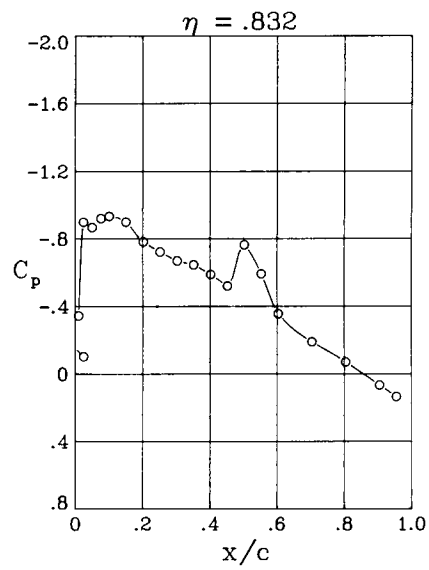
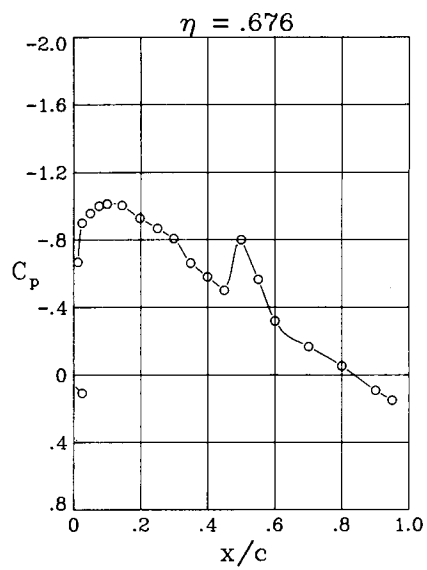
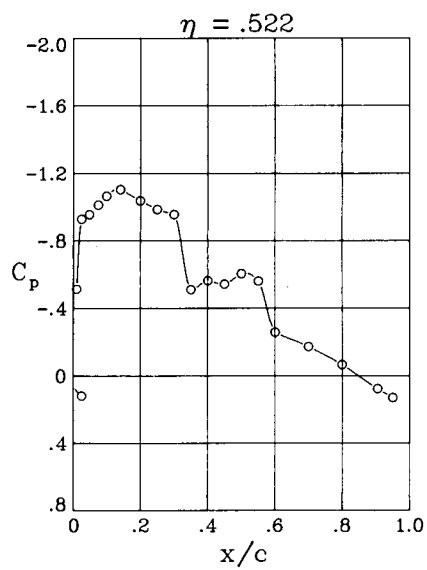
$\alpha = 0.50^\circ$



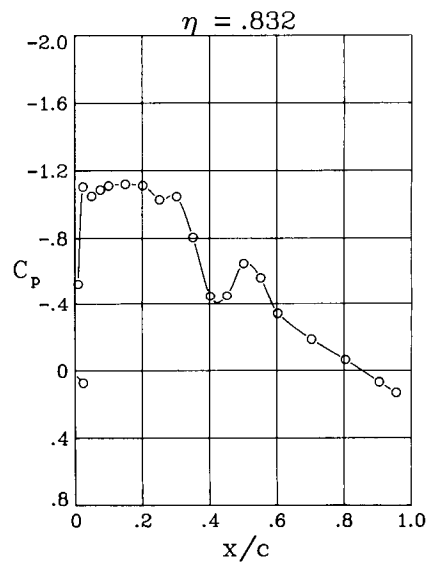
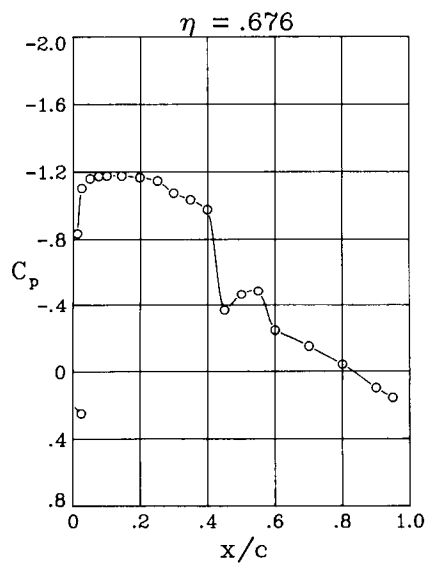
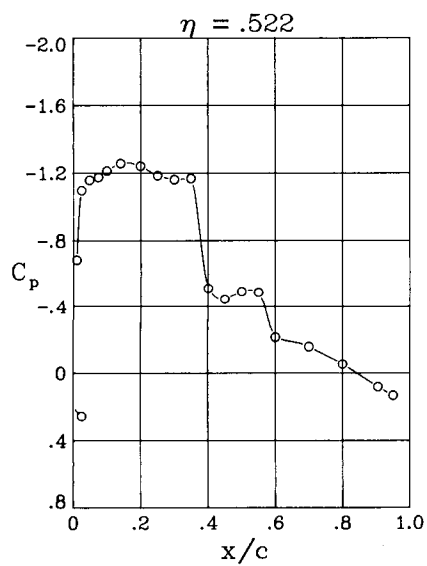
$\alpha = 0.99^\circ$

(c) $M = 0.75$.

Figure 25. Continued.



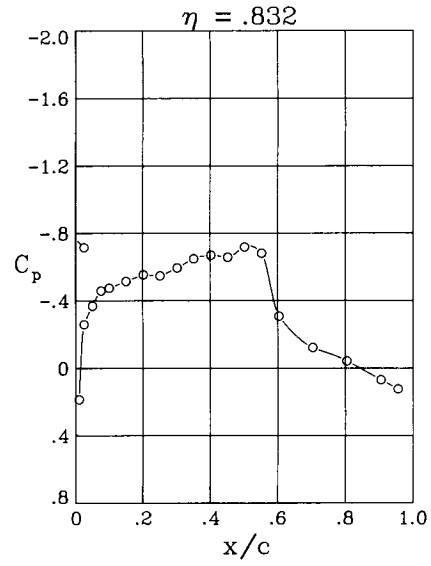
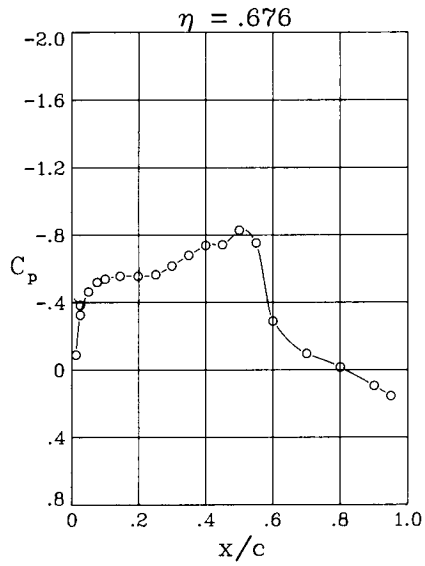
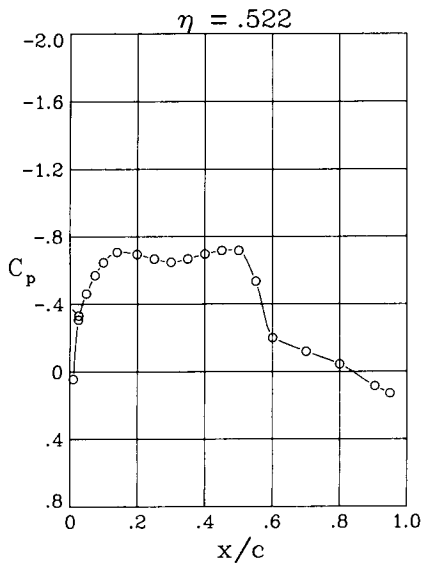
$\alpha = 2.00^\circ$



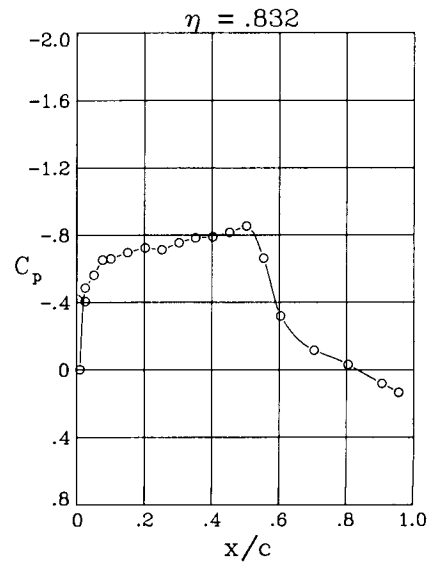
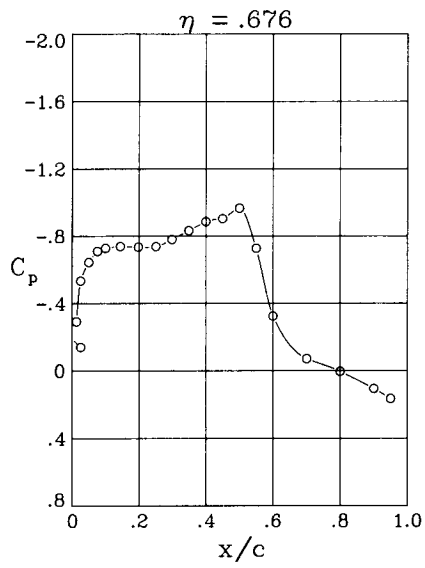
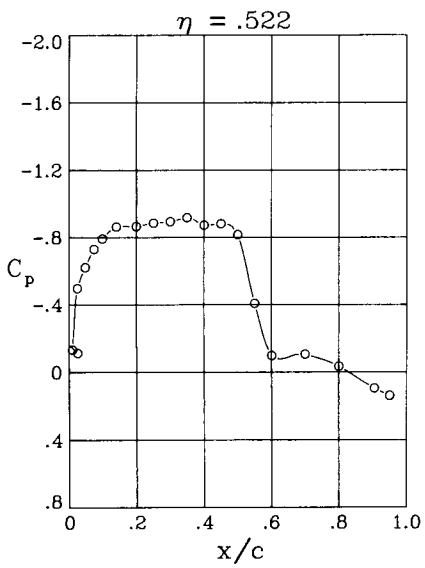
$\alpha = 2.93^\circ$

(c) Concluded.

Figure 25. Continued.



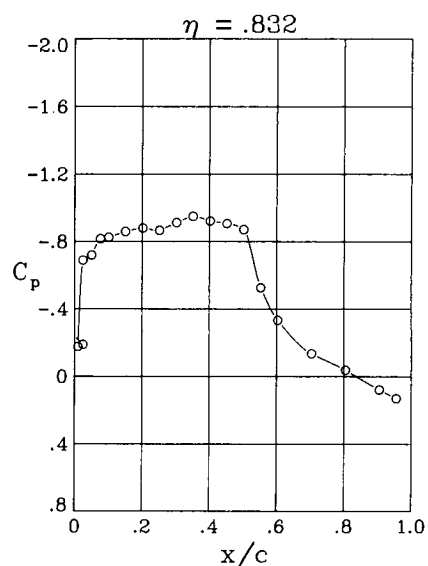
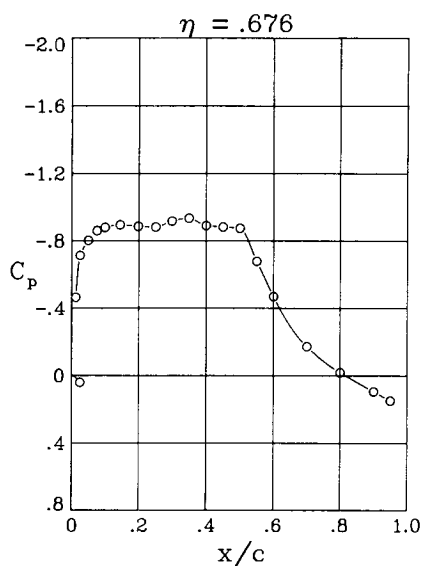
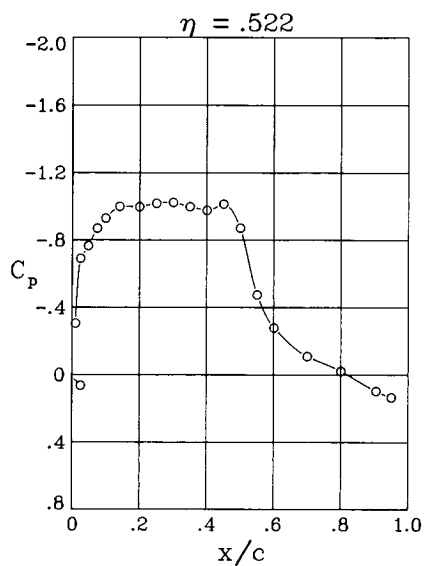
$\alpha = 0.03^\circ$



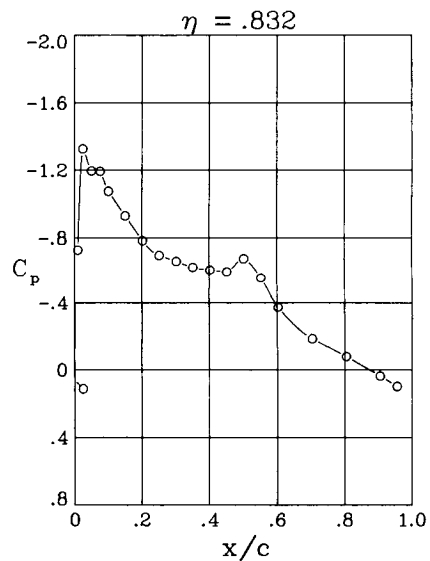
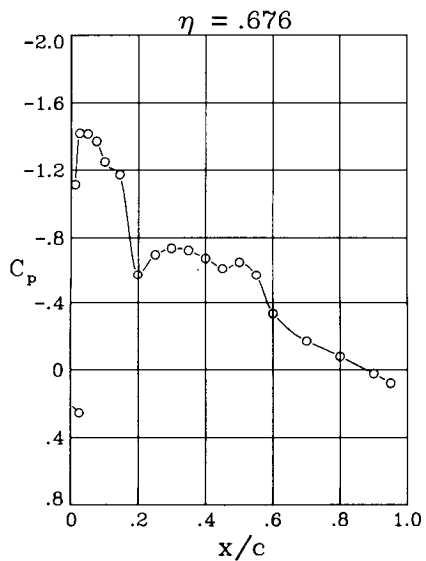
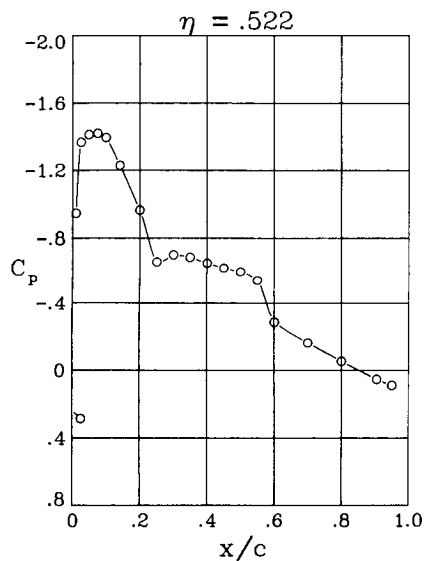
$\alpha = 0.98^\circ$

(d) $M = 0.80$.

Figure 25. Continued.



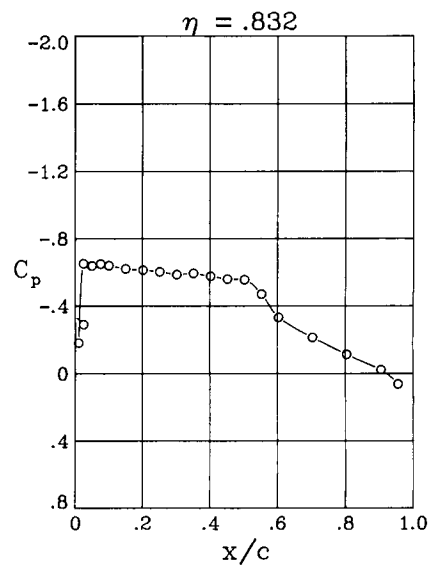
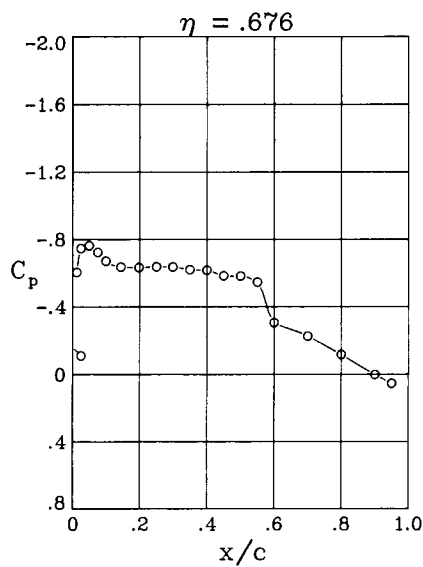
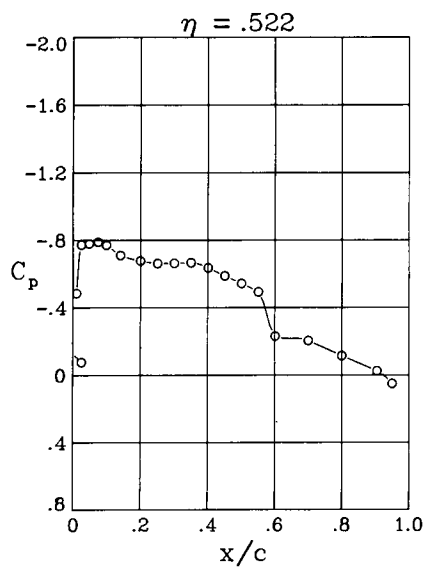
$\alpha = 1.95^\circ$



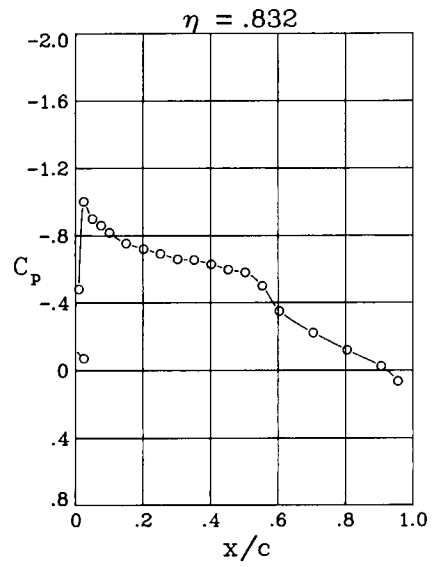
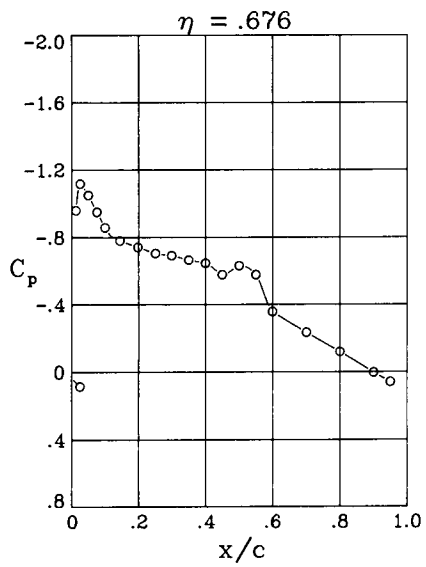
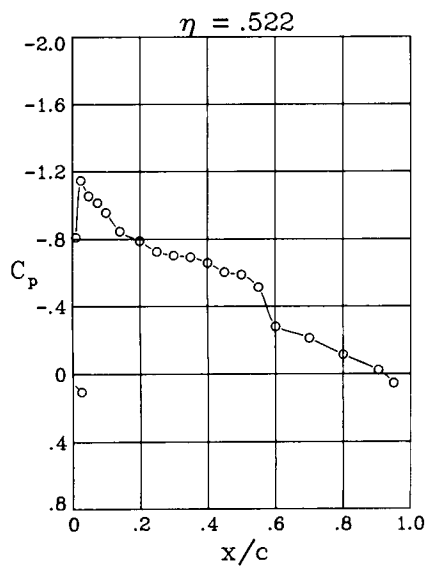
$\alpha = 2.95^\circ$

(d) Concluded.

Figure 25. Concluded.



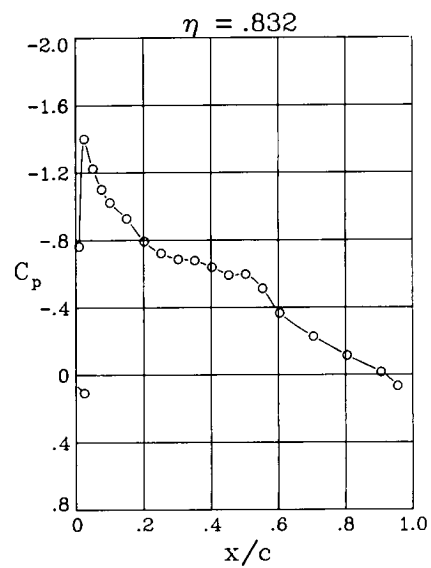
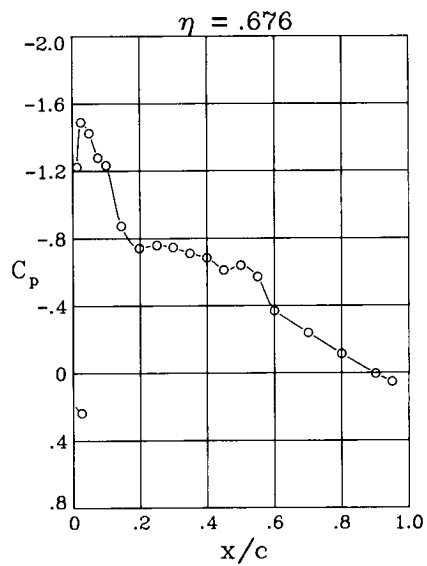
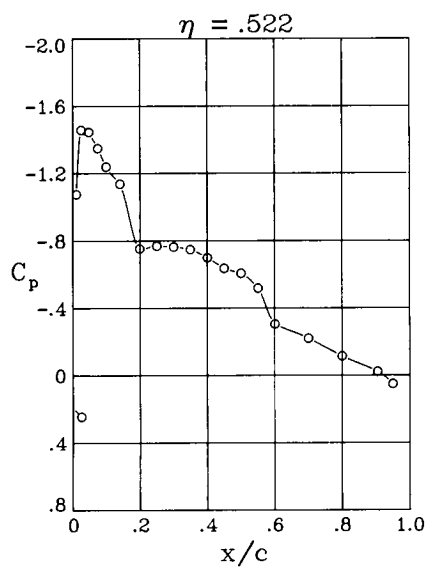
$\alpha = 0.94^\circ$



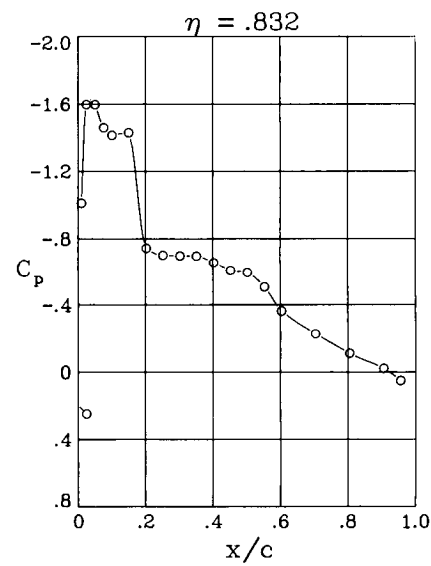
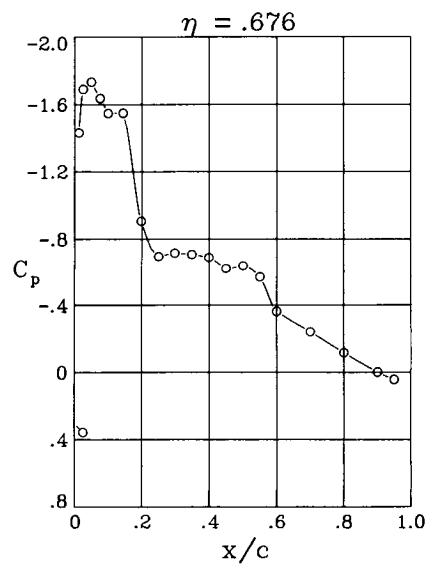
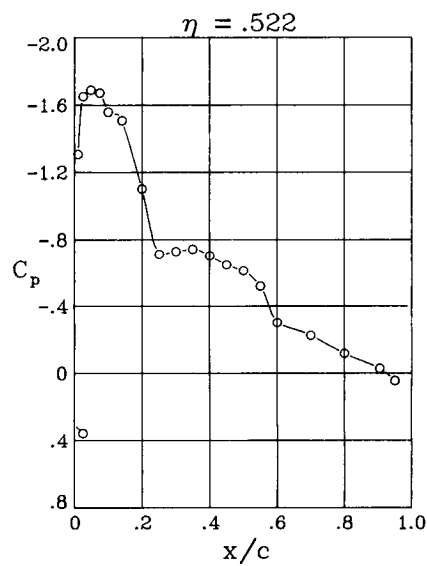
$\alpha = 1.91^\circ$

(a) $M = 0.70$.

Figure 26. Wing pressure distributions for wing C swept 25° .



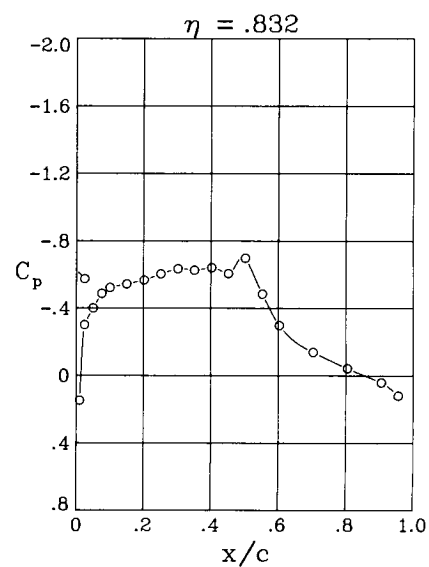
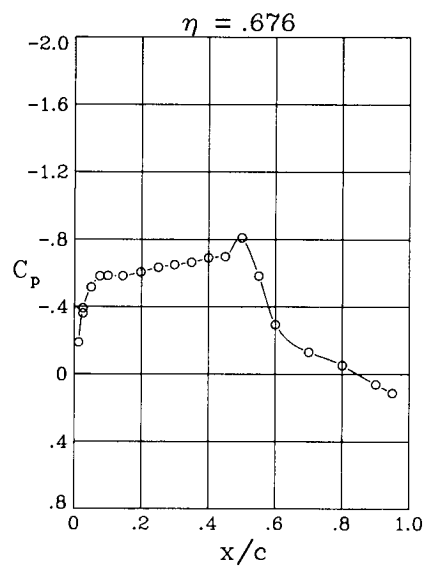
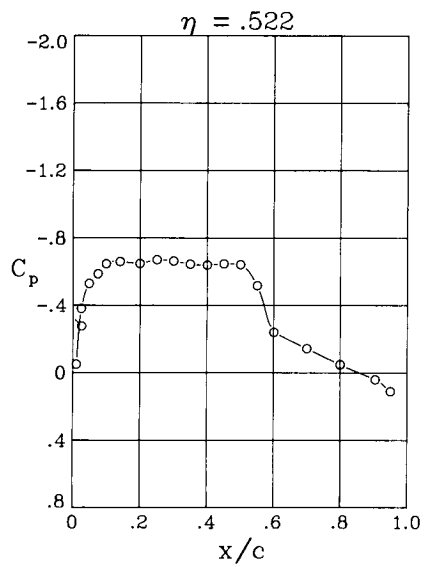
$\alpha = 2.87^\circ$



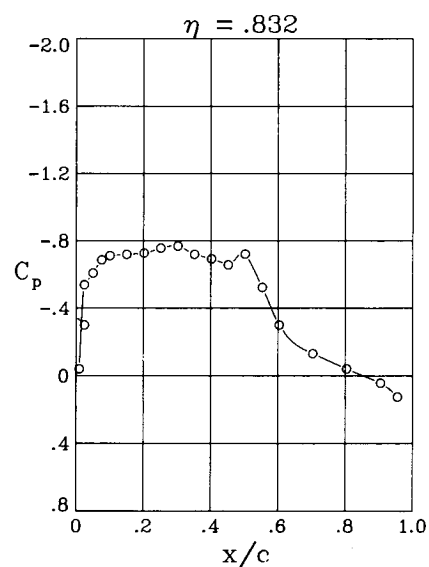
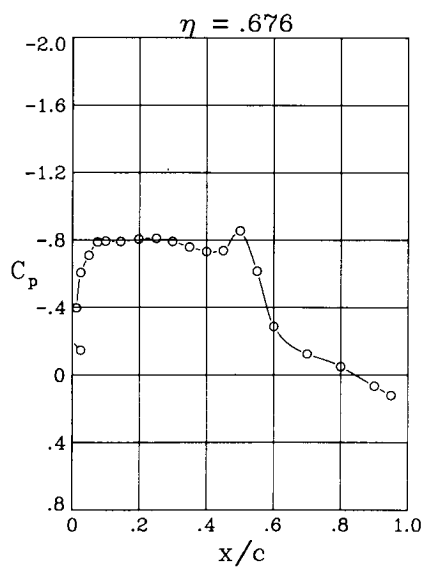
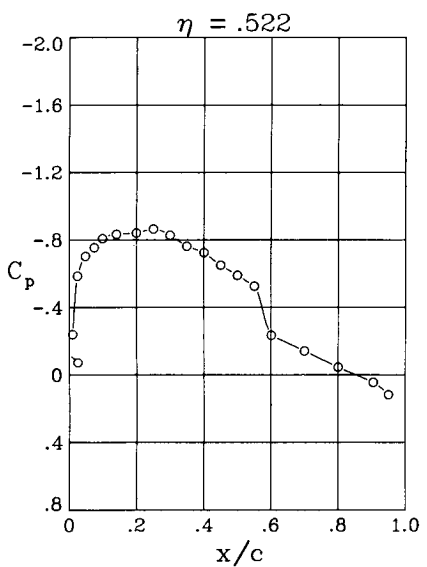
$\alpha = 3.87^\circ$

(a) Concluded.

Figure 26. Continued.



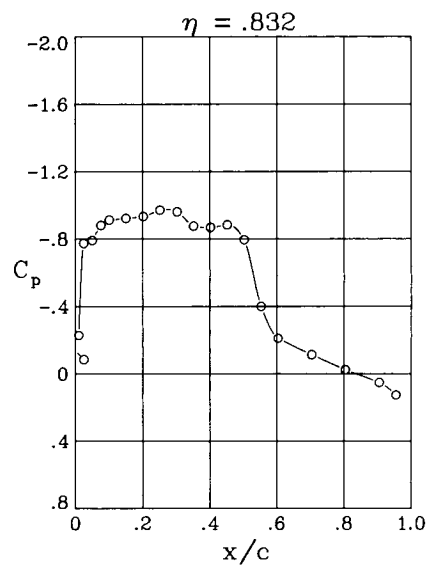
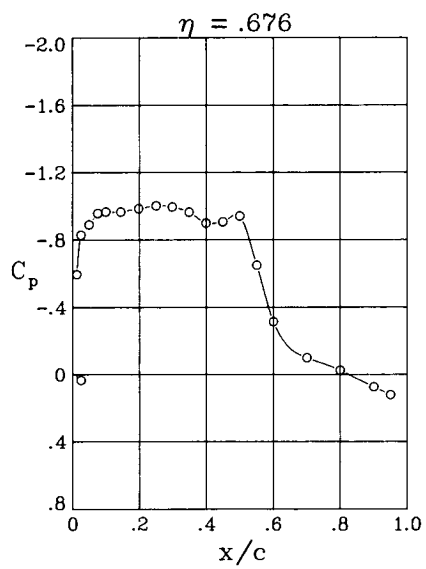
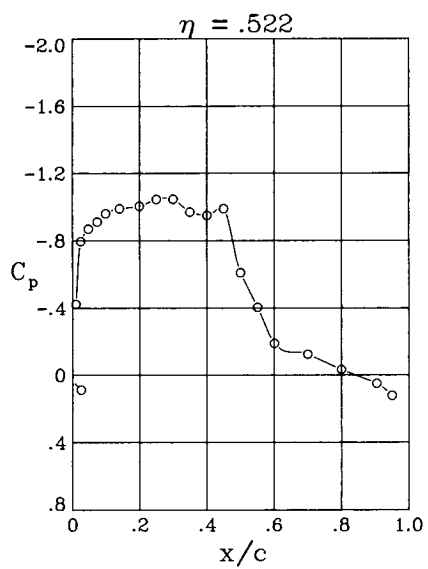
$\alpha = -0.01^\circ$



$\alpha = 0.89^\circ$

(b) $M = 0.80$.

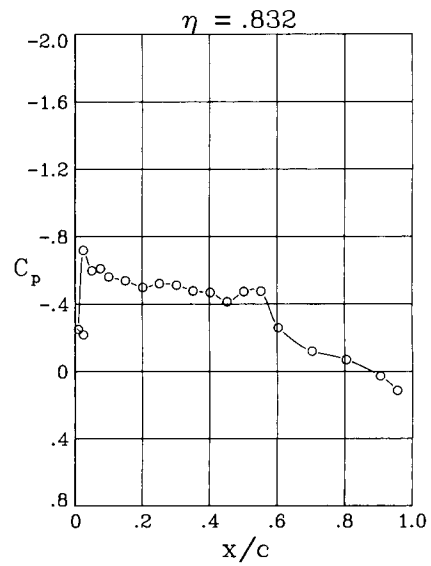
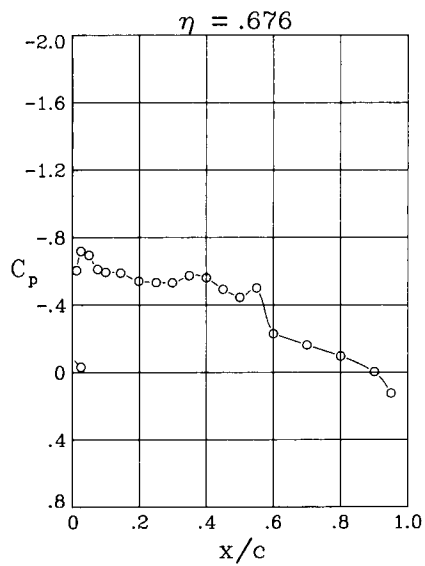
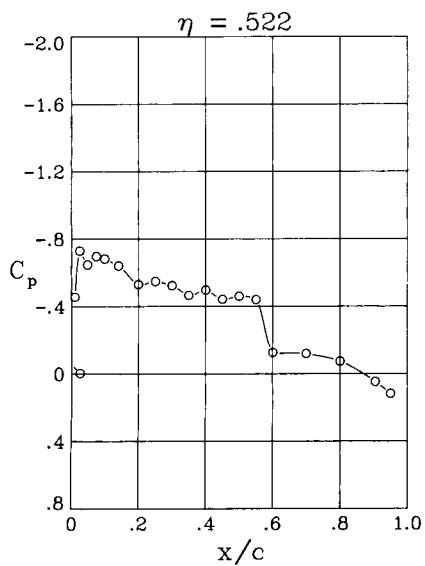
Figure 26. Continued.



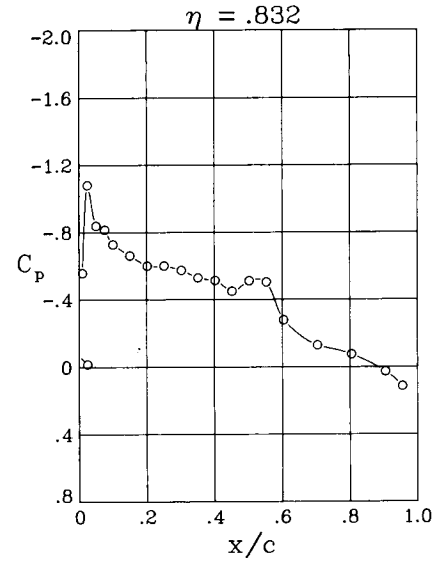
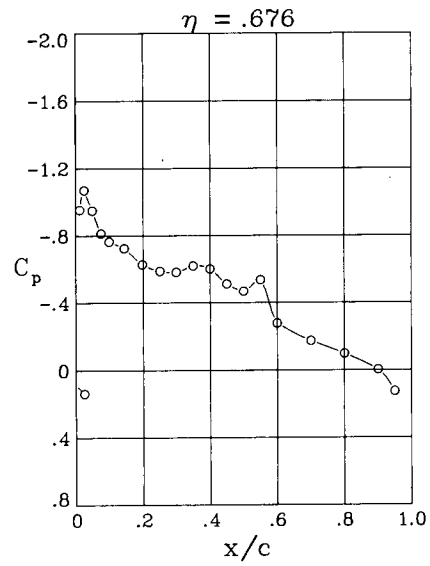
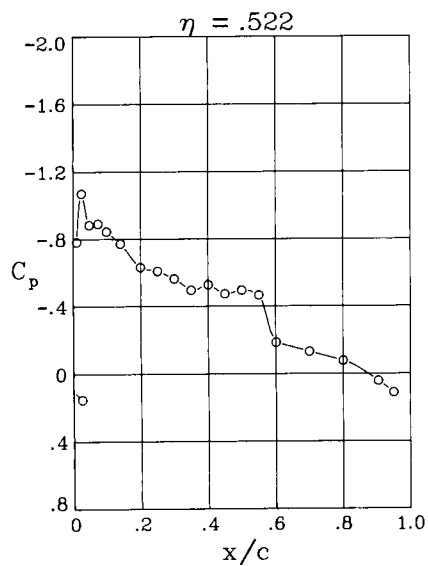
$\alpha = 1.90^\circ$

(b) Concluded.

Figure 26. Concluded.



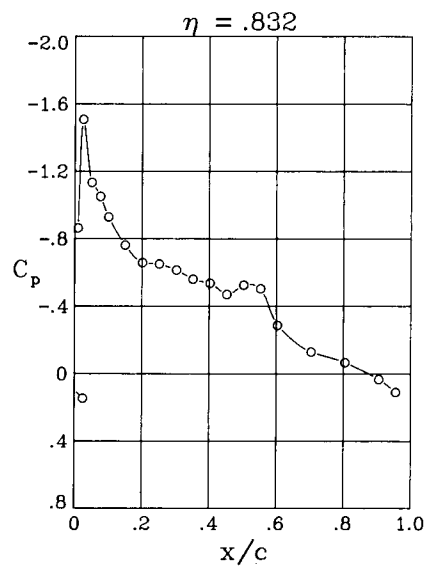
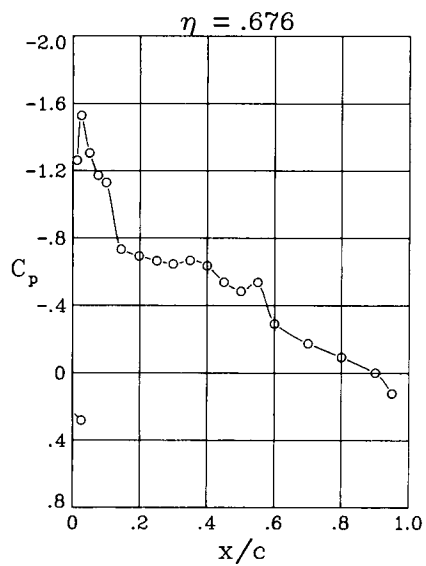
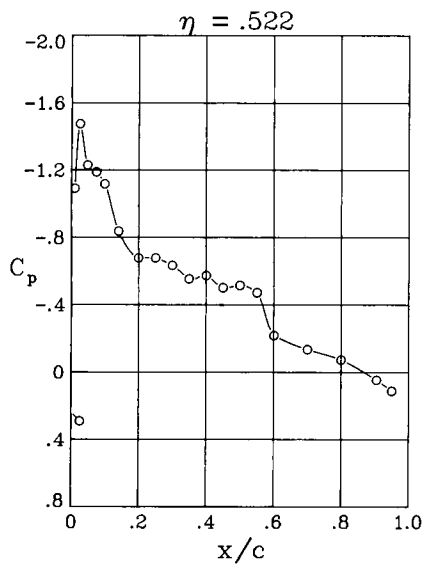
$\alpha = 0.98^\circ$



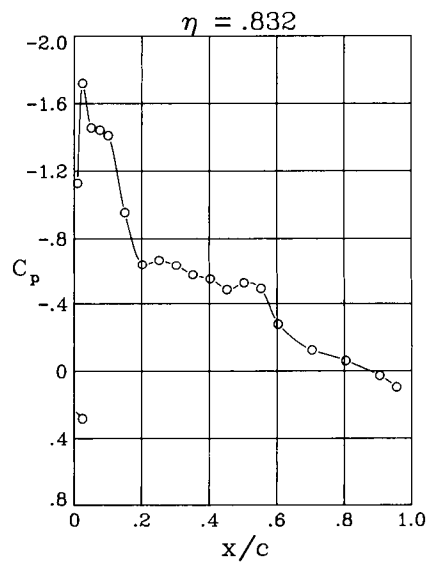
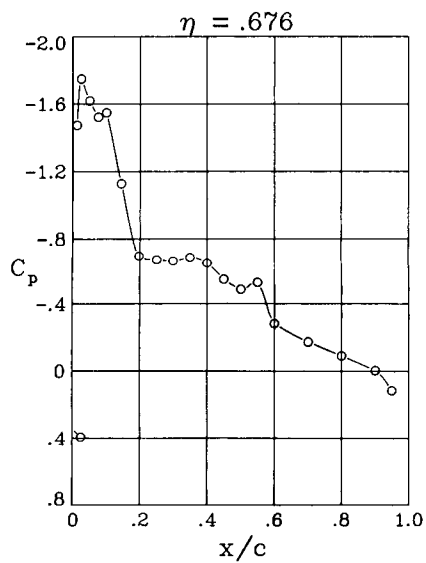
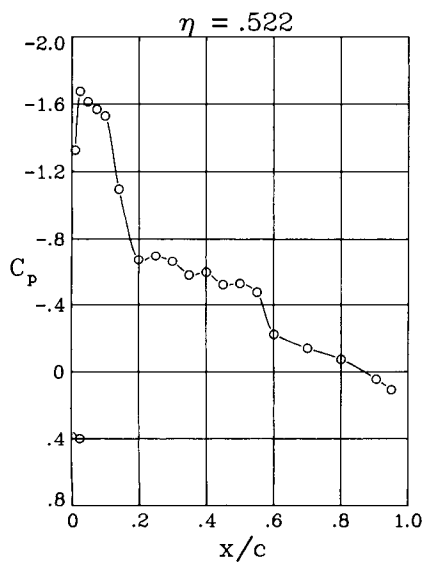
$\alpha = 1.93^\circ$

(a) $M = 0.70$.

Figure 27. Wing pressure distributions for wing C swept 30° .



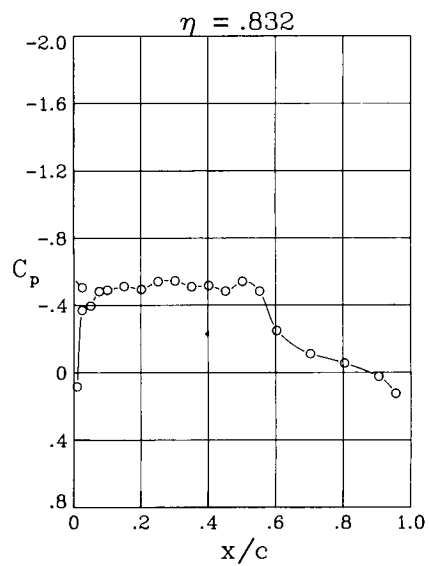
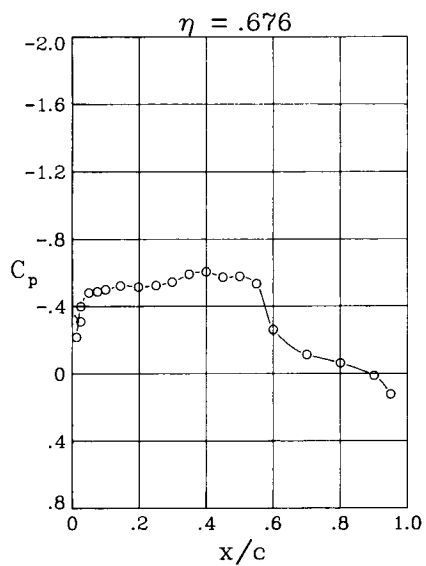
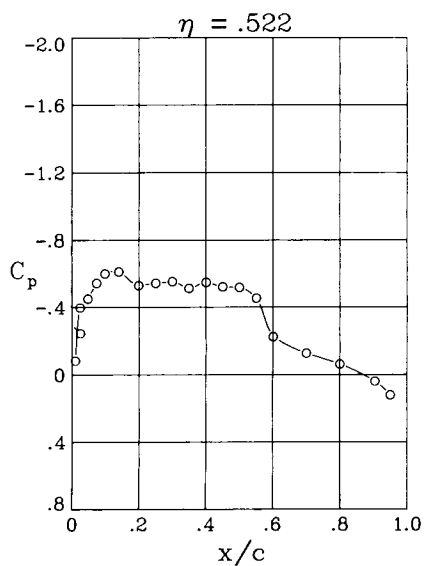
$\alpha = 2.92^\circ$



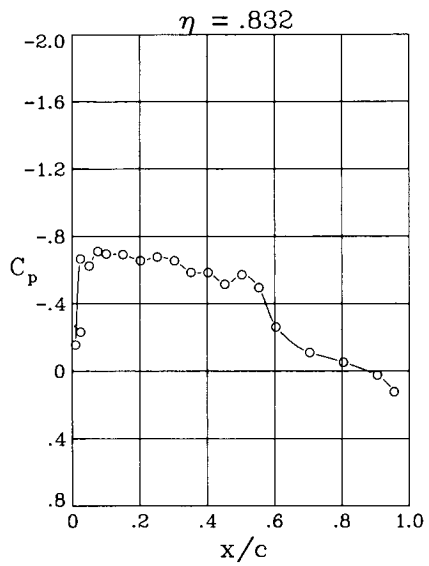
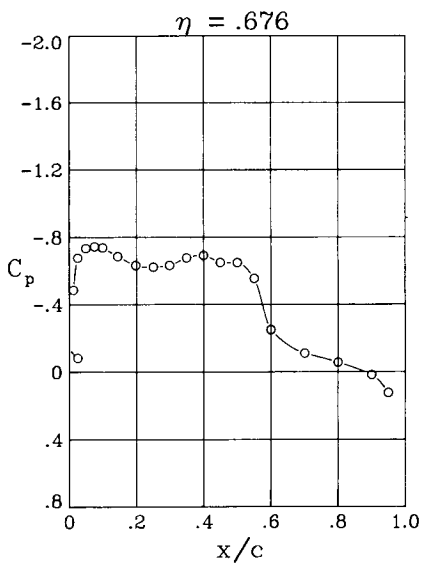
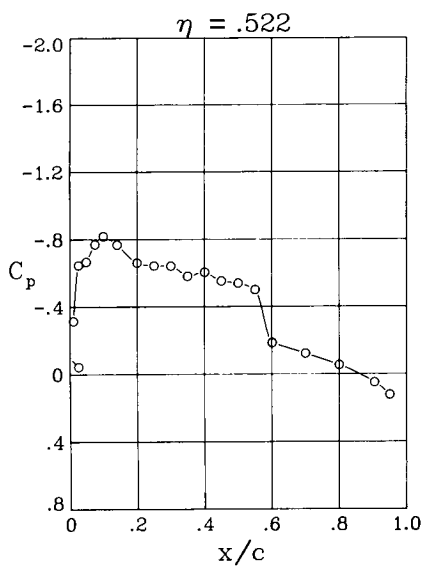
$\alpha = 3.93^\circ$

(a) Concluded.

Figure 27. Continued.



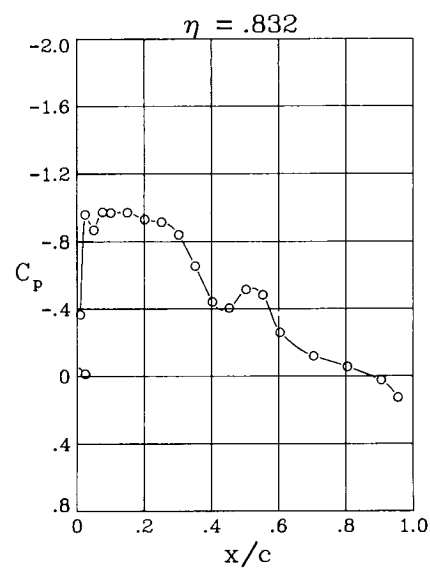
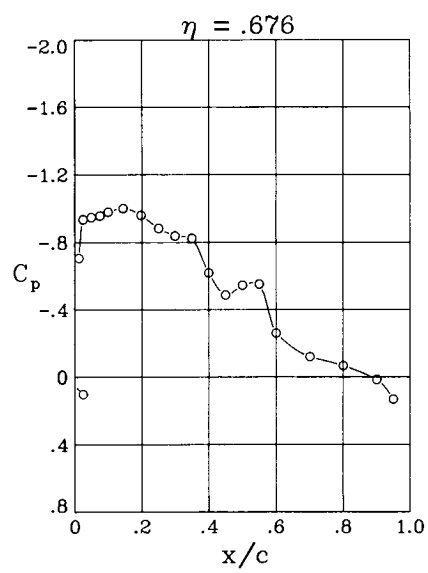
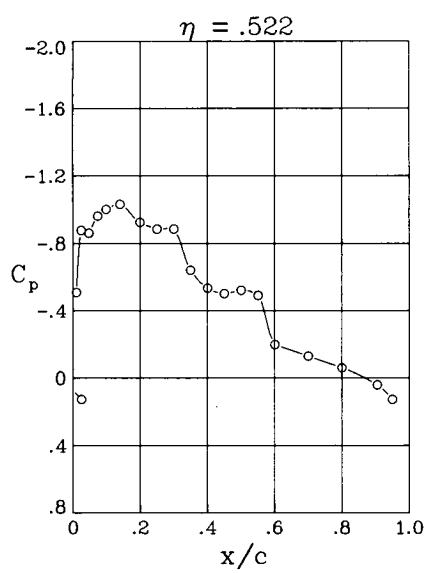
$\alpha = -0.05^\circ$



$\alpha = 0.94^\circ$

(b) $M = 0.80$.

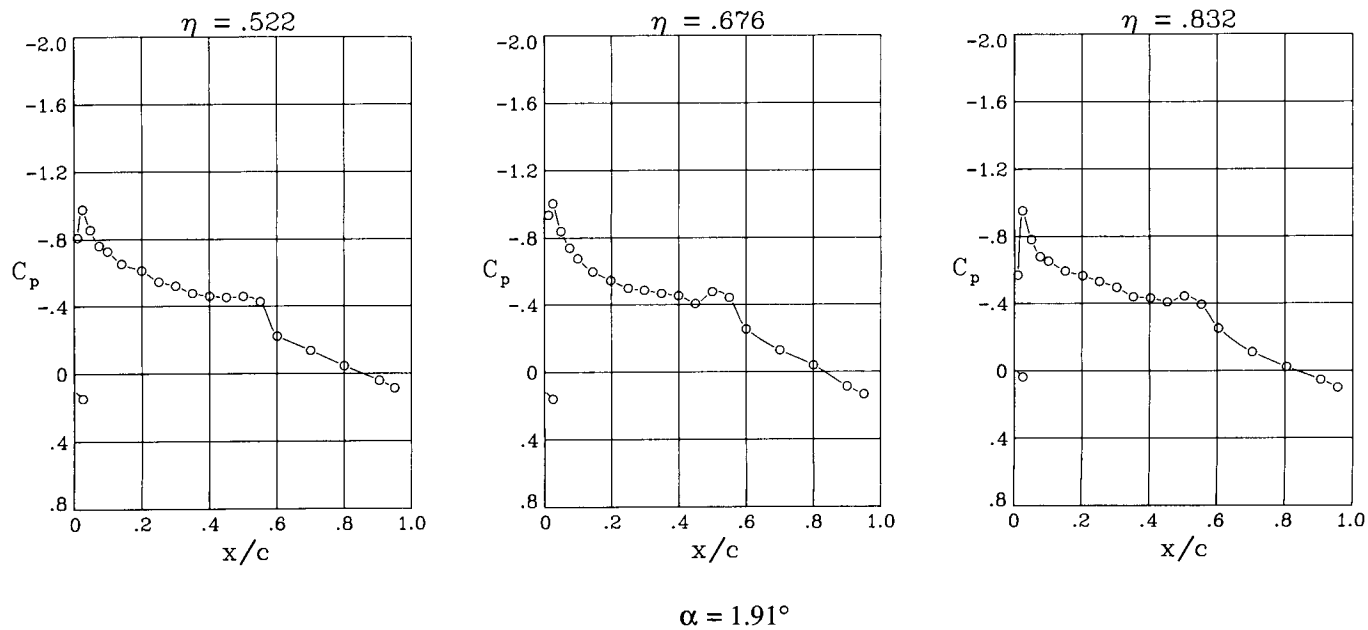
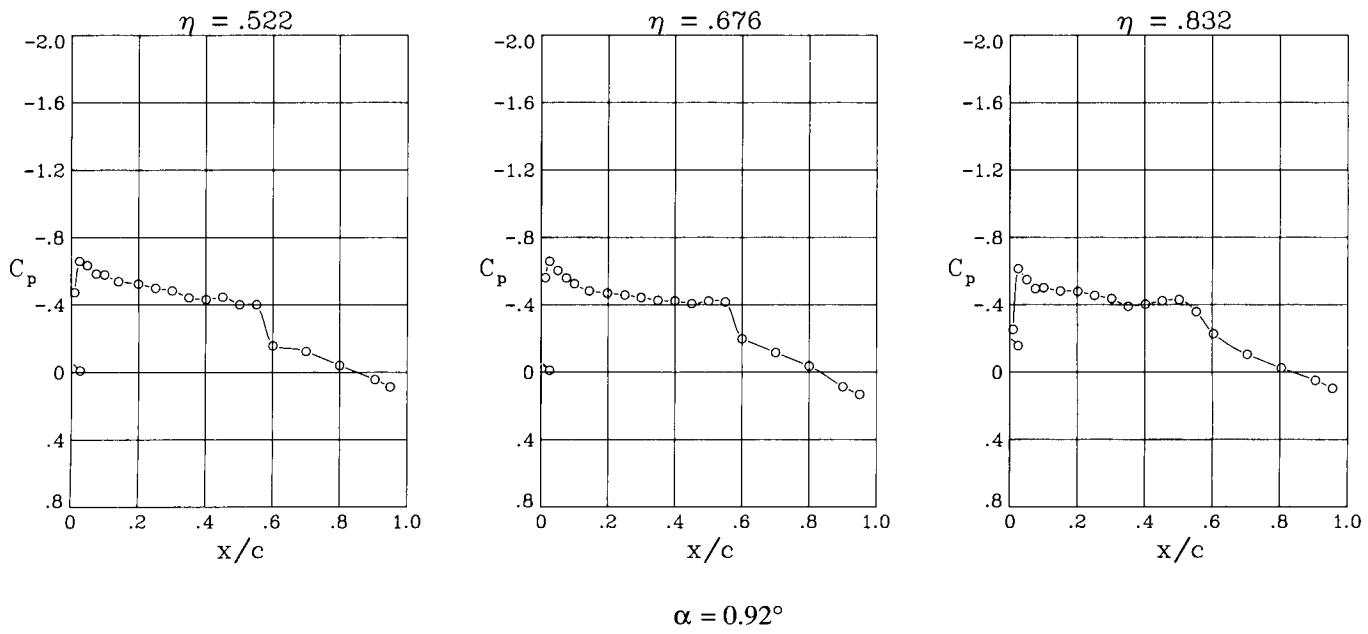
Figure 27. Continued.



$\alpha = 1.92^\circ$

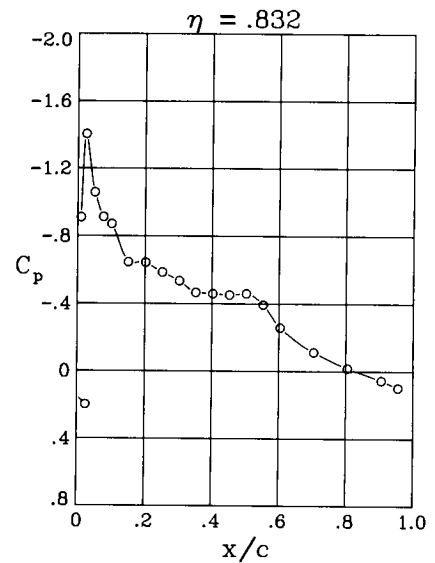
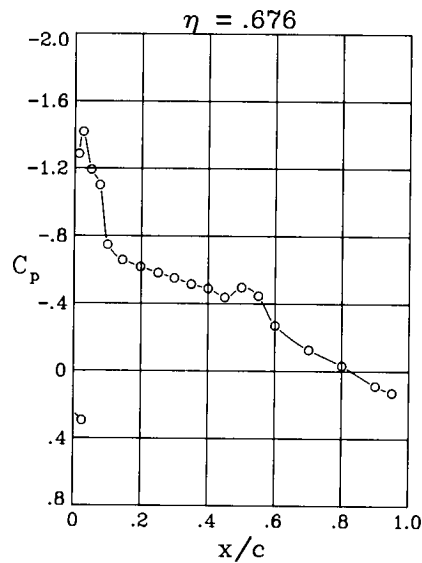
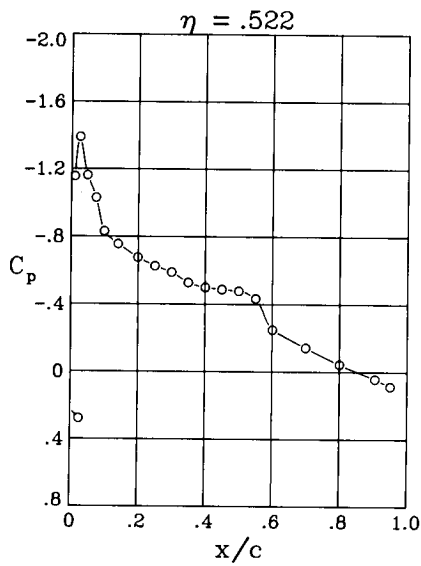
(b) Concluded.

Figure 27. Concluded.

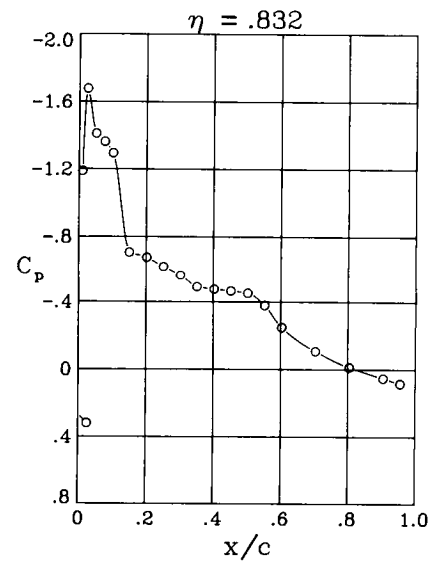
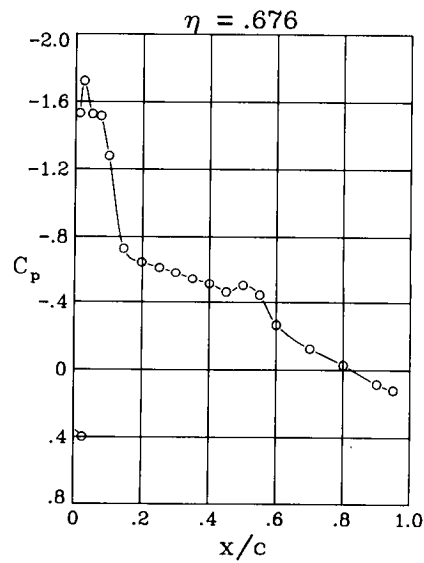
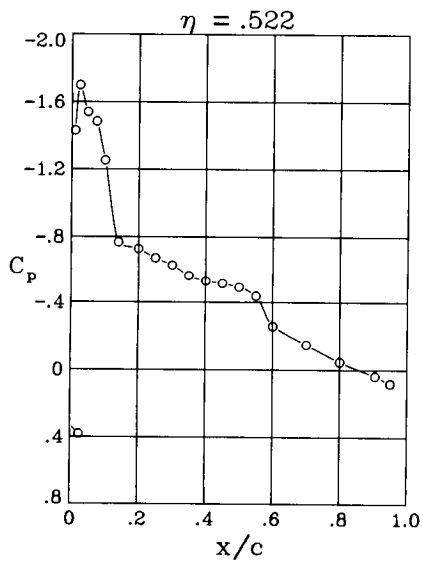


(a) $M = 0.70$.

Figure 28. Wing pressure distributions for wing C swept 35° .



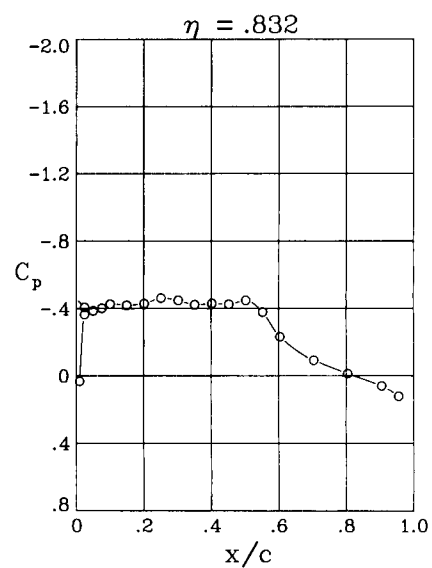
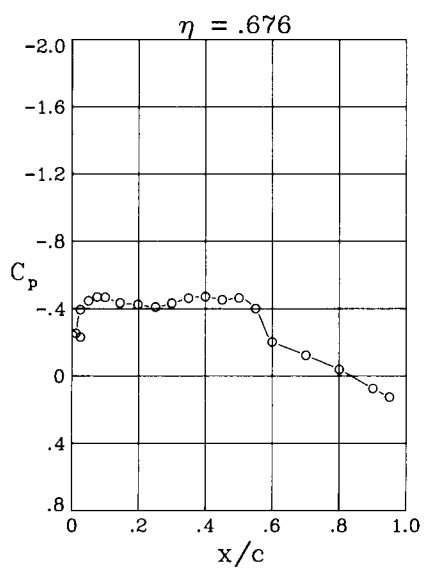
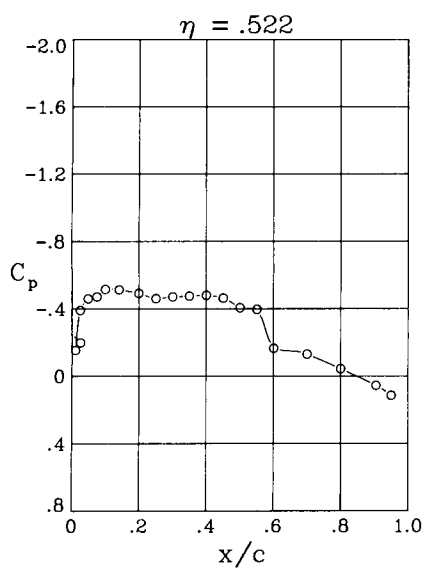
$\alpha = 2.90^\circ$



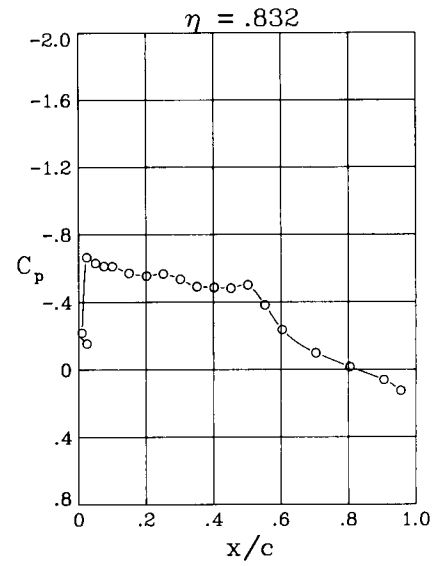
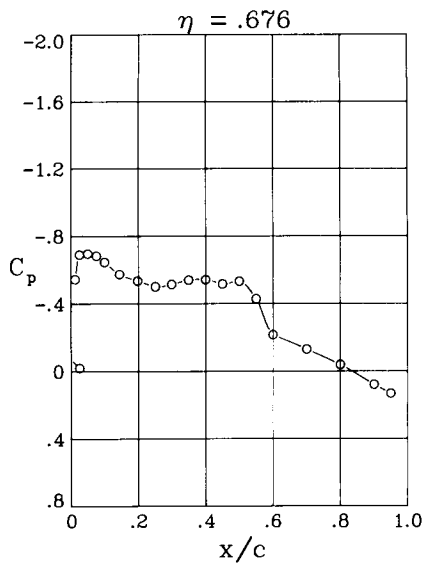
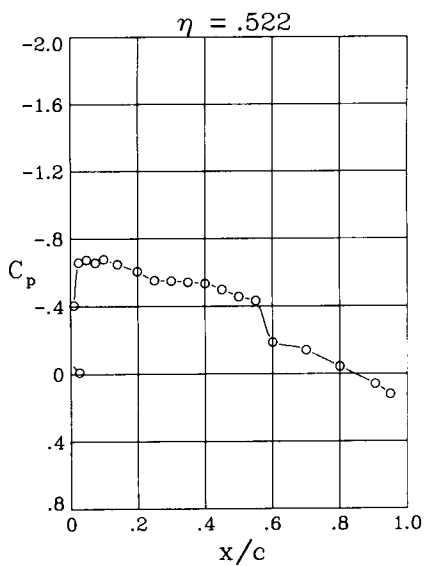
$\alpha = 3.88^\circ$

(a) Concluded.

Figure 28. Continued.



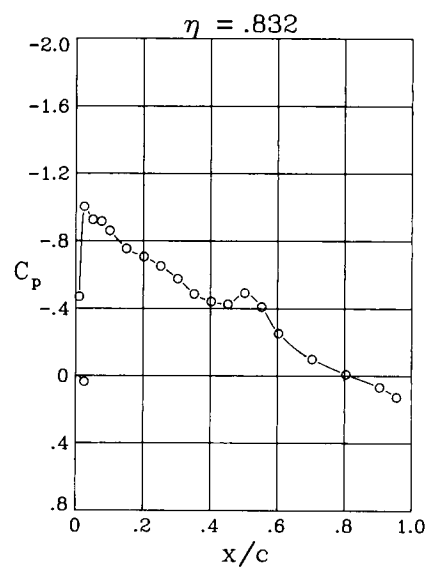
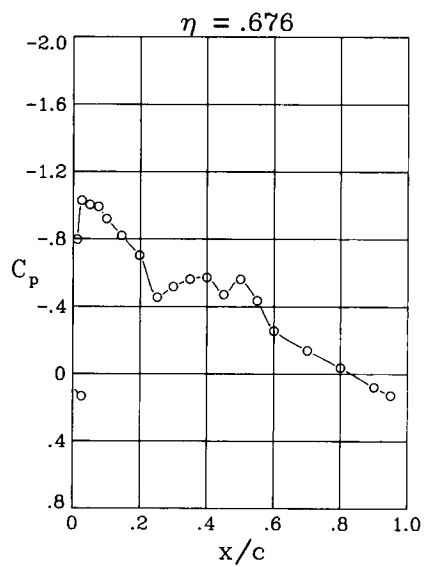
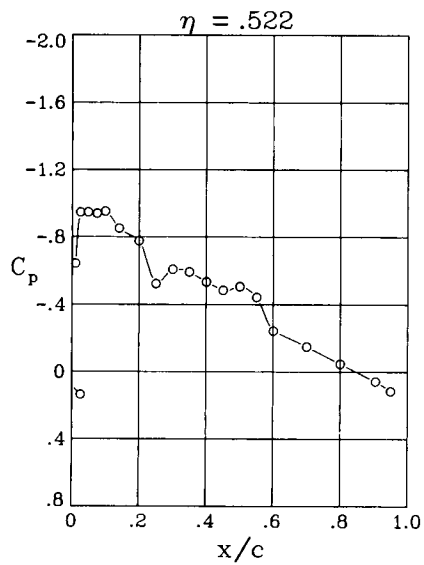
$\alpha = -0.03^\circ$



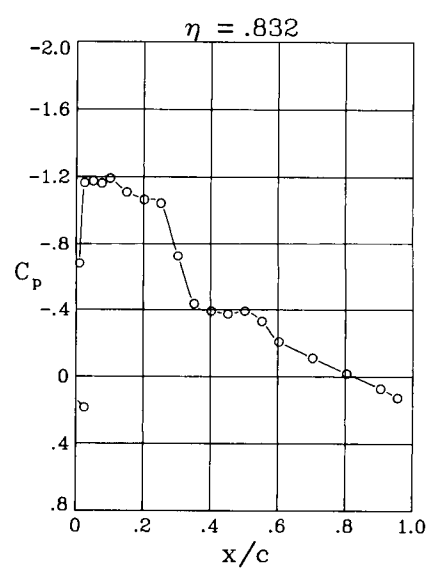
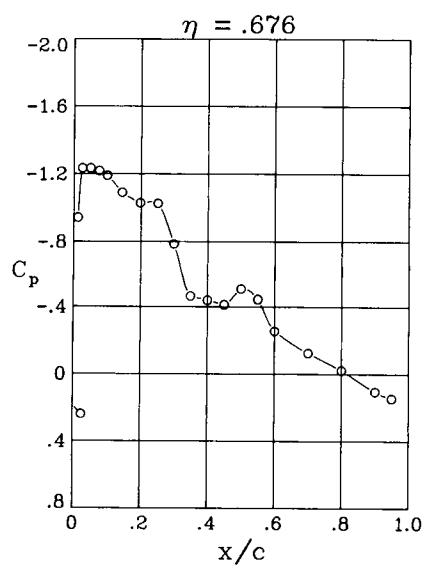
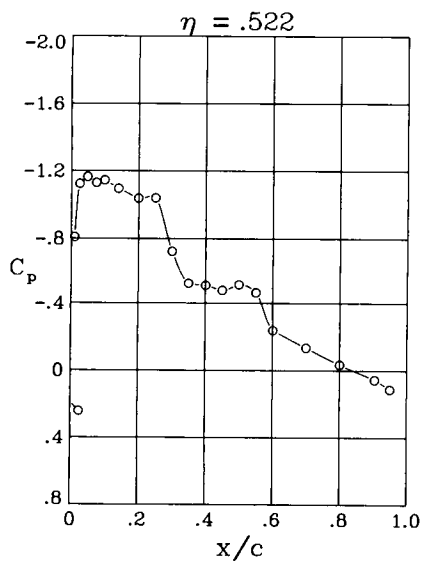
$\alpha = 0.96^\circ$

(b) $M = 0.80$.

Figure 28. Continued.



$\alpha = 1.93^\circ$



$\alpha = 2.90^\circ$

(b) Concluded.

Figure 28. Concluded.



Report Documentation Page

1. Report No. NASA TM-4124	2. Government Accession No.	3. Recipient's Catalog No.	
4. Title and Subtitle Wind-Tunnel Investigation of Aerodynamic Characteristics and Wing Pressure Distributions of an Airplane With Variable-Sweep Wings Modified for Laminar Flow		5. Report Date August 1989	
		6. Performing Organization Code	
7. Author(s) James B. Hallissy and Pamela S. Phillips		8. Performing Organization Report No. L-16493	
		10. Work Unit No. 505-60-21-02	
9. Performing Organization Name and Address NASA Langley Research Center Hampton, VA 23665-5225		11. Contract or Grant No.	
		13. Type of Report and Period Covered Technical Memorandum	
12. Sponsoring Agency Name and Address National Aeronautics and Space Administration Washington, DC 20546-0001		14. Sponsoring Agency Code	
15. Supplementary Notes			
16. Abstract A wind-tunnel investigation has been conducted to evaluate the aerodynamic characteristics and wing pressure distributions of a variable-wing-sweep aircraft having wing panels that were modified to promote laminar flow. The modified wing section shapes were incorporated over most of the exposed outer wing panel span and were obtained by extending the leading edge and adding thickness to the existing wing upper surface forward of 60-percent chord. Two different wing configurations, one designed for a Mach number of 0.7 and one for 0.8, were tested on the model simultaneously, with one wing configuration on the left side and the other on the right. The investigations were conducted at Mach numbers from 0.20 to 0.90 for wing sweep angles of 20°, 25°, 30°, and 35°. Longitudinal, lateral, and directional aerodynamic characteristics of the modified and baseline configurations, and selected pressure distributions for the modified configuration, are presented in graphical form without analysis. A complete tabulation of the pressure data for the modified configuration is available as a microfiche supplement.			
17. Key Words (Suggested by Authors(s)) Aircraft configuration F-14 Laminar flow Transonic wind-tunnel test Longitudinal aerodynamics Lateral-directional aerodynamics Pressure distribution Variable sweep Boundary layer		18. Distribution Statement Unclassified—Unlimited Subject Category 02	
19. Security Classif. (of this report) Unclassified	20. Security Classif. (of this page) Unclassified	21. No. of Pages 226	22. Price A11